DEVELOPMENT OF A NEW ENANTIOSELECTIVE REDUCTION OF KETONE AND FLUOROGENIC DETECTION OF HYDROGEN PEROXIDE

by

Upamanyu Basu

B.Sc., University of Calcutta, 2007

M.Sc., Indian Institute of Technology Bombay, 2009

Submitted to the Graduate Faculty of

The Kenneth P. Dietrich School of Arts and Sciences in partial fulfillment

of the requirements for the degree of

Doctor of Philosophy

University of Pittsburgh

2017

UNIVERSITY OF PITTSBURGH

THE KENNETH P. DIETRICH SCHOOL OF ARTS AND SCIENCES

This dissertation was presented

by

Upamanyu Basu

It was defended on

October 17, 2016

and approved by

Dennis P. Curran, Professor, Department of Chemistry

Paul E. Floreancig, Professor, Department of Chemistry

W. Barry Edwards, Assistant Professor, Department of Radiology

Committee Chair: Kazunori Koide, Associate Professor, Department of Chemistry

DEVELOPMENT OF A NEW ENANTIOSELECTIVE REDUCTION OF KETONE AND FLUOROGENIC DETECTION OF HYDROGEN PEROXIDE

Upamanyu Basu, PhD

University of Pittsburgh, 2017

Aberrant splicing related mutations are related to many diseases including cancers while reactive oxygen species (ROS) imbalance is linked to oxidative cellular damage, ultimately leading to aging and neurodegenerative illness. ROS is also known to protect the cells from foreign pathogens due to their oxidative nature. Herein we have taken two different approaches to study them.

In the first chapter, we discuss an improved synthesis of meayamycins, that are powerful modulators of the spliceosome and are used as tools to study splicing mutations. We examined a new enantioselective reduction of prochiral ketone, en route to the synthesis of meayamycin B. We also described the synthesis of new analogue keto-meayamycin D that probes the potency of meayamycins containing other electrophilic functionalities instead of the epoxide group.

In the second chapter, we discussed the need for new fluorescent turn-on probes for a better understanding of how ROS participates in cellular processes. We describe the syntheses of two new probes for the detection of H_2O_2 that is based on a Mislow-Evans rearrangement. We further studied the stability and kinetics in detail and how they could be beneficial in complimenting the existing probes. Finally, we examined the effect of serum on the Mislow-Evans rearrangement, which is the underlying principle for the H_2O_2 detection.

TABLE OF CONTENTS

LIST OF TABLES

LIST OF FIGURES

LIST OF SCHEMES

LIST OF SPECTRA

LIST OF ABBBREVIATIONS

Ac	acetyl
app	apparent
aq	aqueous
Boc	di-tert-butyl dicarbonate
Br	broad
CSA	camphorsulfonic acid
Cy	cyclohexyl
DCE	dichloroethane
DIBALH	diisobutylaluminum hydride
DIPT	diisopropyl tartarate
DMF	dimethylformamide
DMSO	dimethyl sulfoxide
DNA	deoxyribonucleic acid
dr	diastereomeric ratio
EC_{50}	half maximal effective concentration
ee	enantiomeric excess
er	enantiomeric ratio
ESI	electrospray ionisation
equiv	equivalent
Et	ethyl
GI_{50}	half maximal growth inhibition
h	hour(s)
HBSS	Hank's balanced salt solution
HPLC	high performance liquid chromatography
HRMS	high resolution mass spectrometry
IC_{50}	half maximal inhibitory concentration
IR	infrared
J	coupling constant (NMR)
LCMS	low resolution mass spectrometry
M	molar
Me	methyl
m.p.	melting point
MS	mass spectrum
^{n}Bu	butyl

NMO	N-methylmorpholine
NMR	nuclear magnetic resonance
Ph	phenyl
quant.	quantitative
r.t.	room temperature
R_f	retention factor
RNA	ribonucleic acid
SAR	structure-activity relationship
SF3b	splicing factor 3b
snRNP	small nuclear ribonucleoprotein
T	temperature
TBHP	*t*-butylhydroperoxide
TFA	trifluoroacetic acid
THF	tetrahydrofuran
TLC	thin-layer chromatography
TPAP	tetra-n-propylammonium perruthenate

1.0 INTRODUCTION TO FR901464

In 1996, in the quest for new anticancer agents with novel modes of action, natural products FR901463, FR901464, and FR901465 (Figure 1) were isolated[1-3] by the Fujisawa Pharmaceutical Company from what was initially reported as soil bacteria *Pseudomonas* sp. No. 2663. Later reports indicated *Burkholderia* sp FERM BP-3421 as the source of these natural products.[4] It was reported as having an intriguing biological profile, including being a novel Simian virus 40 (SV40) promoter-dependent transcriptional activator that causes cell cycle arrest at G1 and G2/M phases. All of these natural products exhibited potent anti-proliferative activity against a panel of human cancer cell lines with GI_{50} (concentration required to inhibit 50% of cell growth) values between 0.2 – 1.7 ng/mL.[1-3]

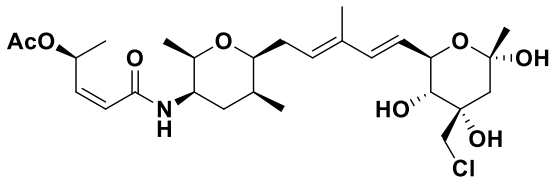

FR901463 (1.1)

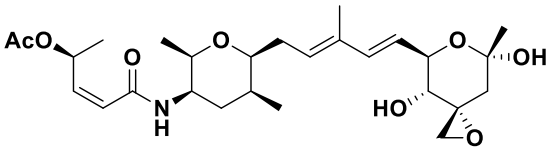

FR901464 (1.2)

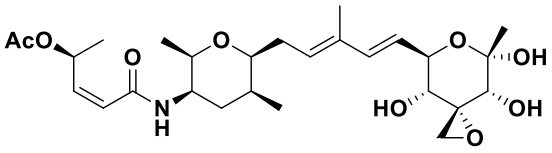

FR901465 (1.3)

Figure 1. Chemical structures of FR901463, FR901464, and FR901465

1.1 PREVIOUS WORK

Current research on the SAR[5-12] of FR901464 indicates that spiroepoxide moiety is crucial to the potency of the molecule. Another important preferred structural attribute includes the presence of a diene moiety, a *cis* enamide. The results of all the SAR studies are summarized in Figure 2:

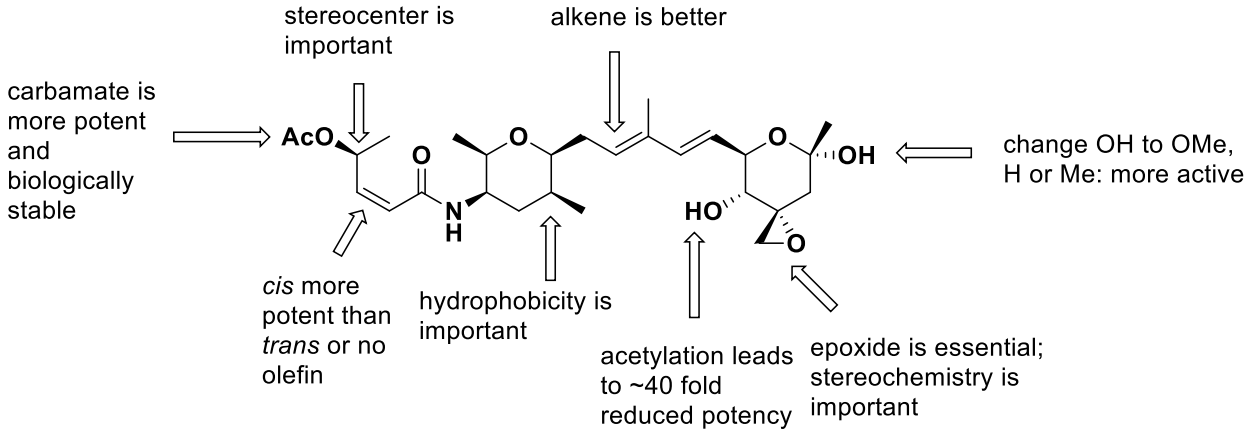

Figure 2. Summary of SAR studies published on FR901464.

In the Koide group, the general approach to the synthesis of meayamycins consisted of synthesizing three key advanced intermediates, the left fragment **1.6**, the side chain acid **1.8,** and the right fragment **1.12**. The synthesis of the left fragment **1.6** relied upon the utilization of a chiral pool synthetic strategy. Starting from (L)-threonine **1.4,** shown in Scheme 1 below, advanced intermediate **1.6** was synthesized in 10 steps via Garner aldehyde **1.5**. The sequence relied upon a key Horner-Wadsworth-Emmons reaction strategy. Carboxylic acid **1.8** was accessed from (S)-lactate ester **1.7**, utilizing another Horner-Wadsworth-Emmons reaction as the key reaction in a 4-step sequence. Finally, the synthesis of right fragment **1.12**, utilized achiral starting materials and a Sharpless asymmetric epoxidation, a Zr/Ag-promoted diastereoselective

alkynylation reaction, a diastereoselective Mislow-Evans rearrangement, and Hg(II) mediated cyclization strategies to set key stereocenters. The overall synthetic plan is shown in Scheme 1 (the specific example of meayamycin B is shown here).

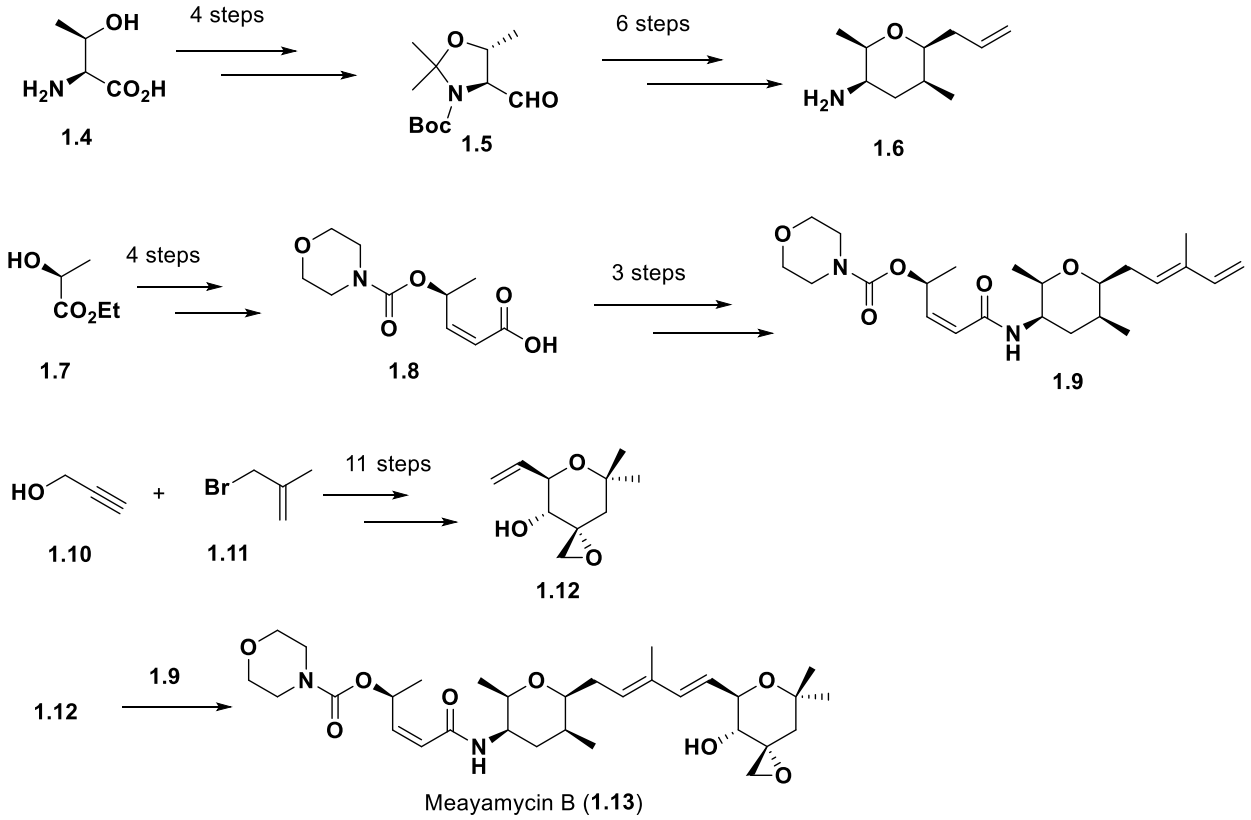

Scheme 1. General approach to FR901464 analogues in the Koide group.

In light of the promising potency of meayamycins towards inhibiting pre-mRNA splicing and cancer-cell growth, there was a need to ensure abundant access to meayamycins to advance its pharmacological studies. However, it became increasingly difficult to support the immense demand (more than 50 requests per year) from other research groups around the world for meayamycins to be used as the tool to study splicing-related projects. To ensure a consistent supply of meayamycins and sufficient material for the further study of their related biological

properties, a safe, scalable, economical, and, most importantly, shortened general synthesis route was required. For this goal, the synthesis of right fragment **1.12** required improvement. The previous synthesis of **1.12** had several drawbacks for scaling up (see Scheme 2 below). First, the Zr/Ag-promoted stereoselective alkynylation reaction to produce **1.17** required stoichiometric amounts of expensive heavy metallic reagents. Second, the use of a selenium reagent was not cost effective. Third, the formation of the tetrahydropyran ring required a stoichiometric quantity of $Hg(OAc)_2$. Most importantly, the scheme was lengthy (11 linear steps from propargyl alcohol).

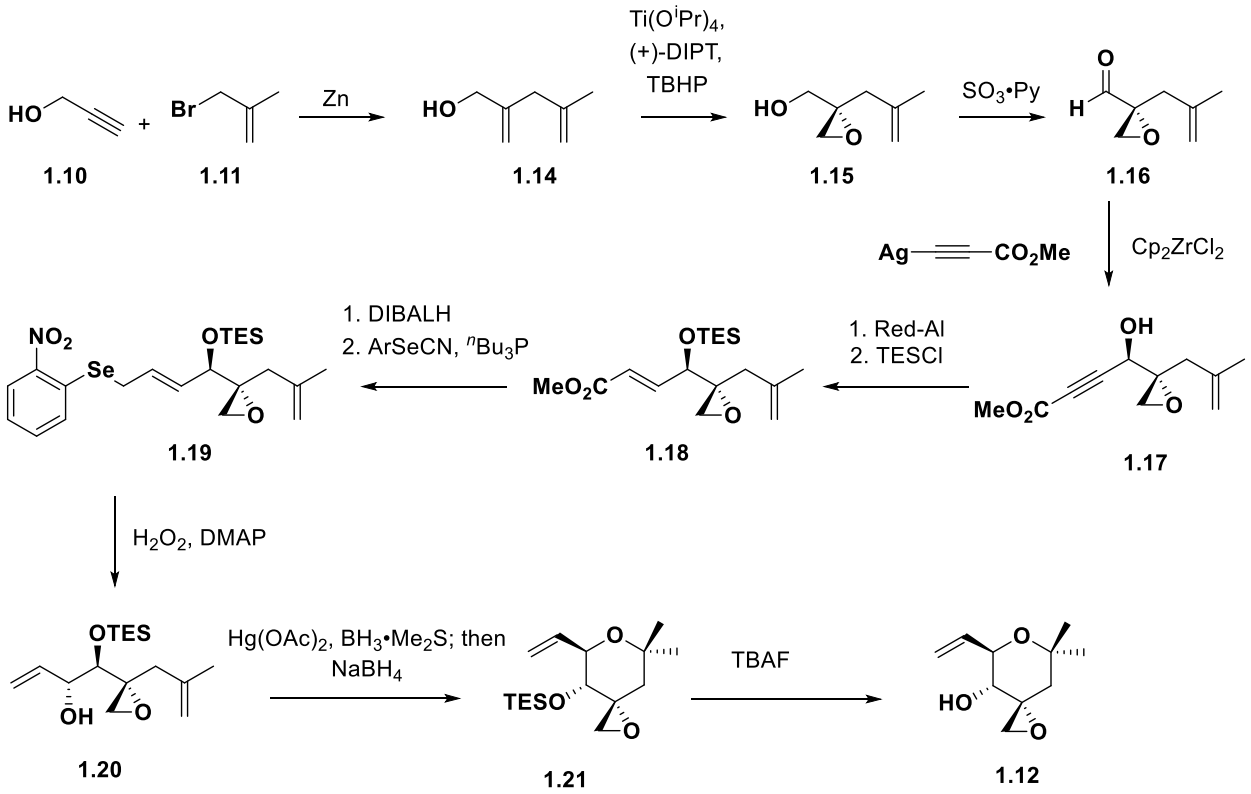

Scheme 2. Previous synthesis of right fragment **1.12.**

It was identified that the synthesis of right fragment **1.12** required improvement, and Dr. Sami Osman, while he was a graduate student in the Koide group, worked on the improved synthesis. To summarize his work, starting from hydroxy ketone **1.22**, silyl enol ether **1.23** was prepared in one step (see Scheme 3 below). This was followed by a Mukaiyama aldol reaction with acrolein (20 equiv) under Kobayashi's condition[13] using 20 mol% of $Yb(OTf)_3 \bullet 6H_2O$ as the Lewis acid catalyst to obtain **1.24** as the aldol product in 75% yield. Regioselective β-elimination using Ac_2O and NaOAc gave enone **1.25** in 60-70% yield.

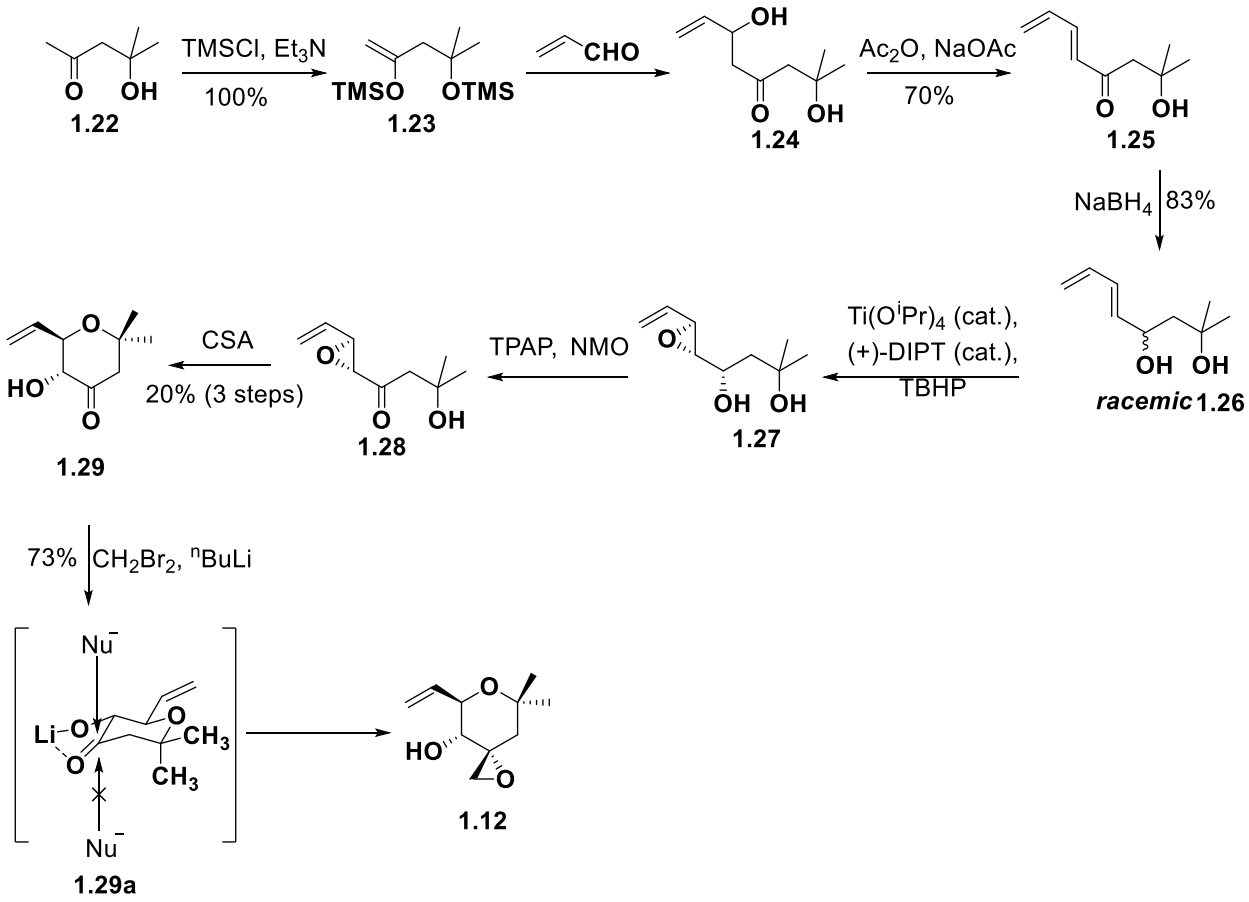

Scheme 3. Previous work on an improved synthesis of right fragment **1.12**.

Dr. Osman's attempts at the enantioselective conversion of **1.25** to epoxyketone **1.28** in one step were unsuccessful and revealed the limitations of some of the other known synthetic methods. For example, Shibasaki's method based on La-BINOL-Ph_3As[14] to induce enantioselective epoxidation required as much as 30 mol% of (*R*)-1,1'-binaphthol (BINOL) ligand to form the epoxyketone in 30% yield and 70% *ee*. The cinchona alkaloid-catalyzed asymmetric Darzens condensation[15] did not provide the desired product even after protecting the tertiary hydroxy group as a TMS or THP ether. Kinetic resolution of racemic epoxy alcohols by an intramolecular epoxide opening catalyzed by [Co^{III}(salen)] complex[16,17] failed to convert racemic **1.28** to enantioenriched **1.29**. A (*R*)-BINOL-phosphoric-acid-based kinetic resolution of racemic epoxide **1.28** to enantioenriched ketone **1.29** was successful in 32% yield with an *ee* of >90%. However, this transformation could not be reproduced.

Finally, a more reproducible approach was realized. Enone **1.25** was reduced with $NaBH_4$ to afford racemic allylic alcohol **1.26**, which was then subjected to Sharpless kinetic resolution[18] to obtain epoxyalcohol **1.27** as one enantiomer. This was then oxidized (Ley oxidation[19]) by using a combination of catalytic tetrapropylammonium perruthenate (TPAP) and stoichiometric 4-methylmorpholine N-oxide (NMO) to obtain chiral epoxyketone **1.28**, which suffered a facile anti-Baldwin/Nicolaou type cyclization[20] under acidic conditions to yield ketone **1.29** in 20% yield over 3 steps. Finally, ketone **1.29** underwent the addition of diastereoselective nucleophilic to produce right fragment **1.12** in 73% yield.

Although a more concise synthesis of the right fragment **1.12** was accomplished, there were still a few problems. Since a kinetic resolution strategy was employed to obtain **1.12**, 50% of the racemic allylic alcohol **1.26** could not be used towards the synthesis. Next, the synthesis utilizes a ketone reduction-alcohol reoxidation strategy to obtain chiral epoxyketone **1.28** from

1.25, which adds redundant steps to the overall synthesis. Finally, using $Yb(OTf)_3 \cdot 6H_2O$ ($12/mmol; vendor: Aldrich) as a catalyst (20 mol %) along with excess acrolein ($0.38/mL; vendor: Aldrich) is not cost effective in large-scale operations. To improve the current synthesis, it was important to utilize an enantioselective reduction of enone to yield optically active allylic alcohol **1.26**. In the following section, we briefly review pioneering research performed in this field.

1.2 ENANTIOSELECTIVE REDUCTION OF KETONE

Reduction of unsymmetrical ketones to alcohols is widely used in organic synthesis. During this reaction, the hydride nucleophile can approach the planar ketone from either face, producing a racemic mixture. Reactions that can selectively deliver the hydride to one face of the prochiral ketone are synthetically useful. This section summarizes the best practical methodologies to achieve an enantioselective reduction of an unsymmetrical ketone. Selected reagents for enantioselective reduction of ketones are summarized in Figure. 3 below.

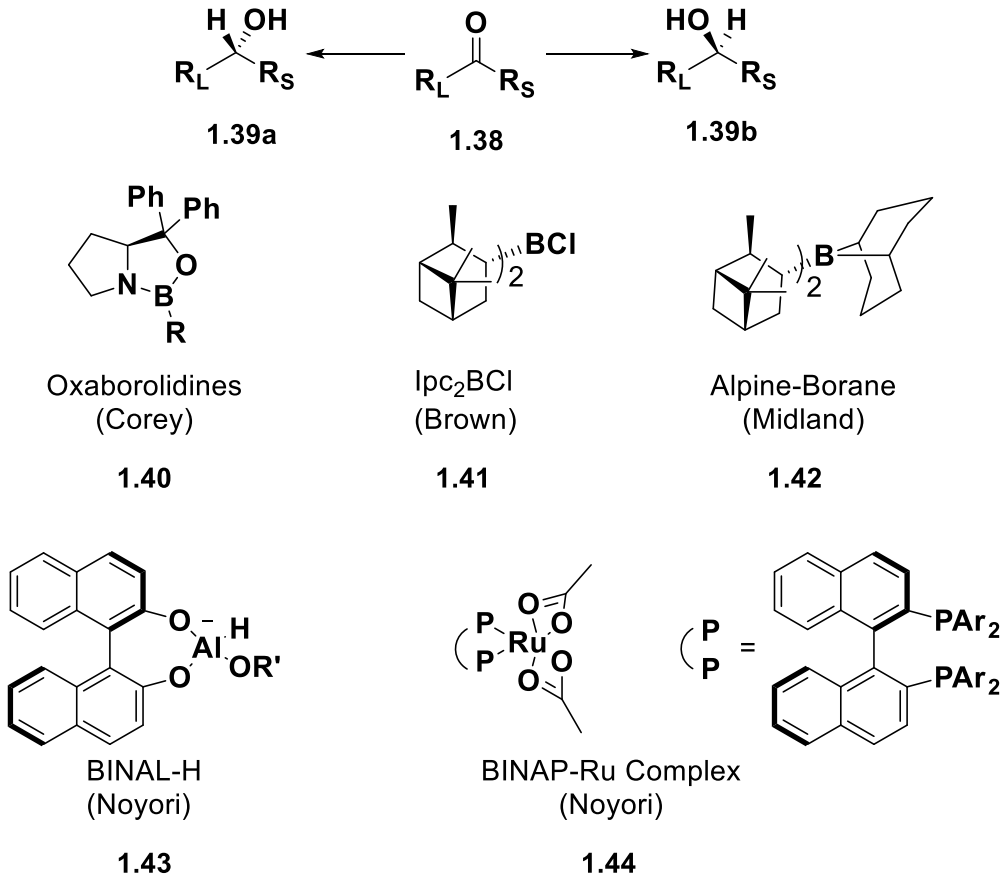

Figure 3. Enantioselective reduction of prochiral ketone and selected reagents for the transformation.

1.2.1 Corey-Bakshi-Shibata (CBS) reduction

Corey and co-workers developed[21-26] a variety of catalysts known as oxazaborolidines that show a high degree of enantioselectivity in the reduction of prochiral ketones. The oxazaborolidine catalysts behave like enzymes in the sense that they bind to both the ketone substrate and borane, thus bringing both reacting entities together. Due to the enzyme-like catalytic nature of

oxazaborolidines, they have also been called chemzymes.[27,28] Corey and his colleagues not only described the structure of the ligand and the mechanism of reduction but also characterized the catalysts by ^{1}H NMR, ^{11}B NMR, and mass spectrometry.[21,22] This method of reduction, popularly known as the Corey-Bakshi-Shibata (CBS) reduction, involves a reducing agent like borane-THF, borane-dimethyl sulfide complex, or catechol borane in conjunction with 1-10 mol% of catalyst. The yield and enantiomeric purity of the alcohol produced is excellent in most cases. Catalyst **1.40** has been successfully used to form the chiral alcohols **1.45-1.52** in high *ee*; see Figure 4 below). Less reactive ketones, like aryl alkyl ketones, with significant steric bias in substituents, have been demonstrated to undergo CBS reduction in very high enantioselectivity. The mechanism proposed[21,22] by Corey et al. is shown in Figure 4 below. In the first step, the catalyst brings ketone and the reducing agent closer to form species **1.40b**, which leads to the reduction of ketone via a six-membered transition state (which has been supported by ^{11}B NMR data). This mechanistic model explains the observed absolute stereochemistry of the reduction. The CBS reduction strategy to impart stereochemical information into a molecule has been extremely popular and has been successfully utilized in the total syntheses of numerous natural products and active pharmaceutical ingredients.[29,30]

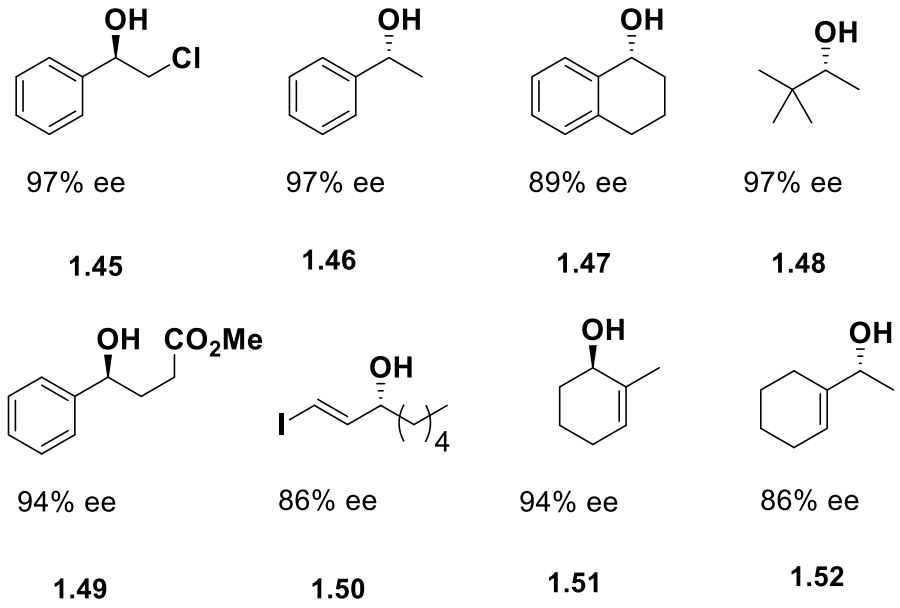

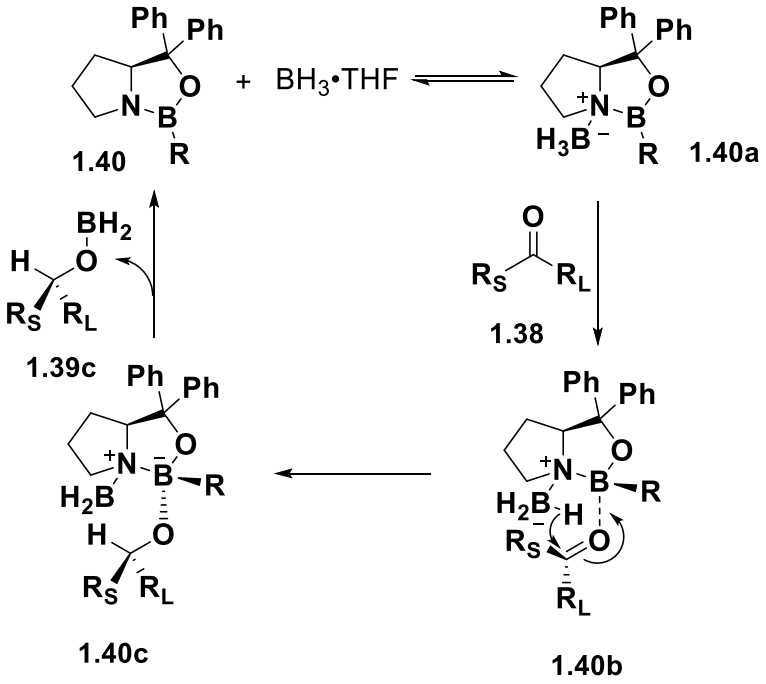

Figure 4. Representative examples of CBS reduction and its proposed mechanism.

1.2.2 Alpine-Borane and Chlorodiisopinocampheylborane (*Ipc_2BCl*)

Similar to other trialkylboranes, Alpine-Borane is inert to many functional groups but quite effective in transferring the β-hydride to one of the prochiral faces of an alkynyl ketone.[31,32] By using this reagent, alkynyl ketones have been reduced selectively in the presence of methyl ketones.[32,33] The reagent is also able to distinguish between an alkynyl and a vinyl group (see Figure 5 below). However, aliphatic ketones, enones, and aryl-alkyl ketones are less reactive and lead to poor enantioselectivity.[33] This drawback was solved by Brown et al. by increasing the Lewis acidity of the boron. In this regard, chlorodiisopinocampheylborane (Ipc_2BCl) was developed.[34] It is a very good reducing agent for the enantioselective reduction of aryl-alkyl ketones and α-tertiary aliphatic ketones (for examples see Figure 5 below). The reagent is not, however, suitable for reducing simple aliphatic ketones and olefinic ketones.[35] Both enantiomers of Alpine-borane and Ipc_2BCl can be easily synthesized from commercially available (+)- and (-)-α-pinene. Mechanistically, a six-membered boat-like transition state is involved for the reduction of unsymmetrical ketone using either reagent.[36] To minimize the steric interaction with the methyl group of the reagent, the larger substituent of the ketone lies in the equatorial position, leading to a syn-planar B-C-C-H arrangement (intermediate **1.58**).[36]

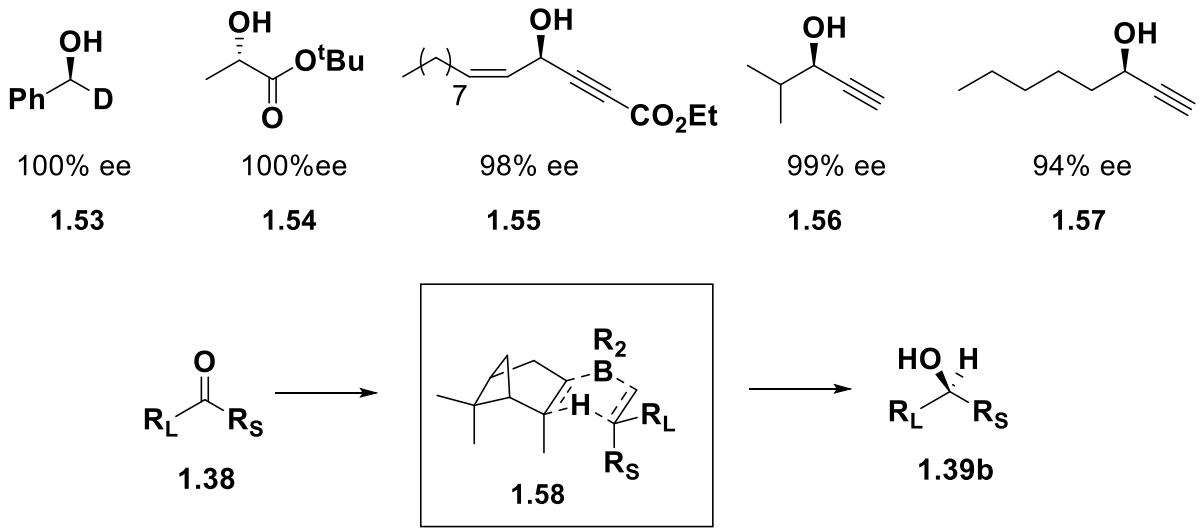

Figure 5. Representative substrate scope and the intermediate that leads to enantioselective reduction.

1.2.3 BINAL-H and Noyori reduction

Chiral reducing agent BINAL-H, derived from the modification of lithium aluminum hydride with equimolar amounts (R)- or (S)-BINOL and ethanol, exhibits exceptionally high enantioselectivity in the reduction of unsymmetrical ketones, including aromatic ketones, alkynylic ketones, olefinic ketones, and deuterium labelled aldehydes.[37,38] The reduction reaction is performed at lower temperatures (-78 ^{o}C or -100 ^{o}C) to obtain better enantioselectivity. The reagent has been successfully used in the reduction of phenacyl bromide to obtain chiral bromohydrin, which was utilized to synthesize optically active (S)-Styrene oxide in 97% ee.[38] The BINAL-H enantioselective reduction has been successfully used in building units of Prostaglandins,[38] among other total syntheses.[39-41] A six-membered transition state has been

proposed to explain the observed stereoselectivity in the reduction of ketones.[39,40] The electronic nature of the substituents differentiates the equatorial unsaturated and axial saturated groups. It is proposed that the alternative, diastereomeric transition state is not favored due to an electronic repulsion between the lone pair on axial O and the axial unsaturated substituent (R_{Un} in **1.63**, Figure 6). Apart from developing the BINAL-H reduction, Noyori introduced the application of chiral phosphine complexes of Ru in the enantioselective hydrogenation of carbonyl compounds.[42] A variety of ketones having α- or β-heteroatoms have been successfully reduced to optically active alcohols with excellent enantioselectivities. β-keto esters are particularly good substrates for Noyori reduction using catalytic Ru-BINAP complex. Noyori reduction has also been reported to affect the dynamic kinetic resolution of racemic α-substituted β-keto esters to furnish optically active alcohols in good yield and with high enantioselectivity. This method has been utilized in the total synthesis of carnitine,[43-45] among other compounds.[46,47] Despite these seminal advances in the enantioselective reduction of unsymmetrical ketones, there is still a need for new catalysts to reduce the likelihood of ketones having a similar steric bias.

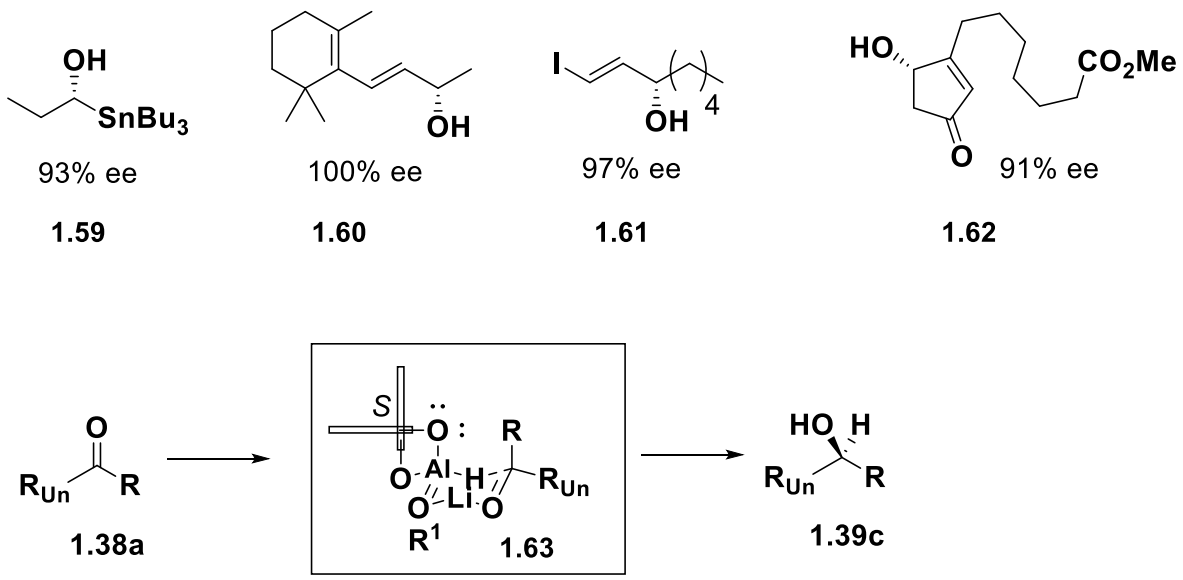

Figure 6. Examples of enantioselective reduction using BINAL-H and a mechanistic rationale.

1.3 RESULTS

With the aforementioned drawbacks in mind, we envisioned that we could bypass the Mukaiyama aldol strategy with a less expensive and scalable strategy involving a Wittig olefination route to enone **1.25** that would eliminate the use of $Yb(OTf)_3 \bullet 6H_2O$. It was also expected that the sequence up to the formation of **1.25** should require only one-column chromatographic purification, which would enable easy access to **1.25**.

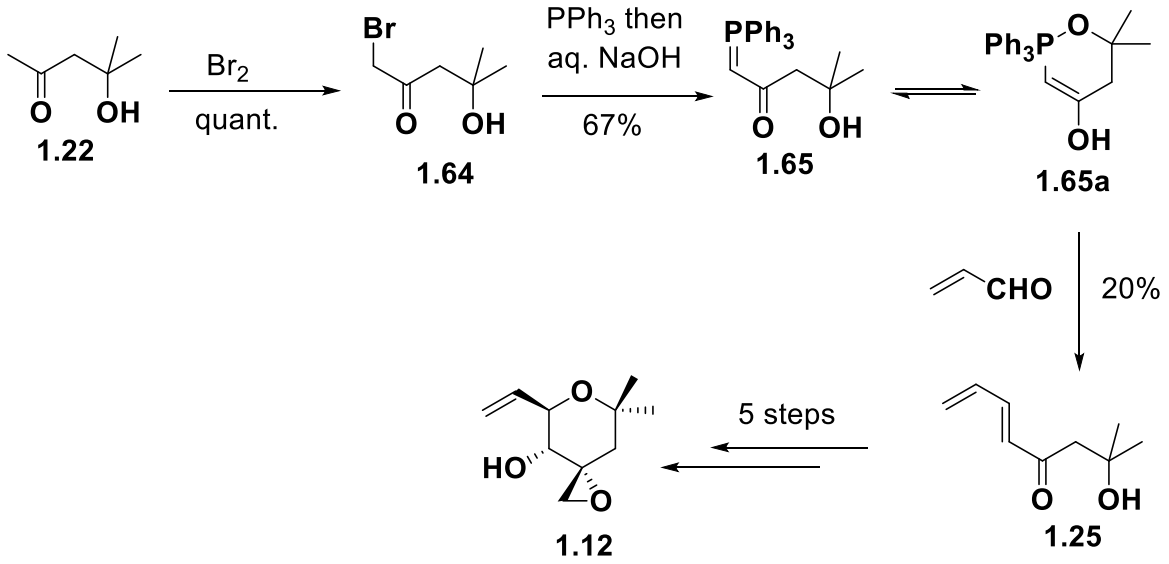

Scheme 4. Wittig reaction approach to right fragment **1.12.**

With this plan in mind, we subjected hydroxyketone **1.22** to bromination conditions in methanol to obtain **1.64** in quantitative yield. The obtained bromoketone **1.64** was refluxed with PPh_3 in benzene, and the precipitated salt was filtered and redissolved in water. The aqueous solution was treated with 2 M NaOH to prepare Wittig reagent **1.65** in 67% yield. It is worth mentioning that **1.65** can be synthesized in >10 g scale without any column chromatography and stored for multiple years without any degradation. With a reliable synthesis of Wittig reagent **1.65**, we subjected it to the Wittig olefination with acrolein under various conditions (Table 1), but unfortunately **1.25** could only be obtained with a maximum yield of 28%. The low yield was presumably due to the stabilized nature of the ylide **1.65**, as shown in structure **1.65a**.[48] Acrolein is also an α,β-unsaturated aldehyde, which rendered it less electrophilic than a typical aldehyde. Although the Wittig reaction strategy was not efficient, the ylide **1.65** could be synthesized from inexpensive reagents and required only extractions to purify. The overall cost for this route was

estimated to be $57.14/mmol of **1.25** (based on cost of reagents and substrates from vendor Aldrich).

Table 1. Conditions tried for the Wittig olefination of **1.65** and acrolein to obtain **1.25**

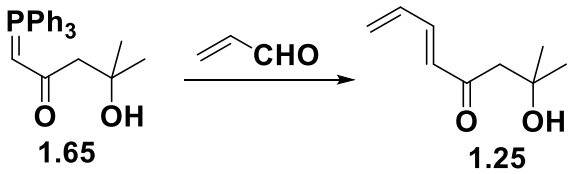

Entry	Solvent	Temp (°C)	Yield (%)
1	THF	65	16
2	CH_2Cl_2	40	28
3	DCE	65	24
4	C_6H_6	80	decomposed
5	DCE/Toluene	80	15
6	Toluene	110	decomposed

Although the unproductive Wittig olefination strategy was a setback, we focused our efforts on the Mukaiyama aldol reaction between **1.23** and acrolein in order to make it more scalable. We decided to try a lower $Yb(OTf)_3•6H_2O$ catalyst loading (20 mol% used previously) and use much less acrolein (20 equiv used previously) without sacrificing the yield of the aldol reaction. Therefore, we performed the same reaction by gradually decreasing the catalyst loading and the amount of acrolein. We found that the catalyst loading could be decreased by >200 times, and the stoichiometry of acrolein used could also be reduced to just 1.5 equivalents without any appreciable loss in yield. It was noted that warming the temperature to room temperature helped decrease reaction time, and furthermore, this did not lead to any side product formation. The optimized conditions for this reaction used only 0.08 mol% $Yb(OTf)_3•6H_2O$ and 1.5 equivalents of acrolein at 1.5 M concentration of **1.23** in Toluene/EtOH/water (4:10:1) for 3 days at 23 °C to

obtain 66% of aldol product **1.24**. The reaction was robust and scalable and enabled us to successfully synthesize 64 g (372 mmol) of **1.24** in one operation.

Table 2. Optimization of conditions for the Mukaiyama aldol reaction between **1.23** and acrolein

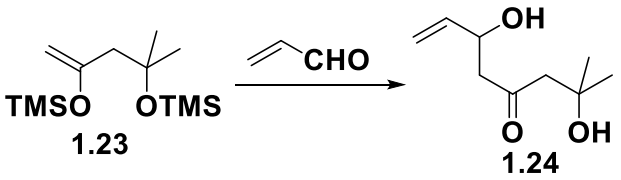

Entry	$Yb(OTf)_3 \cdot 6H_2O$ (mol%)	Acrolein (equiv)	Temp (°C)	Time (d)	Yield (%)
1	20	10	0	1	60-74
2	5.0	3.0	0	1	72
3	2.5	3.0	0	2	75
4	1.0	2.0	23	1	70
5	0.5	2.0	23	1	70
6	0.1	1.5	23	2	67
7	0.08	1.5	23	3	66

With an optimized Mukaiyama aldol procedure, we wondered if we could improve the yield of the regioselective β-elimination of **1.24** leading to **1.25** by using a more hindered Piv_2O ($0.26/mmol, Aldrich) instead of Ac_2O ($0.03/mmol, Aldrich).Thankfully, the yield improved to 83% on a 0.6 mmol scale; however, the cost efficiency for a large-scale operation was a concern (the work in this section is part of a manuscript in preparation).

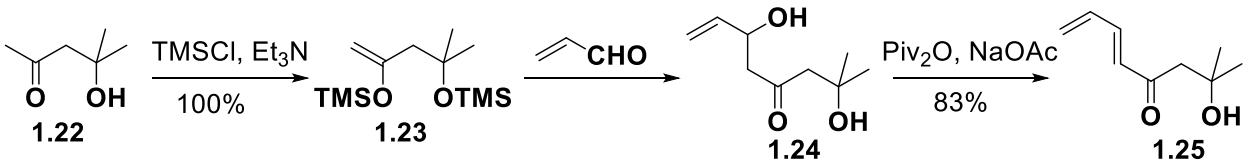

Scheme 5. Optimization of improved synthesis of right fragment **1.12.**

With a scalable route to enone **1.25**, we concentrated our efforts towards enantioselective epoxidation of enone **1.25** to epoxyketone **1.28**. In 2013, List and his colleagues reported a cinchona alkaloid-catalyzed enantioselective epoxidation of α,β-unsaturated ketones based on the formation of chiral iminium ion pair **1.69** (Scheme 6).[49] Unfortunately, the only reaction observed from **1.66** was the deprotection of a THP protecting group under these conditions. This failure may be linked to the failure to form the iminium ion in the first place, due to the presence of the hindered tertiary (protected) alcohol.

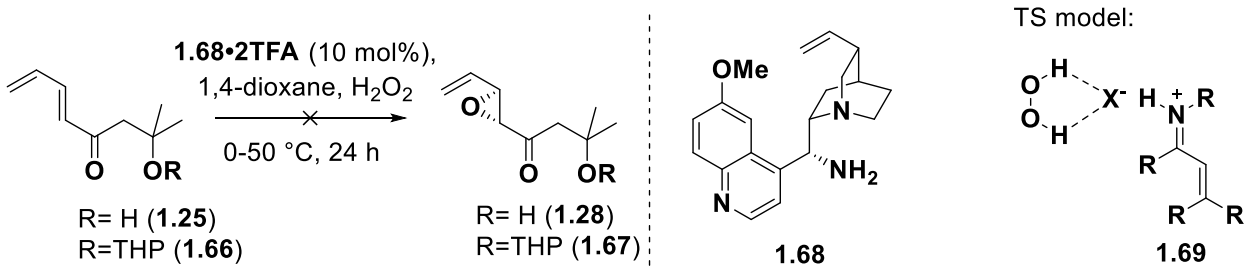

Scheme 6. List's approach to enantioselective epoxidation of α,β-unsaturated ketones.

These unsuccessful trials to asymmetric synthesis of epoxyketone **1.28** led us to divert our strategy to the enantioselective reduction of enone **1.25** to enantioenriched **1.26** so that 50% of allylic alcohol *rac*-**1.26** was not lost during the subsequent Sharpless asymmetric epoxidation/ kinetic resolution step. Despite seminal advances in the enantioselective reduction of carbonyls, our efforts to synthesize enantioenriched **1.26** resulted in unsatisfactory enantioselectivities; for example, the CBS reduction[21] produced enantioenriched **1.26** with a modest 9% *ee* (56% yield). Neither the Noyori asymmetric reduction[37] nor the Brown asymmetric reduction[34] provided the desired product (this section is also part of a manuscript in preparation).

These failures prompted us to develop a new enantioselective reduction of **1.25**. Diastereoselective reduction of chiral β–hydroxyketones have been reported by Shapiro[50] and Evans.[51] Based on these works, we hypothesized that the β–hydroxy functionality of **1.25** could be exploited to induce enantioselectivity to afford enantioenriched **1.26a**. Recent studies[52] have indicated that under mild basic conditions, boric acid can chelate 1,2-diols. Thus, we hypothesized that under similar reaction conditions, **1.25** could form a mixed borate ester **1.70** (Scheme 7) with a chiral bidentate ligand (L*), which would be reduced in a one-pot procedure to obtain the enantioenriched diol **1.26a**.

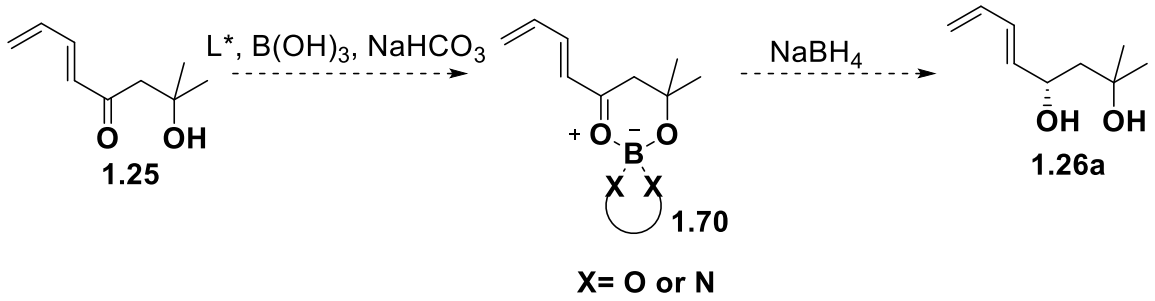

Scheme 7. Hypothesis for the enantioselective reduction of prochiral ketone.

With this hypothesis, several chiral compounds were evaluated as potential ligands L* (see Table 3 below). Although the results of **L1–L4** were discouraging (entries 1–5), the use of axially chiral ligand **L5** (entries 6–11) with $NaBH_4$ produced **1.26** in 84% yield with up to 12:88 *er* (entry 6). Additionally, when the ligand loading was sequentially decreased, comparable enantioselectivities were observed up to 10 mol% loading (entries 7–9). With less than 10 mol% of the ligand, the enantioselectivity eroded (entries 10 and 11). This may be attributed to the competing racemic reduction of ketone **1.25** with $NaBH_4$, which became more prominent at an elevated temperature. Although as much as 20 mol% of **L5** was used in the large-scale

reaction(s), the ligand could be readily recovered (~90% recovery). Encouraged by the result with the $B(OH)_3$-**L5**-$NaBH_4$ system (method A), we wished to optimize and gain insight about this system, so we tested bulky axially chiral ligands, **L6** and **L7**, which did not induce appreciable enantioselectivity. This is presumably because the added steric bulk hindered the formation of the mixed borate ester with the substrate. It should be noted that similar axially chiral reducing agents like BINAL-H,[53] which uses stoichiometric amounts of the chiral ligand, gave good enantioselectivity with ketones in the literature, but when applied to reduce ketone **1.25**, BINAL-H did not yield any product. The optimal reaction conditions were further streamlined by eliminating boric acid; simply premixing **L5** and $NaBH_4$ in MeCN for 1 hour at 23 °C (method B), followed by reduction at -78 to 4 °C over 12 hours led to **1.26a** with up to 2:98 *er*. The **1.26a** thus obtained was transformed to **1.29,** and absolute stereochemistry was determined by comparing it with specific rotation of known **1.29**. Thus, the optimal ligand was determined to be **L5** for the enantioselective reduction of ketone **1.25**.

Table 3. Screening of chiral ligands to induce enantioselectivity

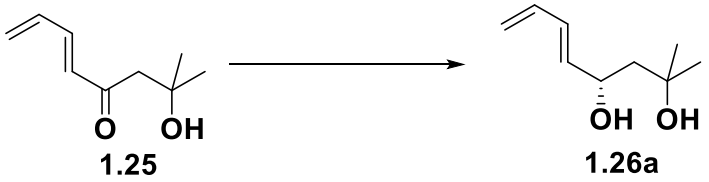

1.25 1.26a

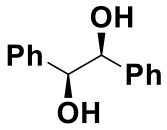

L1

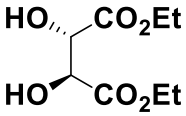

L2

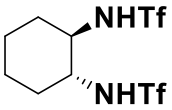

L3

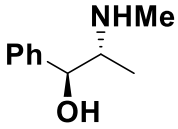

L4

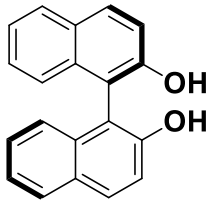

L5

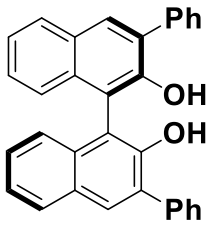

L6

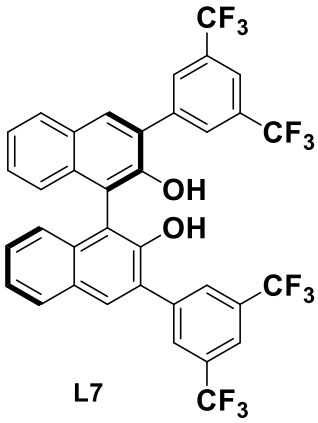

L7

Entry	Ligand (L*)	Amount (mol %)	$NaBH_4$ (mol %)	Yield (%)*	e.r.
1	–	–	100	85	50:50
2	L1	100	40	80	50:50
3	L2	100	50	76	45:55
4	L3	100	30	68	50:50
5	L4	100	30	71	50:50
6	L5	100	30	83	12:88

Table 3 (continued)

Entry	Ligand (L*)	Amount (mol %)	$NaBH_4$ (mol %)	Yield (%)*	e.r.
7	L5	50	30	84	13:87
8	L5	20	30	84	17:83
9	L5	10	30	79	20:80
10	L5	5	30	81	32:68
11	L5	2.5	30	83	40:60
12**	L5	50	50	58	2:98
13**	L5	20	50	79	7:93
14	L6	20	30	70	55:45
15	L7	20	30	73	52:48

To further understand the mechanism, we studied the premixed solution of **L5** (20 mol%) and $NaBH_4$ (30 mol%) by ^{1}H and ^{11}B NMR spectroscopy. A single boron species (δ -20 ppm, q, *J* = 92.8 Hz) was observed in the ^{11}B NMR spectrum besides $NaBH_4$, and the ^{1}H NMR spectrum indicated a loss of C2 symmetry in **L5**. This indicated that **L5** reacted with $NaBH_4$ to form **L5a** (see Scheme 8 below). This reducing agent was not basic enough to react with another hydroxy group in an intramolecular fashion as evident in its ^{11}B NMR spectrum (see experimental section). Although formation of **L5a** was confirmed by ^{11}B NMR studies, the exact mechanism of the enantioselective reduction of enone **1.25** remains shrouded. It must be noted that $NaBH_4$ is essentially insoluble in THF, especially at lower temperatures, and dissolves into solution only

after it reacts with **L5** to form **L5a,** suppressing the background reaction (this section is also part of a manuscript in preparation).

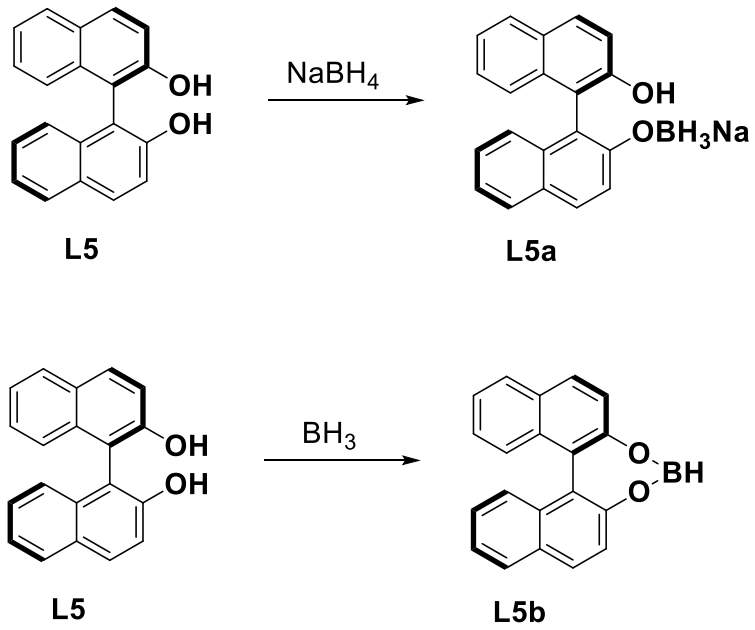

Scheme 8. Observed intermediates generated during the reaction in THF.

We then carried out the subsequent epoxidation of **1.26a** with mCPBA and found that epoxide **1.27** was obtained as a single diastereomer (dr >10:1) in 57% yield (see Scheme 9 below). The result may be explained by Sharpless's proposed model in which the O–C—C=C dihedral angle is estimated to be ~120°.[54] Based on this model, the allylic hydroxy group directs the peracid-mediated oxidation to furnish **1.27** selectively. The stereochemical outcome of this epoxidation is consistent with the transition state TS_{major}; destabilizing steric interactions in transition state TS_{minor} do not favor the formation of the alternative diastereomer **1.27a**. This improved route enabled us to bypass the low yielding Sharpless kinetic resolution strategy (this section is also part of a manuscript in preparation).

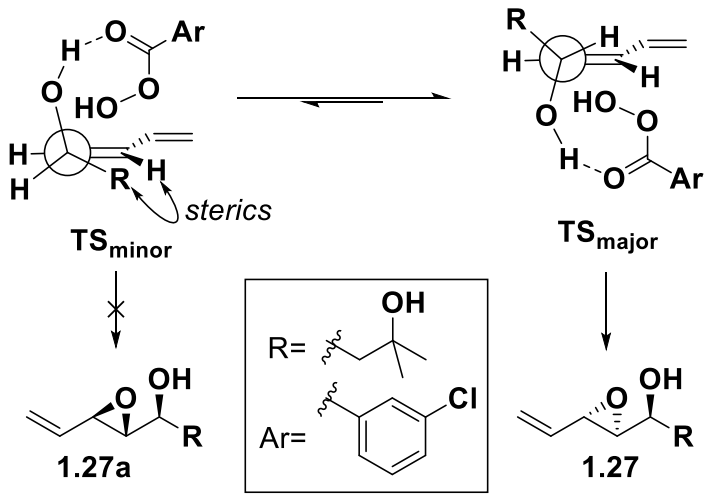

Scheme 9. Rationale for observed diastereoselectivity.

To test the generality of this enantioselective reduction, we tested the reduction of a few prochiral ketones with a premixed solution of **L5** (20 mol%) and $NaBH_4$ (30 mol%), but unfortunately, no appreciable enantioselectivity was observed. We concluded that this approach could not be generalized and, hence, was unreliable. At this point, we revisited our previous strategy to form intermediate **1.70** (see Scheme 7 above). We next planned to form intermediate **1.70** by using BH_3•THF and **L5**.

With this plan, enone **1.25** and prochiral ketones **1.71**, **1.73**, **1.75**, **1.77,** and **1.79** were subjected to a BH_3•THF/ **L5** (1:1) mixture in THF for 1 hour at 0 °C, and the resulting mixture was cooled to -78 °C and exposed to $NaBH_4$ (0.3 equiv) to obtain alcohol (see Table 4 below). Similar to a previous report[62], we observed very good enantioselectivities with stoichiometric amounts of BH_3•THF and **L5**. Although lower loading of BH_3•THF and **L5** led to disappointing results for this enantioselective transformation (entries 3–5, 7), **L5** could be recovered by column chromatography and reused. These observations lead us to hypothesize that catalyst turnover was

a major problem in this transformation. We tried to tackle the turnover problem by adding stoichiometric amounts of a sacrificial alcohol additive (such as ^{t}BuOH, ^{i}PrOH), but it did not improve enantioselectivity. To disfavor the background racemic reduction, we tested milder reducing agents like ^{i}PrOH in basic or neutral conditions as well as HCO_2H and NEt_3 mixtures to no avail. Less reactive reducing agents like sodium triacetoxyborohydride or sodium cyanoborohydride did not lead to any products either.

Table 4. Demonstration of enantioselective reduction on model substrates (absolute stereochemistry was not determined except for **1.26a**)

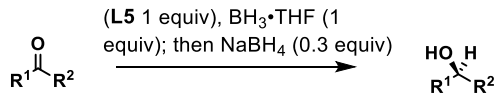

Entry	Ketone	Product[#]	Ligand (mol %)	$NaBH_4$ (mol %)	Yield (%)*	*e.r.*
1	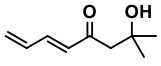 1.25	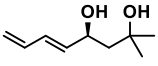 1.26a	100	40	72	2:98
2	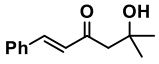 1.71	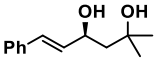 1.72	100	40	69	7:93
3	**1.71**	**1.72**	50	40	76	21:79
4	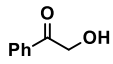 1.73	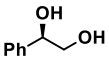 1.74	100	40	71	4:96
5	**1.73**	**1.74**	50	30	78	12:88
6	**1.73**	**1.74**	50	120	88	35:65
7	 1.75	 1.76	100	30	45	49:51
8	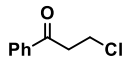 1.77	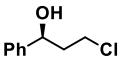 1.78	100	30	49	41:59
9	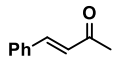 1.79	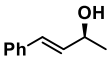 1.80	100	30	40	47:53

With this improved synthesis, we successfully synthesized >1 g of **1.29**. We were interested in studying the effect of substituting the epoxide in the right pyran ring with other electrophiles such as a ketone, so ketone **1.29** was subjected to a cross-metathesis[55] reaction with olefin **1.81** (prepared by Mr. Robert K. Bressin from the Koide group) using catalyst **1.82** to afford analogue **1.83** in 10% yield after two cycles. With this analogue synthesized, we investigated the potency of **1.83**, but unfortunately, cytotoxicity studies indicated that **1.83** was completely inactive, and a GI_{50} value could not be obtained (see Figure 7 below; generated by Ms. Dianne Pham from the Koide group). This result reinstated the importance of epoxide functionality in the FR901464 family of compounds.

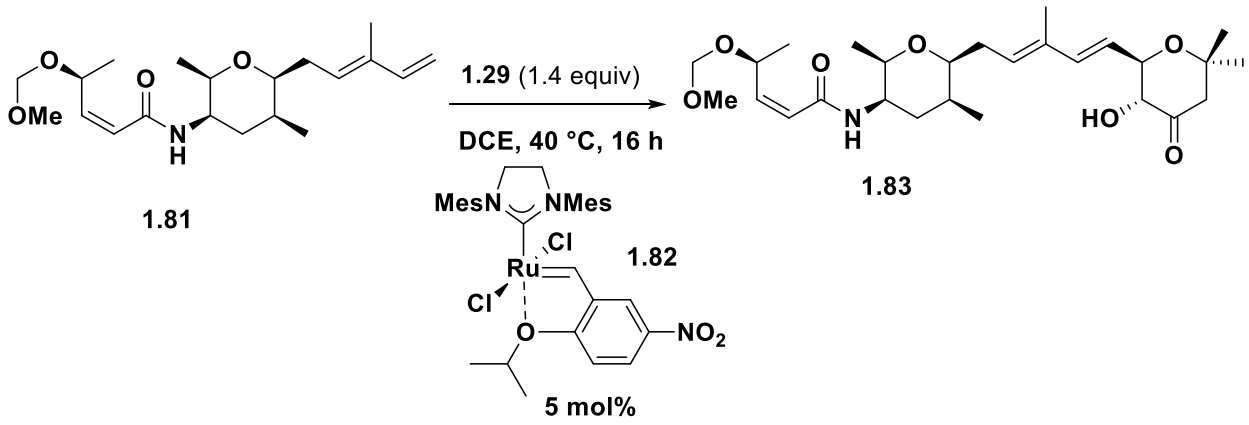

Scheme 10. Synthesis of analogue **1.83.**

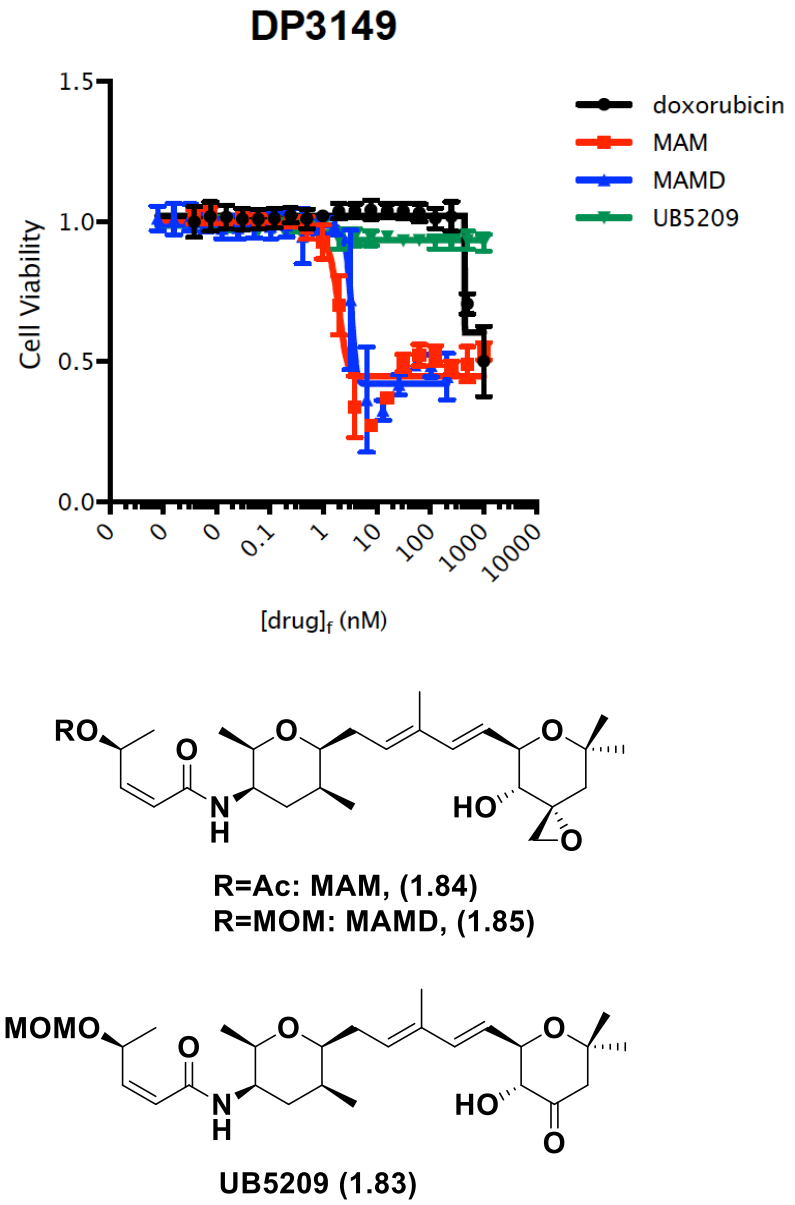

Figure 7. Cytotoxicity studies on **1.83** indicated the importance of epoxide functionality.

1.4 DISCUSSION

To further understand the mechanism of enantioselective reduction, we premixed a solution of **L5** and BH_3•THF (1:1) and studied it by ^{11}B NMR spectroscopy. A boron species **L5b** (δ 27 ppm, doublet) was observed in the ^{11}B NMR spectrum besides BH_3, indicating the formation of a $(RO)_2BH$ species **L5b**. On addition of the ketone substrate, this species was completely consumed, and a single new entity was observed by ^{11}B NMR analysis. It must be noted in THF, sodium borohydride is only sparingly soluble at lower temperatures, and this helps to minimize the background racemic reduction. This complex heterogeneous array of possible reducing agents and their interactions with the substrate makes it challenging to fully understand the mechanistic pathway. More substrate examples involving different functional groups and better enantioselectivity will enable the prediction of a mechanistic model. It is reasonable to expect that the kinetics will be nonlinear and that the enantioselectivity might be substrate specific. Similar nonlinear kinetic studies have been reported in literature.[57] For future work studying the reaction under "incremental," optically pure **L5** may be undertaken. Furthermore, the correlation of product enantiopurity is expected to shed light on the underlying mechanism.

1.5 CONCLUSION

To summarize, the new scheme for right fragment **1.12** took advantage of a new enantioselective reduction of enone **1.25** to allylic alcohol **1.26a** involving chiral ligand **L5**. Two other ketone substrates showed synthetically useful enantioselectivity. The present synthesis is more economical (current and previous schemes: $204/mmol and $753/mmol for right fragment **1.12**, respectively) and requires fewer hazardous reagents. With this improvement, meayamycin B can be synthesized in 11 steps for the longest linear sequence and in 24 steps total. The overall yield of meayamycin B was 0.82% starting from 4-hydroxy-4-methyl-2-pentanone **1.22** and 0.24% from PCl_3. Apart from that, keto-meayamycin D analogue **1.83** was synthesized in 10% yield from **1.29**. When tested for cytotoxicity, it was found to be inactive, which further emphasized the importance of epoxide functionality on the right tetrahydropyran ring.

In the future, there is potential for further improvement of the general route to meayamycins. First and foremost, the endgame cross-metathesis is very poor yielding, and hence, not scalable. Therefore, a more directed Pd-catalyzed cross-coupling reaction-based approach may be beneficial as demonstrated by Nicolaou and coworkers.[56] Second, the synthesis of more physiologically stable and "druggable" analogues may be undertaken. Finally, further studies on enantioselective reduction are required to confirm the exact mechanism. Investigating the mechanism under conditions of nonlinear kinetics, as demonstrated by Blackmond[57] and coworkers, may be helpful to elucidate the mechanism and expand the scope of the substrate.

2.0 INTRODUCTION TO INTRACELLULAR HYDROGEN PEROXIDE

Hydrogen peroxide (H_2O_2), a reactive oxygen species (ROS), is mainly generated in the cell by mitochondrial respiration and is known to play a dichotomous role in the biological system.[58] In aerobic organisms, besides H_2O_2 being known as a potent inducer of oxidative damage-related diseases and ageing and it being reported[58] as a signaling molecule, studies have demonstrated that H_2O_2 is able to protect cells from pathogens. It is also wellknown to be a by-product generated from some basic biochemical reactions catalyzed by enzymes such as glucose oxidase (GOx), alcohol oxidase (AlOx), lactate oxidase (LOx), urate oxidase (UOx), cholesterol oxidase (ChoOx), D-amino acid oxidase (DAAO), glutamate oxidase (GlOx), lysine oxidase (LyOx), oxalate oxidase (OxaOx), and the NADPH oxidase family of enzymes (NOX etc.) Therefore, the study of sensing intracellular H_2O_2 is of practical significance. Conventional techniques for H_2O_2 detection involve fluorimetry, chemiluminescence, fluorescence, electrochemistry, and spectrophotometry.[58–61]

2.1 GENERATION OF ROS IN THE CELL AND ITS IMPLICATIONS

Reactive oxygen species (ROS), including singlet oxygen, superoxide ($O_2^{\bullet-}$), H_2O_2, and hydroxyl radical ($HO^{\bullet-}$), are regarded as powerful intracellular oxidizing agents that are formed as

accidental by-products of aerobic mitochondrial respiration. During aerobic respiration, the oxidative phosphorylation pathway generates a flux of electrons through the respiratory chain that creates a proton gradient across the inner mitochondrial membrane. This generation of a potential gradient is crucial for the generation of ATP.[58–60] During these enzymatic processes and further downstream events in an electron transfer chain (ETC), electrons are added to molecular oxygen, leading to the reduction of O_2 to H_2O. It is during this event that rare electron leakage from the mitochondrial ETC leads to partial reduction of O_2, which, in turn, results in the generation of $O_2^{\bullet-}$ in the cell. It is roughly estimated that up to 0.1-0.5% of the O_2 consumed by the mitochondria leads to an accidental single electron reduction of oxygen to form superoxide ($O_2^{\bullet}$), which subsequently undergoes a dismutation reaction (catalyzed by superoxide dismutase) to form H_2O_2.[60] Hydroxyl radicals $HO^{\bullet-}$ are generated when metal ions (mainly iron and copper) decompose H_2O_2 via a Fenton reaction. Autodefense mechanisms in the cell can generally protect the cells from ROS damage through the help of specific ROS-reducing enzymes (dismutases, catalases, and peroxidases) or non-enzymatic reductants (vitamins A, C, and E and urate and bilirubin). However, unchecked higher concentrations of ROS cause damage to DNA and are known to cause ageing and diseases such as diabetes, Alzheimer's disease, Parkinson's disease, and sepsis, among others.[58-61]

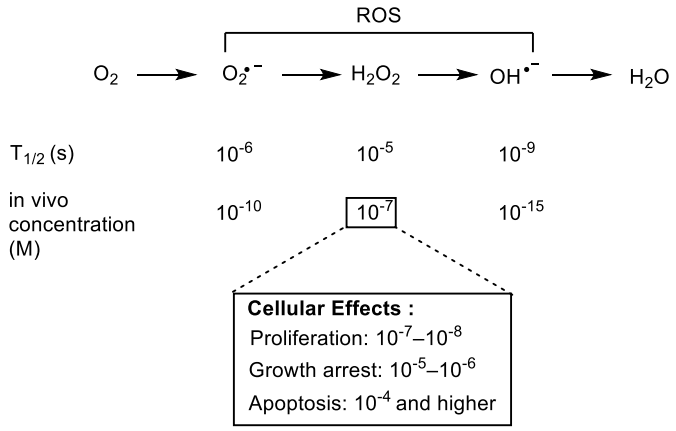

Figure 8. Generation of ROS in the cell and its implications

Different ROS have differing properties in the cell. Owing to their radical nature, ROS like $O_2^{\bullet-}$ and $HO^{\bullet-}$ are more reactive than H_2O_2. Among biologically relevant ROS, H_2O_2 has the highest stability (given by higher half-life $T_{1/2}$ in seconds)[62] and a much higher intracellular concentration (~10^{-7} M). Because H_2O_2 is membrane permeable and diffusible as well as comparatively long-lived and less reactive among all ROS, these factors make it well-suited to be a part of cellular signaling. In *Escherichia coli,* the physiological concentration of H_2O_2 is maintained at around ~0.2 µM, despite minute fluctuations during metabolic activities.[62] It is reported that a physiological concentration of > 0.7 µM H_2O_2 is harmful and leads to growth arrest, while at even higher concentrations, apoptosis is triggered.[62,63]

Aberrant levels of ROS lead to lipid and protein oxidation, as well as DNA damage. The damages incurred by the imbalance of ROS production and antioxidant activity lead to the improper functioning of the organism and accounts for ageing.[62–64] When the cell can no longer repair the damage caused by oxidative stress, cell death occurs by means of apoptosis or necrosis. However, production of ROS is necessary to protect cells from invading pathogens.

Upon ingestion of the pathogen, NOX2 enzymes are activated and produce $O_2^{\bullet-}$, which then dismutates into H_2O_2. H_2O_2, thus formed, undergoes other biochemical reactions that form more reactive species, such as hypochlorous acid, an antimicrobial agent used by the cell.[64]

2.2 REPORTED METHODS FOR HYDROGEN PEROXIDE DETECTION

Since the sequence of cellular events depends on the concentration and locations of H_2O_2, the ability to monitor the spatiotemporal information of H_2O_2 would provide valuable insights into the biology of living organisms. Fluorogenic probes can meet these requirements, and they could be used for detecting H_2O_2. Many methods have been developed for the detection of H_2O_2, including both electrochemical and spectroscopic techniques. Electrochemical methods will not be addressed further because they are not applicable to cell biology. Spectroscopic techniques utilize absorbance, luminescence, and fluorescence. These methods exploit a wide range of chemical characteristics, several of which are discussed below.

2.2.1 Traditional methods of detection for H_2O_2

Traditionally, detection of ROS had largely depended on chemiluminiscent and fluorescent methods. Chemical probes like lucigenin **2.1** and luminol **2.2** were used as chemiluminiscence-based probes, and 2',7'-dichlorodihydrofluorescein diacetate **2.3** (Scheme 11) utilized fluorescence to detect H_2O_2.[65] In a chemiluminescent reaction, the produced product is formed in an excited state that relaxes back to the ground state along with the release of a photon.

Lucigenin **2.1**, when exposed to H_2O_2, forms two molecules of *N*-methylacridone **2.5** by means of a dioxetane intermediate **2.4**. Product **2.5** is generated in the excited state, which on relaxation leads to chemiluminiscence. Although it has been used in chemical biology[66–69] to detect H_2O_2, reports [70–71] have indicated that the species detected by this reaction is superoxide $O_2^{\bullet-}$.

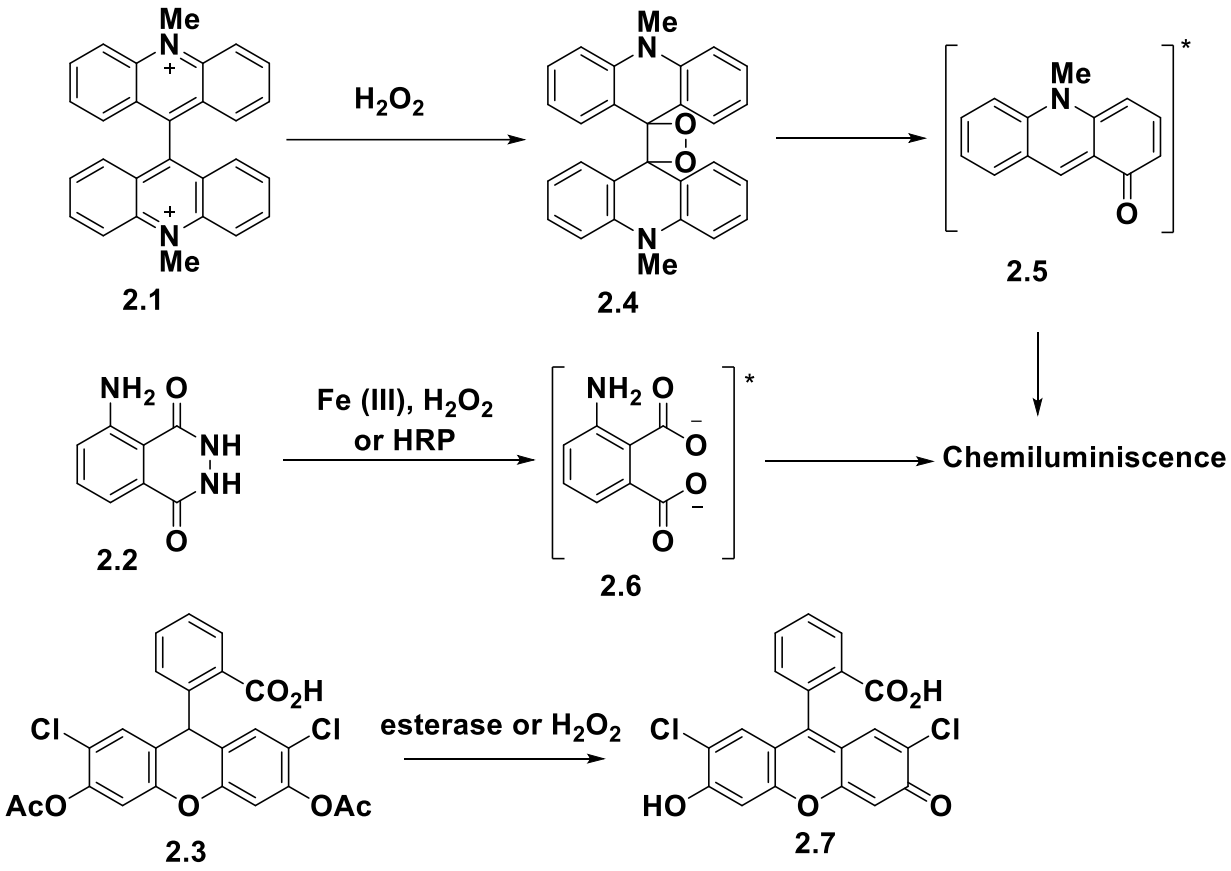

Scheme 11. Traditional methods of H_2O_2 detection.

Luminol **2.2**, another probe that is classically used for the detection of H_2O_2, is based on the oxidation of luminol **2.2** on exposure to H_2O_2 to form excited **2.6** and N_2, which on relaxation releases a photon of wavelength 430 nm.[72] The luminol reaction with H_2O_2 must be catalyzed by either metallic or enzymatic catalysts. The metal-catalyzed reaction has been accomplished using

$Fe(CN)_6^{3-}$.[72] For enzymatic catalysis, Heme-containing compounds within cells and Horseradish peroxidase (HRP) are known to catalyze the luminol reaction.[73,74]

2',7'-Dichlorodihydrofluorescein diacetate **2.3** is a popular ROS sensor that relies on a fluorescence turn-on mechanism to detect ROS.[75] Intracellular esterases cleave the ester functionalities to form 2',7'-dichlorodihydrofluorescein that is membrane impermeable, and on exposure to H_2O_2, gets oxidized to the fluorescent 2',7'-dichlorofluorescein **2.7**. However, reports have demonstrated the sluggish nature of the reaction in the presence of iron. Similar reports have questioned whether these ROS probes react with H_2O_2 at all. For example, reports have proved that luminol analogues can react with $O_2^{\bullet-}$, and Kikuchi et al. have reported that luminol **2.2** can show chemiluminescence with $ONOO^-$ that may be generated from NO and H_2O_2.[76,77] These inadequacies indicate the shortcomings of using luminol and lucigenin probes to detect ROS and hence explain the need for developing a new class of more selective ROS probes.

2.2.2 Enzymatic and genetically encoded probes to detect H_2O_2

HRP-based assays for the estimation of intracellular H_2O_2 concentration are mechanistically based on the formation of an HRP oxidized complex, which in turn oxidizes a reporter molecule.[78] This reporter molecule generally turns fluorescent to nonfluorescent or vice versa. Typically, compounds **2.8** and **2.9**, among others, are used for the detection of intracellular H_2O_2 by the HRP assay method. However, these HRP assay-based detections of intracellular H_2O_2 are not free from errors. For example, intracellular catalase and HRP competes to react with H_2O_2, leading to erroneous fluorescence readouts. Secondly, there exist other intracellular compounds

that can act as HRP substrates, which leads to incorrect interpretations of results. These inaccuracies indicate the inherent problems of using HRP-based assays for the estimation of intracellular H_2O_2.[78–80]

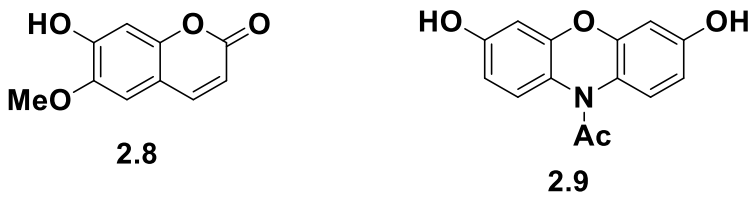

Figure 9. Probes used for intracellular H_2O_2 detection utilizing HRP-based assays.

One of the most specific intracellular H_2O_2 sensors that is widely used in literature is HyPer, which is a genetically encoded fluorogenic protein specific for H_2O_2. It is based on the transcription factor OxyR, isolated from *E. coli* and *S. typhimurium*.[81,82] Mechanistically, the functional domain of the protein OxyR-RD contains two key Cystein residues in a hydrophobic pocket that react with intracellular H_2O_2 to form a disulfide bond. Transfection of this OxyR to a modified fluorescent protein enables detection of H_2O_2. The second-order rate constant for this key oxidation reaction is estimated to be 10^5 M^{-1} s^{-1}.[81,82] Since it is not a reaction based small molecule sensor, it is not discussed any further.

2.2.3 Reaction based organic probes to detect hydrogen peroxide

Several organic probes have been developed to study the dichotomous role played by H_2O_2 in maintaining cellular homeostasis. The Chang group has developed several probes based on boronate functionality while the Nagano group based theirs on the oxidation of benzil.[83,84] It may be argued that both these approaches involve a nucleophilic hydroperoxide anion, HOO^- that

leads to an oxidation-rearrangement sequence and subsequent cleavage by water. Probes based on boronate and benzil moieties react with H_2O_2 pseudo-first-order rate constants of 8.2 x 10^{-3} s^{-1} and 3.4– 4.2 x 10^{-3} s^{-1}, respectively.[83,84] The second-order rate constant for the reaction between H_2O_2 and a boronate ester probe was reported to be 1.38±0.13 $M^{-1}s^{-1}$.[85] Although, these probes are selective for H_2O_2 and do not show interference from other ROS, it is important to note that increased pH increases the rate of reaction. This indicates that these chemistries rely on the presence of the hydroperoxide anion, HOO^-. Under biological conditions, the abundance of this species should be very low, since the pK_a of H_2O_2 is 11.6.

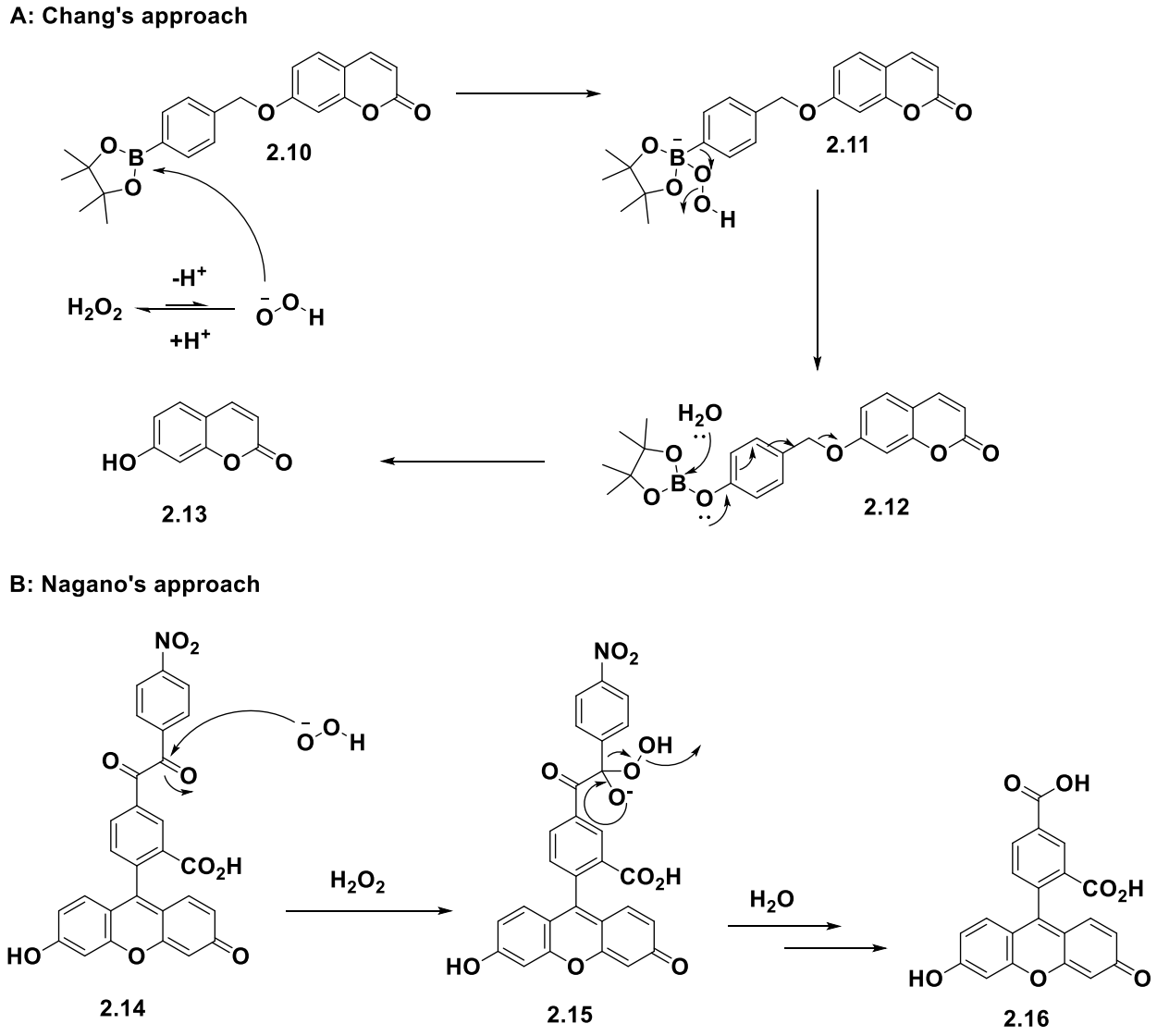

Scheme 12. Detection of hydrogen peroxide by the Nagano and Chang groups

2.2.4 Basis of probe design

The seleno-Mislow-Evans rearrangement employs electrophilic H_2O_2 to oxidize allylic alcohol, and the reaction is known to occur even at 0 °C.[86–88] It was envisioned that an allylic selenide (MESSe; Mislow-Evans H_2O_2 sensor based on selenium, **2.17**) could be oxidized by H_2O_2 to

form fluorogenic **2.21** via a seleno-Mislow-Evans rearrangement. Mechanistically, although it is well-documented that the [2,3] shift occurs very rapidly, the mechanism of the hydrolysis of the selenenate **2.19** is still shrouded. Plausible mechanisms include the oxidation of selenenate **2.19** to seleninate **2.20** followed by facile cleavage (Pathway 1) or a direct cleavage of **2.19** to yield fluorophore **2.21** (Scheme 13). Depending upon whether pathway 1 or 2 is operative, the reaction is supposed to yield **2.23** or **2.24** respectively as a by-product along with acrolein **2.22**.

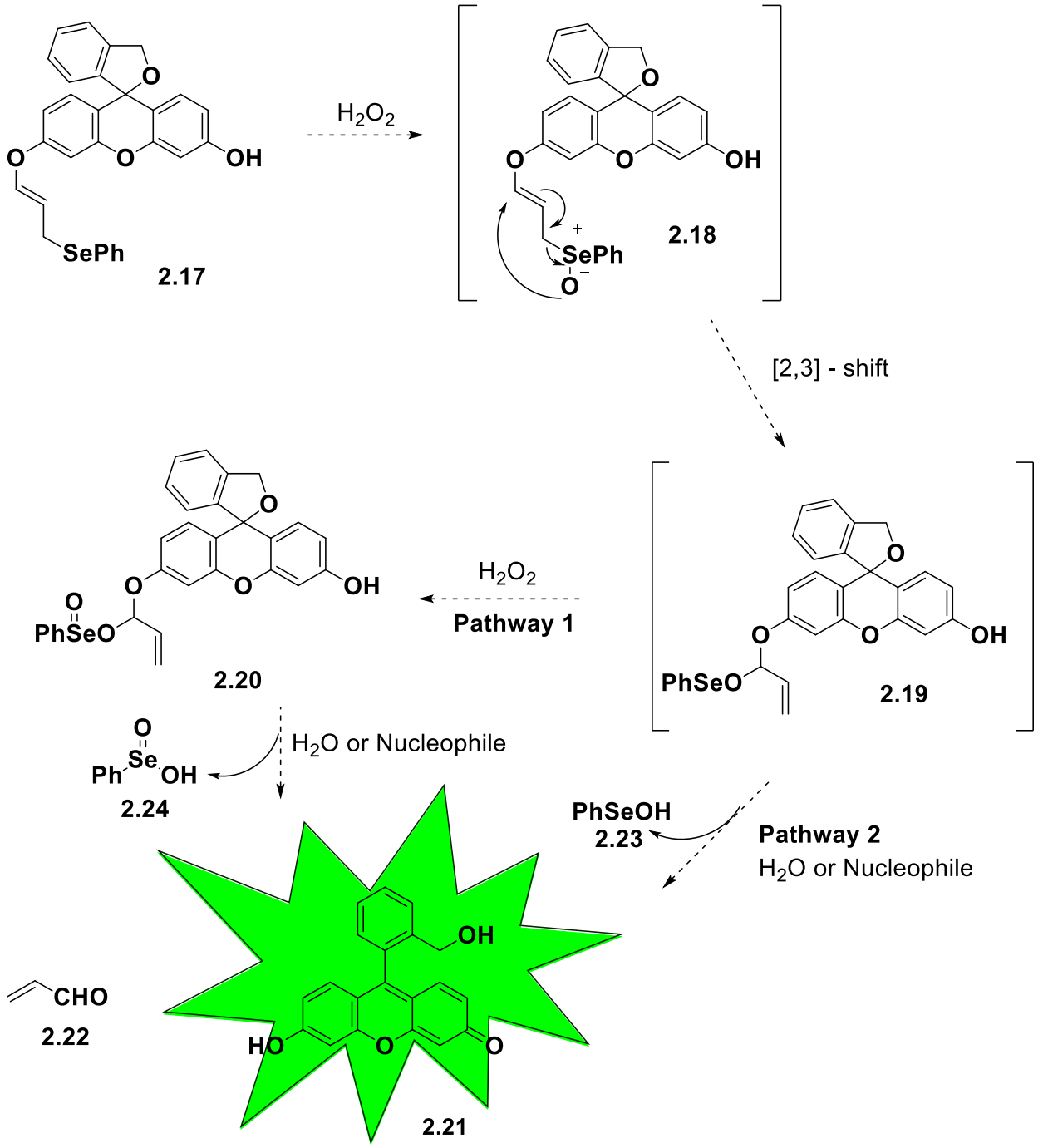

Scheme 13. Rational design of H_2O_2 probe **2.17** and mechanism of H_2O_2 detection.

2.3 RESULTS

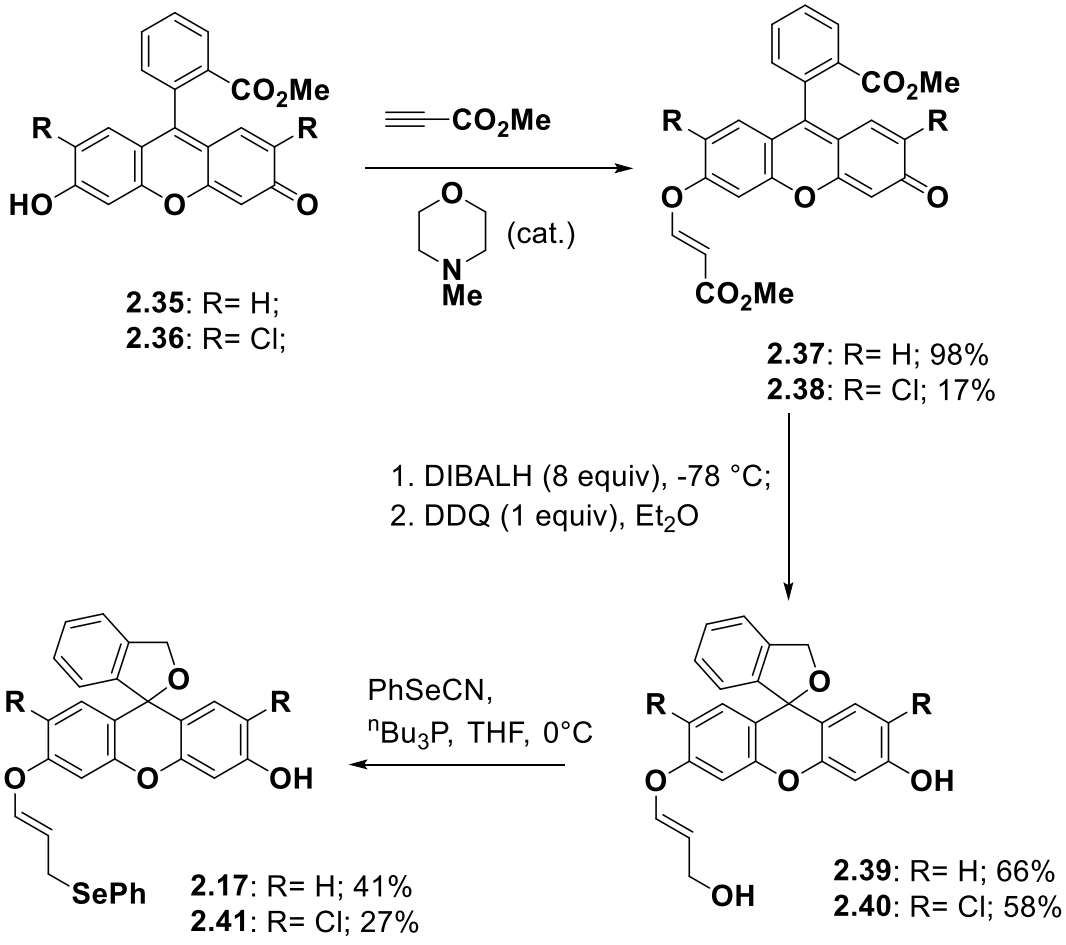

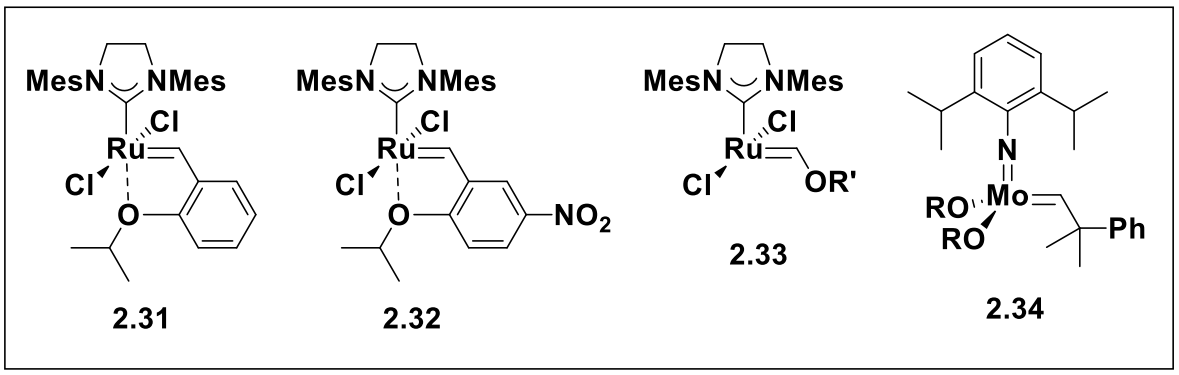

Scheme 14. Synthesis of selenide **2.17.**

2.3.1 Synthesis

Since we already had synthesized **2.28** for a different project,[90] we hypothesized whether the probe **2.17** could be synthesized by cross-metathesis of **2.28** and phenylallylselenide **2.29**. When **2.28** and **2.29** were heated with precatalyst **2.32**[91] at 40–100 °C, **2.17** was obtained in ~0-5% yield along with some organoselenium impurities. The poor yield was not unexpected, as it is well-documented[92–94] that electron-rich olefins like vinyl ethers are poor substrates for [Ru]-catalyzed cross-metathesis. Although olefin metathesis with enol ethers using Mo-catalyzed (such as catalyst **2.34**) conditions are known to be efficient,[92–93] the presence of a free hydroxy group and the air sensitivity of the catalyst rendered this approach unviable. Instead, a Ru-catalyzed approach to perform the same transformation was pursued in this study. It has been reported that although Grubbs first-generation catalyst is ineffective due to the formation of a nonreactive Ru-carbene intermediate (such as **2.33**), a Hoveyda-Grubbs catalyst can furnish a metathesis product in low to moderate yields.[92] The formation of **2.17** could be detected by LC-MS, but further characterization was not possible. With this setback, we hypothesized that we could either modify the catalyst to make it more effective under enol ether-olefin cross-metathesis conditions or change the electronic nature of the olefin, with either plan being a major diversion from the current project. To pursue the second approach (the more reasonable next step), we synthesized vinyl ether **2.30** and subjected it to cross-metathesis with **2.28**. However, this approach also failed to yield probe **2.17** in reproducible yields (typically 0-5%), again due to the formation of similar stable Ru-based Fischer carbene complexes[92-93] The formation of

product could only be confirmed by LC-MS analysis. The low yield and presence of other selenium impurities led us to revisit the synthetic route. As the cross-metathesis approach was ineffective, we pursued a more scalable route to **2.17**. The synthesis of **2.17** started with methyl propiolate undergoing conjugate addition by **2.35**[94] to afford **2.37** in 98% yield. The following DIBAL reduction led to the formation of **2.39** in low-to-moderate yields, possibly due to the hydrolysis of enol ether during the quenching of DIBAL. The final Mitsunobu reaction afforded **2.17** in 41% yield. The dichloro analogue **2.41** was similarly synthesized.

2.3.2 Mechanistic studies

In order to detect any by-products during the reaction of **2.17** and H_2O_2 that might shed light on the mechanism, we decided to study the reaction by crude ^{1}H NMR (300 MHz) analysis. **2.17** was dissolved in DMSO-d_6, and to it was added a substoichiometric amount of H_2O_2. The crude reaction mixture was analyzed against known standards (**2.17** and **2.21**) to identify any by-products. We concluded from the ^{1}H NMR analysis that both **2.21** and acrolein **2.22** were formed during the reaction, which supported our proposed mechanism.

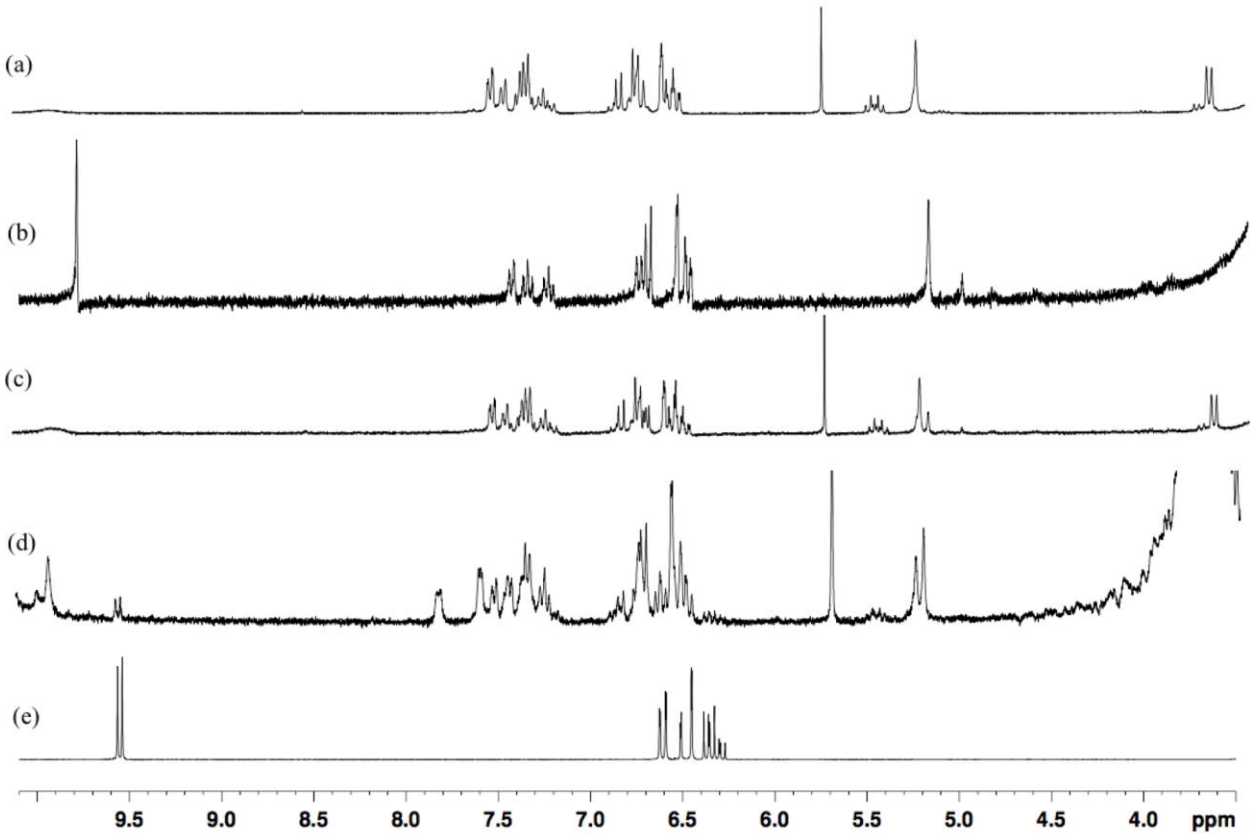

Figure 10. ^{1}H NMR (300 MHz, 293K, DMSO-d_6) of (a) allylic selenide **2.17,** (b) **2.21,** (c) mixture of **2.17** and **2.21,** (d) crude reaction mixture, and (e) acrolein **2.22.**

2.3.3 Stability studies

Organic selenides are known[95] to be prone to oxidative decomposition in the presence of $^{1}O_2$, so we planned to investigate how stable allylic selenide **2.17** was under ambient conditions. To study this stability, the ^{1}H NMR of **2.17** (in DMSO-d_6) was recorded at specified intervals (days 1, 7, 14, 21, 30, and 60), and the solution was exposed to air at room temperature throughout the entire period. It was observed that **2.17** experienced *cis-trans* isomerization of the enol ether with

a half-life of 60 days. Even then, it was quite resistant to oxidative decomposition under ambient light, air, and temperature up to 60 days (<10% acrolein formed in ^{1}H NMR). It must be noted that the mentioned isomerization and further decomposition were more pronounced in protic solvents like CD_3OD or in $CDCl_3$, which are known to contain trace amounts of acid.

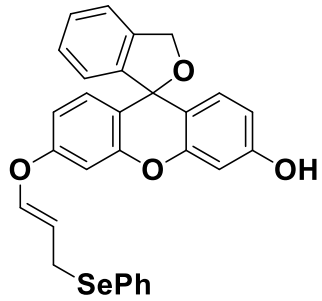

2.17

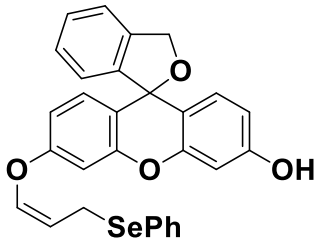

cis-**2.17a**

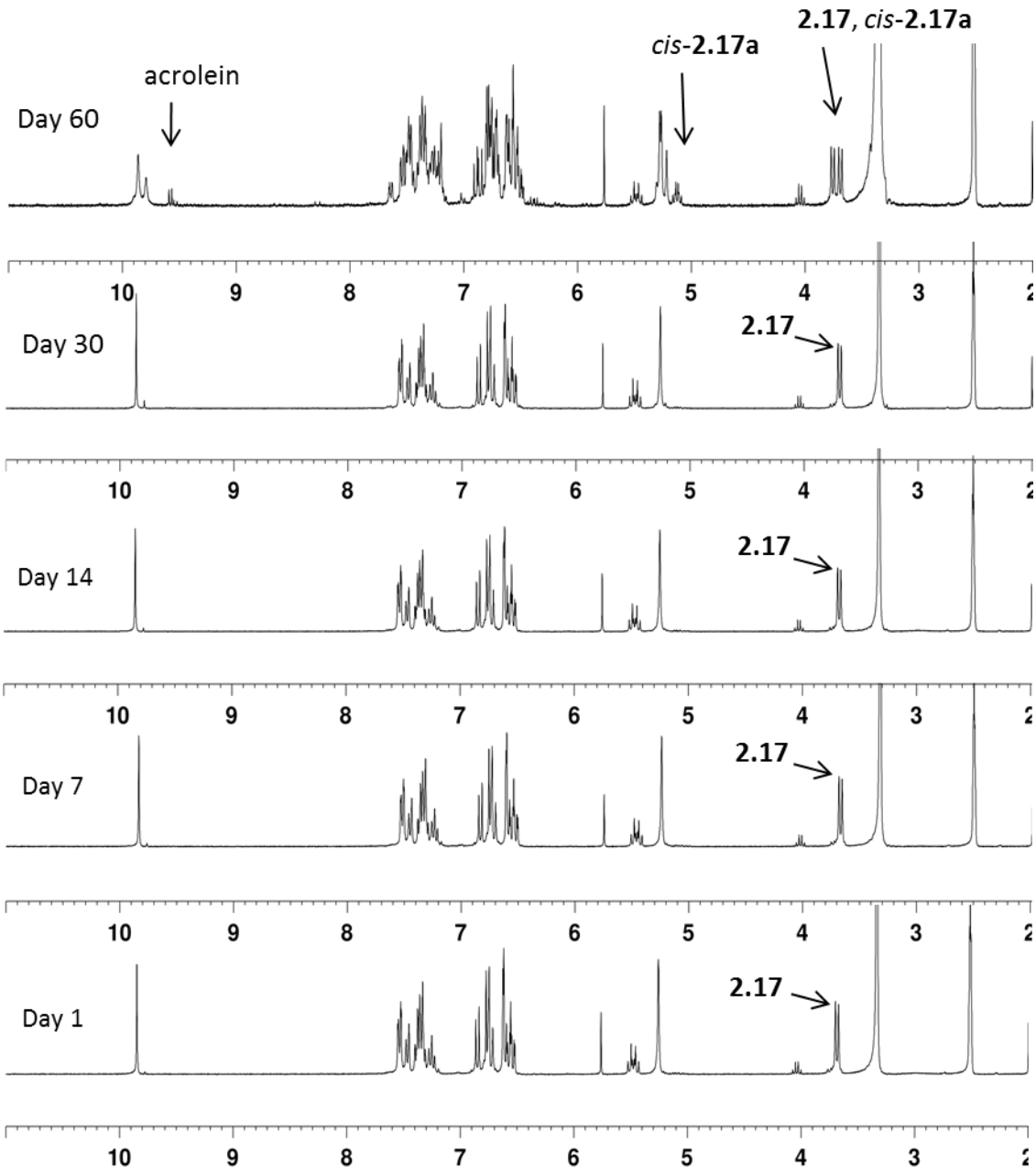

Figure 11. ^{1}H NMR spectra (300 MHz, DMSO-d_6) of **2.17** recorded on days 1, 7, 14, 21, 30, and 60.

2.3.4 Identification of by-products to investigate mechanism

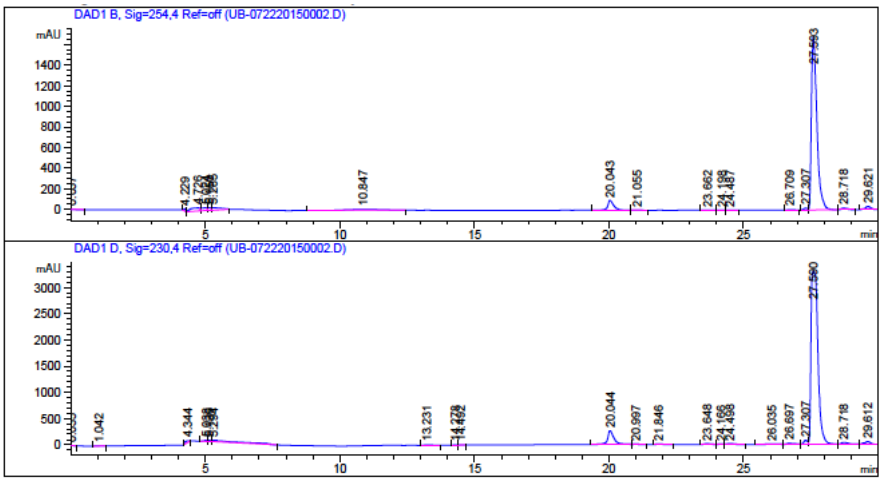

(a)

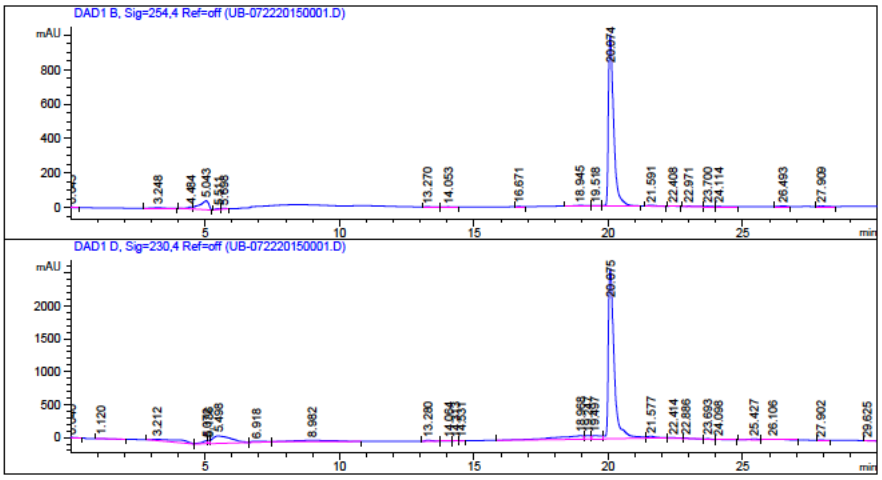

(b)

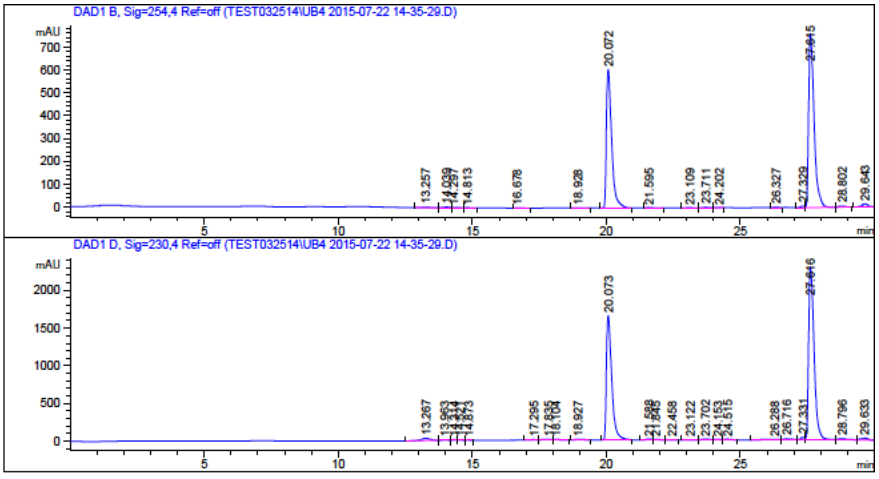

(c)

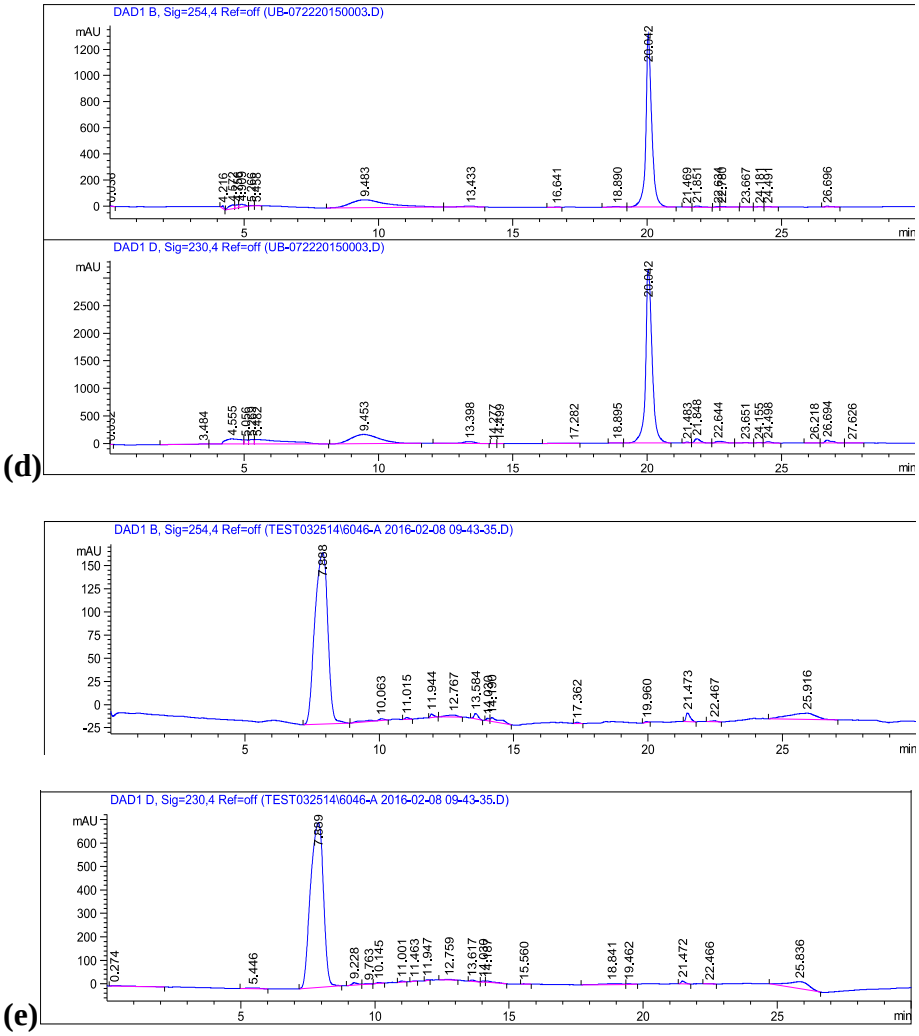

Figure 12. HPLC chromatograms of (a) authentic sample of **2.17**, (b) **2.21**, (c) **2.17**+**2.21**, (d) crude reaction mixture of **2.17** and H_2O_2 (1 equiv), and (e) authentic sample of $PhSeO_2H$ acquired at λ = 254 nm and 230 nm, respectively.

In order to study the by-products that are formed, we investigated the crude reaction mixture with known solutions of **2.17**, **2.21,** and $PhSeO_2H$. As evident from Figure 12, after

HPLC analysis, $PhSeO_2H$ was not observed as a by-product. This indicated that pathway 2 was operative under these conditions, and there was no oxidation of seleninate **2.19**.

2.3.5 Pseudo first-order kinetics and evaluation of second-order rate constant

In order to determine the second-order rate constant of the reaction of **2.17** with H_2O_2, a solution of **2.17** in 5% DMSO in an H 7.5 HEPES buffer was added to an excess of H_2O_2 in a 96 well plate, and the progressive increase in fluorescence was recorded using a plate reader. The relative fluorescence was measured every minute until the reaction was completed. As **2.17** was not fluorogenic, the fluorescence readout was the correlated amount of **2.21** formed, which was the product of the reaction. Based on these pseudo-first-order kinetics, the second-order rate constant of the reaction was calculated (details in experimental section) to be $k = 9.82 \pm 1.11\ M^{-1}s^{-1}$.

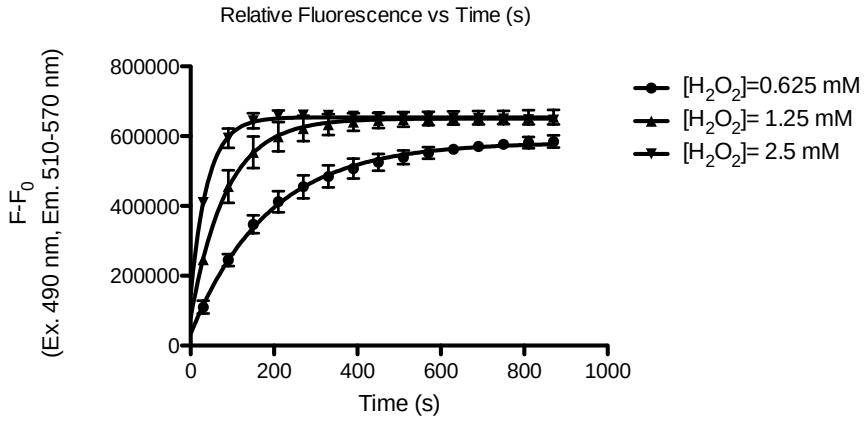

Figure 13. Plot of fluorescence vs. time for the reaction of **2.17** and H_2O_2. Final concentration: $[H_2O_2]$= 0.625 mM, 1.25 mM and 2.5 mM; [**2.17**]= 1.7 μM; 5%MeCN in pH 7.5 HEPES buffer 50 mM. All reactions were performed in triplicate in a 96 well plate.

As evident from the tabulated data (refer to experimental section), after the addition of H_2O_2, the fluorescence signal intensity increased by 25-fold. This somewhat modest increase in the fluorescent turn-on signal may be attributed to the aerial decomposition of **2.17** (in storage for a few months as a solid at 4 °C) to form **2.21**. From the standard curve, the estimated amount of **2.21** in **2.17** as an impurity was calculated to be 2.5%, leading to a higher background F_0 signal. Nevertheless, that does not affect the calculation of rate constant, as shown below.

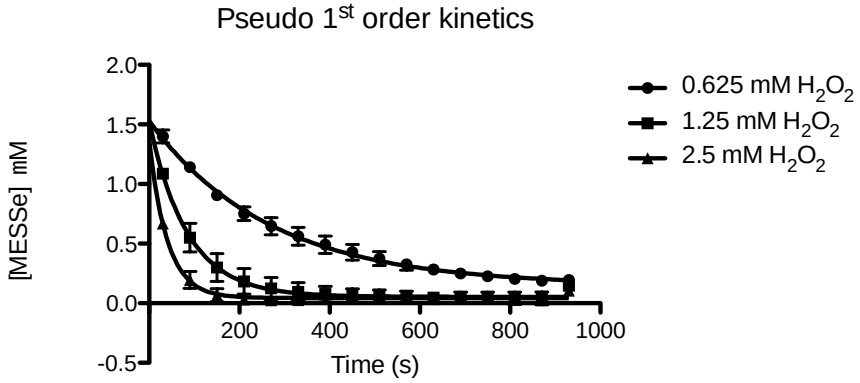

Figure 14. Plot of [**2.17**] vs. time

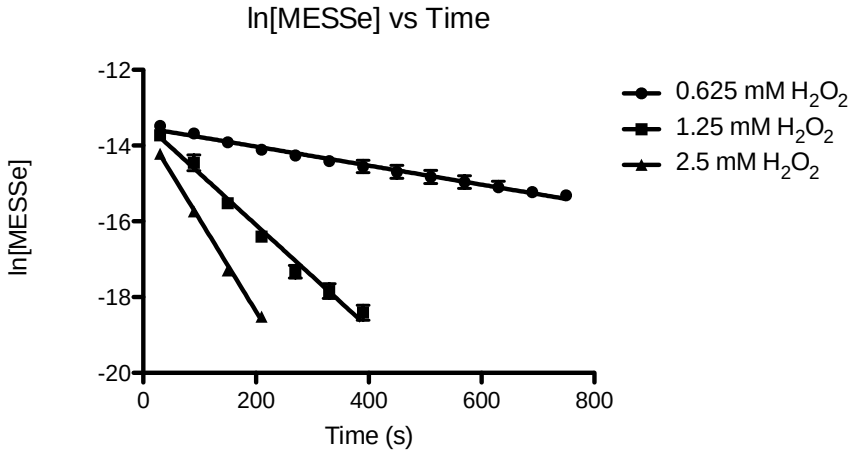

Figure 15. Plot of ln [**2.17**] vs. t to obtain slope (k').

The known concentration of **2.17**, ln [**2.17**] vs. time (s) was plotted to obtain observed rate constants k' as the slope of the linear plot (Figure 15). To determine the second-order rate constant of the reaction of **2.17** with H_2O_2, a solution of **2.17** in 5% DMSO in a pH 7.5 HEPES buffer was diluted with H_2O_2 in a 96-well plate, and the progressive increase in fluorescence was recorded using a plate reader. The relative fluorescence was measured every minute until the reaction was completed. The fluorescence readout was correlated to the amount of **2.21** formed using a standard curve for the **2.21** concentration vs. fluorescence intensity. Based on the pseudo first-order kinetic studies, the second-order rate constant *k* of the reaction was calculated (details in the experimental section) to be 9.82 ± 1.11 $M^{-1}s^{-1}$. Similarly, the pseudo-first-order kinetics of the reaction between **2.41** and H_2O_2 was studied (see experimental section). The second-order rate constant was calculated to be 9.33 ±0.64 M^{-1} s^{-1}. Finally, a solution of **2.17** in 5% DMSO in a pH 7.5 HEPES buffer was incubated with fetal bovine serum (FBS) for 1 hour. It was then subjected to LC-MS analysis to check the stability of the probe under physiological conditions. As no noticeable difference was observed before andafter treatment with serum, it was reported to be stable under physiological conditions.

2.3.6 ROS selectivity and detection of H_2O_2 in biological system

ROS, RNS selectivity studies were performed by Ms. Dianne Pham from the Koide group, and cellular imaging studies were performed in collaboration with Prof. Claudette M. St Croix (University of Pittsburgh). To verify that **2.17** could quantitatively measure H_2O_2 concentrations, **2.17** was incubated with increasing concentrations of H_2O_2. Fluorescence increased linearly with H_2O_2 concentration (Figure 16a), indicating that the probe could be used

to quantify H_2O_2. To determine whether the probe reacts with $O_2^{\bullet-}$, KO_2 was added to a solution of **2.17** buffered at pH 7 for 15 minutes and compared to the reaction with H_2O_2. Since $O_2^{\bullet-}$ is known to spontaneously dismutate to form H_2O_2, increasing amounts of catalase were added to the samples containing KO_2. Selenide **2.17** reacted readily with H_2O_2 while the observed fluorescence from the samples containing KO_2 decreased with increasing catalase concentrations (Figure 16b), indicating that **2.17** did not react with $O_2^{\bullet-}$. Selenide **2.17** was incubated with $^1O_2$ that had been formed by the reaction of Na_2MoO_4 with H_2O_2. A large fluorescence increase was observed only in the samples containing 100 µM of both Na_2MoO_4 and H_2O_2 (Figure 16c). No fluorescence increase was observed in samples containing only Na_2MoO_4, indicating that the probe was not reacting with the Na_2MoO_4. Together, these results indicate that the probe may have reacted with $^1O_2$. However, the addition of NaN_3, a known $^1O_2$ scavenger, did not decrease the fluorescence. Thus, we concluded that the fluorescence observed was not caused by the reaction of **2.17** with $^1O_2$. The addition of excess catalase to verify that **2.17** indeed responded to excess H_2O_2 that had not reacted with the Na_2MoO_4 abolished the fluorescence signal observed in the presence of high concentrations of H_2O_2 (Figure 16).

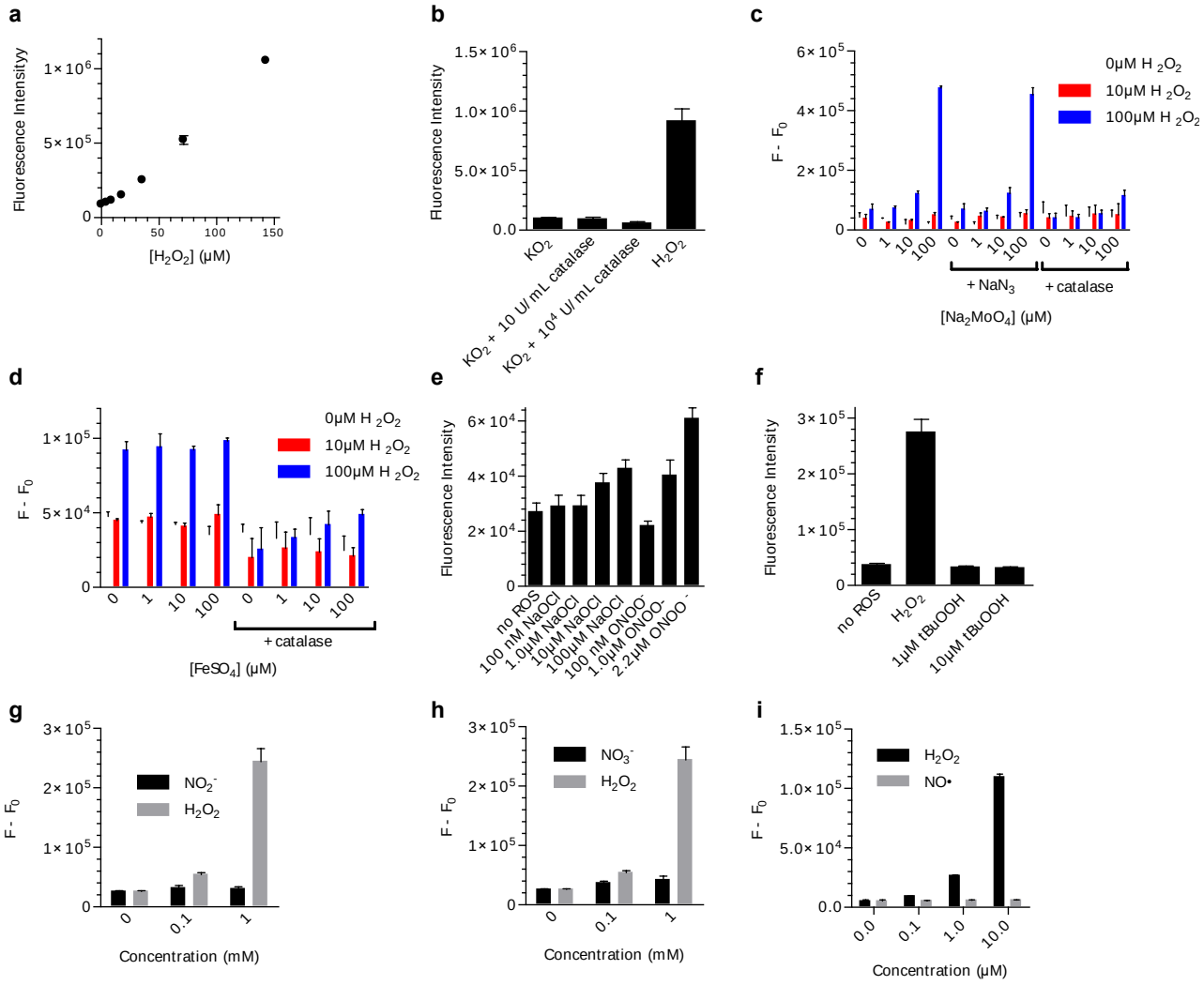

Figure 16. The fluorescence response of **2.17** (1 μM) at pH 7 (a) with increasing concentrations of H_2O_2, (b) $O_2^{\bullet-}$, (c) $^1O_2$, (d) •OH, (e) OCl^- and $ONOO^-$, (f) tBuOOH, (g) NO_2^-, (h) NO_3^-, and (i) NO•. (This is also part of a manuscript in preparation.)

The reactivity of **2.17** with •OH was also tested. •OH was generated from the reaction of Fe^{2+} with H_2O_2; a solution of **2.17** was titrated with $FeSO_4$ and H_2O_2. Fluorescence did not increase as the concentration of $FeSO_4$ increased, indicating that neither $FeSO_4$ nor the •OH

reacted with the probe. The addition of catalase to the solution reduced fluorescence intensity, indicating that the enhanced signals were caused by the reaction of the probe with the H_2O_2 required to produce •OH.

Next, it was investigated whether OCl^-, $ONOO^-$, and ^{t}BuOOH would react with **2.17**. No statistically significant increase in fluorescence intensity was observed with increasing concentrations of OCl^-. A slight increase in fluorescence intensity was observed after increasing the concentration of $ONOO^-$. Reactivity against organic peroxides like ^{t}BuOOH was also probed; no fluorescence was observed even at 100 µM ^{t}BuOOH. The minute or negligible fluorescence signals observed in these studies led us to conclude that the tested ROS do not interfere with the **2.17**-based fluorometric method for H_2O_2.

Reactivity of RNS with **2.17** to produce fluorescence was also scrutinized; **2.17** was exposed to either NO_2^-, NO_3^-, or NO• at various concentrations. The fluorescence change over the first 15 minutes was reported for NO_2^- and NO_3^- in Figures 16g and 16h, respectively. No concentration dependence was observed with either NO_2^- or NO_3^-, indicating that **2.17** did not react with these RNS. Similar results were obtained for NO• (Figure 16i). These results suggest that **2.17** did not react with NO_2^-, NO_3^- or NO•.

Attempts to image H_2O_2 within cells were also made. Cells were incubated with 0.5 µM **2.17** for 15 minutes prior to imaging. After washing with Hank's Balanced Salt Solution (HBSS) and replacing the media, H_2O_2 was added. Within 30 seconds, a significant increase in fluorescence was observed in HeLa cells (Figure 17a). Punctuates were observed in cytoplasm, suggesting that **2.17** may have localized within mitochondria. Attempts to monitor endogenous ROS production upon stimulation with 10 µM ionomycin in pH 7 (from a 10 mM stock solution)

in RAW cells resulted in a significant response relative to the baseline fluorescence within 30 seconds of the addition of 10 µM ionomycin (Figures 17b and 17c).

To confirm the mitochondrial localization of **2.17**, endothelial cells were simultaneously treated with **2.17** and MitoTracker Red for 20 minutes (Figure 17d). Time-lapse imaging showed that fluorescence continued to increase over time in response to 10 µM ionomycin. The overlap of the green and red fluorescence indicates that the probe was indeed localized to mitochondria. The diffusion of both the green and red fluorescence indicates that stimulation with ionomycin likely induced changes in mitochondrial membrane potential or permeability, causing the contents to leak out.

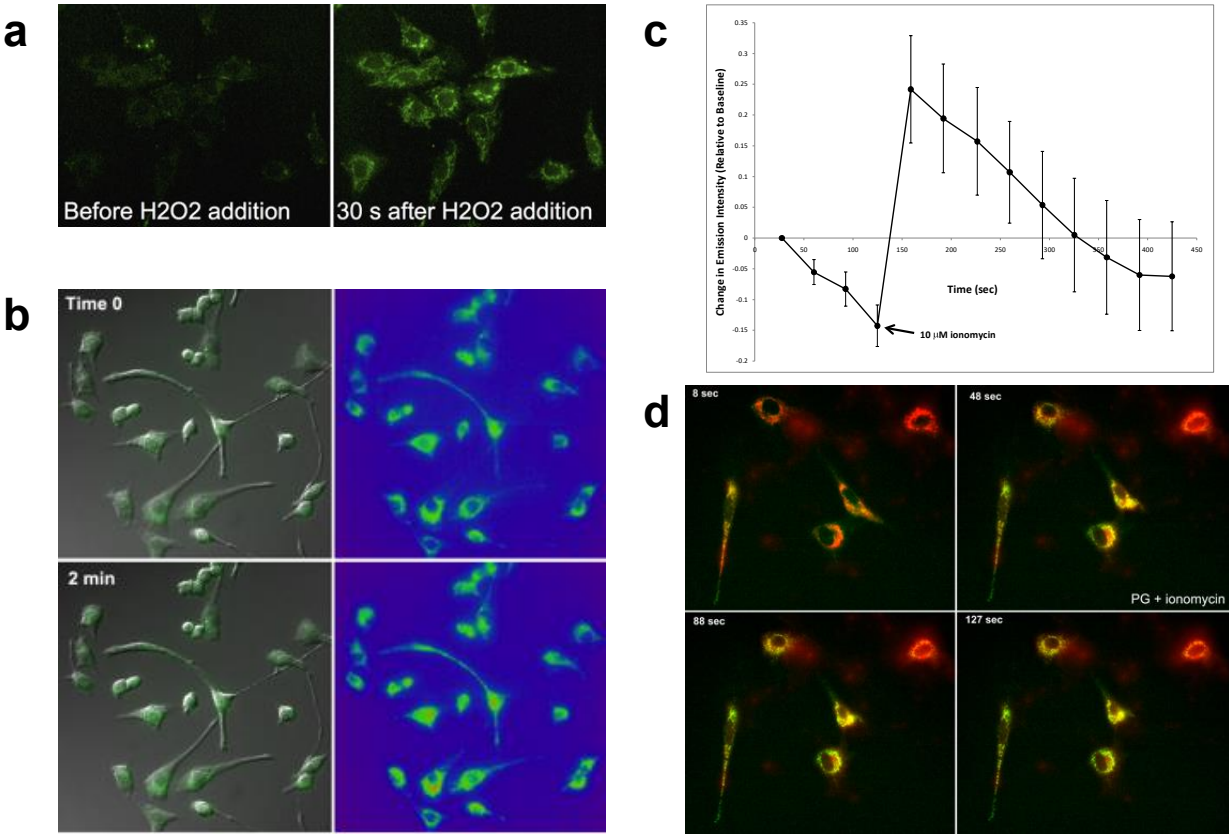

Figure 17. Cellular images using **2.17**. (a) HeLa cells treated with **2.17** showed a significant fluorescence increase after the addition of H_2O_2. (b) RAW macrophages loaded with 0.5 µM

2.17 for 15 minutes showed (c) a significant response within 30 seconds of the addition of 10 μM ionomycin. Fluorescence channel (green) and pseudo-color shown. (d) Colocalization studies with MitoTracker Red and stimulation by ionomycin revealed increased fluorescence intensity found localized to mitochondria in endothelial cells. (This is also part of a manuscript in preparation.)

2.4 DISCUSSION

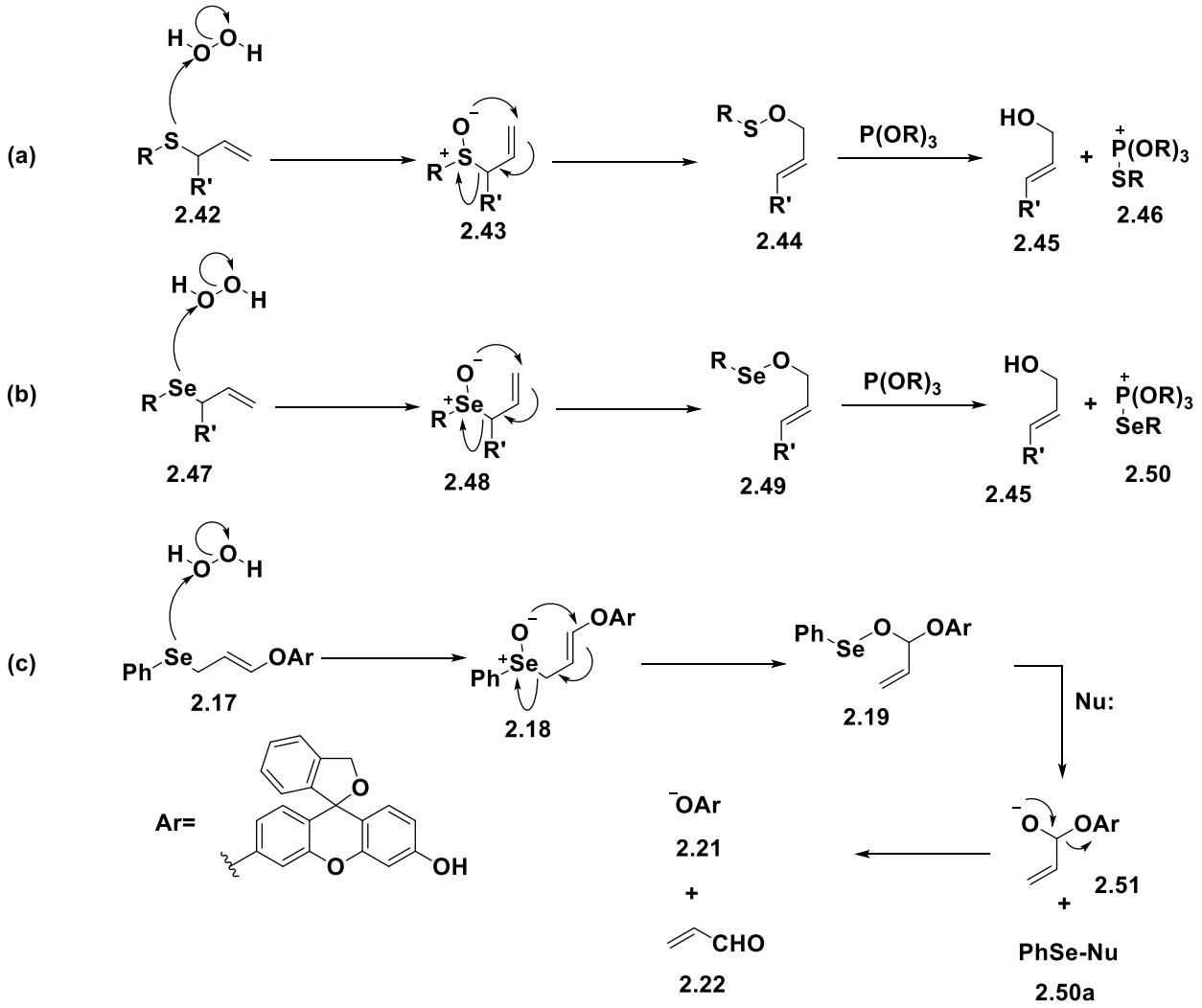

Scheme 15. Comparison of Mislow-Evans rearrangement and seleno-Mislow-Evans rearrangement.

When **2.17** is exposed to H_2O_2, after the formation of selenoxide **2.18**, a seleno-Mislow-Evans rearrangement generates a fluorescence signal. In the Mislow-Evans reaction[96] (Scheme 16), sulfide **2.42** first undergoes oxidation by H_2O_2 to form the allylic sulfoxide **2.43**. Following this,

a [2,3]-sigmatropic shift occurs to form the sulfenate ester **2.44**. A nucleophilic attack by phosphite and the resulting cleavage of the S-O bond then occur to form the corresponding allylic alcohol **2.45**. The formation of **2.44** from **2.43** was determined to be the rate-determining step.[97] The "rearrangement-cleavage" occurs with a rate constant of 2.2 – 4.2 $\times 10^4$ s^{-1}.[98] The seleno-Mislow-Evans reaction (Scheme 16) proceeds in a similar fashion to the Mislow-Evans reaction. Upon oxidation of the selenide **2.47**, the selenoxide **2.48** forms. A [2,3]-sigmatropic shift furnishes the resulting selenenate **2.49**. This attack on the selenium atom by a nucleophile such as a thiol or water results in the cleavage of the Se-O bond to form alcohol **2.45**. The initial oxidation of selenium is expected to be faster than that of sulfur as H_2O_2 is known to react preferentially with selenium in the presence of sulfur. Hence, cellular thiols should not interfere with **2.17**.[99] However, unlike the Mislow-Evans reaction, the cleavage of the Se-O bond of **2.49** to form **2.45** was the rate-limiting step (unpublished results by Dr. Sami Osman); therefore, similar rate constants for the rearrangement-cleavage in the seleno-Mislow-Evans reaction do not exist in the literature. However, since similar seleno-Mislow-Evans are performed under -30 ˚C, while the Mislow-Evans reaction must be heated to occur, it is reasonable to assume that the rate of the seleno-Mislow Evans reaction is much faster.

Mechanistically, two possible pathways exist for the reaction of **2.17** with H_2O_2. In both mechanisms (Scheme 13), oxidation of **2.17** and the following deprotonation yields the selenoxide **2.18**. A [2,3]-sigmatropic shift occurs to give selenenate **2.19**. From this point, the mechanisms diverge; in the presence of a nucleophile, **2.19** either collapses to fluorescent **2.21** or **2.19** is reoxidized to selenanate **2.20**, which yields **2.21**. However, from the HPLC studies, it was concluded that only the first mechanism was underway since $PhSeO_2H$ was not detected.

2.5 CONCLUSION

To summarize, selenide **2.17** was synthesized, and it was demonstrated that it reacts with hydrogen peroxide in a concentration-dependent manner without any interference from other ROS and RNS species. The kinetics of the reaction between **2.17** and hydrogen peroxide were studied, and it was calculated that **2.17** reacts about 7 times faster than boronate ester-based H_2O_2 probes. It was confirmed that selenenate **2.19** collapsed to form **2.21** when **2.17** was treated with hydrogen peroxide (Pathway 2) since $PhSeO_2H$ was not observed in crude reaction mixtures. It was demonstrated that a solution of **2.17** was somewhat resistant to aerial oxidation (*cis-trans* isomerization $t_{1/2}$= 60 days).

Although *in vitro* studies to detect hydrogen peroxide in cells were successful, it is possible that the somewhat hydrophobic nature of **2.17** may be a concern for *in vivo* animal studies, and, in future, more hydrophilic probes may be synthesized. The introduction of polar sulfonate groups may be helpful to improve aqueous solubility and, hence, improve *in vivo* monitoring.

APPENDIX A

EXPERIMENTAL SECTION

All reactions were carried out with freshly distilled solvents under anhydrous conditions, unless otherwise noted. All of the flasks used for carrying out reactions were dried in an oven at 80 °C prior to use. Unless specifically stated, the temperature of a water bath during the evaporation of organic solvents using a rotary evaporator was about 35±5 °C. All of the syringes in this study were dried in an oven at 80 °C and stored in a dessicator over Drierite®. Tetrahydrofuran (THF) was distilled over Na metal and benzophenone. Methylene chloride (CH_2Cl_2) was distilled over calcium hydride. Acetonitrile was distilled from CaH_2 and stored over 3Å molecular sieves. Yields refer to chromatographically and spectroscopically (^{1}H NMR) homogenous materials, unless otherwise stated. All reactions were monitored by thin-layer chromatography (TLC) carried out on 0.25-mm Merck silica gel plates (60F-254) using UV light (254 nm) for visualization or anisaldehyde in ethanol or 0.2% ninhydrin in ethanol as a developing agents and heat for visualization. Silica gel (230–400 mesh) was used for flash column chromatography. A rotary evaporator was connected to a water aspirator that produced a vacuum pressure of approximately 60 mmHg when it was connected to the evaporator. NMR spectra were recorded on a Bruker Advance spectrometer at 300 MHz, 400 MHz, 500 MHz, 600 MHz or 700 MHz.

The chemical shifts are given in parts per million (ppm) on a delta (δ) scale. The solvent peak was used as a reference value, for ^{1}H NMR: $CHCl_3$ = 7.27 ppm, CH_3OH = 3.31 ppm, DMSO = 2.50 ppm, acetone = 2.05 ppm, for ^{13}C NMR: $CDCl_3$ = 77.00 ppm, CD_3OD = 49.00 ppm, DMSO-d_6 = 49.10 ppm, and acetone-d_6 = 29.40 ppm. The following abbreviations are used to indicate the multiplicities: s = singlet; d = doublet; t = triplet; q = quartet; m = multiplet; br = broad. High-resolution mass spectra were recorded on a VG 7070 spectrometer. Low-resolution mass spectra [LCMS (ESI)] were recorded on a Shimadzu LCMS-2020. Infrared (IR) spectra were collected on a Mattson Cygnus 100 spectrometer. Samples for acquiring IR spectra were prepared as a thin film on a NaCl plate by dissolving the compound in CH_2Cl_2 and then evaporating the CH_2Cl_2.

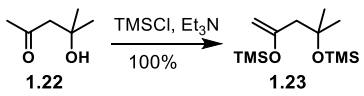

1.22 **1.23**

Preparation of enol ether **1.23**: A 2-L round-bottomed flask equipped with a Teflon-coated magnetic stir bar containing ketone **1.22** (50.2 mL, 406 mmol) was purged with argon. Et_3N (170 mL, 1.22 mol) and TMSCl (130 mL, 1.0 mol) were added to the flask at 23 °C and the mixture was stirred at the same temperature for 30 min. A solution of NaI (132 g, 448 mmol; dried overnight under high vacuum in a 140 °C sand bath) in dry MeCN (1 L; dried over 4Å molecular sieves overnight) was added to the reaction mixture over 1 h at the same temperature. The mixture was stirred for an additional 3.5 h, then diluted with ice-cold H_2O (1.5 L). The mixture was extracted with EtOAc (3 × 500 mL). The combined organic layers were dried over Na_2SO_4, filtered through a cotton plug, and concentrated *in vacuo*. The resulting crude residue of

enol ether **1.23** (106 g, quantitative yield) was used directly in the next step without further purification.

Data for enol ether **1.23**: IR (film): ν_{max} = 2961, 1620, 1321, 1251, 1042 cm^{-1}; ^{1}H NMR (300 MHz, $CDCl_3$, 293 K): δ 4.07 (*br* s, 1H; C*H*$_2$=), 4.08 (br s, 1H; C*H*$_2$=), 2.21 (s, 2H; -C*H*$_2$-), 1.28 (s, 6H; *Me*$_2$C(OTMS)), 0.23 (s, 9H; TMS), 0.12 (s, 9H; TMS); ^{13}C NMR (100 MHz, $CDCl_3$, 293 K): δ 157.0, 92.7, 73.8, 51.8, 29.9, 2.7, 0.04; HRMS of **1.23** was not obtainable.

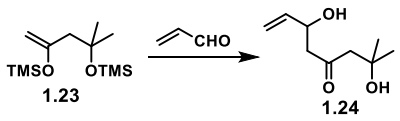

1.23 **1.24**

Preparation of hydroxy ketone **1.24**: To a 250-mL round-bottomed flask equipped with a Teflon-coated magnetic stir bar containing **1.23** (13.030 g, 50.00 mmol), was added toluene (13.4 mL) and acrolein (5.0 mL, 75 mmol). The flask was cooled on an ice-water bath (0 °C external temperature), then a solution of $Yb(OTf)_3$•$6H_2O$ (25.0 mg, 40.3 μmol) in H_2O/EtOH (1:10 v/v, 36.6 mL) was added. The mixture was stirred at room temperature for 3 d and then concentrated *in vacuo*. The crude residue was purified by flash chromatography (10→60% EtOAc in hexanes) on silica gel (1.5 L) to afford hydroxy ketone **1.24** as colorless oil (6.031 g, 70% yield).

Data for hydroxy ketone **1.24**: R_f = 0.18 (40% EtOAc in hexanes); IR (film): ν_{max} = 3410 (br O-H), 2974, 2932, 1701 (C=O), 1378, 1144 cm^{-1}; ^{1}H NMR (300 MHz, 1% CD_3OD in $CDCl_3$, 293 K): δ 5.87 (ddd, *J* = 16.8, 10.4, 5.6 Hz, 1H; CH_2=C*H*), 5.31 (ddd, *J* = 16.8, 1.2, 1.2 Hz, 1H; C*H*$_2$=CH), 5.16 (ddd, *J* = 10.4, 1.2, 1.2 Hz, 1H; C*H*$_2$=CH), 4.61 (ddddd, *J* = 8.8, 6.0, 6.0, 1.2, 1.2 Hz, 1H; C*H*(OH)), 2.73–2.63 (m, 4H; C*H*$_2$C(O)C*H*$_2$), 1.25 (s, 6H; C*Me*$_2$); ^{13}C NMR (100 MHz,

$CDCl_3$, 293 K): δ 212.5, 138.8, 115.3, 69.8, 68.6, 54.2, 50.5, 29.4; HRMS (ESI+) calcd. for $C_9H_{17}O_3$ $[M + H]^+$ 173.1178, found 173.1184.

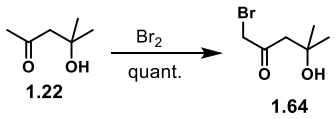

Preparation of bromo ketone **1.64**: To a 250-mL round-bottomed flask equipped with a Teflon-coated magnetic stir bar was added ketone **1.22** (10.01 g, 86.10 mmol) in MeOH (60.0 mL), and the stirred solution was cooled to 0 °C. To the mixture was added Br_2 (4.40 mL, 86.10 mmol) dropwise using a syringe, and the resultant mixture was slowly warmed to 23 °C over 3 h. The mixture was poured into H_2O (200 mL) and extracted with CH_2Cl_2 (50 mL × 4). The combined organic layers were dried over Na_2SO_4, filtered through a cotton plug, and concentrated *in vacuo* to afford bromo ketone **1.64** as yellow oil (16.601 g, 99% yield).

Data for bromo ketone **1.64**: R_f = 0.57 (60% EtOAc in hexanes); IR (film): ν_{max} = 3433 (br O-H), 2975, 2249, 1715 (C=O), 1465, 1382, 1173, 1057, 978, 911, 733 cm^{-1}; ^1H NMR (300 MHz, 1% CD_3OD in $CDCl_3$, 293 K): δ 3.89 (s, 2H; CH_2Br), 2.72 (s, 2H; C(O)CH_2), 1.18 (s, 6H; CMe_2); ^{13}C NMR (125 MHz, $CDCl_3$, 293 K): δ 202.8, 70.0, 51.0, 35.6, 29.4; HRMS (EI+) calcd. for $C_6H_{12}BrO$ $[M\text{-}OH+H]^+$ 179.0066, found 178.9959.

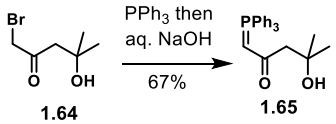

Preparation of ylide **1.65**: To a 250-mL round-bottomed flask equipped with a Teflon-coated magnetic stir bar was added **1.64** (10.02 g, 51.31 mmol), benzene (80.0 mL), PPh_3 (14.22

g, 53.86 mmol) and the solution was stirred at 23 °C for 7 h. The mixture was poured into H_2O (1 L) and extracted with CH_2Cl_2 (100 mL × 3). The aqueous layer was treated with 4 M NaOH (15.0 mL, 60.0 mmol) and extracted with CH_2Cl_2 (100 mL × 4). The combined organic layers were dried over Na_2SO_4, filtered through a cotton plug, and concentrated *in vacuo* to afford crude ylide **1.65**. This ylide was washed with hexanes (100 mL × 3) until TLC analysis showed absence of PPh_3 to obtain ylide **1.65** as a yellowish white solid (12.302 g, 67% yield).

Data for ylide **1.65**: R_f = 0.24 (40% EtOAc in hexanes); IR (film): ν_{max} = 3266 (br O-H), 3057, 2967, 1675 (C=O), 1528, 1437, 1404, 1282, 1106, 998 cm^{-1}; ^1H NMR (300 MHz, 1% CD_3OD in $CDCl_3$, 293 K): δ 7.65–7.43 (m, 15H; P*Ph*$_3$), 3.80–3.71 (d, *J* = 26.1 Hz, 1H; C*H*=PPh_3), 2.43 (s, 2H; C(O)C*H*$_2$), 1.24 (s, 6H; C*Me*$_2$); ^{13}C NMR (125 MHz, $CDCl_3$, 293 K): δ 192.9, 133.1 (d, *J* = 10.0 Hz), 132.2 (d, *J* = 2.5 Hz), 129.0 (d, *J* = 11.3 Hz), 126.3 (d, *J* = 90.0 Hz), 70.1, 55.7 (d, *J* = 103.8 Hz), 50.3 (d, 13.8), 29.7; HRMS (EI+) calcd. for $C_{24}H_{26}O_2P$ $[M+H]^+$ 377.1665, found 377.1675. m.p.: 184.5–185.2 °C.

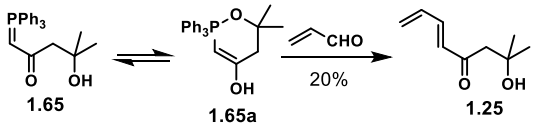

Preparation of enone **1.25** (Method A): To a 250-mL round-bottomed flask equipped with a Teflon-coated magnetic stir bar and a reflux condenser was added ylide **1.65** (12.320 g, 32.75 mmol), CH_2Cl_2 (105 mL) at 23 °C, to which acrolein (4.3 mL, 64 mmol) was added dropwise. The mixture was refluxed at 40 °C for 24 h, and then concentrated *in vacuo*. The resulting crude residue was purified by flash chromatography (10→50% EtOAc in hexanes) on silica gel (200 mL) to afford enone **1.25** as pale yellow oil (1.41 g, 28% yield).

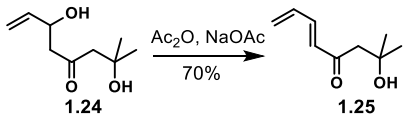

Preparation of enone **1.25** (Method B): To a 1-L round-bottomed flask equipped with a Teflon-coated magnetic stir bar was added **1.24** (24.292 g, 141.07 mmol), DCE (40 mL), Ac_2O (13.35 mL, 141.1 mmol) and NaOAc (3.472 g, 42.33 mmol). The mixture was stirred in a 60 °C oil bath for 24 h. The mixture was cooled to 23 °C, then diluted with EtOAc (250 mL) and saturated aqueous sodium bicarbonate (200 mL). The organic layer was separated, dried over Na_2SO_4, filtered through a cotton plug, and concentrated *in vacuo*. The crude residue was purified by flash chromatography (10→50% EtOAc in hexanes) on silica gel (1 L) to afford enone **1.25** as pale yellow oil (15.238 g, 70% yield).

Preparation of enone **1.25** (Method C): To a 25-mL round-bottomed flask equipped with a Teflon-coated magnetic stir bar was added **1.24** (110 mg, 0.60 mmol), DCE (1.0 mL), Piv_2O (0.14 mL, 0.70 mmol) and NaOAc (25.1 mg, 0.30 mmol). The mixture was stirred in a 60 °C oil bath for 24 h. The mixture was cooled to 23 °C, then diluted with CH_2Cl_2 (5.0 mL) and saturated aqueous sodium bicarbonate (5.0 mL). The organic layer was separated, dried over Na_2SO_4, filtered, and concentrated *in vacuo*. The crude residue was purified by flash chromatography (10→50% EtOAc in hexanes) on silica gel (10 mL) to afford enone **1.25** as pale yellow oil (77.1 mg, 83% yield).

Data for enone **1.25**: R_f = 0.33 (40% EtOAc in hexanes); IR (film): ν_{max} = 3437 (br O-H), 2973, 1678 (C=O), 1204, 1110 cm^{-1}; ^1H NMR (300 MHz, 1% CD_3OD in $CDCl_3$, 293 K): δ 7.16 (dd, *J* = 15.6 Hz, 10.8 Hz, 1H; C*H*=CH- C(O)), 6.48 (ddd, *J* = 16.8, 10.8, 10.8 Hz, 1H; CH_2=C*H*-CH=CH-C(O)), 6.18 (d, *J* = 15.6 Hz, 1H; CH=C*H*-C(O)), 5.72 (dd, *J* = 16.8, 0.3 Hz,

1H, C*H*$_2$=CH), 5.60 (dd, *J* = 10.8, 0.3 Hz, 1H; C*H*$_2$=CH), 2.77 (s, 2H; C(O)C*H*$_2$), 1.29 (s, 6H; C*Me*$_2$); ^{13}C NMR (75 MHz, $CDCl_3$, 293 K): δ 202.0, 143.6, 135.0, 131.0, 127.4, 69.9, 50.5, 29.4; HRMS (EI+) calcd. for $C_9H_{14}O_2$ $[M\text{-}CH_3]^+$ 139.0759, found 139.0756.

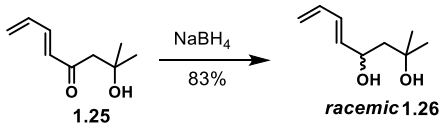

Preparation of allylic alcohol **1.26**: A 250-mL round-bottomed flask equipped with a Teflon-coated magnetic stir bar was added **1.25** (2.40 g, 15.4 mmol) and MeOH (60 mL). The mixture was cooled to 0 °C and $NaBH_4$ (1.16 g, 30.8 mmol) was added over 15 min. The mixture was stirred at the same temperature for 30 min, then diluted with saturated aqueous NH_4Cl (50 mL). MeOH was removed *in vacuo*, then the resulting mixture was extracted with Et_2O (3 × 40 mL). The organic layer was washed with aqueous NH_3 (5 mL x 2), brine (10 mL), dried over Na_2SO_4, filtered through a cotton plug, and concentrated *in vacuo*. Allylic alcohol **1.26** was used directly in the next step (2.30 g, 95% yield).

Data for allylic alcohol **1.26**: R_f = 0.30 (40% EtOAc in hexanes); IR (film): ν_{max} = 3369, 3088, 3040, 2973, 2935, 1654, 1605, 1467, 1380, 1326, 1253, 1153, 1058, 1004, 952, 908, 857, 768 cm^{-1}; ^{1}H NMR (300 MHz, 1% CD_3OD in $CDCl_3$, 293 K): δ 6.25 (ddd, *J* = 16.2, 10.2, 10.2 Hz, 1H; C*H*=CH$_2$), 6.25 (dd, *J* = 14.4, 10.5 Hz, 1H; CH$_2$=CH-C*H*), 5.53 (dd, *J* = 14.7, 6.3 Hz, 1H; CH=C*H*– CH(OH)), 5.05 (dd, *J* = 14.4, 0.3 Hz, 1H; C*H*$_2$=CH), 4.93 (dd, *J* = 10.2, 0.3 Hz, 1H; C*H*$_2$=CH), 4.40 (*app* dt, *J* = 7.8, 6.3 Hz, 1H; C*H*(OH)), 1.60 (dd, *J* = 14.4, 10.8, 1H; CH(OH)-C*H*$_2$), 1.43 (dd, *J* = 14.4, 2.4, 1H; CH(OH)-C*H*$_2$), 1.20 (s, 3H; *Me*), 1.11 (s, 3H; *Me*);

^{13}C NMR (75 MHz, $CDCl_3$, 293 K): δ 136.4, 130.2, 130.0, 117.1, 71.3, 69.8, 47.5, 31.4, 27.6. HRMS (ESI+) calcd. for $C_9H_{17}O_2$ $[M+H]^+$ 157.1223, found 157.1229.

Enantioselective reduction of ketone:

General procedure:

(Method A) To a clean and dry 10 mL round-bottomed flask was added $NaHCO_3$, H_3BO_3 and Ligand (**L***) (1:1:1) and stirred in 10:1 MeOH/water mixture (2 mL) at 23 °C. After 1 h, the mixture was concentrated *in vacuo* and water was removed by adding MeOH (4 mL × 3) and concentrating under reduced pressure to obtain a white solid, to which was added enone **1.25** (31 mg, 0.2 mmol) in 1 mL THF and stirred at 23 °C. After 1 h, the solution was cooled to -78 °C and $NaBH_4$ (2.3 mg, 0.06 mmol, 0.3 equiv) was added. The mixture was slowly warmed to 23 °C over 12 h and was quenched with saturated aqueous NH_4Cl (1.0 mL), and THF was removed *in vacuo*. The resulting mixture was extracted with Et_2O (3 × 5 mL). The combined organic layers were washed with brine, conc. NH_3 and dried over Na_2SO_4, filtered through a cotton plug, and concentrated *in vacuo*. The crude residue was purified by flash chromatography (5→30% EtOAc in hexanes) on silica gel (10 mL) to afford **1.26a** as a clear oil. A solution of **1.26a** was prepared in 5% ^{i}PrOH in hexanes (1mg/mL). The enantiomeric ratio was determined by chiral HPLC with (S,S)-Whelk-O 1 column [eluent: 5:95 ^{i}PrOH/hexanes; 1.0 mL/min flow rate, detection: 231 nm; $\mathbf{t}_R$ 7.7min, $\mathbf{t}_R$ 8.2 min.]

(Method B) To a clean and dry 10 mL round-bottomed flask was added (R)-1,1'-binaphthol (**L5**) (0.04 mmol, 20 mol%) and stirred with $NaBH_4$ (0.5 equiv) in MeCN (2 mL) at 23 °C. After 1 h, the mixture was concentrated *in vacuo* to obtain a white solid, which was resuspended in dry THF (1 mL) and cooled to -78 °C. To it was added enone **1.25** (31 mg, 0.2 mmol) in 0.5 mL THF and slowly warmed to 0 °C over 16 h. The mixture was quenched with

saturated aqueous NH_4Cl (1.0 mL), and THF was removed *in vacuo*. The resulting mixture was extracted with Et_2O (3 × 5 mL). The combined organic layers were washed with conc. NH_3 (2 mL) to remove any $B(OH)_3$, dried over Na_2SO_4, filtered through a cotton plug, and concentrated *in vacuo*. The crude residue was purified by flash chromatography (5→30% EtOAc in hexanes) on silica gel (10 mL) to afford allylic alcohol **1.26a** as clear oil. A solution of **1.26a** was prepared in 5% ^{i}PrOH in hexanes (1mg/mL). The enantiomeric ratio was determined by chiral HPLC with (S,S)-Whelk-O 1 column [eluent: 5:95 ^{i}PrOH/hexanes; 1.0 mL/min flow rate, detection: 231 nm; $\mathbf{t}_R$ 7.7min, $\mathbf{t}_R$ 8.2 min.]

(Method C) To a clean and dry 500 mL round-bottomed flask was added (R)-1,1'-binaphthol (**L5**) 18.9 g (66 mmol, 100 mol%), dissolved in dry THF (120 mL) and cooled to 0 °C. To it was added dropwise BH_3•THF (66.0 mL, 1 equiv, 1 M in THF) over 20 min, and stirred for another 1 h at the same temperature. To this reaction **1.25** (or ketone substrate) in 120 mL THF was added dropwise over 45 min at 0 °C. After an additional 1 h the mixture cooled to -78 °C and $NaBH_4$ (832 mg, 0.3 equiv) was added slowly in 4 portions over 2 h and allowed to warm to 23 °C over 12 h. The reaction mixture was then quenched with 100 mL sat. NH_4Cl at 0 °C and stirred for 30 min. The mixture was concentrated *in vacuo* to remove THF, followed by vacuum filtration to remove a precipitated white solid. The obtained white precipitate was recrystallized from hot hexanes to recover (R)-1,1'-binaphthol (**L5**) 12.1 g (42 mmol, 63% recovery). The aqueous layer was extracted with EtOAc (3 × 50 mL). The combined organic layers were washed with conc. NH_3 (20 mL) to remove any $B(OH)_3$, dried over Na_2SO_4, filtered through a cotton plug, and concentrated *in vacuo*. The crude residue was purified by flash chromatography (5→30% EtOAc in hexanes) on silica gel (400 mL) to afford alcohol **1.26a** (7.30 g, 71%) as clear oil. A solution of the product was prepared in 5% ^{i}PrOH in hexanes (1mg/mL). The

enantiomeric ratio was determined by chiral HPLC with (S,S)-Whelk-O 1 column [For compound **1.26a**: eluent: 5:95 ^{i}PrOH/hexanes; 1.0 mL/min flow rate, detection: 231 nm; $\mathbf{t}_R$ 7.7min, $\mathbf{t}_R$ 8.2 min.

Data for allylic alcohol **1.26a**: $[\alpha]_D^{21}$ -3.5 (*c* 1.0, CH_2Cl_2).

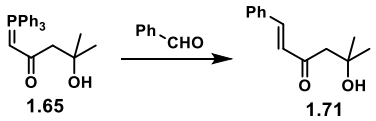

Preparation of enone **1.71**: To a 50-mL round-bottomed flask equipped with a Teflon-coated magnetic stir bar and a reflux condenser was added ylide **1.65** (376 mg, 1 mmol), CH_2Cl_2 (5 mL) at 23 °C, to which PhCHO (2 mmol) was added dropwise. The mixture was refluxed at 40 °C for 4 h, and then concentrated *in vacuo*. The resulting crude residue was purified by flash chromatography (10→50% EtOAc in hexanes) on silica gel (200 mL) to afford enone **1.71** as pale yellow oil (151 mg, 74% yield).

Data for enone **1.71**: R_f = 0.56 (40% EtOAc in hexanes); IR (film): ν_{max} = 3459 (br O-H), 3030, 2970, 1675 (C=O), 1501, 1200, 1130 cm^{-1}; ^{1}H NMR (300 MHz, 1% CD_3OD in $CDCl_3$, 293 K): δ 7.60 (d, *J* = 16.2 Hz, 1H; Ph-C*H*=CH), 7.57–7.55 (m, 2H; *Ar*), 7.42–7.26 (m, 3H; *Ar*), 6.76 (d, *J* = 16.2 Hz, 1H; Ph-CH=C*H*), 2.86 (s, 2H; CH_2), 1.32 (s, 6H; CMe_2); ^{13}C NMR (75 MHz, $CDCl_3$, 293 K): δ 201.6, 143.7, 134.2, 130.9, 129.0, 128.5, 126.9, 70.0, 51.0, 29.5. HRMS (ESI+) calcd. for $C_{13}H_{17}O_2$ $[M+H]^+$ 205.1150, found 205.1158.

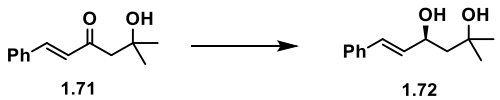

Preparation of **1.72**: Prepared by general method C described above.

Data for allylic alcohol **1.72**: R_f = 0.40 (40% EtOAc in hexanes); IR (film): ν_{max} = 3369, 3088, 3030, 2973, 2935, 1654, 1503, 1464, 1390, 1329, 1244, 1153, 1058, 1004, 957 cm^{-1}; ^1H NMR (400 MHz, 1% CD_3OD in $CDCl_3$, 293 K): δ 7.38 (d, *J* = 7.2 Hz, 1H; Ar), 7.33 (app t, *J* = 7.2, Hz, 1H; Ar), 7.23 (d, *J* = 7.2 Hz, 1H; Ar), 6.63 (d, *J* = 16.0 Hz, 1H; Ph-C*H*=CH), 6.25 (dd, *J* = 16.0, 6.4 Hz, 1H; Ph-CH=C*H*), 4.72 (d, *J* = 8.0 Hz, 1H; CH=CH-C*H*), 1.88 (dd, *J* = 14.4, 10.8 Hz, 1H; CH_2 axial), 1.68 (dd, *J* = 14.4, 2.4 Hz, 1H; CH_2 equatorial), 1.39 (s, 3H; *Me*), 1.30 (s, 3H; *Me*); ^{13}C NMR (100 MHz, $CDCl_3$, 293 K): δ 136.7, 132.2, 129.8, 128.6, 127.7, 126.5, 71.7, 70.8, 48.0, 32.0, 27.8. HRMS (ESI+) calcd. for $C_{13}H_{19}O_2$ $[M+H]^+$ 207.1307, found 207.1301.

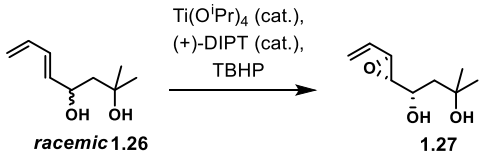

Preparation of epoxy alcohol **1.27**: A 250-mL round-bottomed flask equipped with a Teflon-coated magnetic stir bar containing enantioenriched **1.26a** (2.30 g, 14.7 mmol) was purged with argon. CH_2Cl_2 (60 mL) and 4Å molecular sieves (3.10 g) were added to the flask. The mixture was cooled to -20 °C (external temperature), then Ti(O^iPr)$_4$ (0.38 g, 1.34 mmol), (+)-DIPT (0.50 g, 2.10 mmol) and ^{t}BuOOH solution in isooctane (1.4 mL, 8.0 mmol) were added sequentially at the same temperature. The mixture was stirred at the same temperature for 13 h, then diluted with 1 M NaOH (50 mL), Celite ® (3.0 g), Na_2SO_4 (3.0 g), NaCl (3.0 g). The mixture was stirred for 40 min, then filtered through a pad of Celite® and Florisil mixture. The filtrate was concentrated *in vacuo*, and the resulting crude residue was purified by flash chromatography (10→70% EtOAc in hexanes with 1% NEt_3) on silica gel (200 mL) to afford unreacted allylic alcohol **1.26a** and epoxy alcohol **1.27** as clear oils (1.38 g, ca. 55%) with

impurities of titanium and tartrate. The recovered **1.26a** was resubjected to the same conditions to afford **1.27** (1.80g, ca. 71% after 2 cycles) as clear oil with minor impurities. The impure epoxy alcohol **1.27** was used in the next step without further purification. The % *ee* was not determined at this stage due to the presence of impurities.

Data for epoxy alcohol **1.27**: R_f = 0.35 (60% EtOAc in hexanes); IR (film): ν_{max} = 3400, 2977, 2932, 1645, 1425, 1371, 1255, 1147, 1064, 1022, 929, 905, 796, 737 cm^{-1}; ^1H NMR (300 MHz, 1% CD_3OD in $CDCl_3$, 293 K): δ 5.89 (ddd, *J* = 17.4, 10.5, 6.9 Hz, 1H; CH_2=C*H*), 5.31 (dd, *J* = 17.4, 0.3 Hz, 1H; C*H*$_2$=CH), 5.23 (d, *J* = 10.5 Hz, 1H; C*H*$_2$=CH), 4.11–4.17 (m, 2H; CH_2=CH-C*H*-C*H*), 3.33 (dd, *J* = 9.3, 3.3 Hz, 1H; C*H*(OH)), 1.96 (dd, *J* = 14.4, 3.3 Hz, 1H; C*H*$_2$), 1.70 (dd, *J* = 14.4, 3.3 Hz, 1H; C*H*$_2$), 1.45 (s, 3H; C*Me*$_2$), 1.21 (s, 3H; C*Me*$_2$); ^{13}C NMR (75 MHz, $CDCl_3$, 293 K): δ 136.3, 118.5, 76.4, 75.1, 73.1, 70.3, 70.1, 43.5, 31.2, 23.0.

Preparation of epoxy alcohol **1.27**: A 25-mL round-bottomed flask equipped with a Teflon-coated magnetic stir bar containing enantioenriched **1.26a** (43 mg, 0.28 mmol) was dissolved in CH_2Cl_2 (2 mL) and was cooled to 0 °C (external temperature). To the stirred solution was added $NaHCO_3$ (46 mg, 0.55 mmol) and mCPBA (52 mg, 0.30 mmol) sequentially and stirred at the same temperature for 1 h, then stirred at 23 °C for 1 h. The reaction was then quenched with saturated $Na_2S_2O_3$ solution and extracted with CH_2Cl_2 (10 mL × 3) and the combined organic layers were dried over Na_2SO_4, filtered through a cotton plug, and concentrated *in vacuo*. The crude residue was purified by flash chromatography (5→50% EtOAc in hexanes) on silica gel (15 mL) to afford epoxy alcohol **1.27** as clear oil (27 mg, 57% yield).

Data for epoxy alcohol **1.27**: $[\alpha]_D^{21}$ -2.8 (*c* 0.9, CH_2Cl_2).

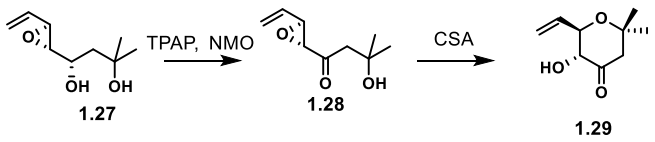

Preparation of ketone **1.29**: To a 250-mL round-bottomed flask equipped with a Teflon-coated magnetic stir bar containing **1.27** (911 mg) was added CH_2Cl_2 (200 mL), 4Å molecular sieves (3.30 g), TPAP (101 mg, 0.29 mmol), and NMO (2.50 g, 18.4 mmol) at 23 °C. The mixture was stirred at the same temperature for 40 min, then filtered through a plug of silica. The filtrate was concentrated to approximately 200 mL of CH_2Cl_2 remaining in the flask. To the flask was added CSA (860 mg, 3.70 mmol) at 23 °C. The mixture was stirred at the same temperature for 19 h, then Et_3N (0.1 mL) was added. The mixture was concentrated *in vacuo*, and the crude residue was purified by flash chromatography (10→30% EtOAc in hexanes) on silica gel (50 mL) to afford ketone **1.29** as clear oil (650 mg, 70% yield, over 2 steps).

Data for epoxy ketone **1.28**: R_f = 0.33 (40% EtOAc in hexanes); IR (film): ν_{max} = 3403 (br, O-H), 2974, 2930, 1709 (C=O), 1442, 1199, 1135 cm^{-1}; ^1H NMR (300 MHz, $CDCl_3$, 293 K): δ 5.56 (ddd, *J* = 17.2, 11.1, 6.0 Hz, 1H; CH_2=C*H*), 5.55 (dd, *J* = 17.2, 2.5 Hz, 1H; C*H*$_2$=CH), 5.41 (dd, *J* = 11.1, 2.5 Hz, 1H; C*H*$_2$=CH), 3.49 (dd, *J* = 6.0, 2.1 Hz, 1H; CH_2=CH-C*H*-O), 3.38 (d, *J* = 2.1 Hz, 1H; O-C*H*-C(O)), 2.67 (d, *J* = 17.1 Hz, 1H; C(O)C*H*$_2$), 2.50 (d, *J* = 17.1 Hz, 1H; C(O)C*H*$_2$), 1.28 (s, 3H, *Me*), 1.27 (s, 3H, *Me*); ^{13}C NMR (175 MHz, $CDCl_3$, 293 K): δ 207.9, 133.0, 121.8, 69.8, 61.2, 57.9, 47.9, 29.5, 29.4; HRMS (EI+) calcd. for $C_9H_{13}O_2$ $[M\text{-}OH]^+$ 153.0916, found 153.0910. Due to unstable nature of **1.28**, further characterization was not possible.

Data for ketone **1.29**: R_f = 0.35 (30% EtOAc in hexanes); IR (film): ν_{max} = 3474 (br, O-H), 2975, 2934, 1723 (C=O), 1374, 1240, 1107, 1080 cm^{-1}; ^1H NMR (300 MHz, 1% CD_3OD in

C_6D_6, 293 K): δ 6.06 (ddd, *J* = 17.1, 10.5, 4.8 Hz, 1H; CH_2=C*H*), 5.53 (ddd, *J* = 17.1, 1.8, 1.8 Hz, 1H; C*H*$_2$=CH), 5.17 (ddd, *J* = 10.5, 1.8, 1.8 Hz, 1H; C*H*$_2$=CH), 3.86 (dd, *J* = 9.0, 6.8 Hz, 1H; C*H*$_2$=CH-C*H*), 3.63 (d, *J* = 9.0 Hz, 1H; C*H*(OH)), 2.67 (d, *J* = 13.2 Hz, 1H; C(O)C*H*$_2$), 2.52 (d, *J* = 13.2 Hz, 1H; C(O)C*H*$_2$), 1.00 (s, 3H; *Me*), 0.75 (s, 3H; *Me*); ^{13}C NMR (75 MHz, $CDCl_3$, 293 K): δ 207.4, 135.5, 118.0, 77.9, 76.7, 76.4, 51.5, 30.8, 23.6; HRMS (ESI+) calcd. for $C_9H_{15}O_3$ $[M + H]^+$ 171.1021, found 171.1006. $[\alpha]_D$ ^{20} +28.1 (*c* 1.0, CH_2Cl_2).

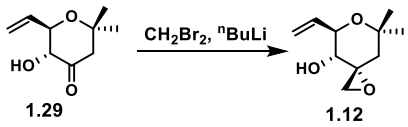

1.29 1.12

Preparation of epoxide **1.12**: A 25-mL round-bottomed flask equipped with a Teflon-coated magnetic stir bar containing ketone **1.29** (200 mg, 1.18 mmol) was purged with N_2. To the flask was added THF (12.0 mL) and CH_2Br_2 (246 mg, 1.42 mmol). The flask was cooled to -78 °C, then ^{n}BuLi (1.60 mL, 2.60 mmol) was added. The mixture was stirred for 7 h, while warming the cooling bath to 20 °C. The reaction mixture was quenched with saturated aqueous NH_4Cl (15.0 mL), and THF was removed *in vacuo*. The resulting mixture was extracted with Et_2O (3 × 15 mL). The combined organic layers were dried over Na_2SO_4, filtered through a cotton plug, and concentrated *in vacuo*. The crude residue was purified by flash chromatography (5→30% EtOAc in hexanes) on silica gel (40 mL) to afford epoxide **1.12** as clear oil (157 mg, 73% yield).

Spectroscopic data for epoxide **1.12** matched that in *J. Am. Chem. Soc.* **2007**, *129*, 2648–2659.

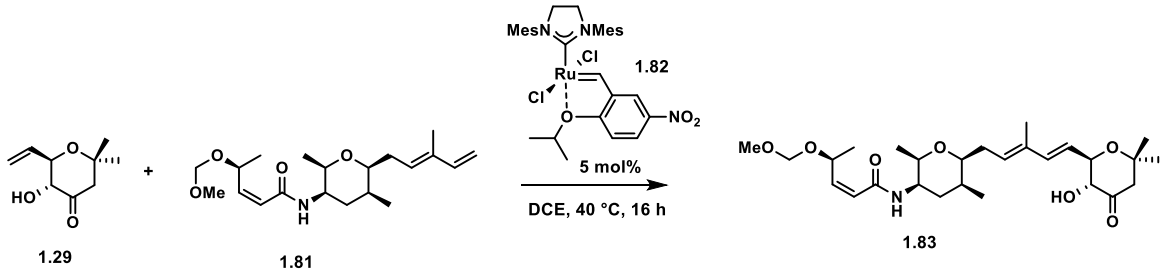

Preparation of ketone **1.83**: A 10-mL round-bottomed flask equipped with equipped with a Teflon-coated magnetic stir bar containing diene **1.55** (35 mg, 0.1 mmol, prepared by Mr. Robert K. Bressin) and alkene **1.29** (34 mg, 0.2 mmol) was charged with DCE (0.3 mL), **1.56** (3.2 mg, 0.0048 mmol). The mixture was stirred in an oil bath for 2 h at 40 °C, then added **1.82** (2.1 mg, 0.0031 mmol), and the mixture was stirred for an additional 14 h, then concentrated *in vacuo*. The crude residue was purified by flash chromatography (10→100% EtOAc in hexanes) on silica gel (5 mL) to afford **1.83** as oil (3.5 mg). The recovered starting materials were subjected to the same reaction conditions and purified to obtain **1.83** (1.5 mg) as oil (combined yield: 5 mg, 10% after 2 cycles). Some of this material was purified by preparative-TLC (EtOAc) and used for biological experiments.

Data for ketone **1.83***:* R_f = 0.32 (70% EtOAc in hexanes); IR (film): ν_{max} = 3399 (br, O-H), 2974, 2924, 1730 (C=O), 1665 (C=O), 1517, 1463, 1383, 1260, 1218, 1077, 1033 cm^{-1}; $[\alpha]_D^{17}$ +3.45 (*c* 0.3, CH_2Cl_2); ^1H NMR (500 MHz, 1% CD_3OD in $CDCl_3$, 293 K): δ = 6.44 (d, *J* = 15.5 Hz, 1, 7-H), 5.99 (dd, *J* = 11.5, 8.0 Hz, 1H, 3'-H), 5.86 (br d, *J* = 8.5 Hz, 1H, N-H), 5.74–5.70 (m, 2H, 2'-H, 6-H), 5.56 (dd, *J* = 7.0, 7.0 Hz, 1H, 9-H), 5.43–5.37 (m, 1H, 4'-H), 4.69 (d, *J* = 7.0 Hz, 1H, 6'-H), 4.63 (d, *J* = 7.0 Hz, 1H, 6"-H), 4.02 (dd, *J* = 9.0, 3.0 Hz, 1H, 4-H), 3.98–3.93 (m, 2H, 5-H, 14-H), 3.67 (dq, *J* = 7.0, 2.0 Hz, 1H, 15-H), 3.53 (ddd, *J* = 7.0, 7.0, 2.0 Hz, 1H, 11-H), 3.37 (s, 3H, *Me*OCH_2O), 2.68 (d, *J* = 13.0 Hz, 1H, 2_{axial}-H), 2.53 (d, *J* = 13.0 Hz, 1H,

$2_{equatorial}$-H), 2.42–2.37 (m, 1H, 10-H), 2.27–2.21 (m, 1H, 10-H), 1.94–1.92 (m, 2H, 12-H, 13-H), 1.80–1.77 (m, 1H, 13-H), 1.80 (s, 3H, 18-H), 1.45 (s, 3H, 17-H), 1.33 (d, J = 6.5 Hz, 3H, 4'-H), 1.22 (s, 3H, 17-H), 1.14 (d, J = 6.5 Hz, 3H, 16-H), 1.02 (d, J = 6.5 Hz, 3H, 19-H); ^{13}C NMR (100 MHz, $CDCl_3$, 293 K): δ = 207.4, 165.1, 147.2, 138.1, 134.5, 130.1, 129.7, 124.0, 122.3, 95.1, 80.8, 69.6, 55.4, 51.5, 47.1, 35.9, 32.0, 30.9, 29.7, 29.0, 23.7, 21.0, 17.8, 15.2, 12.6; HRMS (ESI+) calcd. for $C_{30}H_{46}N_2O_8Na$ $[M + Na]^+$ 494.3112, found 494.3104.

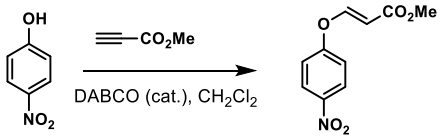

4-nitrophenol 2.25

Preparation of enoate **2.25**: To a stirred solution of 4-nitrophenol (4.0 g, 28.6 mmol) in anhydrous CH_2Cl_2 (100 mL) was added 1,4-diazabicyclo[2.2.2]octane (321 mg, 10 mol %) at 25 °C. To the reaction mixture, methyl propiolate (4.56 mL, 57.2 mmol) were added dropwise over 15 min, and stirring continued for 12 h at the same temperature. The reaction mixture was quenched with saturated aqueous NH_4Cl (15.0 mL), organic layer was separated in a separatory funnel and the resulting aqueous layer was extracted with CH_2Cl_2 (2 × 15 mL). The combined organic layers were dried over Na_2SO_4, filtered through a cotton plug, and concentrated *in vacuo*. The crude residue was purified by flash column chromatography (10→30% EtOAc in hexanes) on silica gel (500 mL). The resulting pale brown solid product was recrystallized from EtOAc and hexanes to yield enoate **2.25** as a white crystalline solid (4.74 g, 74%).

Data for **2.25:** M.p. = 104.0–105.0 °C; R_f = 0.33 (50% EtOAc in hexanes); IR (film) 1715 (C=O), 1660, 1611, 1501, 937, 855, 844, 748, 729 cm $^{-1}$; ^{1}H NMR (300 MHz, 293 K, $CDCl_3$) δ: 8.29 (ddd, 2H, J = 9.3, 3.3, 2.1 Hz; $(CH)_2CNO_2$), 7.82 (d, 1H, J = 12.0 Hz;

ArOC*H*=CHCO$_2$Me), 7.20 (ddd, 2H, *J* = 9.3, 3.3, 2.1 Hz; OC(C*H*)$_2$), 5.78 (d, 1H, *J* = 12.0 Hz; ArOCH=C*H*CO$_2$Me), 3.77 (s, 1H; O*Me*); ^{13}C NMR (75 MHz, 293K, $CDCl_3$) δ: 166.8, 160.2, 156.0, 144.4, 126.1, 117.6, 105.1, 51.7; HRMS (ESI+) calcd. for $C_{10}H_9NO_5$ $[M+H]^+$ 224.0559, found 224.0573.

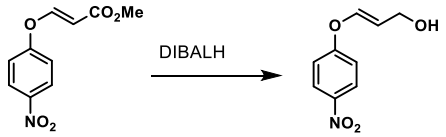

2.25 **2.26**

Preparation of alcohol **2.26**: To a dry 50-mL round-bottom flask are added enoate **2.25** (300 mg, 1.34 mmol) and a Teflon magnetic stir bar. The flask was purged continuously with nitrogen to replace all air. With a syringe, anhydrous CH_2Cl_2 (5 mL) was added and **2.25** dissolved by continuous stirring. The solution was cooled to -78 °C with a dry ice bath for about 15 min. To the flask was added 1M DIBALH in hexanes (3.39 mL, 3.39 mmol) via syringe, dropwise over 2–3 min. After 10 min, the reaction mixture was stirred for 2 h at 0 °C under a nitrogen atmosphere. The reaction mixture was quenched with saturated Rochelle's salt (10 mL) under air and warmed to 25 °C. The mixture was transferred to a 30-mL separatory funnel and extracted with CH_2Cl_2 (3 × 10 mL). The combined extracts were washed with brine (20 mL), dried over anhydrous Na_2SO_4, filtered through a cotton plug, and rotatory evaporated *in vacuo* to yield alcohol **2.26** as an orange-brown solid (236 mg, 87%), which formed an inseparable mixture of *cis* and *trans* isomers (0.3:1) on overnight storage in the freezer.

Data for **2.26:** m.p. = 43.0–44.0 °C; R_f = 0.26 (70% EtOAc in hexanes); IR (film) 3409 (broad, O-H), 1591, 1519, 1343, 1249, 1169, 1113, 702 cm $^{-1}$; ^{1}H NMR (300 MHz, 293K, $CDCl_3$) δ: 8.24 (ddd, 2H, *J* = 9.3, 3.3, 2.1 Hz; (C*H*)$_2$CNO$_2$), 7.09 (ddd, 2H, *J* = 9.3, 3.3, 2.1 Hz;

OC(C*H*)$_2$), 6.76 (dt, 1H, *J* = 12.0, 1.4 Hz; C*H*=CHCH$_2$OH), 5.74 (dt, 1H, *J* = 12.0, 6.6 Hz; CH=C*H*CH$_2$OH), 4.25 (dd, 2H, *J* = 6.6, 1.4 Hz CH=CHC*H*$_2$OH); ^{13}C NMR (100 MHz, 293K, $CDCl_3$) δ: 161.7, 142.9, 142.7, 126.0, 116.4, 114.9, 59.5; HRMS (ESI+) calcd. for $C_9H_9NO_4$ $[M+H]^+$ 196.0610, found 196.0614.

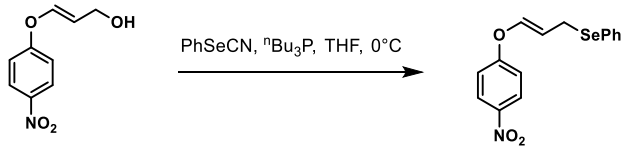

2.26 **2.27**

Preparation of alcohol **2.27: 2.27** was prepared using the following general procedure described below.

Data for **2.27:** Yield: 88%; R_f = 0.68 (20% EtOAc in hexanes); ^{1}H NMR (300 MHz, 293K, $CDCl_3$) δ: 8.14 (ddd, 2H, *J* = 9.0, 3.3, 2.1 Hz; *Ar* (cis)), 8.09 (ddd, 2H, *J* = 9.0, 3.3, 2.1 Hz; *Ar* (trans)), 7.59–7.55 (m, 3H; *Ph*), 7.32–7.20 (m, 2H; *Ph*), 6.86 (ddd, 1H, *J* = 9.0, 3.3, 2.1 Hz; *Ar* (cis)), 6.65 (ddd, 1H, *J* = 9.0, 3.3, 2.1 Hz; *Ar* (trans)), 6.35 (ddd, 1H, *J* = 6.0, 1.2, 1.2 Hz; *cis*-C*H*=CHCH$_2$), 6.21 (ddd, 1H, *J* = 12.0, 1.2, 1.2 Hz; *trans*-C*H*=CHCH$_2$), 5.71 (ddd, 1H, *J* = 12.0, 8.4, 8.4 Hz; *trans*-CH=C*H*CH$_2$), 5.27 (ddd, 1H, *J* = 6.0, 8.4, 8.4 Hz; *cis*-CH=C*H*CH$_2$), 3.68 (dd, 2H, *J* = 8.4, 0.9 Hz; *cis*-CH=CHC*H*$_2$), 3.51 (dd, 2H, *J* = 8.4, 0.9 Hz; *trans*-CH=CHC*H*$_2$); HRMS (TOF MS ES+) calcd. for $C_9H_9NO_4$ $[M+H]^+$ 196.0610, found 196.0614. The compound was not further characterized due to presence of inseparable impurities.

Synthesis: The following general procedure was utilized for the synthesis of allylic selenide **2.17** and **2.41**.

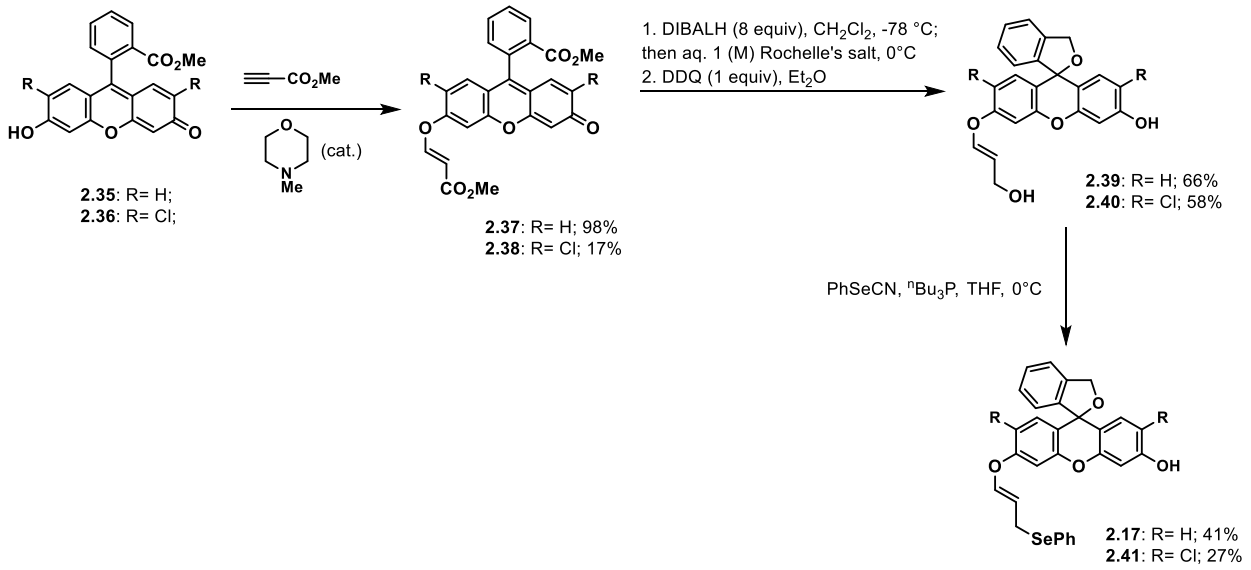

Scheme 16. General route to allylic selenide **2.17**

General procedure:

Preparation of **2.37***:* To a suspension of **2.35**[74] (1.00 g, 3.00 mmol) in dry CH_2Cl_2 (50 mL) was added N-methylmorpholine (30 mg, 0.30 mmol) and methyl propiolate (270 mg, 3.20 mmol) under a nitrogen atmosphere at 23 °C. After stirring the reaction mixture for 24 h at the same temperature, 3 g SiO_2 gel was added and the mixture was concentrated *in vacuo*. The resulting crude residue was purified by flash column chromatography (10→40% EtOAc in hexanes) on SiO_2 gel (200 mL) to obtain compound **2.37** (1.27 g, 98%) as an orange solid.

Data for **2.37**: mp 192.0–194.0 °C; R_f: 0.25 (70% EtOAc in hexanes); IR (film): ν_{max} = 3060, 2923, 1722 (C=O), 1642 (C=O), 1639 (C=O), 1595, 1522, 1444, 1378, 1267, 1247, 1191, 1158, 1133, 1106, 1081, 854, 707 cm^{-1}; ^1H NMR (300 MHz, $CDCl_3$, 293 K): δ 8.25 (dd, *J* = 7.5, 1.5 Hz, 1H; *Ar*), 7.85 (d, *J* = 12.0 Hz, 1H; ArO-C*H*=CH-CO_2Me), 7.79 (ddd, *J* = 7.5, 7.5, 1.2 Hz, 1H; *Ar*), 7.72 (ddd, *J* = 7.5, 7.5, 1.2 Hz, 1H; *Ar*), 7.33 (dd, *J* = 7.5, 1.2 Hz, 1H; *Ar*), 7.18 (d, *J* = 2.4 Hz, 1H; *Ar*), 6.98 (d, *J* = 9.0 Hz, 1H; *Ar*), 6.89 (dd, *J* = 9.6, 1.8 Hz, 1H; *Ar*), 6.87 (d, *J* = 9.6

Hz, 1H, *Ar*), 6.56 (dd, *J* = 9.6, 1.8 Hz, 1H; *Ar*), 6.46 (d, *J* = 1.8 Hz, 1H; *Ar*), 5.79 (d, *J* = 12.0 Hz, 1H; ArO-CH=C*H*-CO_2Me), 3.76 (s, 3H; -CO_2Me), 3.66 (s, 3H; -CO_2Me); ^{13}C NMR (75 MHz, $CDCl_3$, 293 K): δ 185.9, 166.8, 165.5, 159.0, 158.5, 156.2, 153.4, 148.7, 134.3, 132.9, 131.3, 130.7, 130.6, 130.4, 130.2, 129.9, 129.3, 119.3, 118.1, 114.1, 106.4, 105.2, 104.8, 52.5, 51.6; HRMS (ESI+) calcd. for $C_{25}H_{19}O_7$ $[M+H]^+$ 431.1110, found 431.1125.

Preparation of **2.39**: A 1M solution of DIBALH in hexanes (1.8 mL, 1.8 mmol) was added dropwise to a flask containing **2.37** (100 mg, 0.23 mmol) in dry CH_2Cl_2 (1.5 mL) under a nitrogen atmosphere at -78 °C. After stirring the reaction mixture for 15 min at the same temperature, the flask was warmed to 23 °C. The mixture was stirred at the same temperature for an additional 2 h and then the reaction was quenched with 1M aqueous Na,K-tartrate (2 mL) at 0 °C. After stirring the mixture for 3 h at 23 °C, 5 mL Et_2O and DDQ (57 mg, 0.25 mmol) was added at 0 °C and stirred at the same temperature for 1 h. The combined organic and aqueous layers were filtered through a pad of Celite and the pad was rinsed with EtOAc. The filtrate was dried under Na_2SO_4, filtered through a cotton plug, and concentrated *in vacuo*. The resulting crude residue was purified by flash column chromatography (10→60% EtOAc in hexanes) on SiO_2 gel (20 mL) to obtain compound **2.39** (57 mg, 66%) as a pale yellow solid and byproduct **2.21** (14 mg, 20%) as an orange solid.

Data for **2.39***:* mp 169.0–170.0 °C; R_f: 0.52 (70% EtOAc in hexanes); IR (film): ν_{max} = 3378 (O–H), 2923, 2853, 1673, 1601, 1480, 1434, 1409, 1266, 1173, 1114, 1004, 926, 854, 722 cm^{-1}; ^{1}H NMR (300 MHz, 1% CD_3OD in $CDCl_3$, 293 K): δ 7.36–7.37 (m, 2H; *Ar*), 7.23–7.28 (m, 1H; *Ar*), 6.91 (d, *J* = 2.4 Hz, 1H; *Ar*), 6.88 (br s, 1H; *Ar*), 6.84 (d, *J* = 2.4 Hz, 1H; *Ar*), 6.77 (d, *J* = 8.4 Hz, 1H; *Ar*), 6.68–6.70 (m, 1H; *Ar*), 6.70 (d, *J* = 12.0, 1.8 Hz, 1H; ArO-C*H*=CH-),

6.60 (d, *J* = 2.4 Hz, 1H; *Ar*), 6.52 (dd, *J* = 8.7, 2.4 Hz, 1H; *Ar*), 5.57 (ddd, *J* = 12.0, 7.2, 7.2 Hz, 1H; -CH=C*H*-CH_2OH), 5.29 (s, 2H; Ar-CH_2-O), 4.15 (dd, *J* = 7.2, 1.8 Hz, 2H; -CH=CH-CH_2OH); ^{13}C NMR (75 MHz, CD_3OD, 293 K): δ 154.0, 153.0, 149.6, 149.5, 143.9, 143.5, 138.6, 129.6, 129.1, 128.5, 128.4, 123.0, 120.9, 120.0, 118.0, 116.5, 116.4, 113.5, 104.5, 103.0, 83.0, 72.0, 58.0; HRMS (ESI+) calcd. for $C_{23}H_{19}O_5$ $[M+H]^+$ 375.1227, found 375.1209.

Preparation of **2.17**: A 10-mL round-bottomed flask equipped with a Teflon-coated magnetic stir bar containing **2.39** (85 mg, 0.23 mmol) was purged with argon. THF (1.2 mL) was added to the flask at 0 °C and to it was added $^{n}Bu_3P$ (67 µL, 0.27 mmol) and PhSeCN (29 µL, 0.23 mmol) sequentially. The mixture was stirred at the same temperature for 30 min and was quenched with sat. NH_4Cl. The mixture was extracted with EtOAc (3 × 15 mL). The combined organic layers were dried over Na_2SO_4, and concentrated *in vacuo*. The resulting crude residue was purified by flash column chromatography (SiO_2, eluent: 5%→25% EtOAc in hexanes; 30 mL each) to obtain **2.17** (48 mg, 41%) as pale yellow solid

Data for **2.17***:* mp 125.5–126.5 °C; R_f: 0.56 (40% EtOAc in hexanes); IR (film): ν_{max} = 3286 (O-H), 2923, 2853, 2360, 1664, 1609, 1496, 1458, 1427, 1331, 1266, 1247, 1210, 1177, 1111, 997, 928, 846, 804, 757, 737, 691 cm^{-1}; ^{1}H NMR (300 MHz, 1% CD_3OD in $CDCl_3$, 293 K): δ 7.56 (dd, *J* =6.0, 1.2 Hz, 2H; *Ar*), 7.36–7.34 (m, 2H; *Ar*), 7.32–7.31 (m, 3H; *Ar*), 7.27–7.26 (m, 1H; *Ar*), 6.88 (d, *J* = 7.5 Hz, 1H; *Ar*), 6.83 (dd, *J* = 8.1, 8.1 Hz, 2H; *Ar*), 6.66 (d, *J* = 2.4 Hz, 1H; *Ar*), 6.54 (m, 3H; *Ar*), 6.30 (d, *J* = 12.0 Hz, 1H; -C*H*=CH-CH_2SePh), 5.57 (ddd, *J* = 12.0, 8.4, 8.4 Hz, 1H; -CH=C*H*-CH_2SePh), 5.27 (s, 2H; Ar-CH_2-O), 3.45 (dd, *J* = 8.1, 0.9 Hz, 2H; -CH=CH-CH_2SePh); ^{13}C NMR (75 MHz, $CDCl_3$, 293 K): δ 157.5, 156.5, 151.4, 151.3, 144.6, 143.1, 139.0, 134.4, 130.1, 130.0, 129.4, 129.2, 128.9, 128.4, 128.2, 127.7, 123.9, 120.7, 119.1,

117.0, 112.5, 111.8, 110.4, 103.6, 102.7, 83.6, 72.0, 25.6; HRMS (ESI-) calcd. for $C_{29}H_{21}O_4Se$ $[M-H]^+$ 513.0610, found 513.0610.

The following compounds were synthesized following the general procedure described above.

Data for **2.38***:* Yield: 17% (orange solid); mp 202.0-203.0 °C; R_f: 0.20 (40% EtOAc in hexanes); IR (film): ν_{max} = 3065, 2951, 1719, 1652, 1625, 1592, 1525, 1433, 1336, 1273, 1236, 1173, 1111, 1084, 1041, 998 cm^{-1}; ^1H NMR (300 MHz, $CDCl_3$, 293 K): δ 8.37 (dd, *J* =7.8, 1.2 Hz, 1H; *Ar*), 7.87–7.75 (m, 2H; *Ar*), 7.77 (d, *J* = 12.0 Hz, 1H; -C*H*=CH-CO_2Me), 7.34 (dd, *J* = 7.8, 1.2 Hz, 1H; *Ar*), 7.03 (s, 1H; *Ar*), 6.98 (s, 1H; *Ar*), 6.62 (s, 1H; *Ar*), 5.84 (d, *J* = 12.0 Hz, 1H; -CH=C*H*-CO_2Me), 3.79 (s, 3H; -CO_2*Me*), 3.74 (s, 3H; -CO_2*Me*); ^{13}C NMR (100 MHz, CD_3OD, 293 K): δ 178.0, 166.4, 165.2, 157.5, 155.9, 154.5, 151.4, 148.5, 136.1, 133.5, 133.4, 131.7, 130.5, 130.4, 129.8, 128.8, 127.3, 121.1, 119.3, 118.6, 106.5, 106.3, 105.8, 52.7, 51.8; HRMS (ESI+) calcd. for $C_{25}H_{17}Cl_2O_7$ $[M+H]^+$ 499.0346, found 499.0331.

Data for **2.40***:* Yield: 58% (yellow solid); m.p 204.2–205.0 °C; R_f: 0.26 (60% EtOAc in hexanes); IR (film): ν_{max} = 3378, 2921, 2851, 1673, 1601, 1480, 1434, 1409, 1266, 1173, 1114, 1004, 922, 864, 722 cm^{-1}; ^1H NMR (300 MHz, CD_3OD, 293 K): δ 7.53 (s, 1H; *Ar*), 7.417.40 (m, 2H; *Ar*), 7.33–7.27 (m, 1H; *Ar*), 6.93 (s, 1H; *Ar*), 6.89 (s, 1H; *Ar*), 6.86 (d, *J* = 7.5 Hz, 1H; *Ar*), 6.81 (s, 1H; *Ar*), 6.74 (s, 1H; *Ar*), 6.69 (d, *J* = 12.0 Hz, 1H; -C*H*=CH-CH_2OH), 5.64 (ddd, *J* = 12.0, 6.9, 6.9 Hz, 1H; -CH=C*H*-CH_2OH), 5.29 (s, 2H; Ar-CH_2O), 4.13 (d, *J* = 6.9 Hz, 1H; -CH=CH-CH_2OH); ^{13}C NMR (75 MHz, CD_3OD, 293 K): δ 154.0, 152.9, 149.6, 149.5, 143.9, 143.5, 138.6, 129.6, 129.1, 128.5, 128.4, 123.0, 120.9, 120.1, 118.0, 116.5, 116.4, 113.5, 104.5,

103.0, 83.0, 72.0, 58.0; HRMS (ESI+) calcd. for $C_{23}H_{17}Cl_2O_5$ $[M+H]^+$ 443.0448, found 443.0450.

Data for **2.41***:* Yield: 27% (yellow foam); R_f: 0.30 (20% EtOAc in hexanes); IR (film): ν_{max} = 3242 (O-H), 2917, 1664, 1625, 1605, 1479, 1435, 1409, 1350, 1266, 1245, 1174, 1107, 1024, 874, 734 cm^{-1}; ^1H NMR (300 MHz, CD_3CN, 293 K): δ 7.54–7.51 (m, 3H; *Ar*), 7.40–7.32 (m, 5H; *Ar*), 6.91 (s, 1H; *Ar*), 6.88 (s, 1H; *Ar*), 6.82 (s, 1H; *Ar*), 6.38 (s, 1H; *Ar*), 6.38 (br d, *J* = 12.0 Hz, 1H; ArO-C*H*=CH-CH_2SePh), 5.58 (dt, *J* = 12.0, 8.4 Hz, 1H; -CH=C*H*-CH_2SePh), 5.29 (s, 1H; Ar-C*H*$_2$OH), 3.57 (dd, *J* = 8.4, 0.9 Hz, 2H; -CH=CH-C*H*$_2$SePh); ^{13}C NMR (150 MHz, CD_3CN, 293 K): δ 154.1, 153.7, 150.2, 150.1, 145.6, 143.3, 139.5, 134.7, 130.6, 130.5, 130.3, 130.2, 130.1, 129.6, 129.5, 128.6, 124.0, 122.4, 121.4, 118.9, 117.0, 113.4, 105.2, 104.6, 83.3, 79.1, 73.6, 25.0; HRMS (ESI-) calcd. for $C_{29}H_{19}Cl_2O_4Se$ $[M-H]^+$ 580.9820, found 580.9826.

Pseudo first order kinetics and evaluation of second order rate constant

Calibration curve for **2.21**:

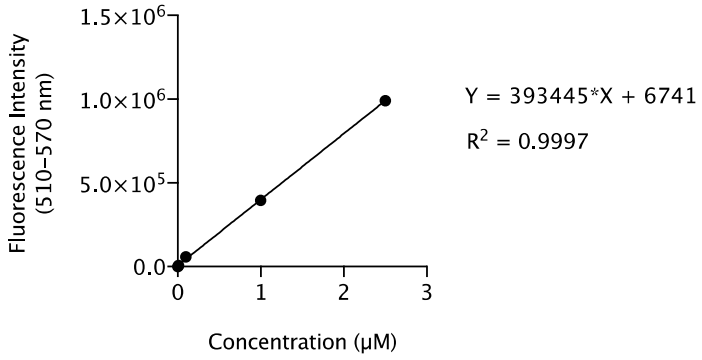

Figure 18. Calibration curve for **2.21**

Volume: 200 μL

5% MeCN in 50mM pH 7.5 HEPES buffer

Raw data for studying pseudo first order kinetics:

Rate= k'[**2.17**]; where k'= k[H_2O_2]

Final concentration: [H_2O_2]= 0.625 mM, 1.25 mM and 2.5 mM; [**2.17**]= 1.7 μM; 5% MeCN in pH 7.5 HEPES buffer 50 mM. All reactions were performed in triplicate in a 96 well plate.

Table 5. Raw data for kinetics study

F_0= 24616 units

	F-F_0 (515 nm); [H_2O_2]= 0.625 mM			F-F_0 (515 nm); [H_2O_2]= 1.25 mM			F-F_0 (515 nm); [H_2O_2]= 2.5 mM		
time(s)	Exp. 1	Exp. 2	Exp. 3	Exp. 1	Exp. 2	Exp. 3	Exp.1	Exp. 2	Exp. 3
30	145691	101161	83026	255659	258915	225047	425024	405551	398309
90	220196	277036	236883	364712	517271	484926	539467	612814	630136
150	301900	391059	348470	463364	607290	590662	601940	657981	671943
210	355049	458596	422910	514663	641798	639332	627168	666435	680181
270	390358	499861	473964	549297	656229	660178	636230	665190	679336
330	421561	522358	509584	572635	661539	664254	638753	666173	674138
390	450025	534705	536252	589797	665178	666753	641141	663899	664993
450	477638	541922	555207	601493	663842	669367	640270	661893	664413
510	501767	546290	569868	606377	663608	673539	639383	659509	664003
570	524121	550122	581518	612207	662594	675671	637346	658746	663104

630	543908	551490	591076	614405	663947	677477	637422	656826	661222
690	559985	551741	599176	616203	663123	679640	636174	654911	659002
750	570897	553475	603780	616371	663595	679888	634294	654494	657410
810	580693	553568	609902	614783	663765	683016	631953	653606	654988
870	587536	552326	614108	614819	662173	685799	631346	651140	655338

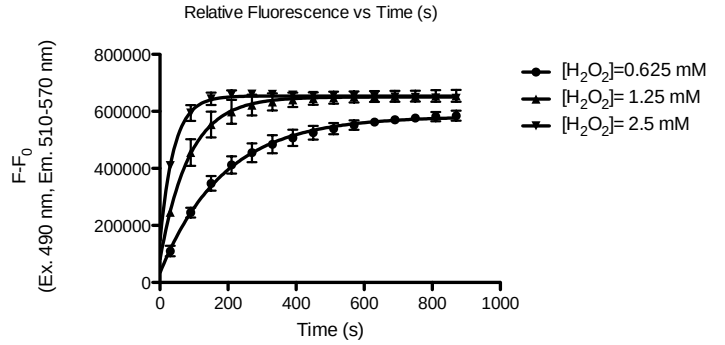

Figure 19. Plot of relative fluorescence vs time

Calculating [**2.17**] from the standard curve of **2.21**. Fluorescence Intensity = 389700•[**2.21**] + 7480; R^2 = 0.9997. From the calculated values of [**2.17**] the following graph was plotted.

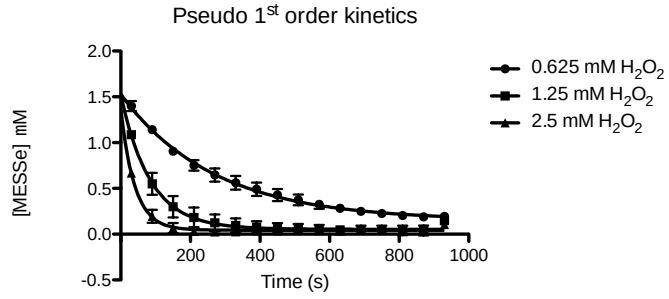

Figure 20. Plot of [**2.17**] vs time

With the known values of [**2.17**], ln[**2.17**] vs time (s) was plotted to obtain observed rate constants k' as the slope of the linear plot (Figure 21).

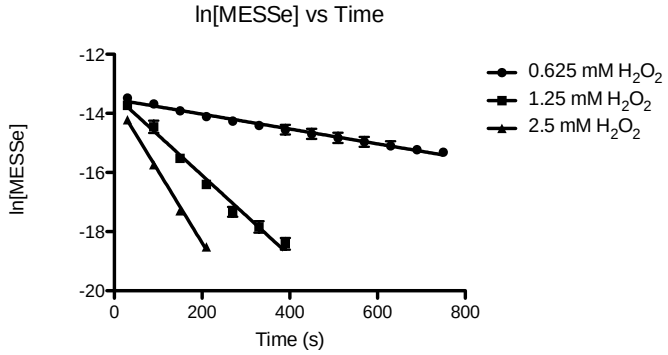

Figure 21. Plot of ln[**2.17**] vs t to obtain slope (k')

Table 6. Slope (k') obtained from the plot of ln [**2.17**] vs time.

$[H_2O_2]$ (mM)	Slope k' (s^{-1})
2.5	0.02432
1.25	0.01359
0.625	0.00251

From Figure 21, three values of k' were obtained for three different concentrations of H_2O_2. Under pseudo first order conditions, k'= k$[H_2O_2]$. So, a plot of observed rate constant k' vs $[H_2O_2]$ yielded the second order rate constant k as the slope of the linear plot. After all calculations, it was found that second order rate constant k=9.82 ± 1.11 $M^{-1}s^{-1}$.

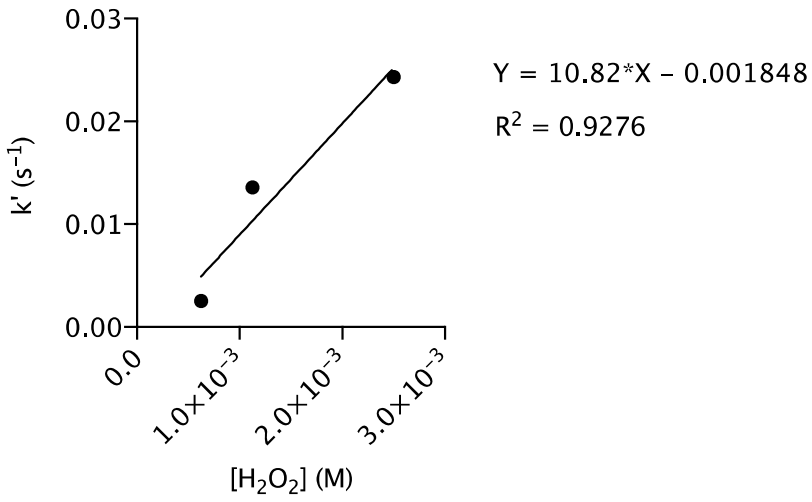

Figure 22. Plot of k' vs time to obtain second order rate constant k.

Similarly, the second order rate constant for reaction of H_2O_2 with **2.41** was also calculated from the following plots.

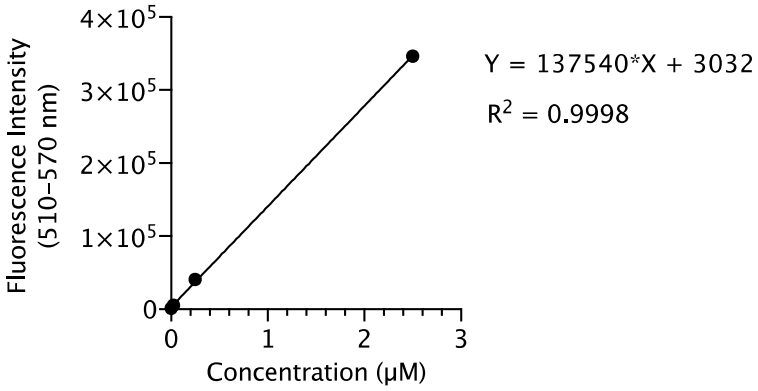

Figure 23. Calibration curve for Pittsburgh Green

Volume: 200 μL

5% DMSO in 50mM pH 7.5 HEPES buffer

F_0= 974.222 arbitrary units (before addition of H_2O_2)

[**2.41**]= 2.5 μM

$[H_2O_2]$ = 250, 125, 62.5 μM respectively

Table 7. Raw data for calculation of pseudo 1st order rate constant for **2.41**

	$F-F_0$ (515 nm); $[H_2O_2]$= 62.5 μM			$F-F_0$ (515 nm); $[H_2O_2]$= 125 μM			$F-F_0$ (515 nm); $[H_2O_2]$= 250 μM		
time(s)	Exp. 1	Exp. 2	Exp. 3	Exp. 1	Exp. 2	Exp. 3	Exp.1	Exp. 2	Exp. 3
30	64532	60839	72341	51068	40954	29407	20933	20713	17895
90	94055	84890	99777	61620	54853	38434	26549	26261	22833
150	126168	110059	125746	75450	68745	48938	32203	32013	27511
210	151144	132904	151809	88218	82399	59492	38434	38112	32023
270	174202	154143	173840	99254	94711	69782	45581	45714	38555
330	195425	176762	196268	110291	106912	80261	54391	53856	46349
390	214125	195309	213903	120534	118426	90136	61465	61141	55115
450	235080	213946	228931	132699	129729	101653	68335	68705	62745
510	251284	232113	245365	142828	140659	113203	74962	76129	70760
570	267145	247451	259690	152548	149939	120429	82980	83409	78331
630	277115	262327	273899	163508	160682	132151	89955	91138	85442
690	280646	276049	285043	174252	170447	142735	98437	100429	95200
750	285014	290726	296951	184048	179818	153582	105665	107760	102828
810	291608	306540	310230	193989	188931	160835	113559	114196	111796
870	298779	319772	321793	203331	197010	172486	119974	121528	117097

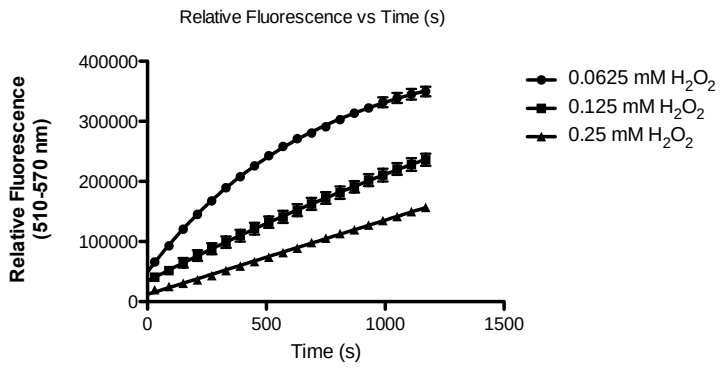

Figure 24. Relative fluorescence vs time plot

[**2.41**]= 2.5 μM

[H_2O_2] = 250, 125, 62.5 μM respectively

As evident from the tabulated data, after addition of H_2O_2, the fluorescence signal intensity increases by >300 times. (For example, in the table 7 at t=870 s and [H_2O_2]= 62.5 μM, F_{final}/F_0= 321793/974=330)

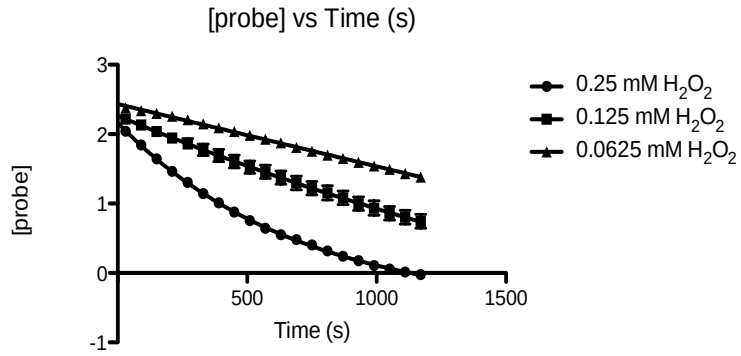

Figure 25. Plot of [**2.41**] vs time

With the known values of [**2.41**], ln[**2.41**] vs time (s) was plotted to obtain observed rate constants k' as the slope of the linear plot (Figure 26).

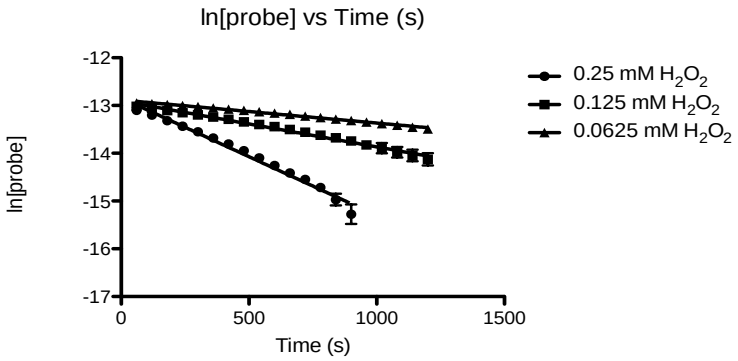

Figure 26. Plot of ln[**2.41**] vs time

Table 8. Slope (k') obtained from the plot of ln[**2.41**] vs time

From the plot of ln[**2.41**] vs time, pseudo 1st order rate constant was obtained as follows:

$[H_2O_2]$ (mM)	k' (s^{-1})
0.25	0.002461
0.125	0.0009606
0.0625	0.0004826

The tabulated values of k' were plotted against $[H_2O_2]$ to obtain 2nd order rate constant as $k=9.33 \pm 0.64\ M^{-1}\ s^{-1}$.

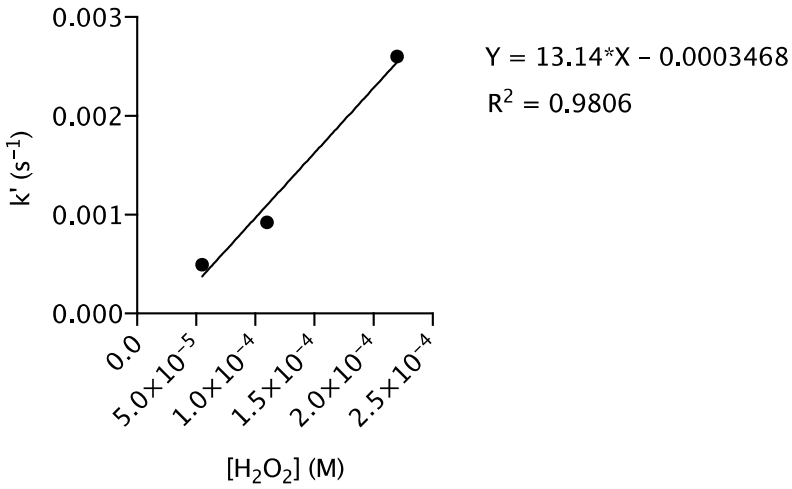

Figure 27. Plot of k' vs [H_2O_2]

Chiral HPLC chromatogram (Method A) :

1. Negative control (no added chiral ligand; racemic reaction performed in MeOH)

racemic **1.26**

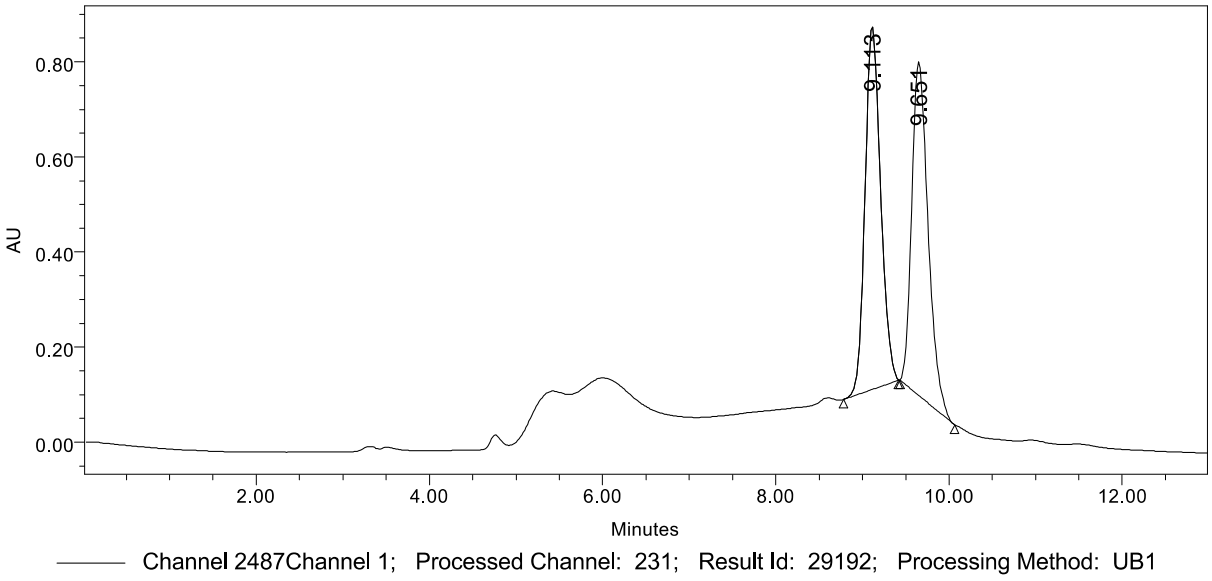

Processed Channel Descr.: 231

	Processed Channel Descr.	RT	Area	% Area	Height
1	231	9.113	9493518	50.64	762861
2	231	9.651	9254415	49.36	701357

Figure 28. Racemic **1.26**

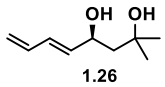

1.26

2. Ligand **L1** (1 equiv) in THF (Method A)

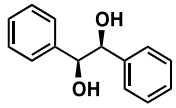

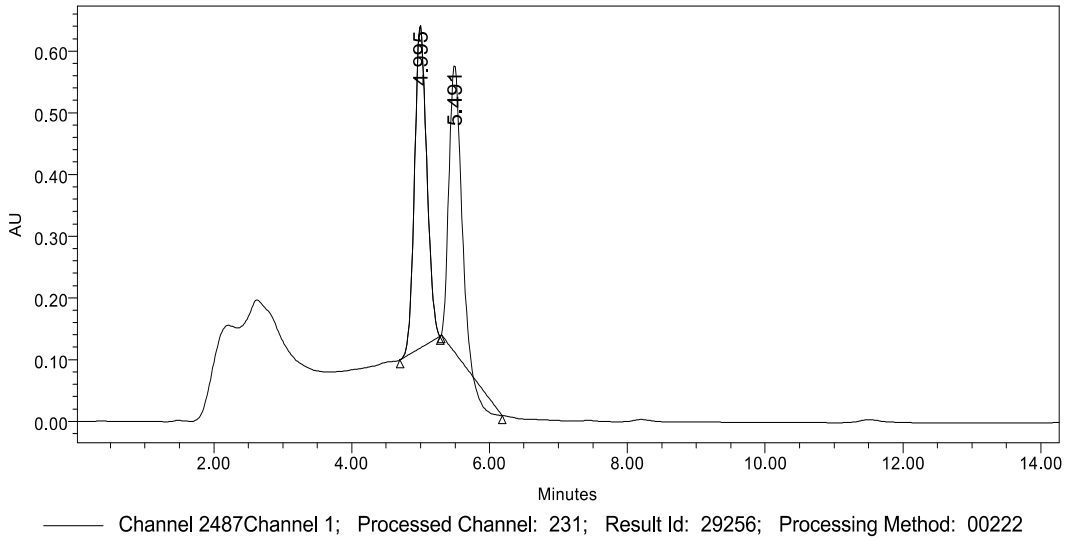

Processed Channel Descr.: 231

	Processed Channel Descr.	RT	Area	% Area	Height
1	231	4.995	6435054	50.83	522712
2	231	5.491	6224552	49.17	464438

Figure 29. Trial with ligand **L1**

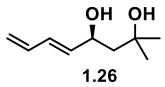

1.26

3. Ligand **L2** (1 equiv) in THF (Method A)

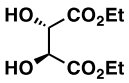

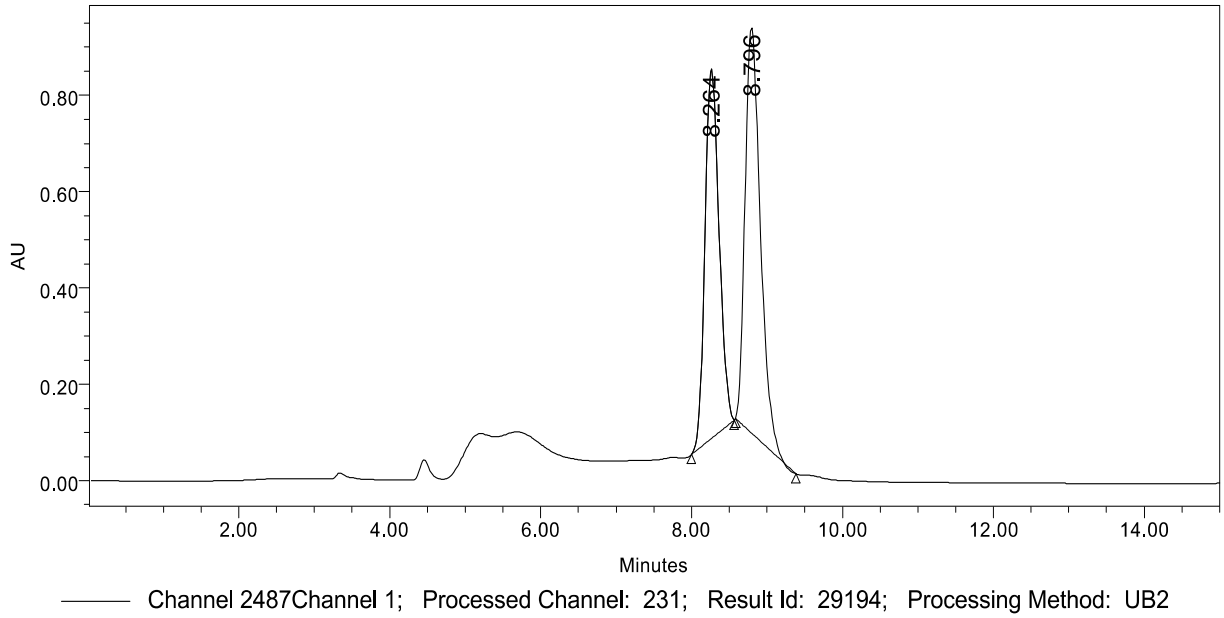

Processed Channel Descr.: 231

	Processed Channel Descr.	RT	Area	% Area	Height
1	231	8.264	9959254	45.55	767145
2	231	8.796	11907045	54.45	841530

Figure 30. Trial with ligand **L2**

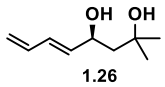

1.26

4. Ligand **L3** (1 equiv) in THF (Method A)

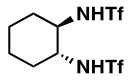

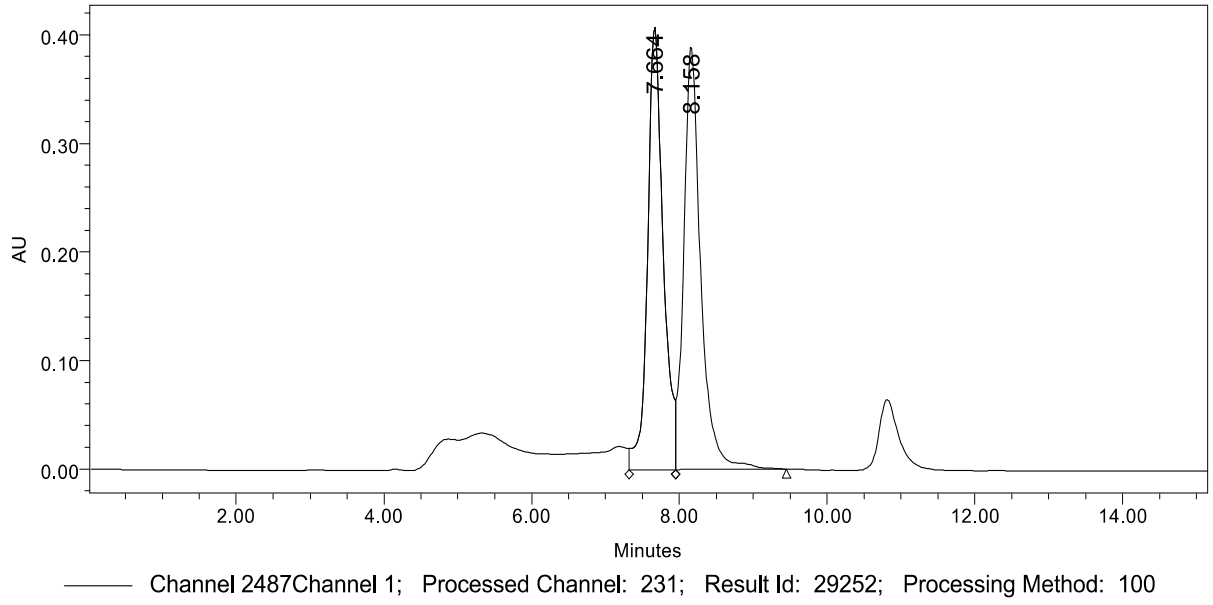

Processed Channel Descr.: 231

	Processed Channel Descr.	RT	Area	% Area	Height
1	231	7.664	5991732	49.08	407413
2	231	8.158	6215597	50.92	390108

Figure 31. Trial with ligand **L3**

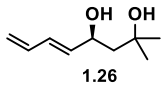

1.26

5. Ligand **L4** (1 equiv) in THF (Method A)

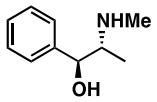

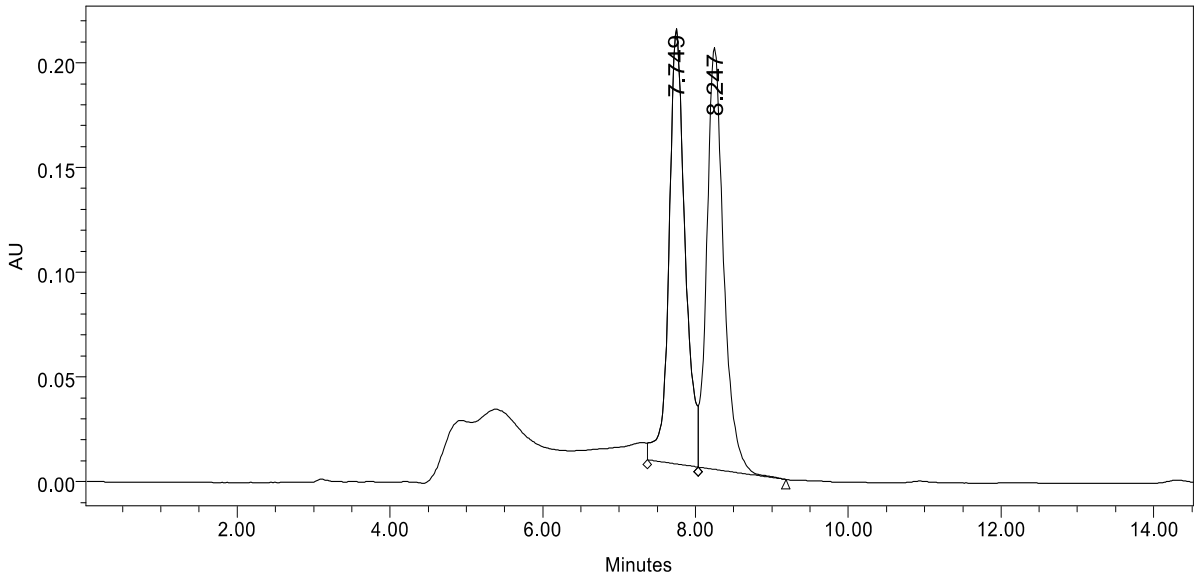

Processed Channel Descr.: 231

	Processed Channel Descr.	RT	Area	% Area	Height
1	231	7.749	3044610	49.78	207677
2	231	8.247	3071264	50.22	201316

Figure 32. Trial with ligand **L4**

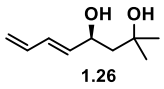

1.26

6. Ligand **L5** (1 equiv) in THF (Method A)

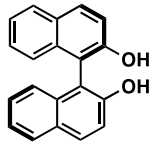

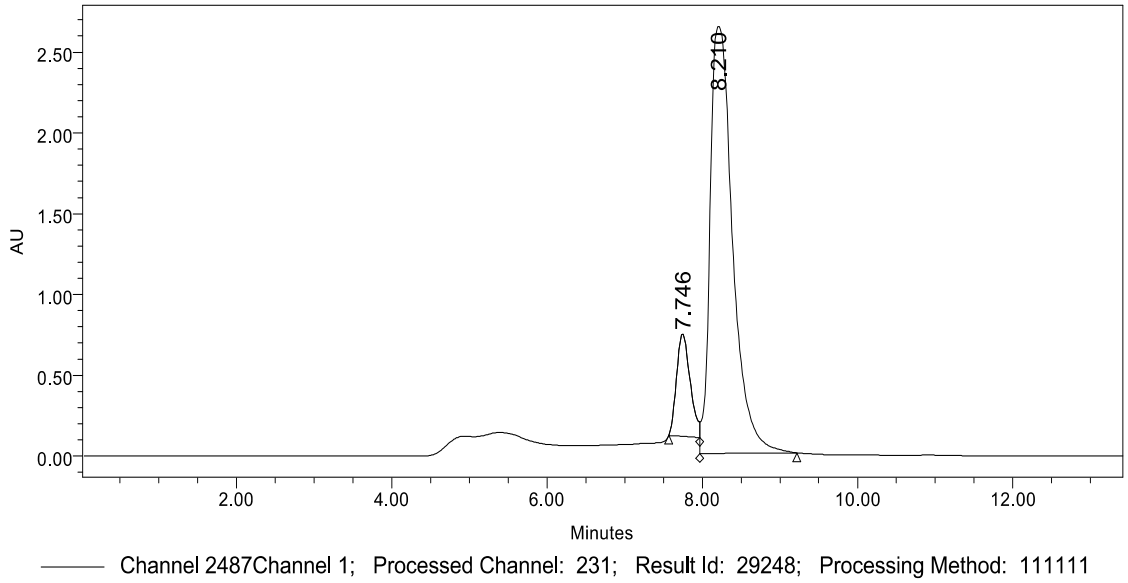

Processed Channel Descr.: 231

	Processed Channel Descr.	RT	Area	% Area	Height
1	231	7.746	7689715	12.56	633285
2	231	8.210	53558088	87.44	2646427

Figure 33. Trial with ligand **L5**

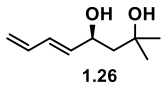

1.26

7. Ligand **L5** (0.5 equiv) in THF (Method A)

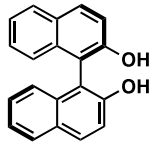

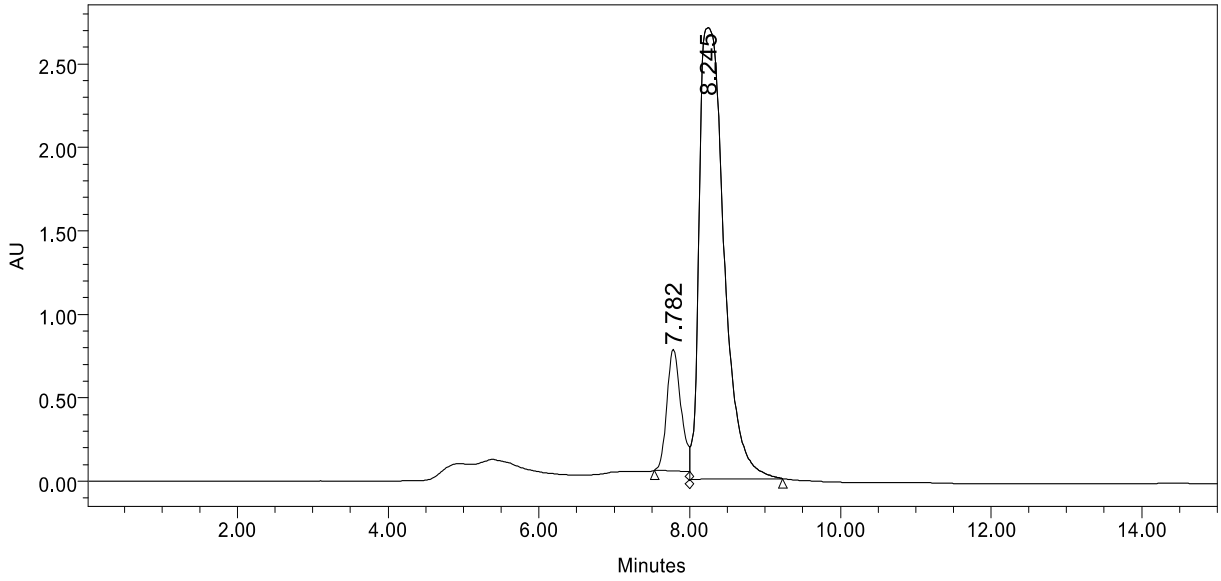

Processed Channel Descr.: 231

	Processed Channel Descr.	RT	Area	% Area	Height
1	231	7.782	9411261	13.19	728126
2	231	8.245	61952347	86.81	2705571

Figure 34. Trial with 0.5 equiv ligand **L5**

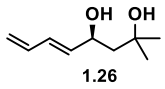

1.26

8. Ligand **L5** (0.2 equiv) in THF (Method A)

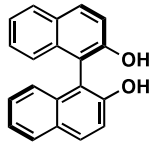

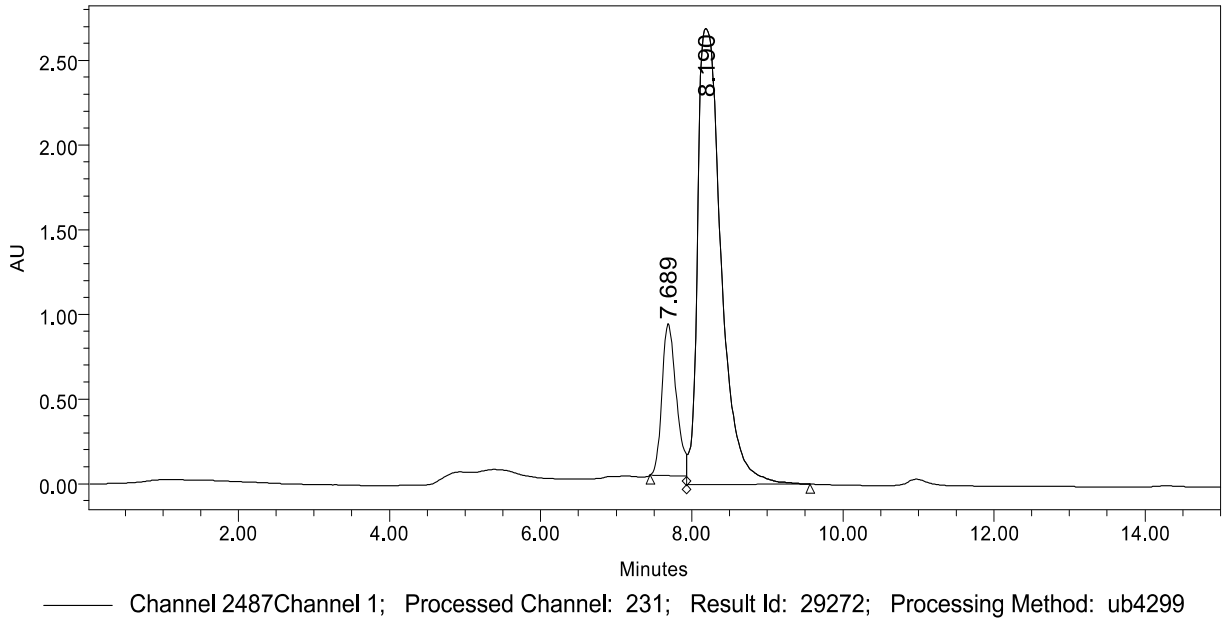

Processed Channel Descr.: 231

	Processed Channel Descr.	RT	Area	% Area	Height
1	231	7.689	11731510	16.74	899630
2	231	8.190	58353857	83.26	2693925

Figure 35. Trial with 0.2 equiv ligand **L5**

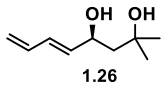

1.26

9. Ligand **L5** (0.1 equiv) in THF (Method A)

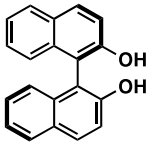

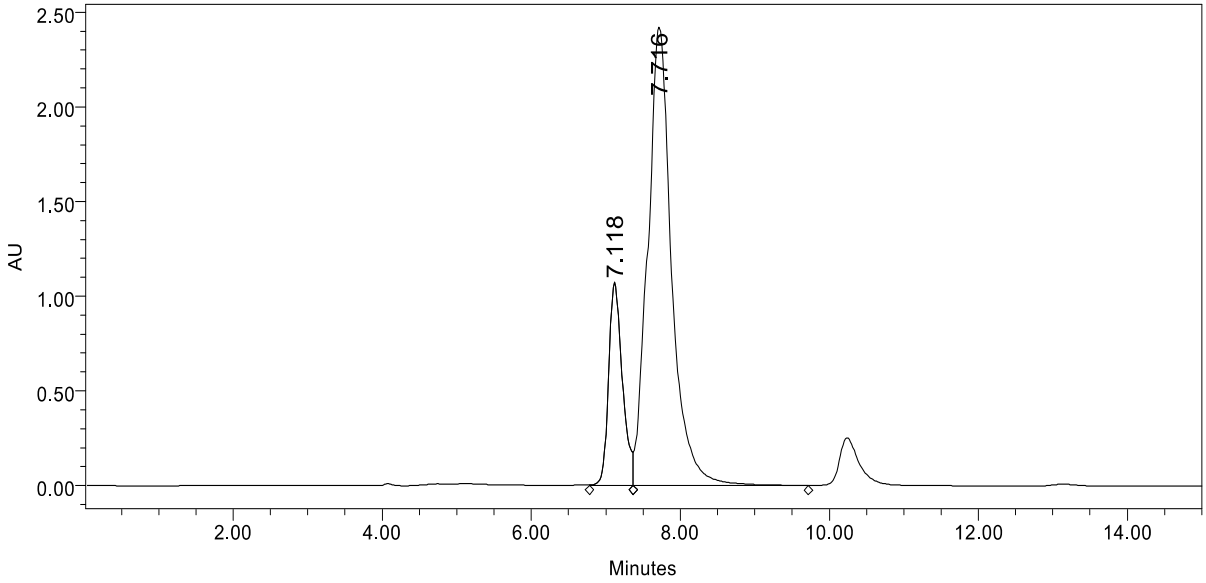

Processed Channel Descr.: 231

	Processed Channel Descr.	RT	Area	% Area	Height
1	231	7.118	13778486	20.36	1072350
2	231	7.716	53883773	79.64	2420818

Figure 36. Trial with 0.1 equiv ligand **L5**

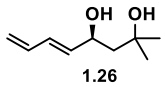

1.26

10. Ligand **L5** (0.05 equiv) in THF (Method A)

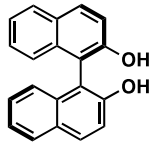

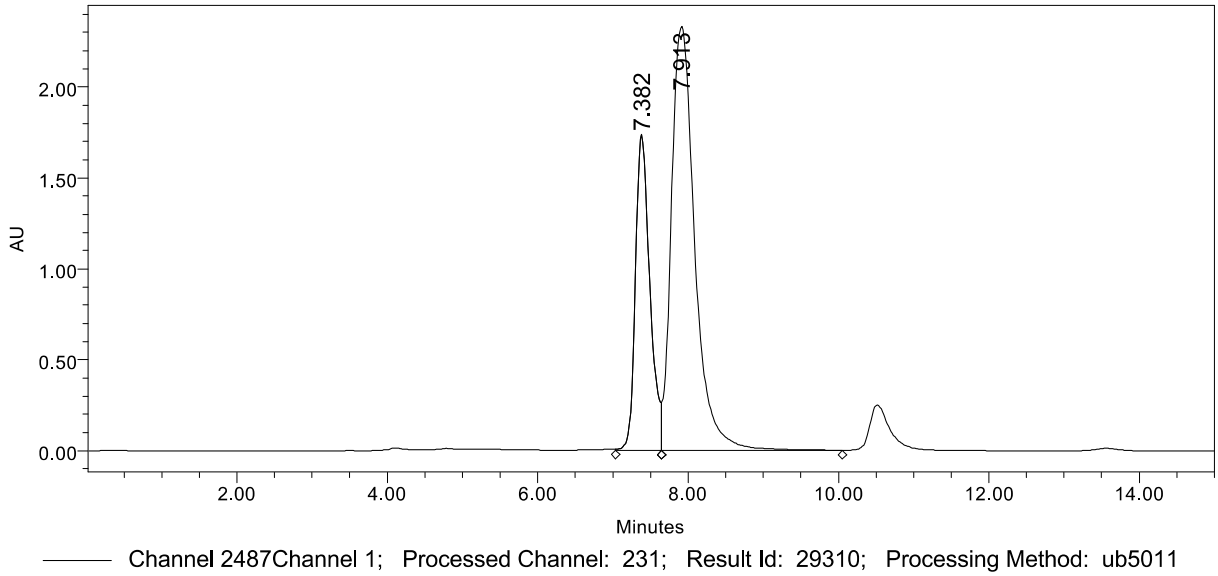

Processed Channel Descr.: 231

	Processed Channel Descr.	RT	Area	% Area	Height
1	231	7.382	23241163	31.52	1735669
2	231	7.913	50487265	68.48	2330938

Figure 37. Trial with 0.05 equiv ligand **L5**

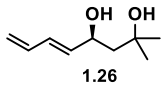

1.26

11. Ligand **L5** (0.02 equiv) in THF (Method A)

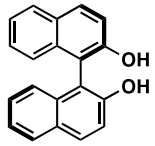

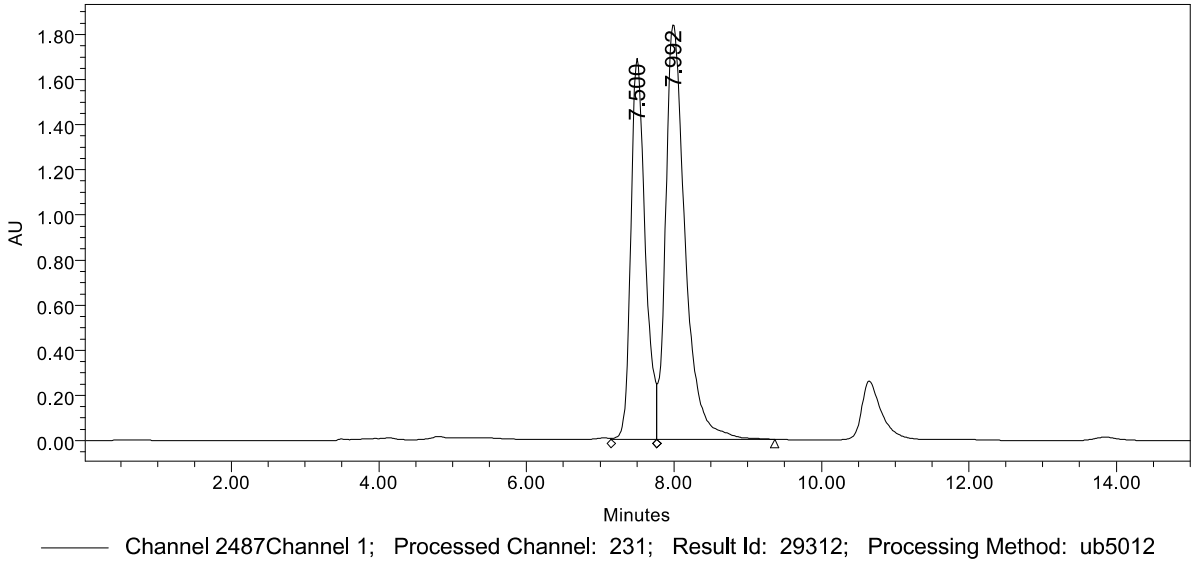

Processed Channel Descr.: 231

	Processed Channel Descr.	RT	Area	% Area	Height
1	231	7.500	22997415	40.45	1688843
2	231	7.992	33862941	59.55	1841789

Figure 38. Trial with 0.02 equiv ligand **L5**

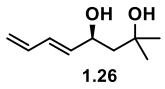

1.26

12. Ligand **L5** (0.5 equiv) in MeCN (method B)

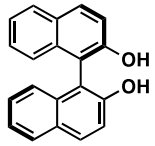

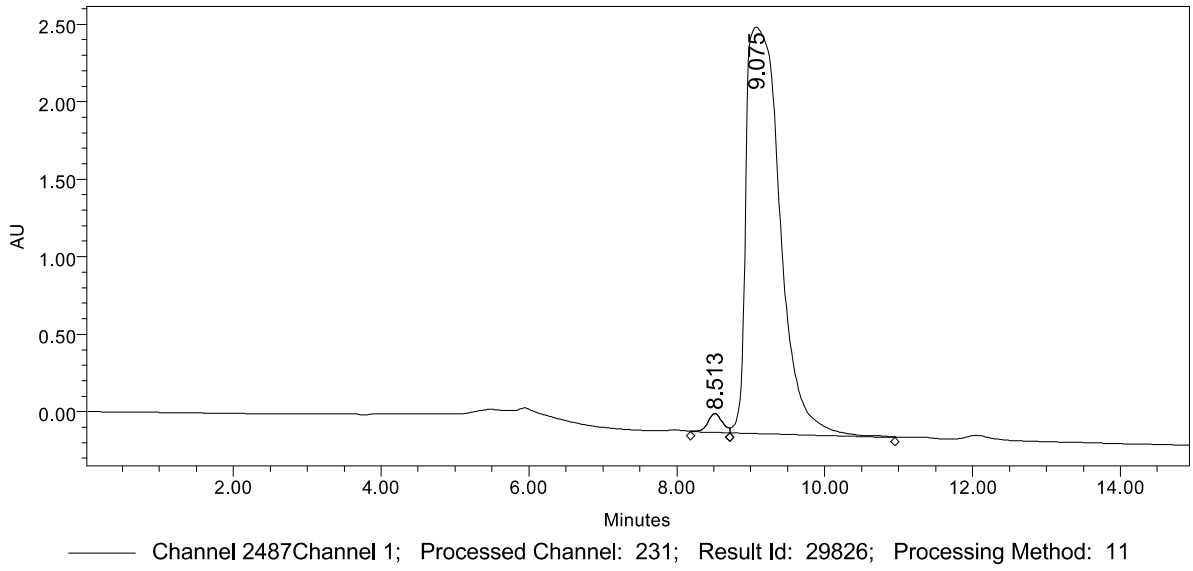

Processed Channel Descr.: 231

	Processed Channel Descr.	RT	Area	% Area	Height
1	231	8.513	1649310	1.93	121458
2	231	9.075	83678611	98.07	2621253

Figure 39. Trial with 0.5 equiv ligand **L5** in MeCN

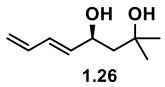

1.26

13. Ligand **L5** (0.2 equiv) in MeCN (method B)

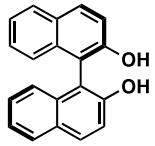

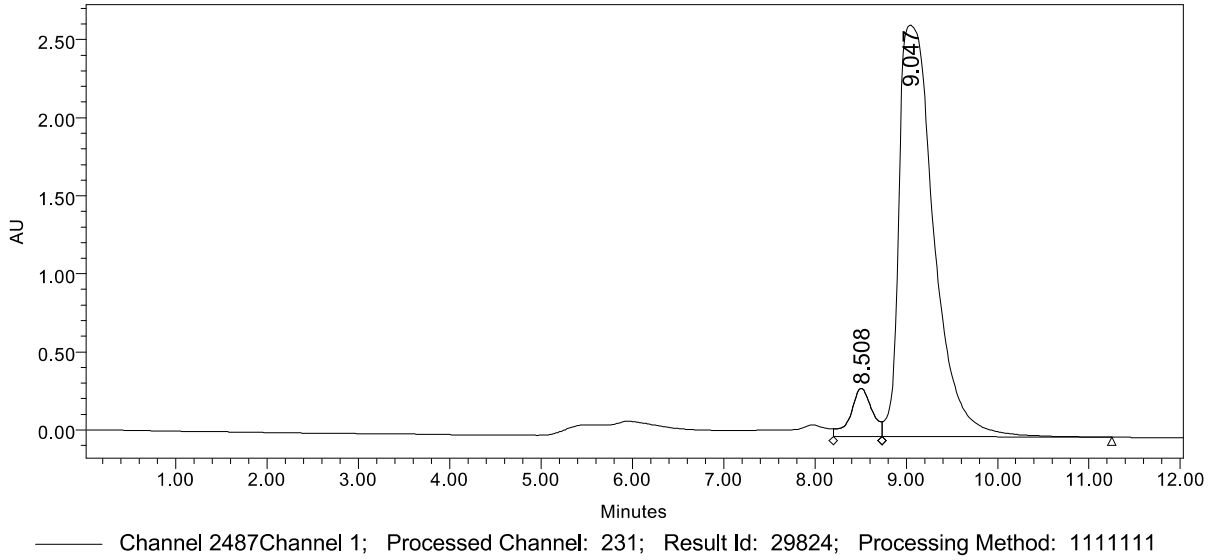

Processed Channel Descr.: 231

	Processed Channel Descr.	RT	Area	% Area	Height
1	231	8.508	5008728	6.69	308966
2	231	9.047	69895266	93.31	2635816

Figure 40. Trial with 0.2 equiv ligand **L5** in MeCN

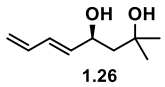

1.26

14. Ligand **L6** (0.2 equiv): (Note: 4% ^{i}PrOH in hexanes was used as eluent; crude reaction mixture was analysed without column chromatography)

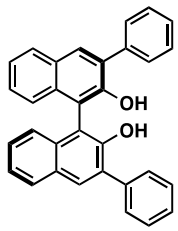

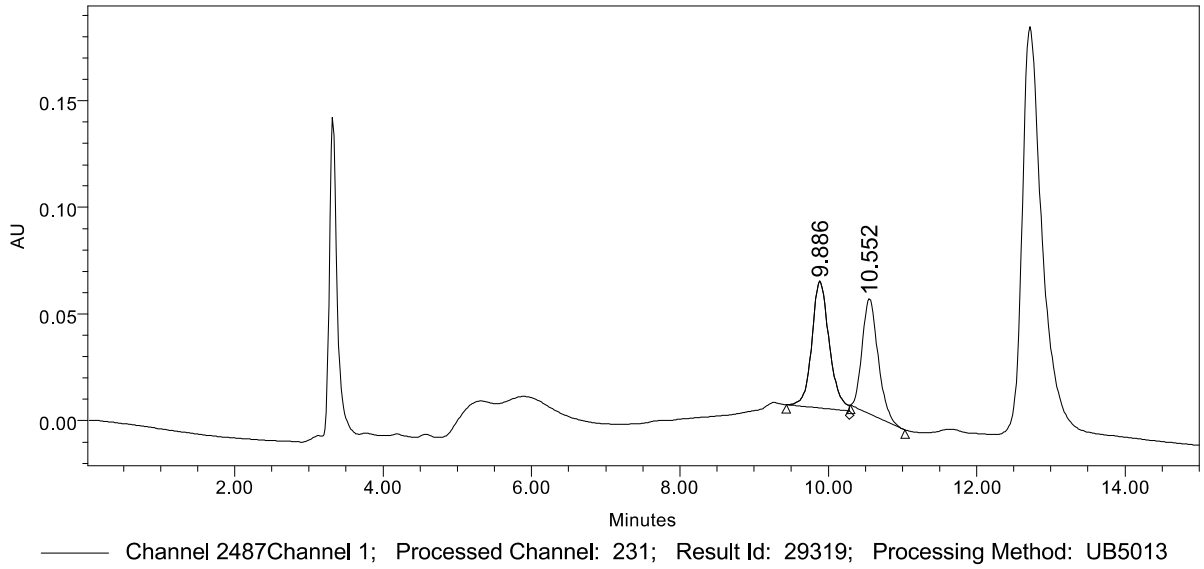

Processed Channel Descr.: 231

	Processed Channel Descr.	RT	Area	% Area	Height
1	231	9.886	977847	54.95	59492
2	231	10.552	801718	45.05	53823

Figure 41. Trial with ligand **L6**

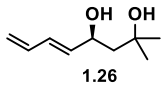

1.26

15. Ligand **L7** (0.2 equiv): (Note: 4% ^{i}PrOH in hexanes was used as eluent)

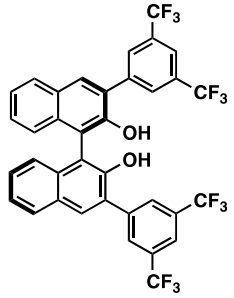

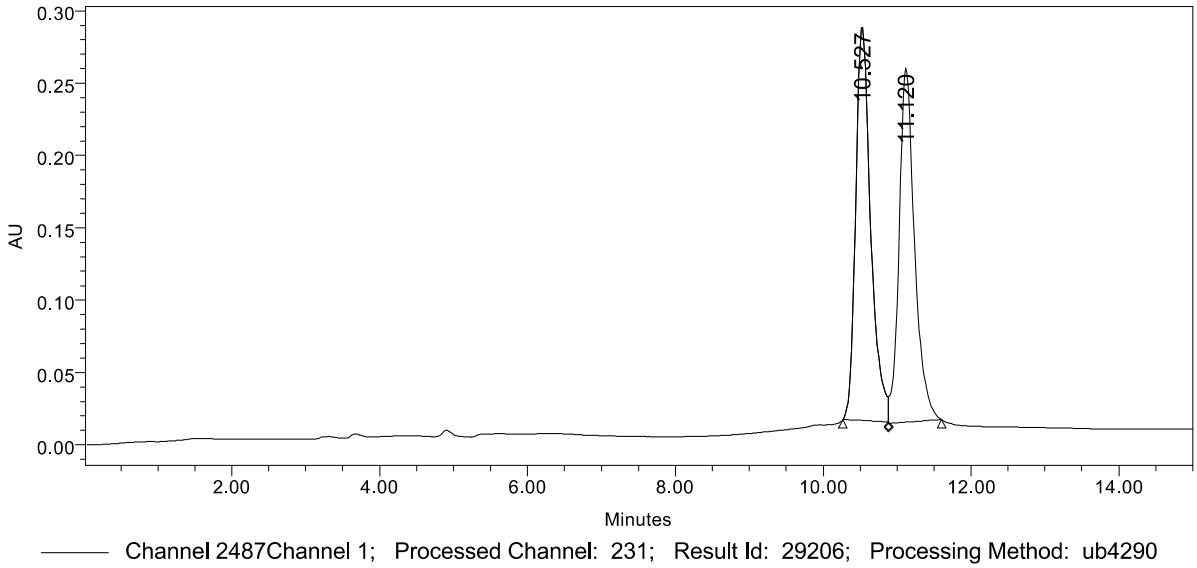

Processed Channel Descr.: 231

	Processed Channel Descr.	RT	Area	% Area	Height
1	231	10.527	3826058	51.83	272379
2	231	11.120	3556481	48.17	244843

Figure 42. Trial with ligand **L7**

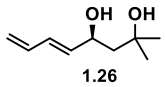

1.26

16. Ligand **L5** (1 equiv) (method C)

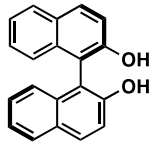

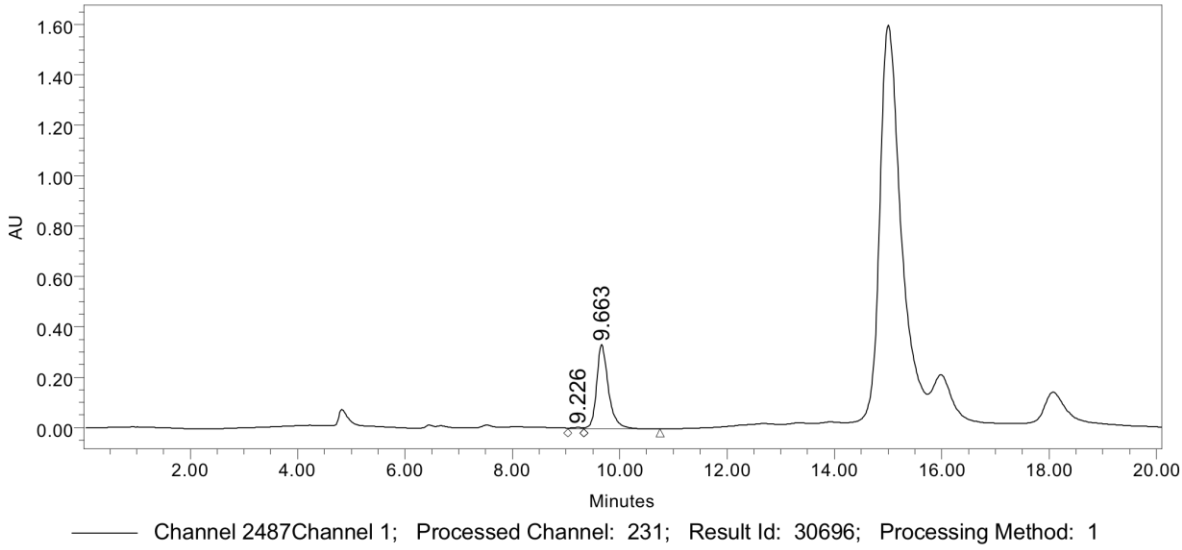

Processed Channel Descr.: 231

	Processed Channel Descr.	RT	Area	% Area	Height
1	231	9.226	91530	1.75	6459
2	231	9.663	5152085	98.25	335162

Figure 43. Trial with ligand **L5** (method C)

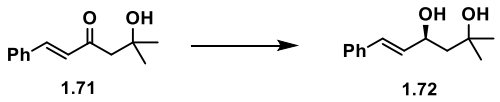

17. Ligand **:** none

Elution: 4% ^{i}PrOH in hexanes

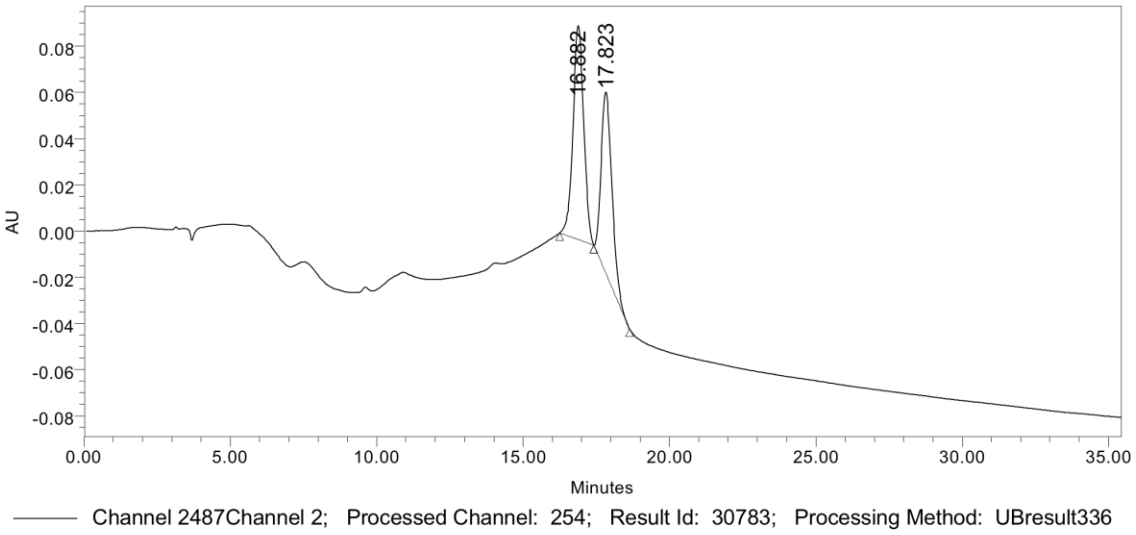

Processed Channel Descr.: 254

	Processed Channel Descr.	RT	Area	% Area	Height
1	254	16.882	2363721	53.89	92521
2	254	17.823	2022617	46.11	78279

Figure 44. Racemic **1.72**

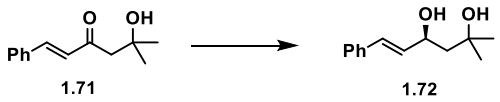

18. Ligand **: L5** (1 equiv) (method C)

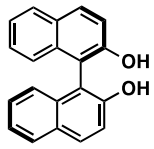

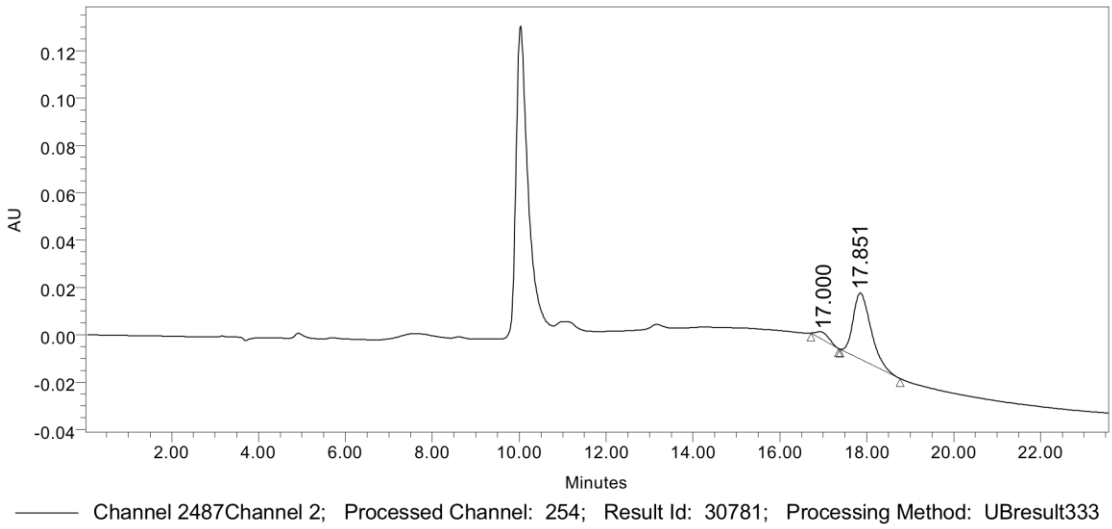

Processed Channel Descr.: 254

	Processed Channel Descr.	RT	Area	% Area	Height
1	254	17.000	61371	7.14	3083
2	254	17.851	798309	92.86	27978

Figure 45. Enantioenriched **1.72** with **L5**

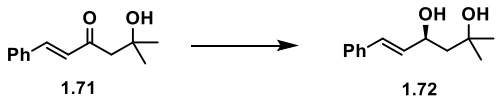

19. Ligand **: L5** (0.5 equiv) (method C)

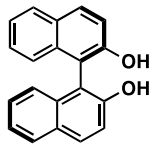

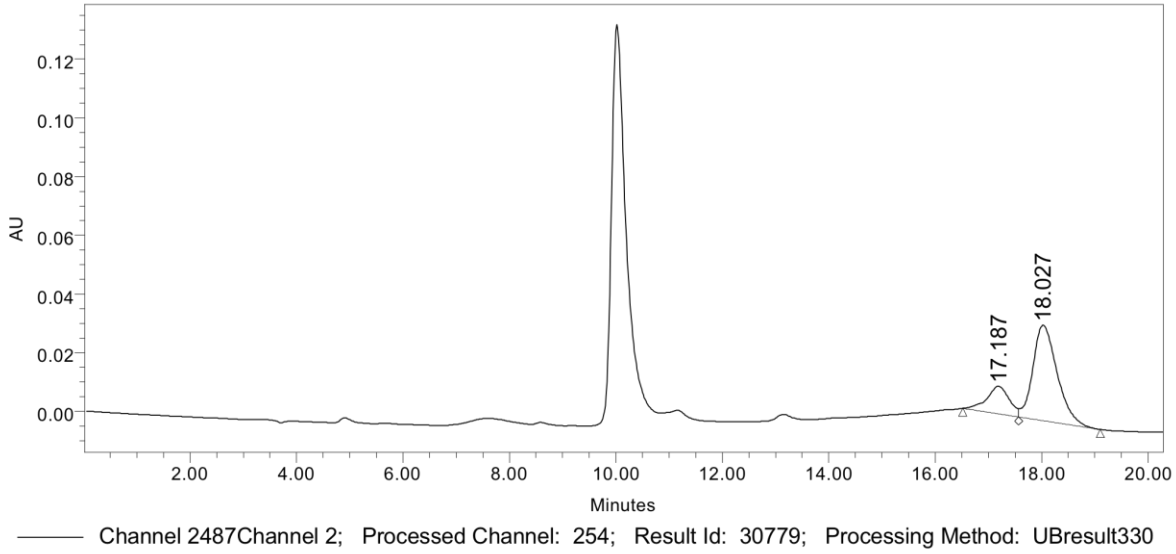

Processed Channel Descr.: 254

	Processed Channel Descr.	RT	Area	% Area	Height
1	254	17.187	280584	21.39	9416
2	254	18.027	1031347	78.61	32576

Figure 46. Enantioenriched **1.72** with **L5** (0.5 equiv)

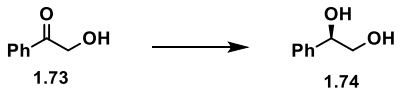

20. Ligand**:** none

Elution: 5% ^{i}PrOH in hexanes

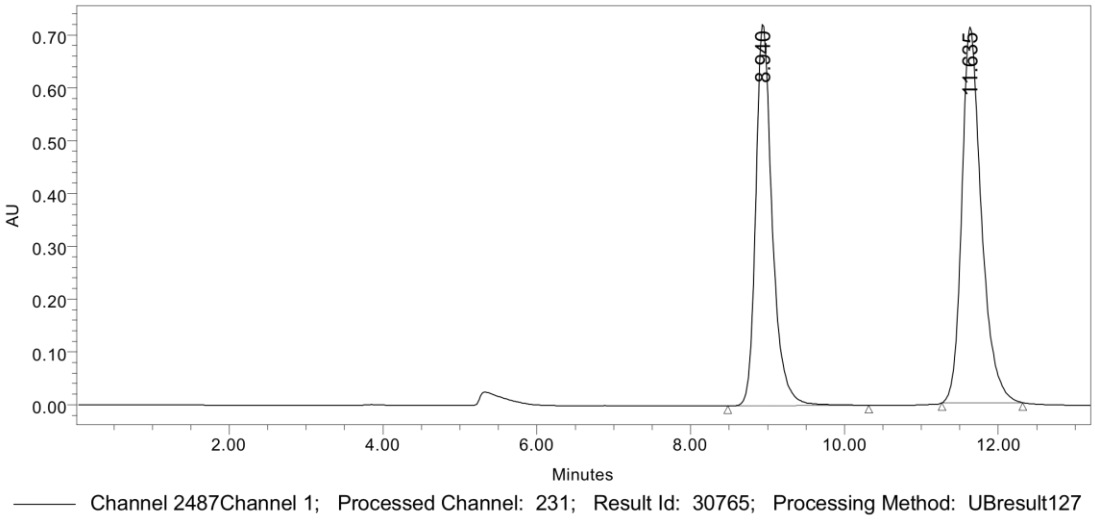

Processed Channel Descr.: 231

	Processed Channel Descr.	RT	Area	% Area	Height
1	231	8.940	10670168	48.40	722933
2	231	11.635	11377349	51.60	686839

Figure 47. Racemic **1.74**

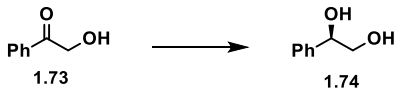

21. Ligand **: L5** (1 equiv) (method C)

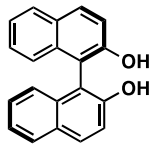

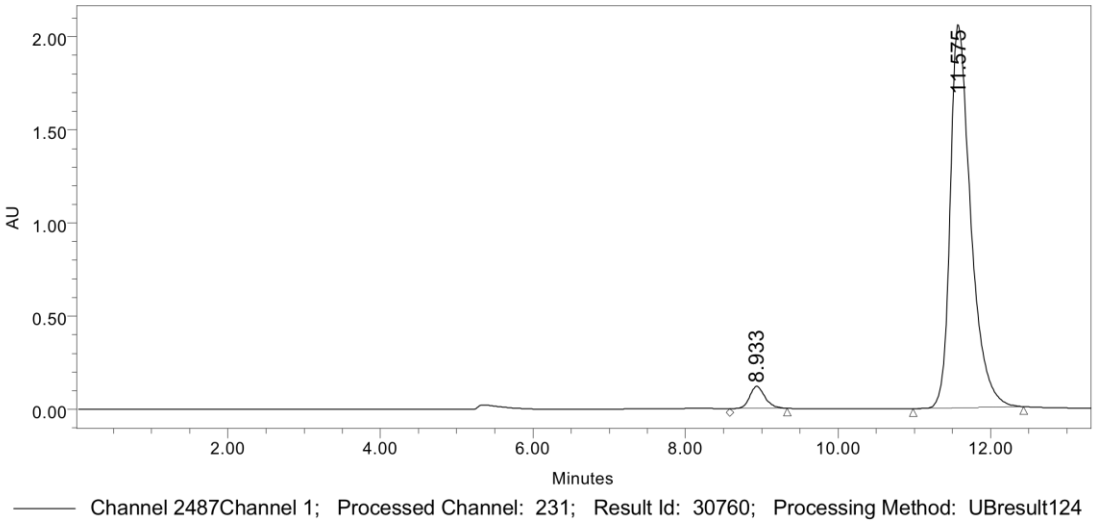

Processed Channel Descr.: 231

	Processed Channel Descr.	RT	Area	% Area	Height
1	231	8.933	1650060	4.11	119151
2	231	11.575	38525666	95.89	2061707

Figure 48. Enantioenriched **1.74** with **L5**

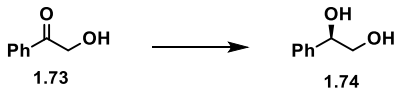

22. Ligand **: L5** (0.5 equiv) (method C)

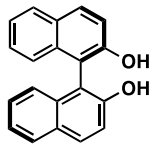

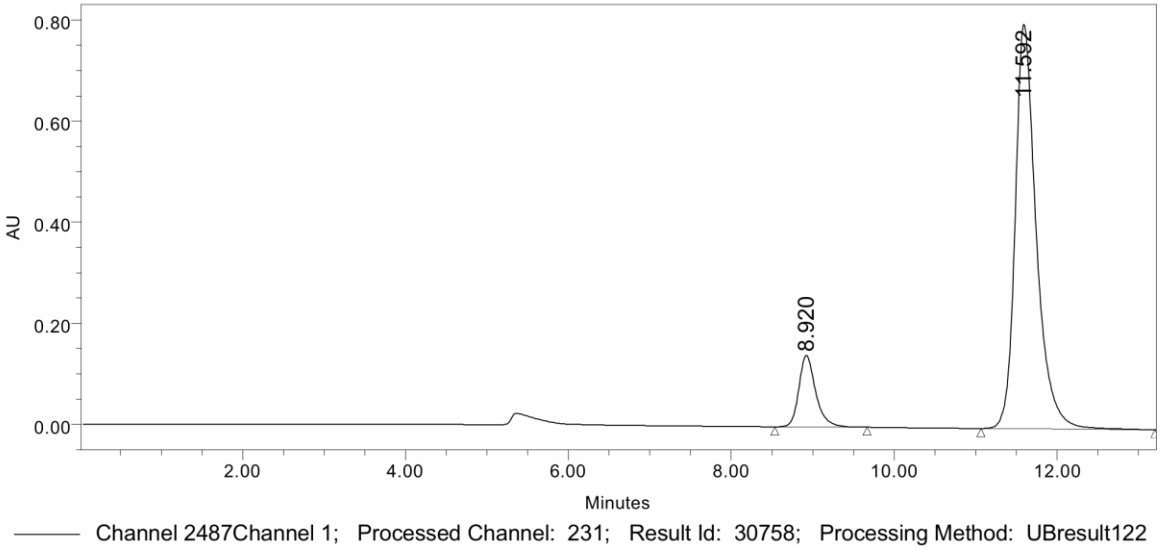

Processed Channel Descr.: 231

	Processed Channel Descr.	RT	Area	% Area	Height
1	231	8.920	2037160	12.39	142197
2	231	11.592	14402109	87.61	802426

Figure 49. Enantioenriched **1.74** with **L5** (0.5 equiv)

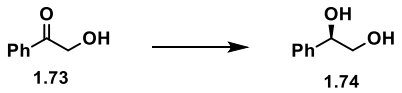

23. Ligand **: L5** (0.5 equiv), excess $NaBH_4$ (method C)

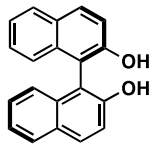

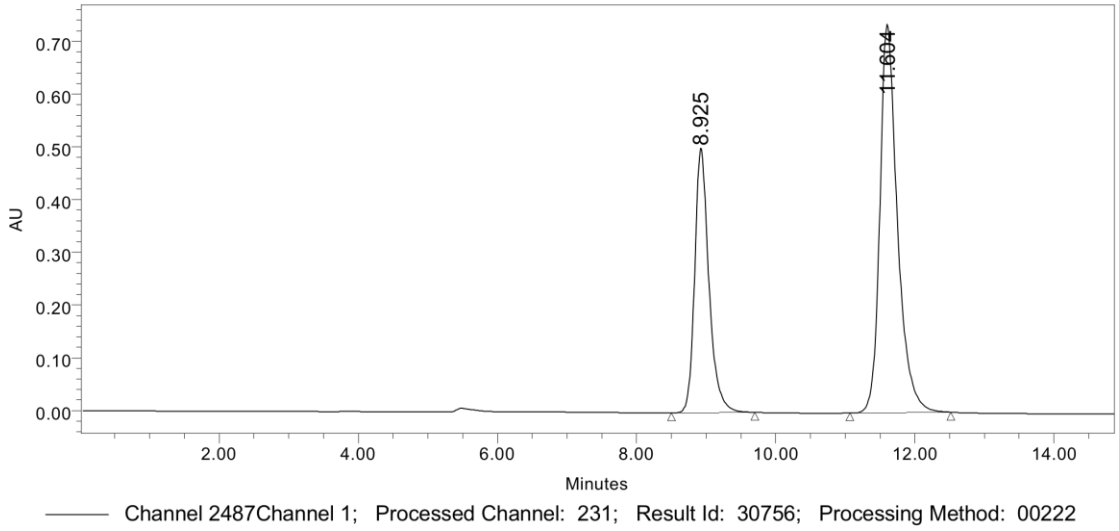

Processed Channel Descr.: 231

	Processed Channel Descr.	RT	Area	% Area	Height
1	231	8.925	7120256	35.45	503015
2	231	11.604	12967052	64.55	736754

Figure 50. Enantioenriched **1.74** with **L5** (0.5 equiv) and excess $NaBH_4$

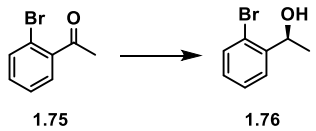

1.75 1.76

24. Ligand **:** none (method C)

Elution: 1% ^{i}PrOH in Hexanes

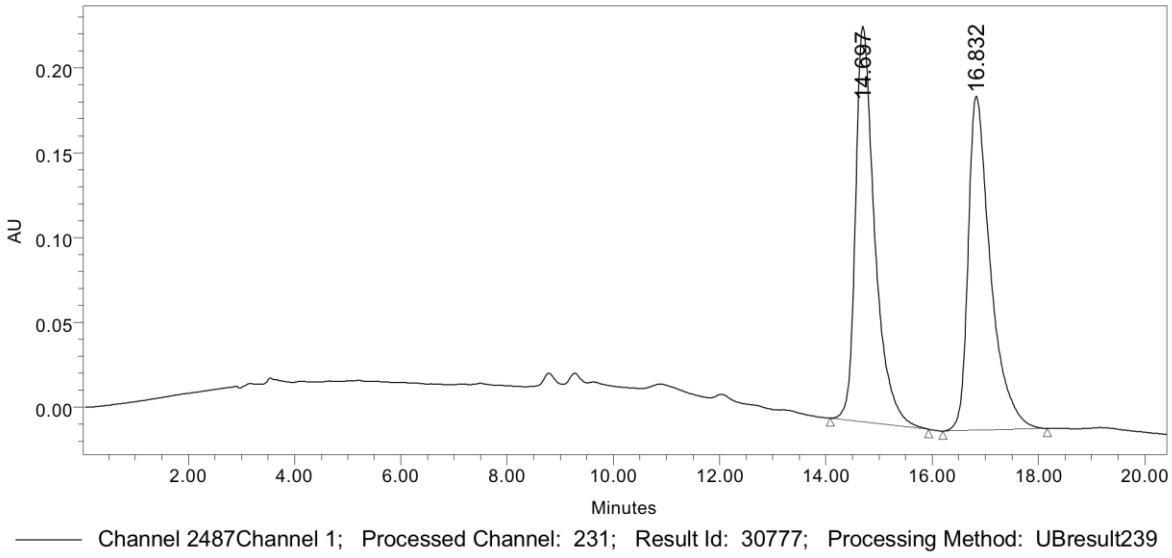

Processed Channel Descr.: 231

	Processed Channel Descr.	RT	Area	% Area	Height
1	231	14.697	5872107	50.48	233141
2	231	16.832	5759685	49.52	196743

Figure 51. Racemic **1.76**

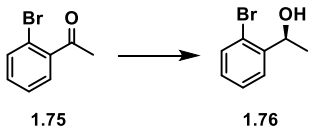

1.75 1.76

25. Ligand **: L5** 1 (equiv) (method C)

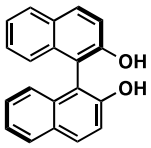

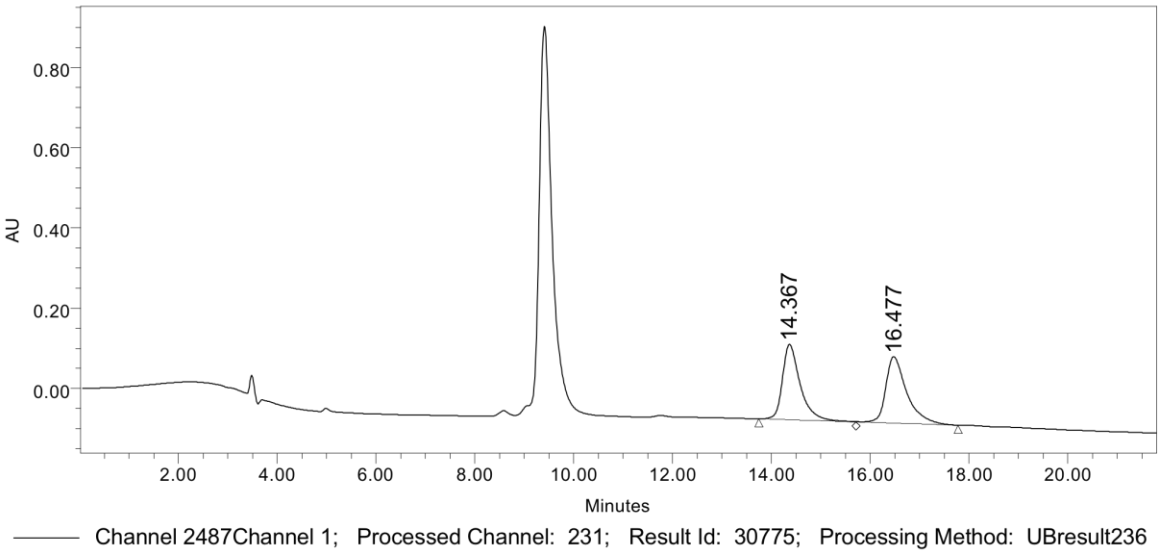

Processed Channel Descr.: 231

	Processed Channel Descr.	RT	Area	% Area	Height
1	231	14.367	4686103	48.94	187948
2	231	16.477	4889904	51.06	165588

Figure 52. Trial with **L5** to synthesize enantioenriched **1.76**

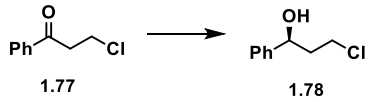

26. Ligand **:** none

Elution: 1% ^{i}PrOH in Hexanes

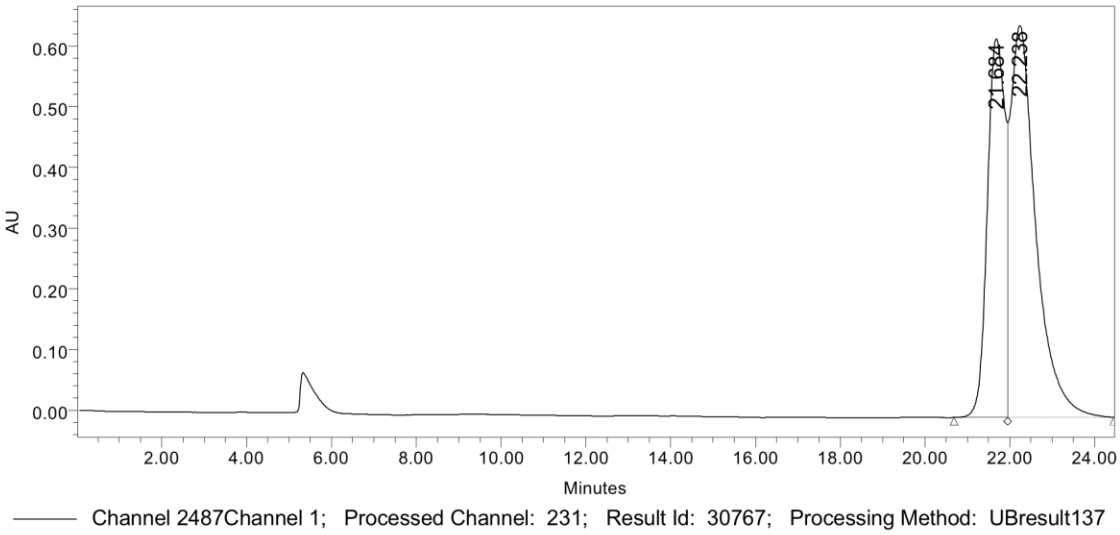

Processed Channel Descr.: 231

	Processed Channel Descr.	RT	Area	% Area	Height
1	231	21.684	18058806	40.06	624065
2	231	22.238	27022381	59.94	645482

Figure 53. Racemic **1.78**

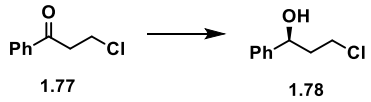

27. Ligand **: L5** (1 equiv) (method C)

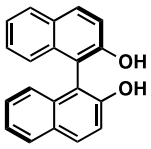

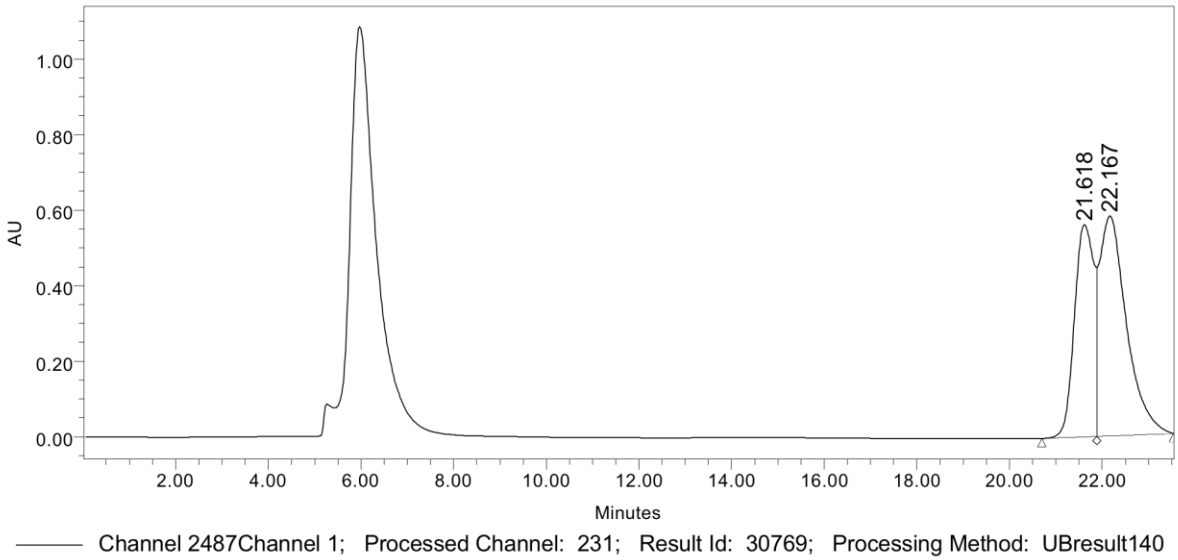

Processed Channel Descr.: 231

	Processed Channel Descr.	RT	Area	% Area	Height
1	231	21.618	16428458	41.02	562457
2	231	22.167	23620625	58.98	582512

Figure 54. Trial with **L5** to synthesize enantioenriched **1.78**

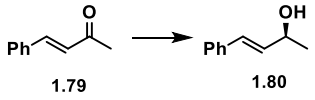

1.79 1.80

28. Ligand **:** none (method C)

Elution: 1% ^{i}PrOH in hexanes

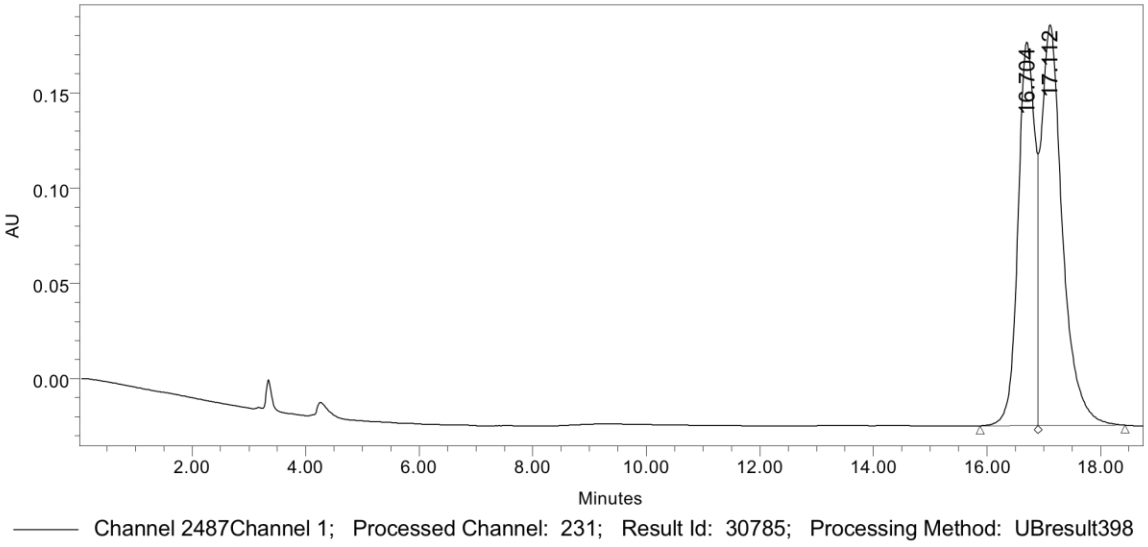

Processed Channel Descr.: 231

	Processed Channel Descr.	RT	Area	% Area	Height
1	231	16.704	4188091	43.17	201405
2	231	17.112	5512302	56.83	210348

Figure 55. Racemic **1.80**

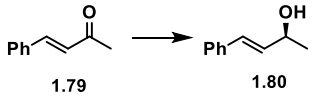

29. Ligand **: L5** (1 equiv) (method C)

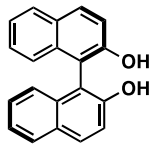

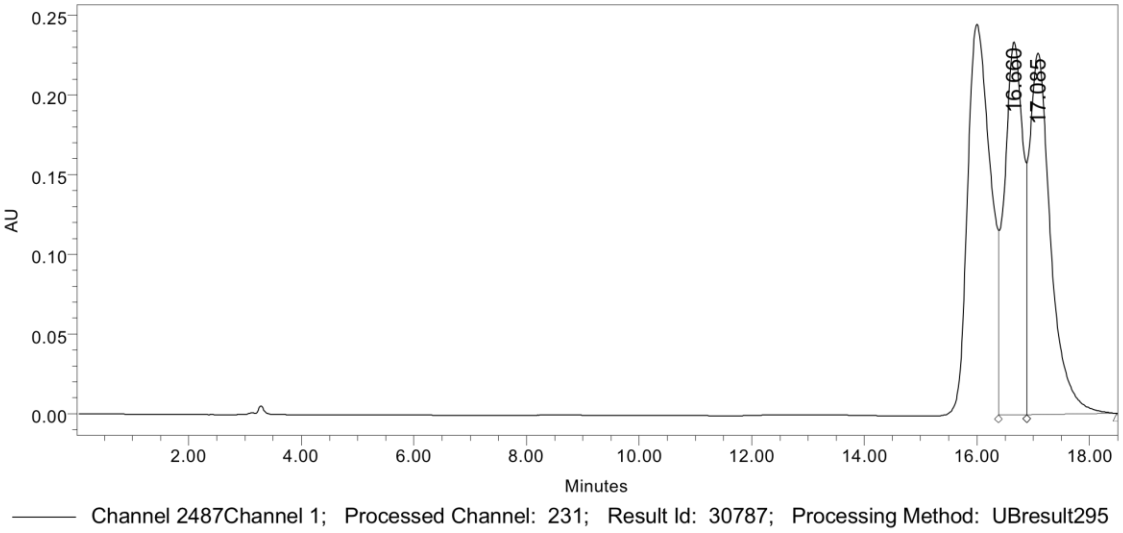

Processed Channel Descr.: 231

	Processed Channel Descr.	RT	Area	% Area	Height
1	231	16.660	5432322	47.62	233974
2	231	17.085	5975404	52.38	226833

Figure 56. Trial with **L5** to synthesize enantioenriched **1.80**

SPECTRA

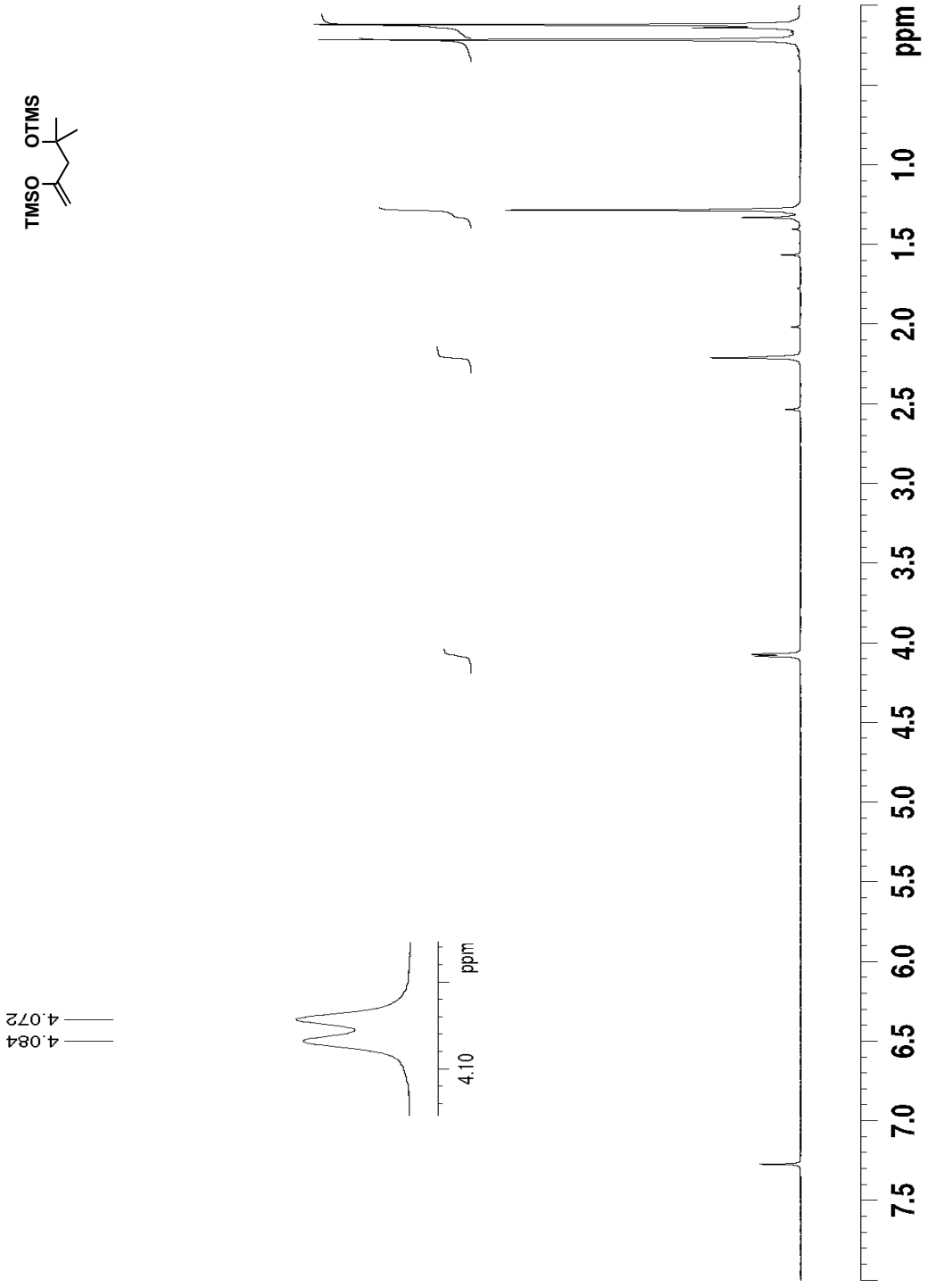

Spectrum 1. ^{1}H NMR spectrum of silyl enol ether **1.23** (300 MHz, $CDCl_3$, 293K)

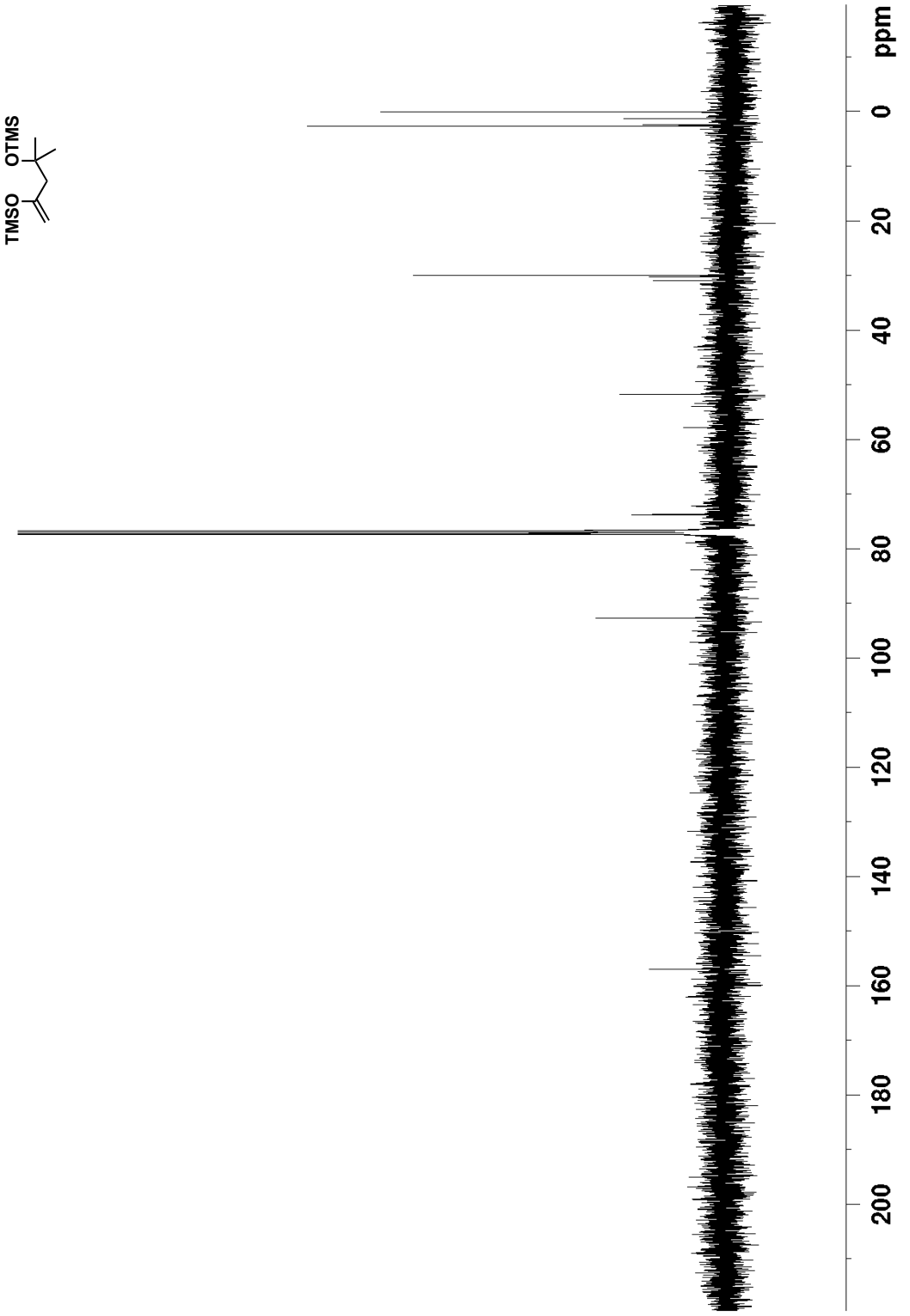

Spectrum 2. ^{13}C NMR spectrum of silyl enol ether **1.23** (100 MHz, $CDCl_3$, 293K)

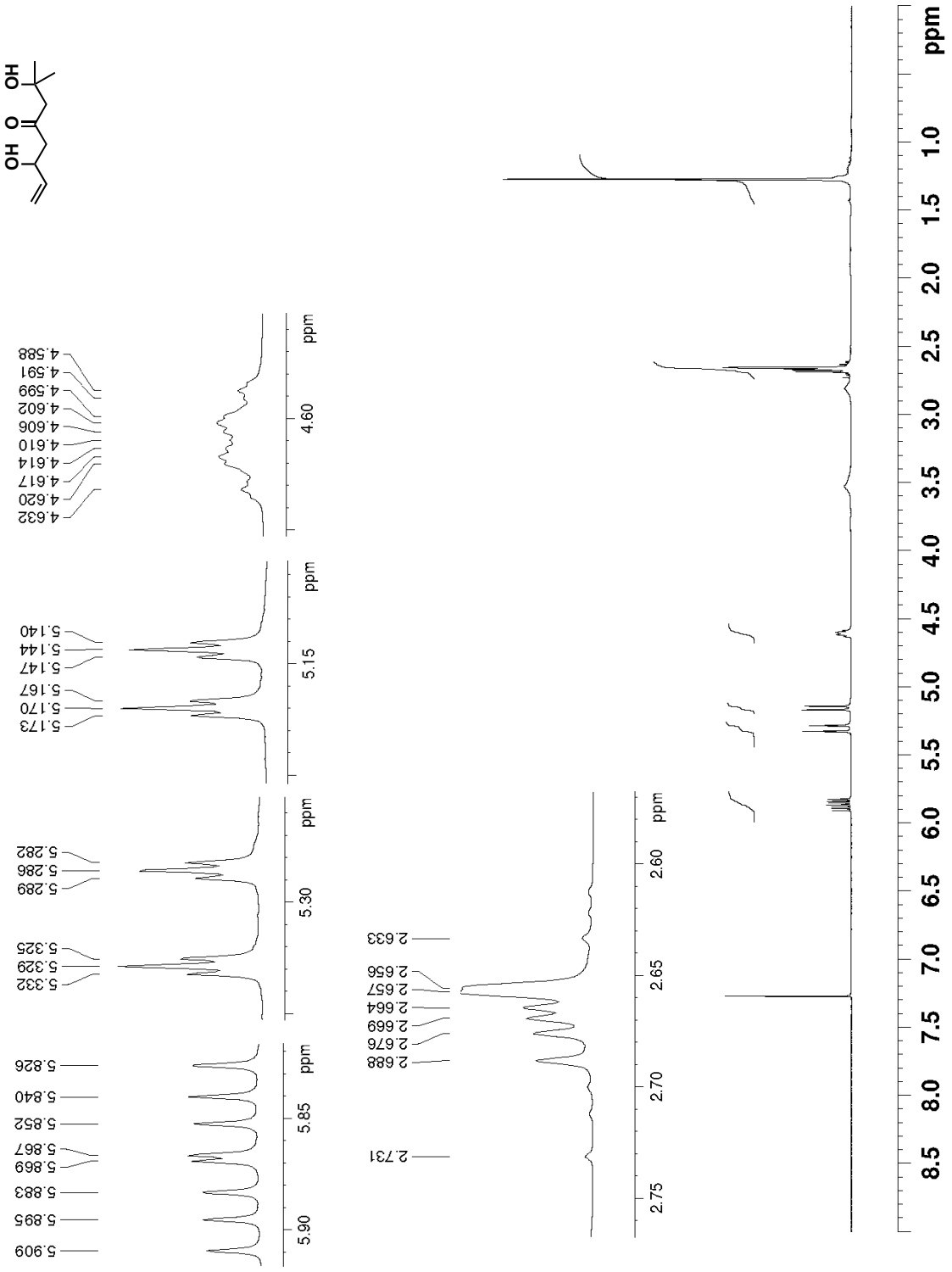

Spectrum 3. ^{1}H NMR spectrum of allylic alcohol **1.24** (300 MHz, 1% CD_3OD in $CDCl_3$, 293K)

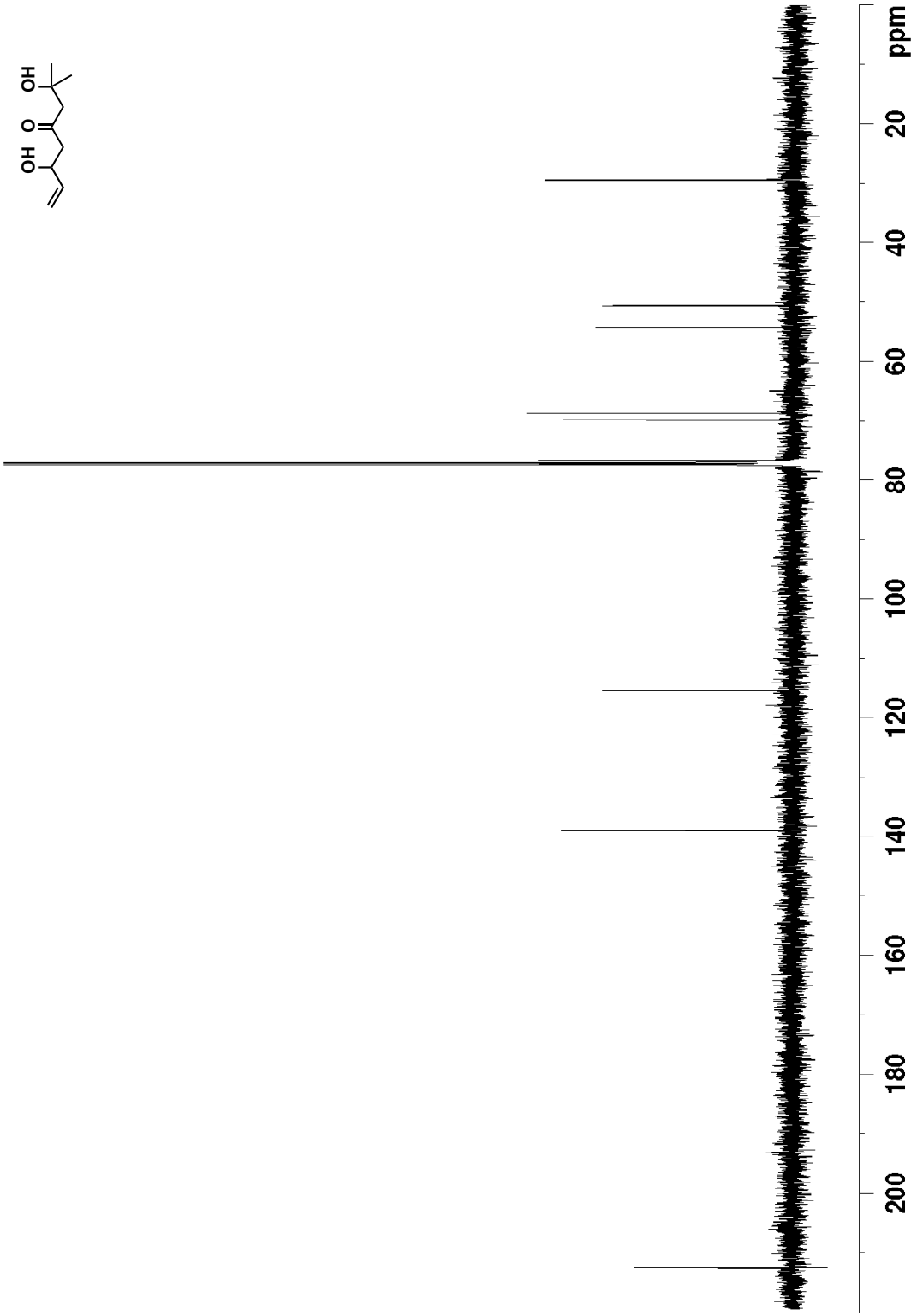

Spectrum 4. ^{13}C NMR spectrum of allylic alcohol **1.24** (100 MHz, $CDCl_3$, 293K)

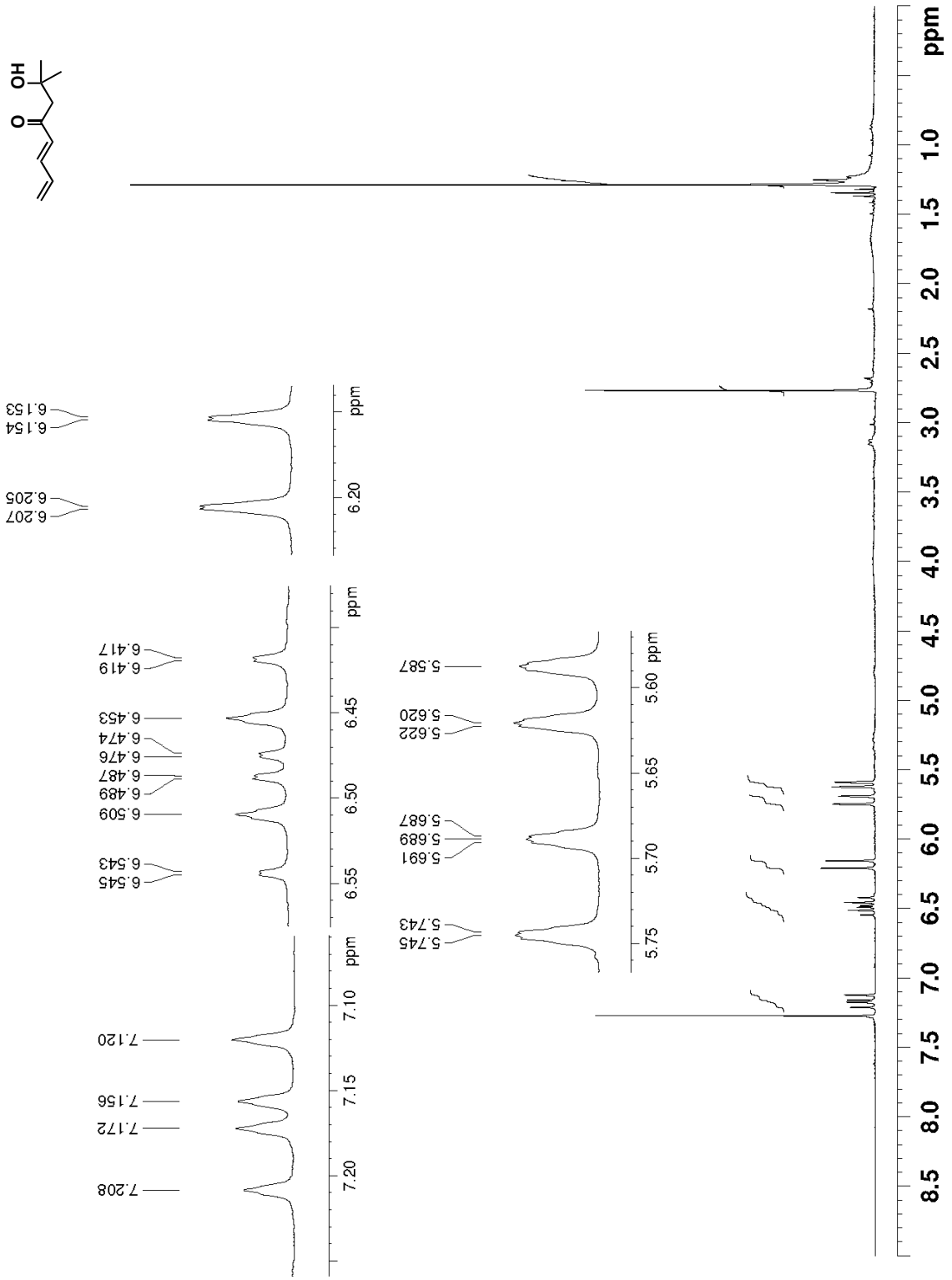

Spectrum 5. ^{1}H NMR spectrum of enone **1.25** (300 MHz, 1% CD_3OD in $CDCl_3$, 293K)

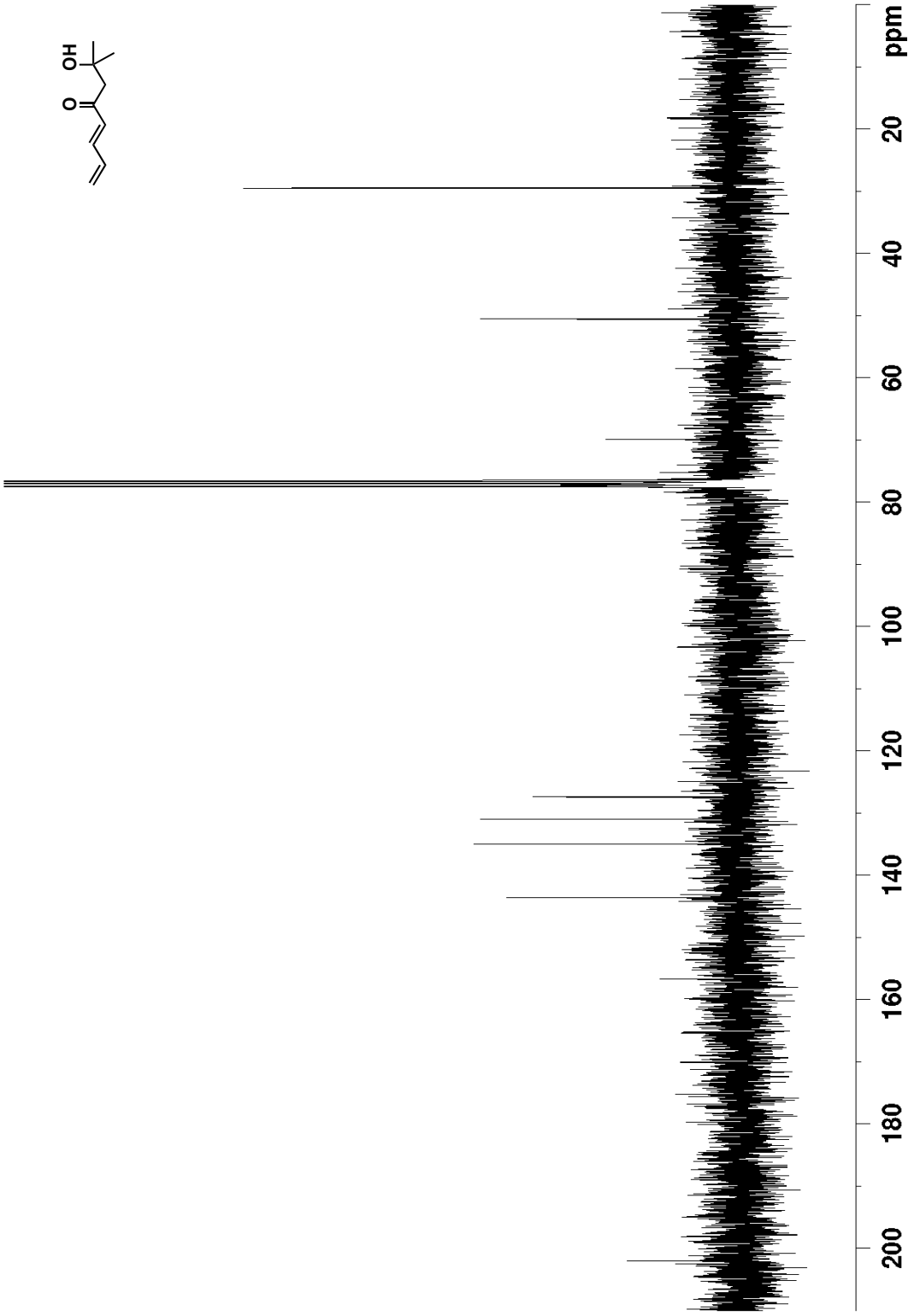

Spectrum 6. ^{13}C NMR spectrum of enone **1.25** (75 MHz, $CDCl_3$, 293K).

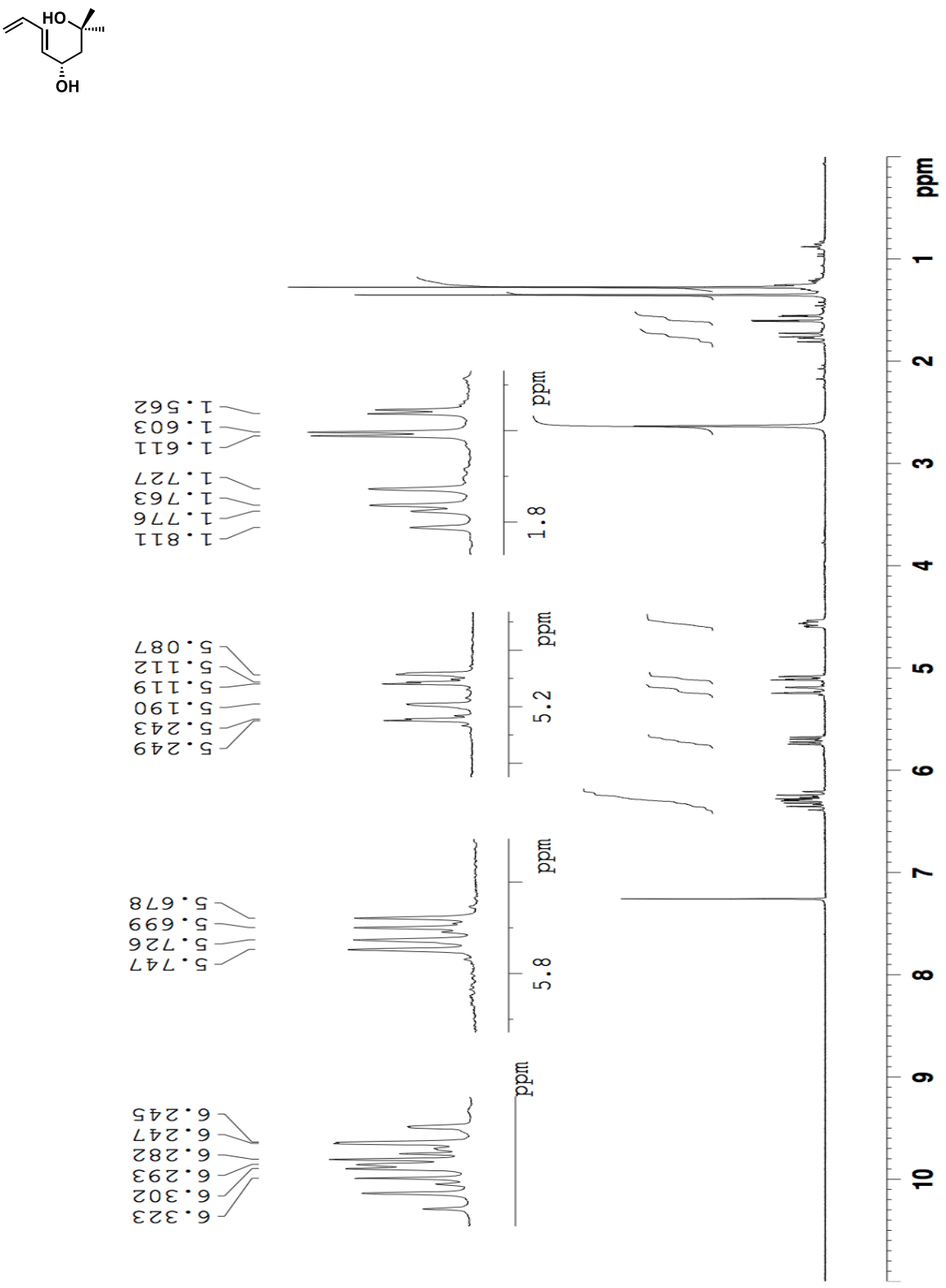

Spectrum 7. ^{1}H NMR spectrum of **1.26** (300 MHz, $CDCl_3$, 293K).

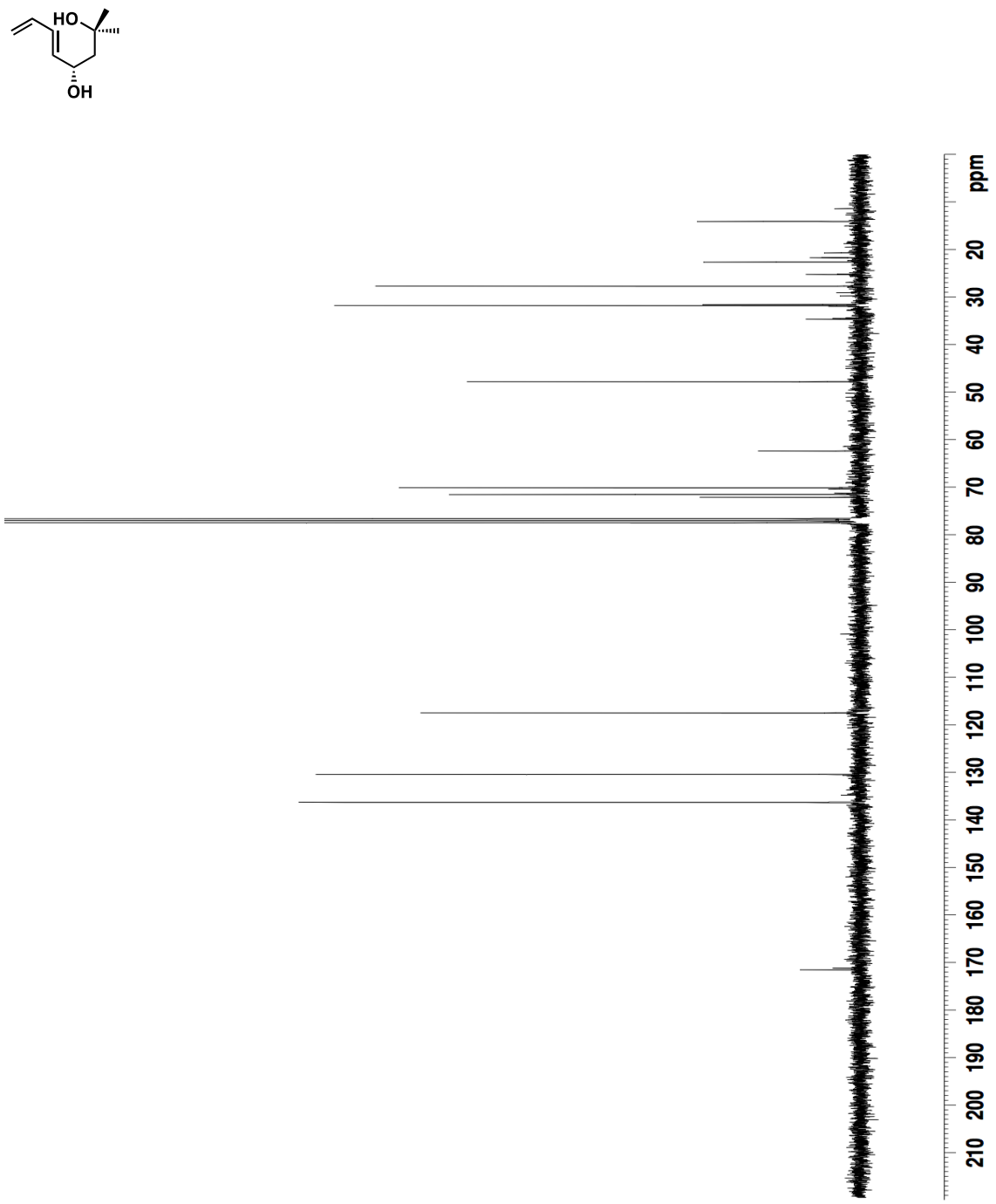

Spectrum 8. ^{13}C NMR spectrum of **1.26** (75 MHz, $CDCl_3$, 293K).

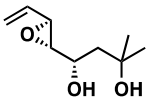

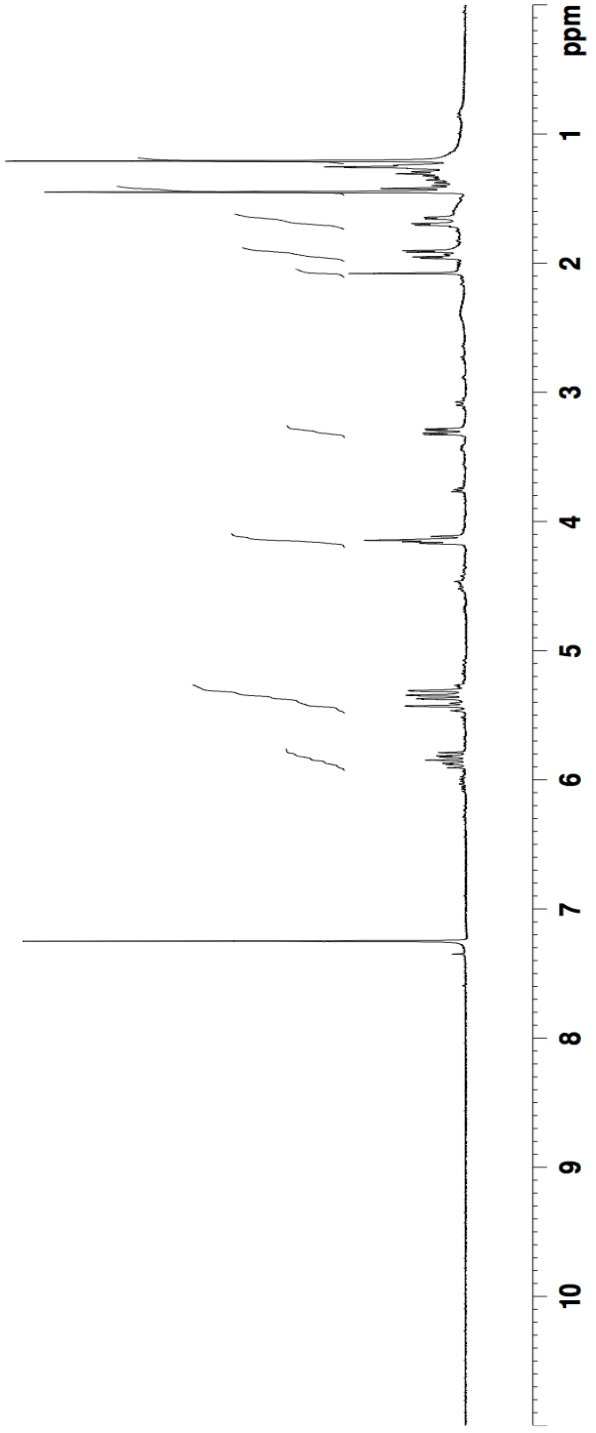

Spectrum 9. ^{1}H NMR spectrum of **1.27** (300 MHz, $CDCl_3$, 293K).

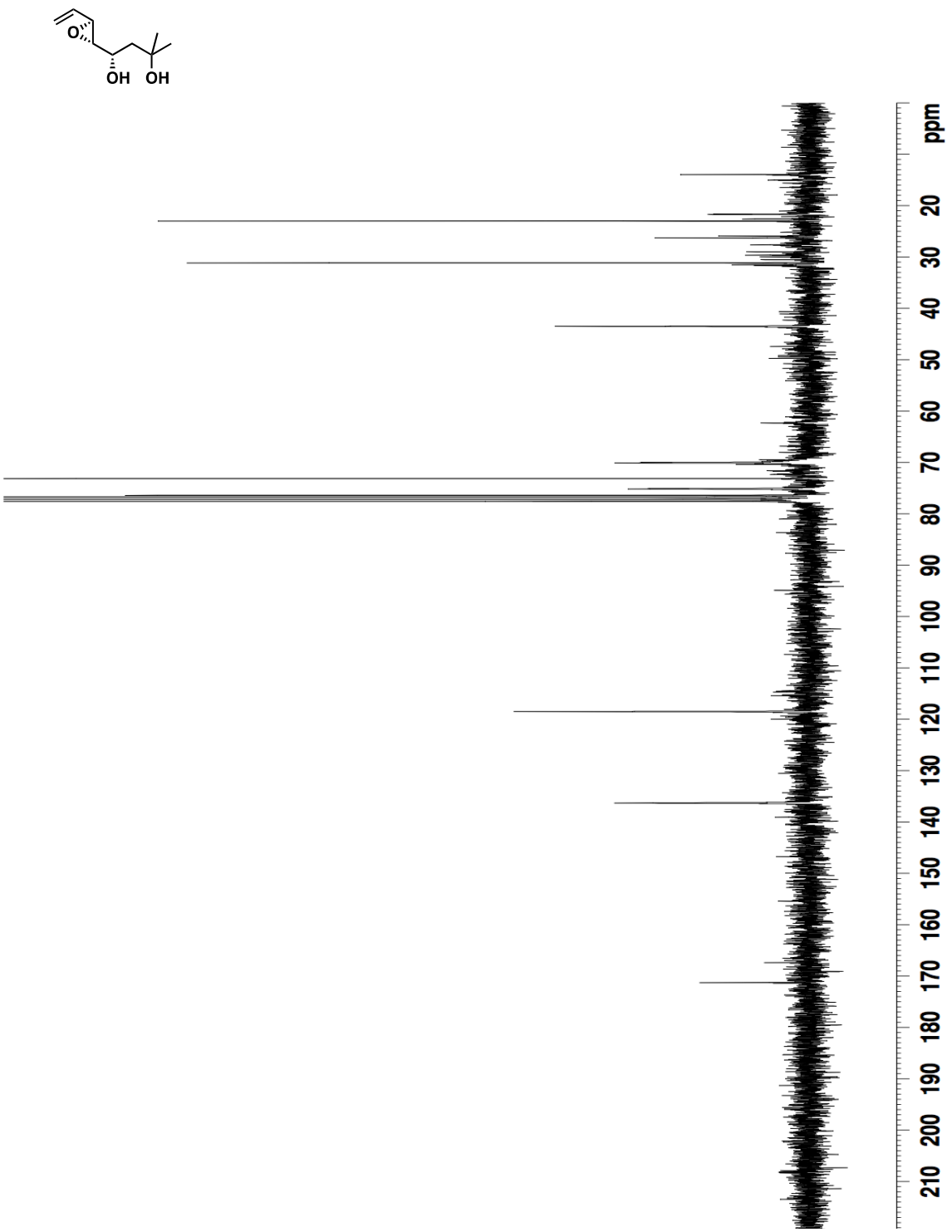

Spectrum 10. ^{13}C NMR spectrum of epoxide **1.27** (75 MHz, $CDCl_3$, 293K).

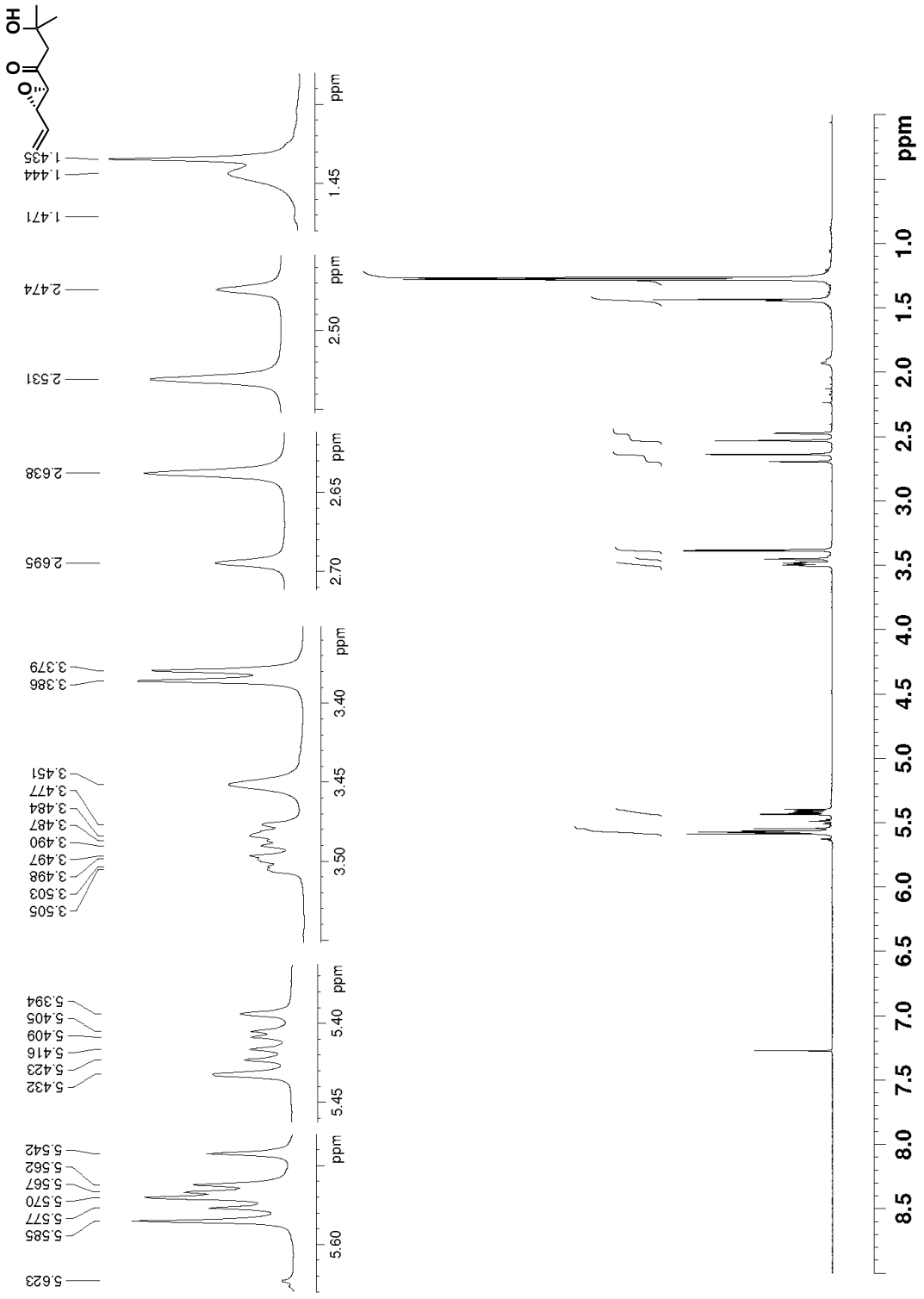

Spectrum 11. ^{1}H NMR of epoxide **1.28** (300 MHz, $CDCl_3$, 293K)

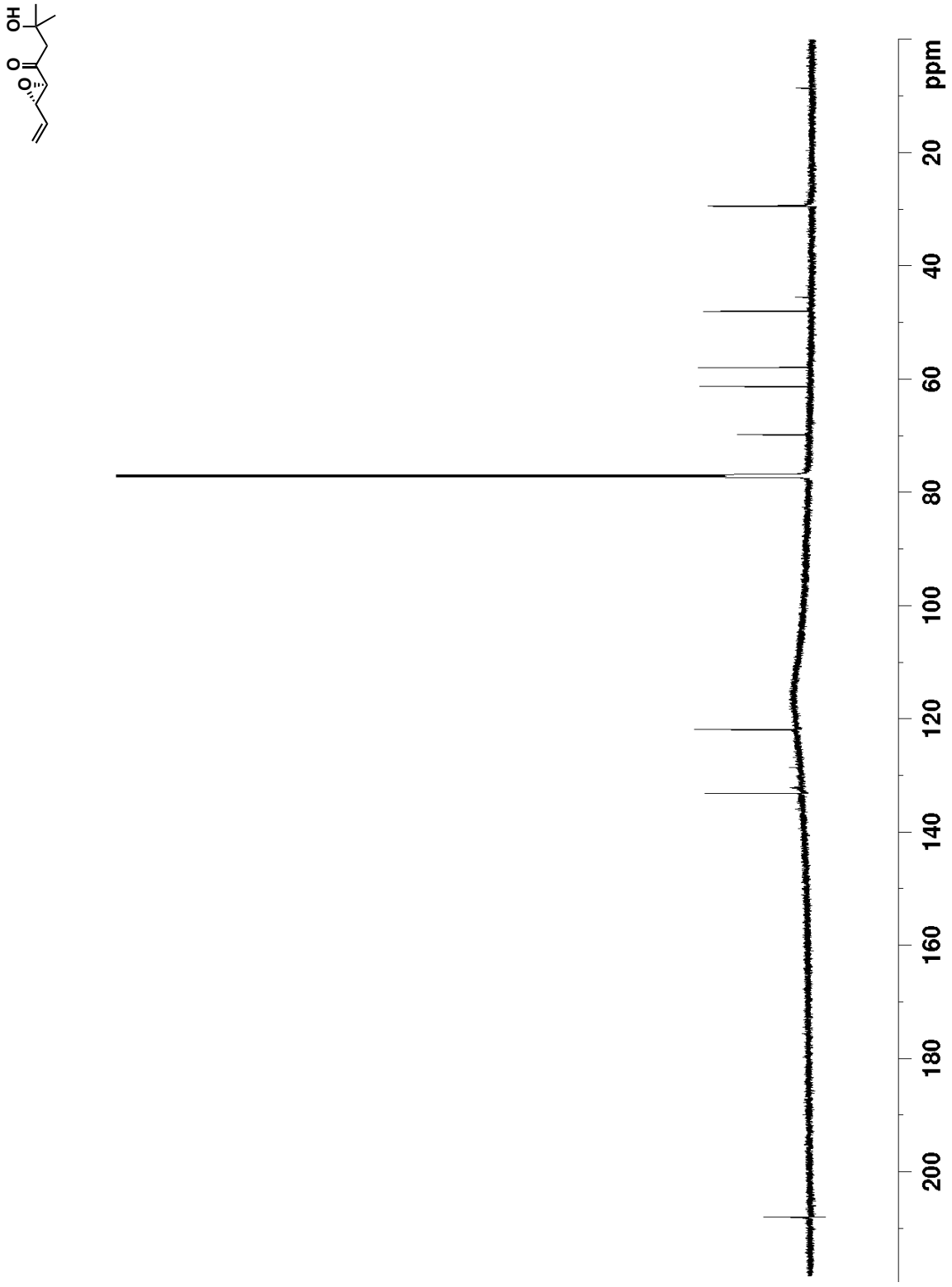

Spectrum 12. ^{13}C NMR spectrum of epoxide **1.28** (175 MHz, $CDCl_3$, 293K)

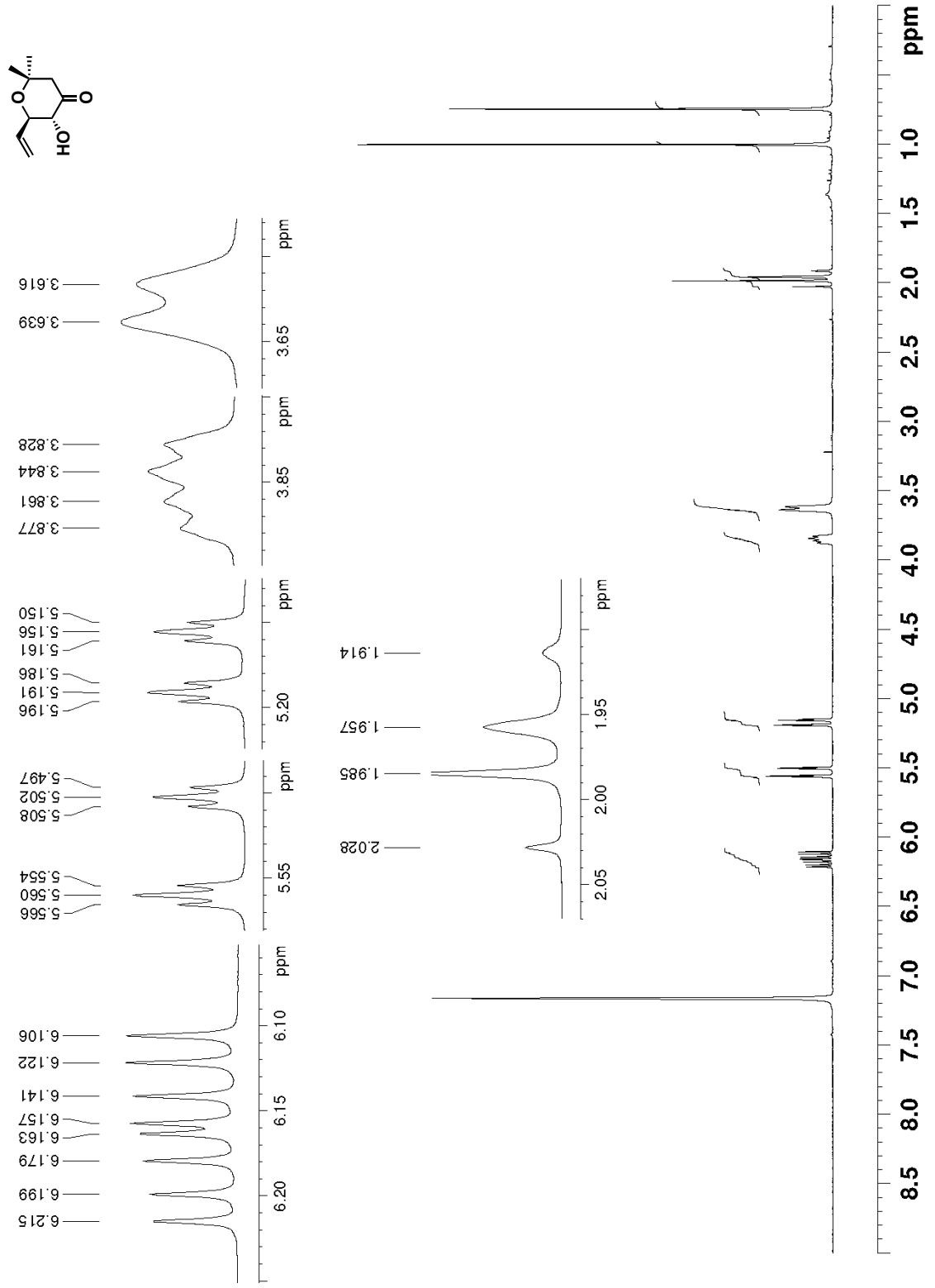

Spectrum 13. ^{1}H NMR spectrum of ketone **1.29** (300 MHz, 1% CD_3OD in C_6D_6, 293K)

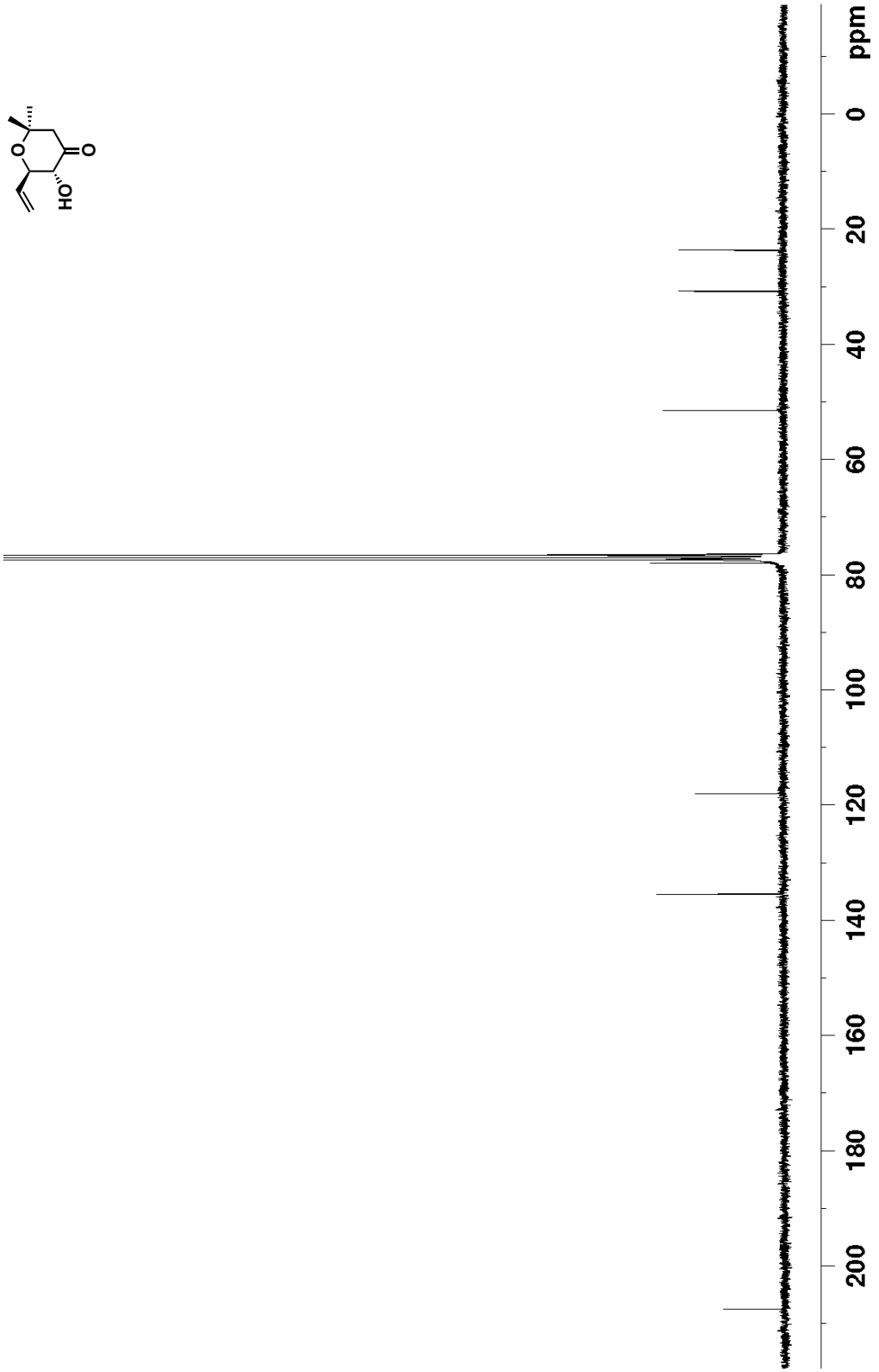

Spectrum 14. ^{13}C NMR spectrum of ketone **1.29** (100 MHz, $CDCl_3$, 293K)

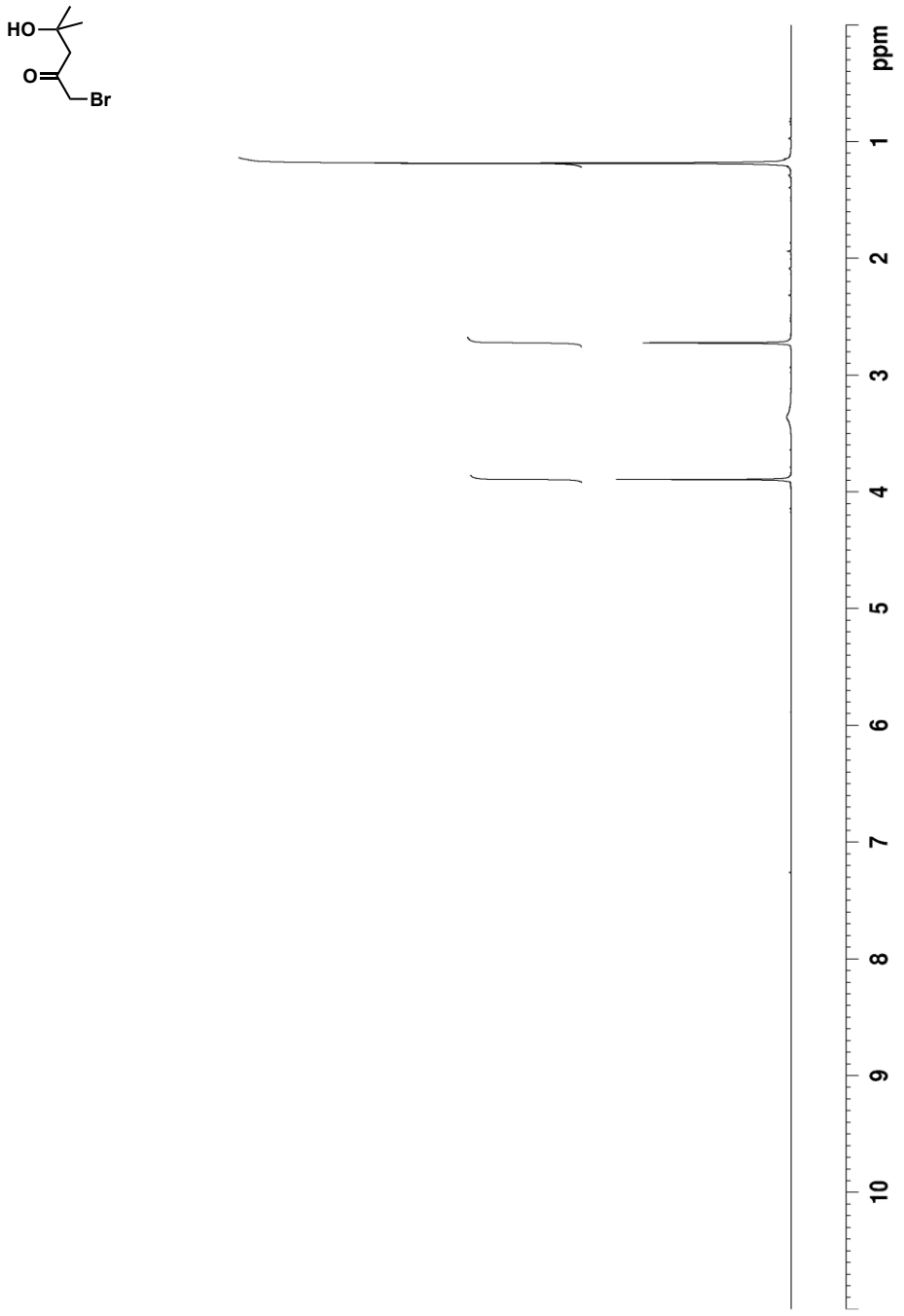

Spectrum 15. ^{1}H NMR spectrum of **1.64** (300 MHz, 1% CD_3OD in C_6D_6, 293K)

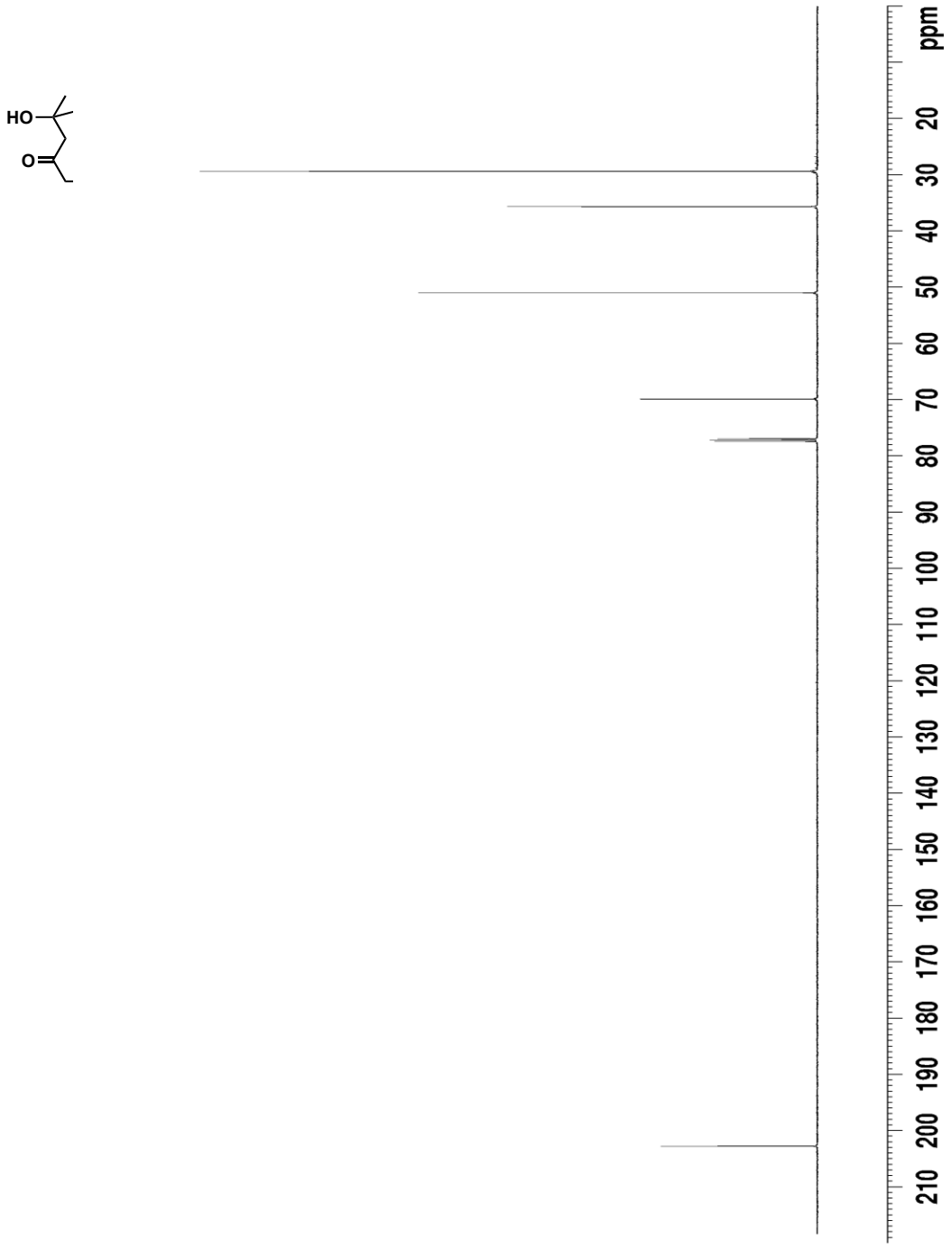

Spectrum 16. ^{13}C NMR spectrum of **1.64** (125 MHz, 1% CD_3OD in C_6D_6, 293K)

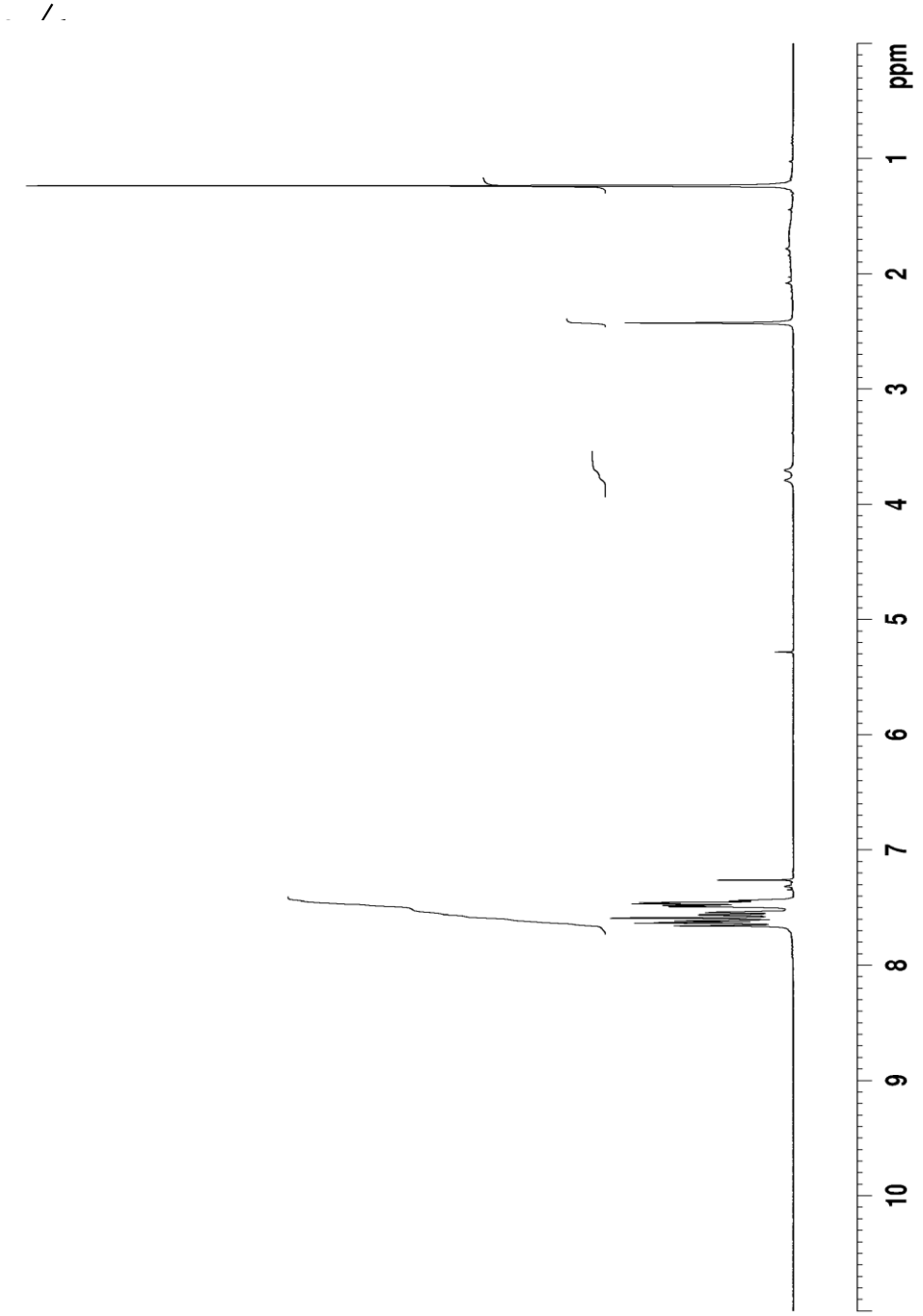

Spectrum 17. ^{1}H NMR spectrum of **1.65** (300 MHz, 1% CD_3OD in C_6D_6, 293K)

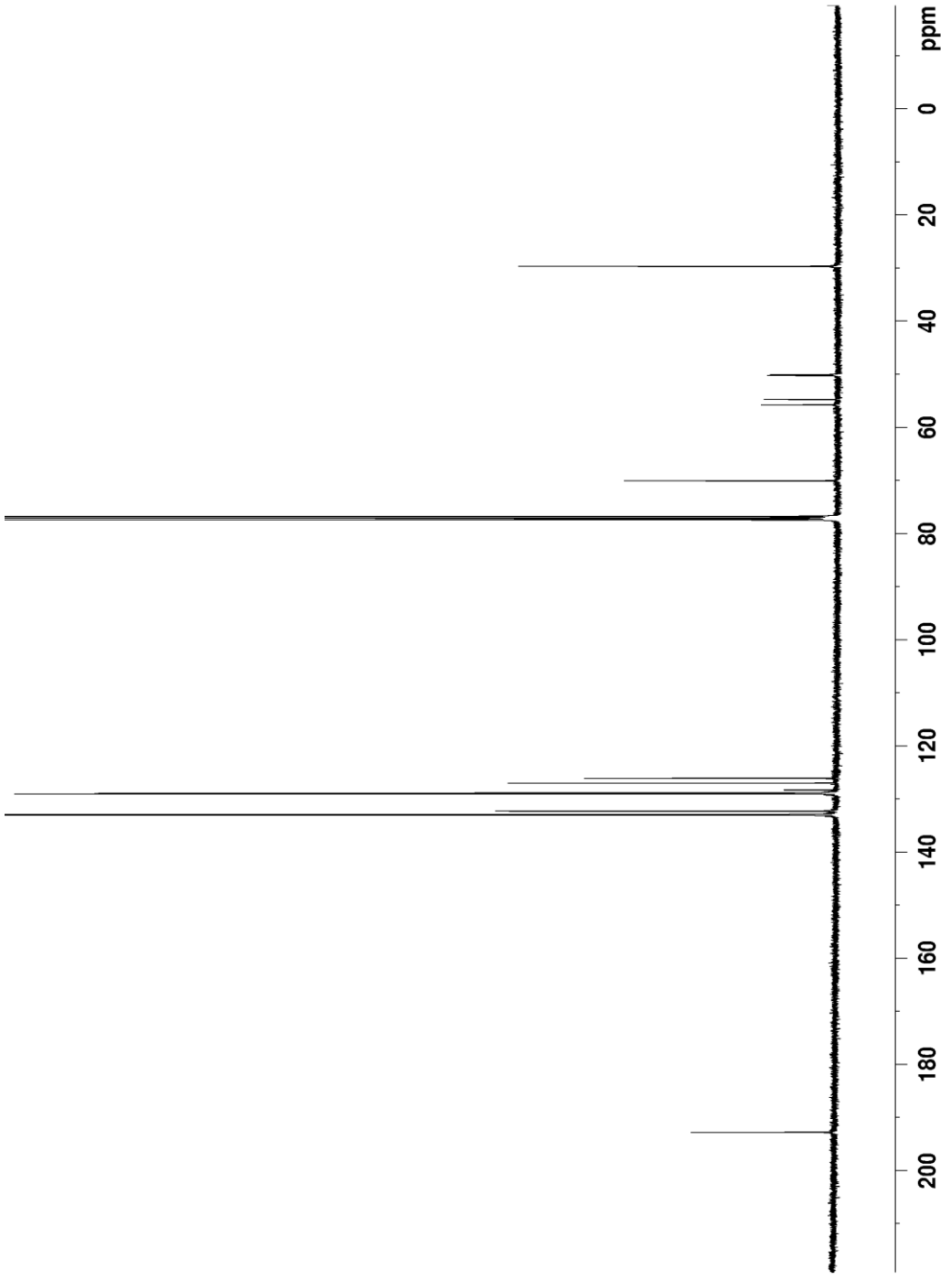

Spectrum 18. ^{13}C NMR spectrum of **1.65** (75 MHz, $CDCl_3$, 293K)

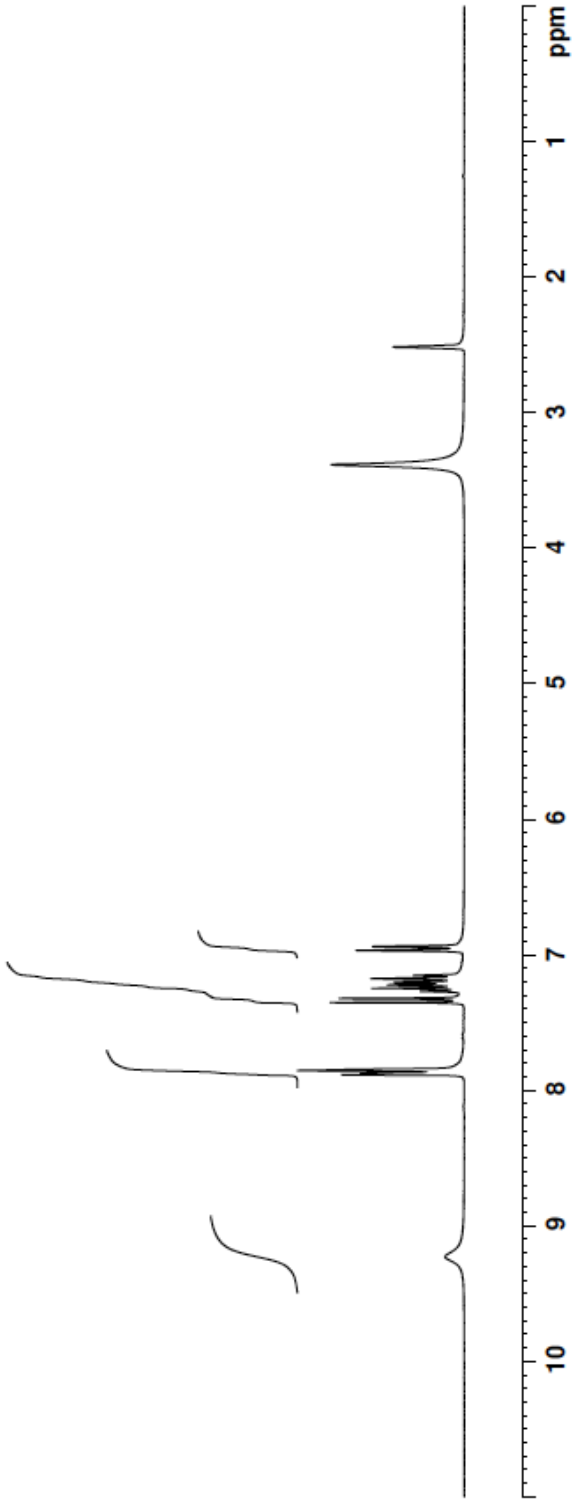

Spectrum 19. ^{1}H NMR spectrum of **L5** (300 MHz, DMSO-d_6, 293K)

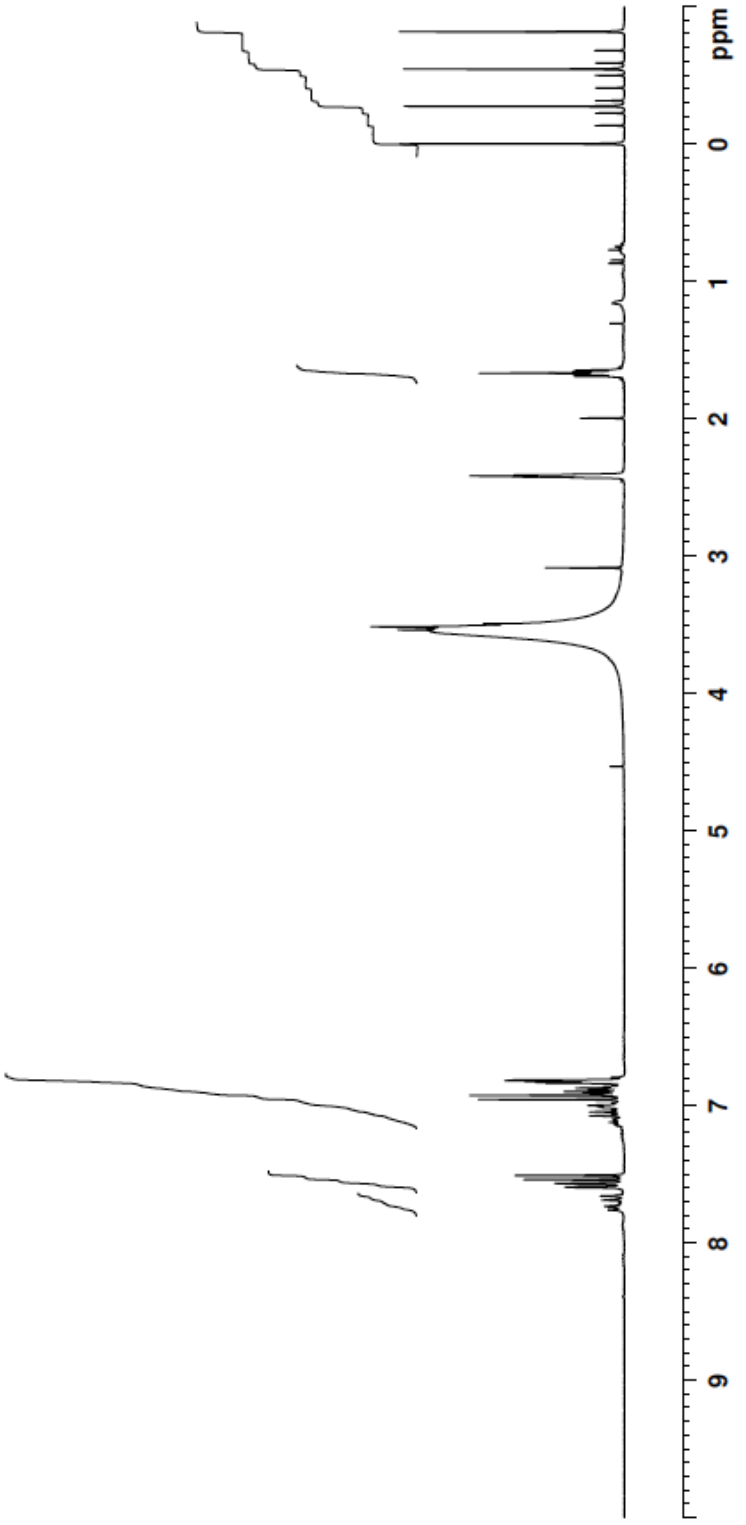

Spectrum 20. ^{1}H NMR spectrum of **L5**+$NaBH_4$ (300 MHz, DMSO-d_6, 293K)

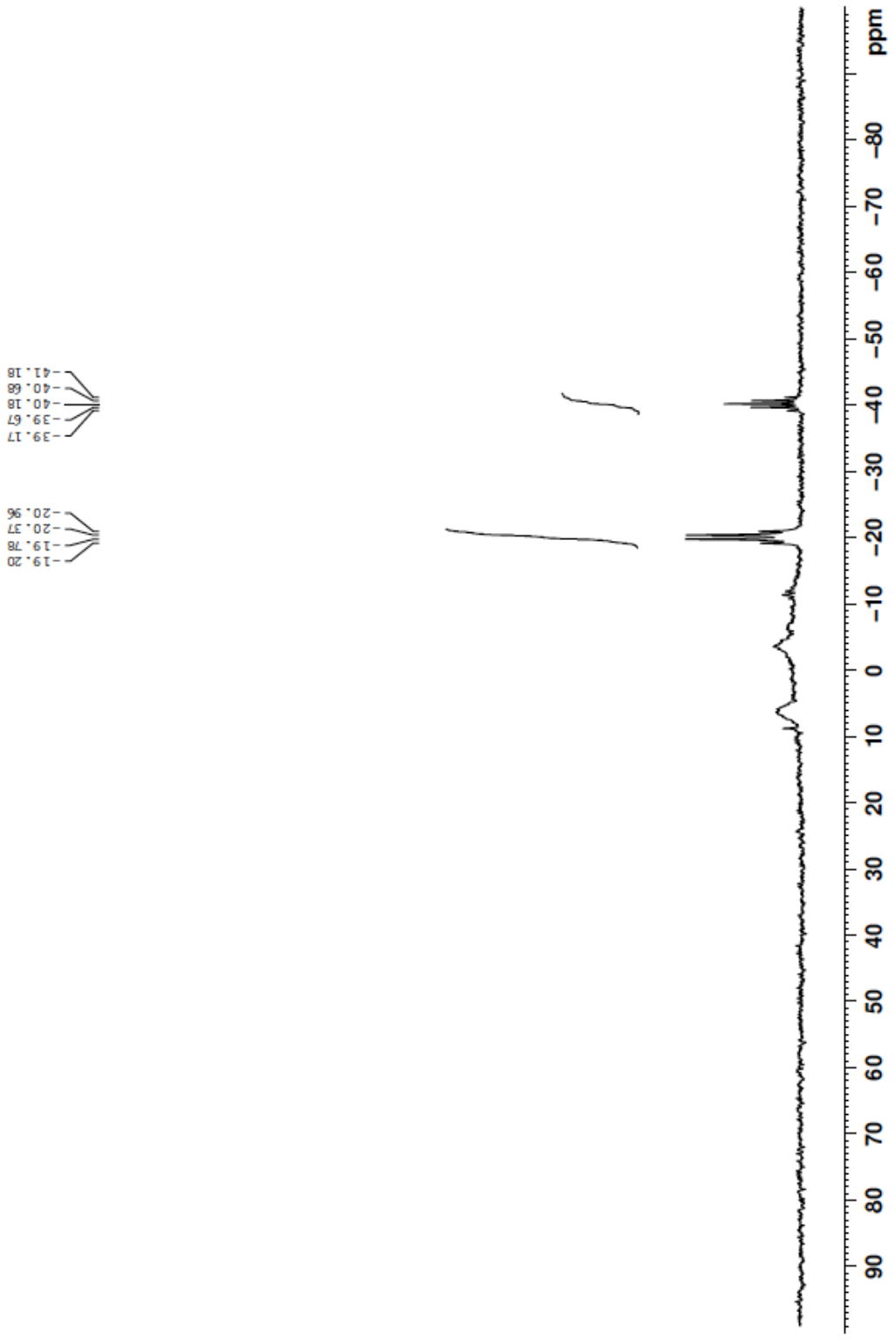

Spectrum 21. ^{11}B NMR spectrum of **L5**+$NaBH_4$ (160 MHz, CD_3CN, 293K)

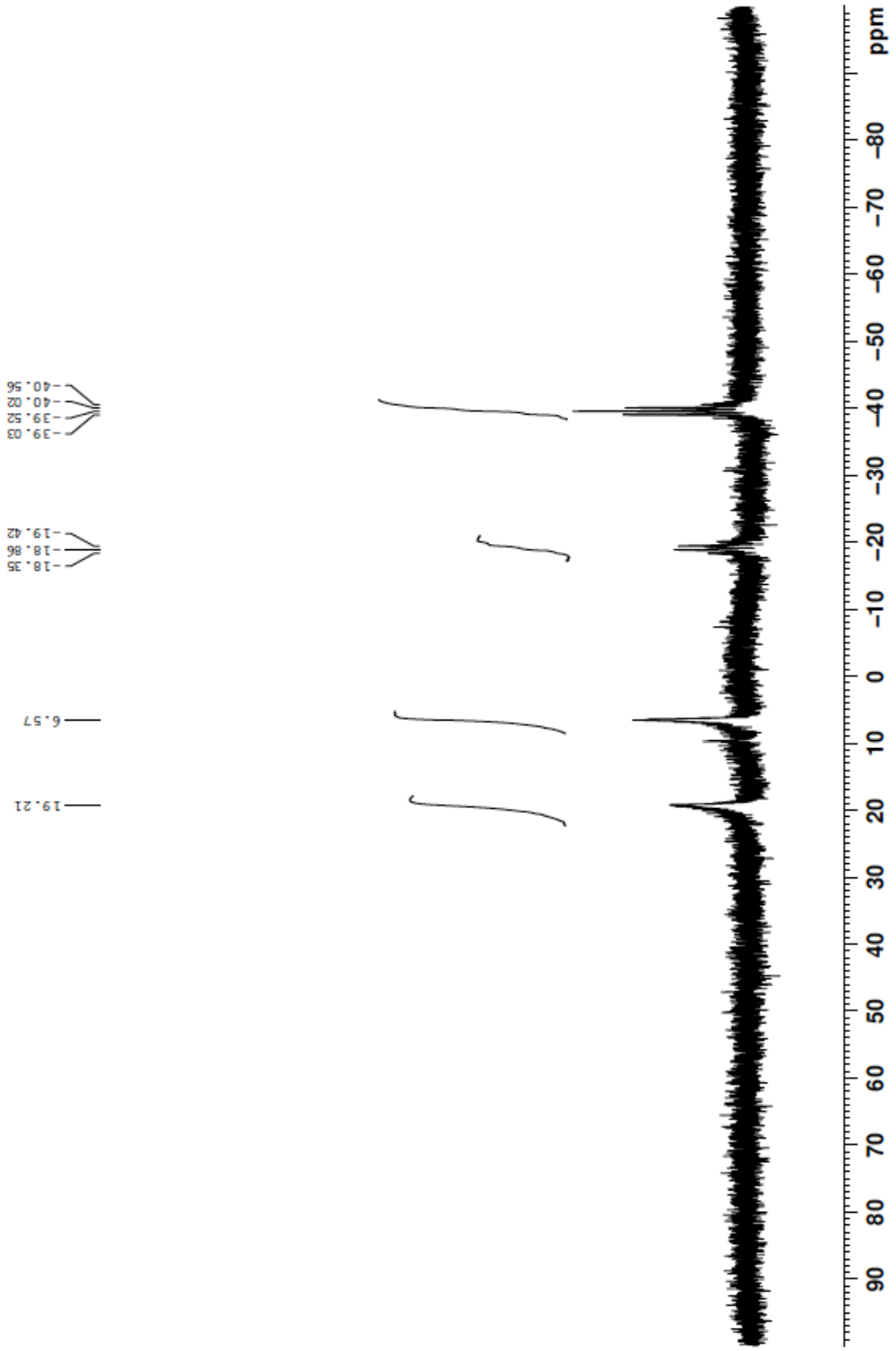

Spectrum 22. ^{11}B NMR spectrum of **L5**+$NaBH_4$+ ketone **1.25** (160 MHz, 293K)

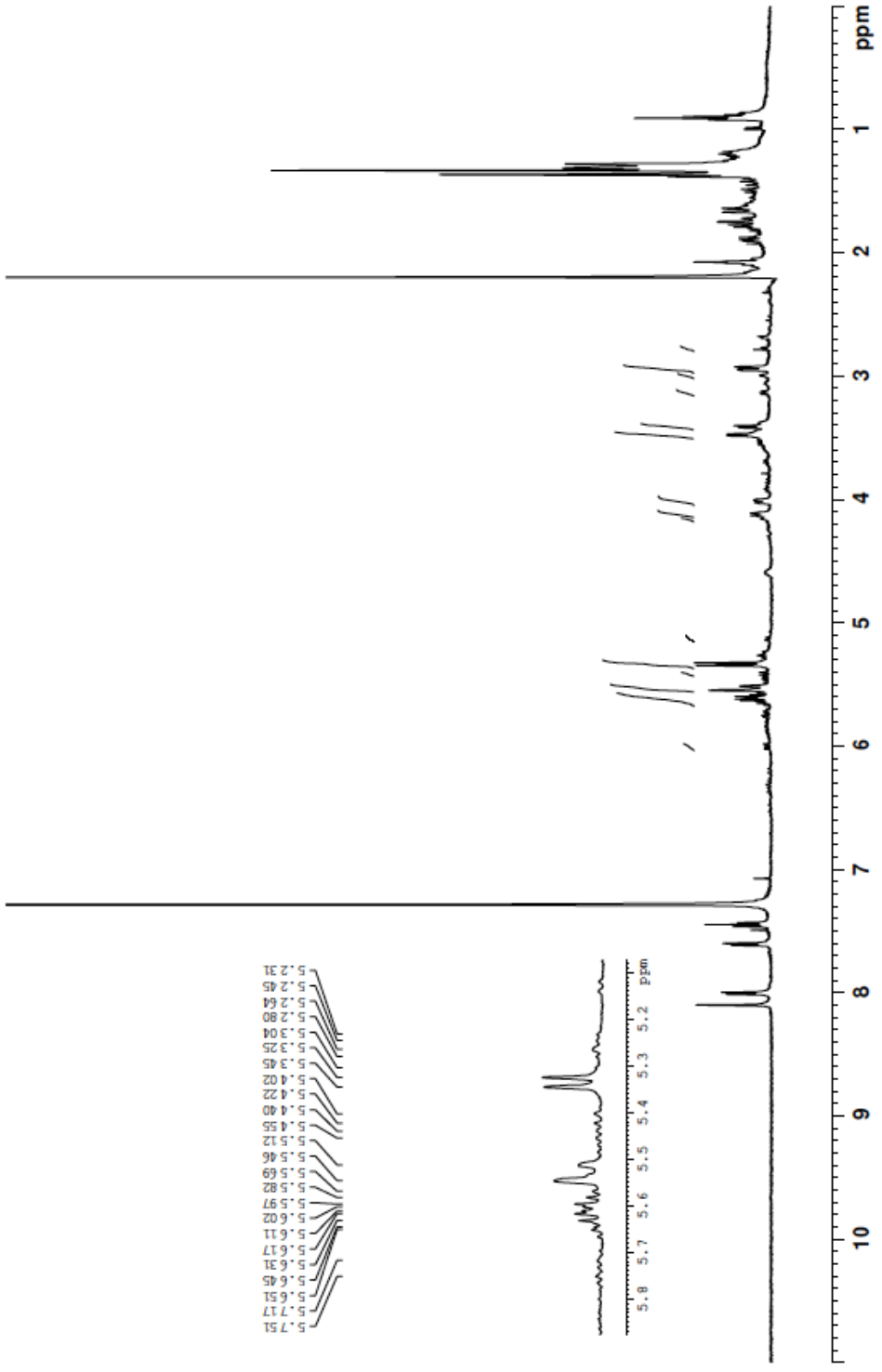

Spectrum 23. Crude ^{1}H NMR spectrum of epoxidation of **1.27** with mCPBA (500 MHz, $CDCl_3$, 293K)

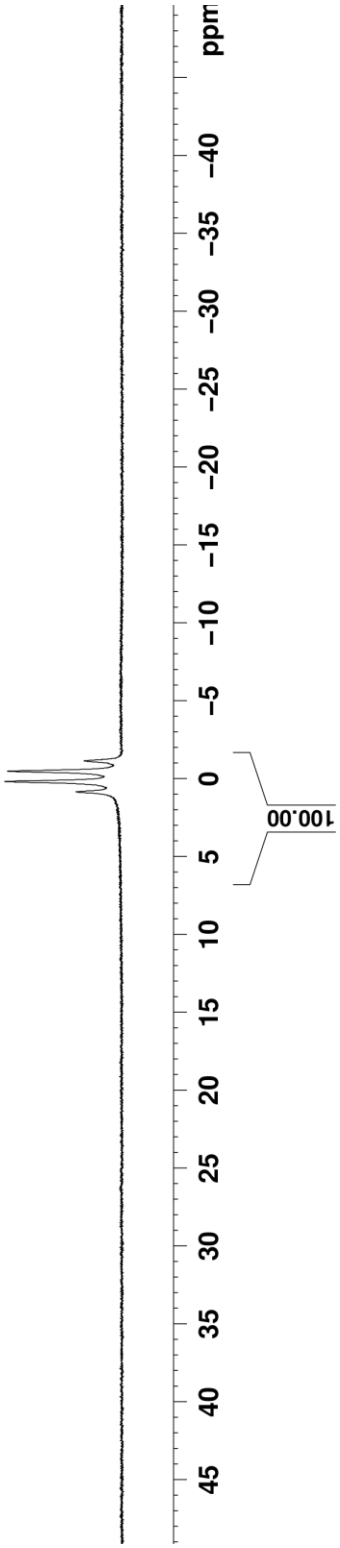

Spectrum 24. ^{11}B NMR spectrum of BH_3 (160 MHz, 293K)

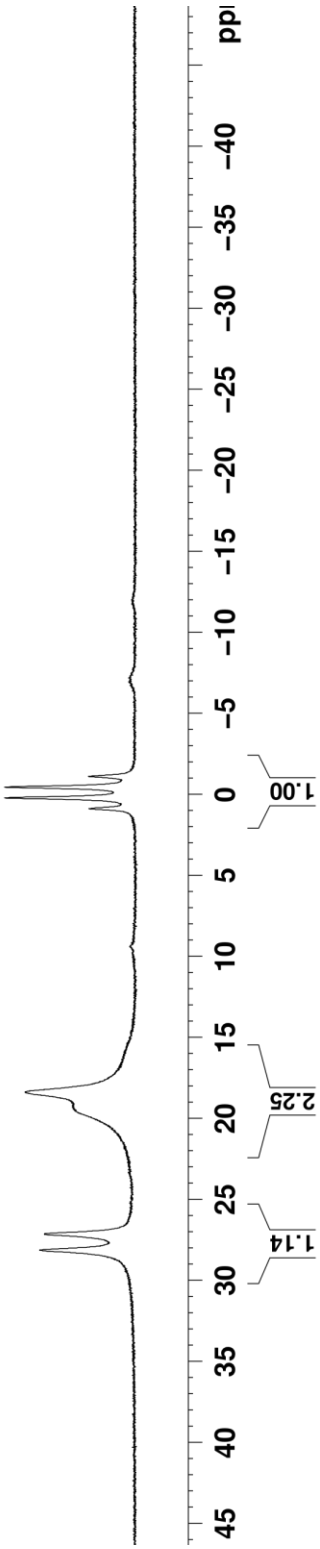

Spectrum 25. ^{11}B NMR spectrum of **L5**+BH_3 (160 MHz, 293K)

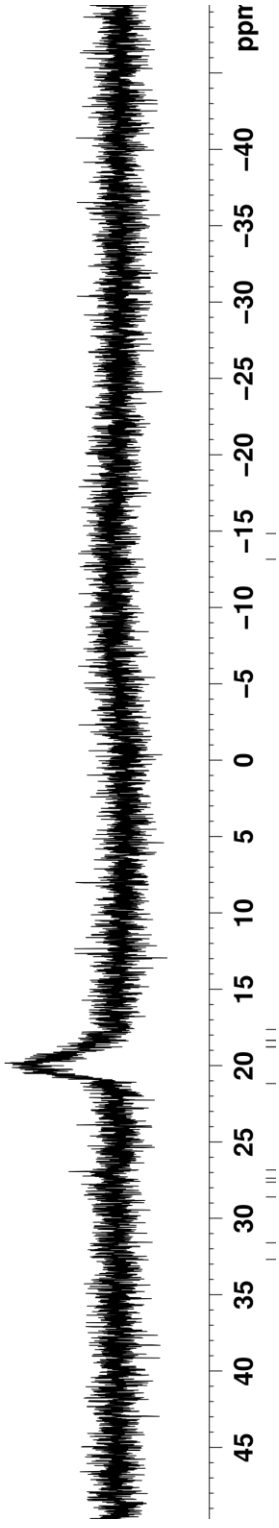

Spectrum 26. ^{11}B NMR spectrum of **L5**+BH_3 followed by addition of ketone (160 MHz, 293K)

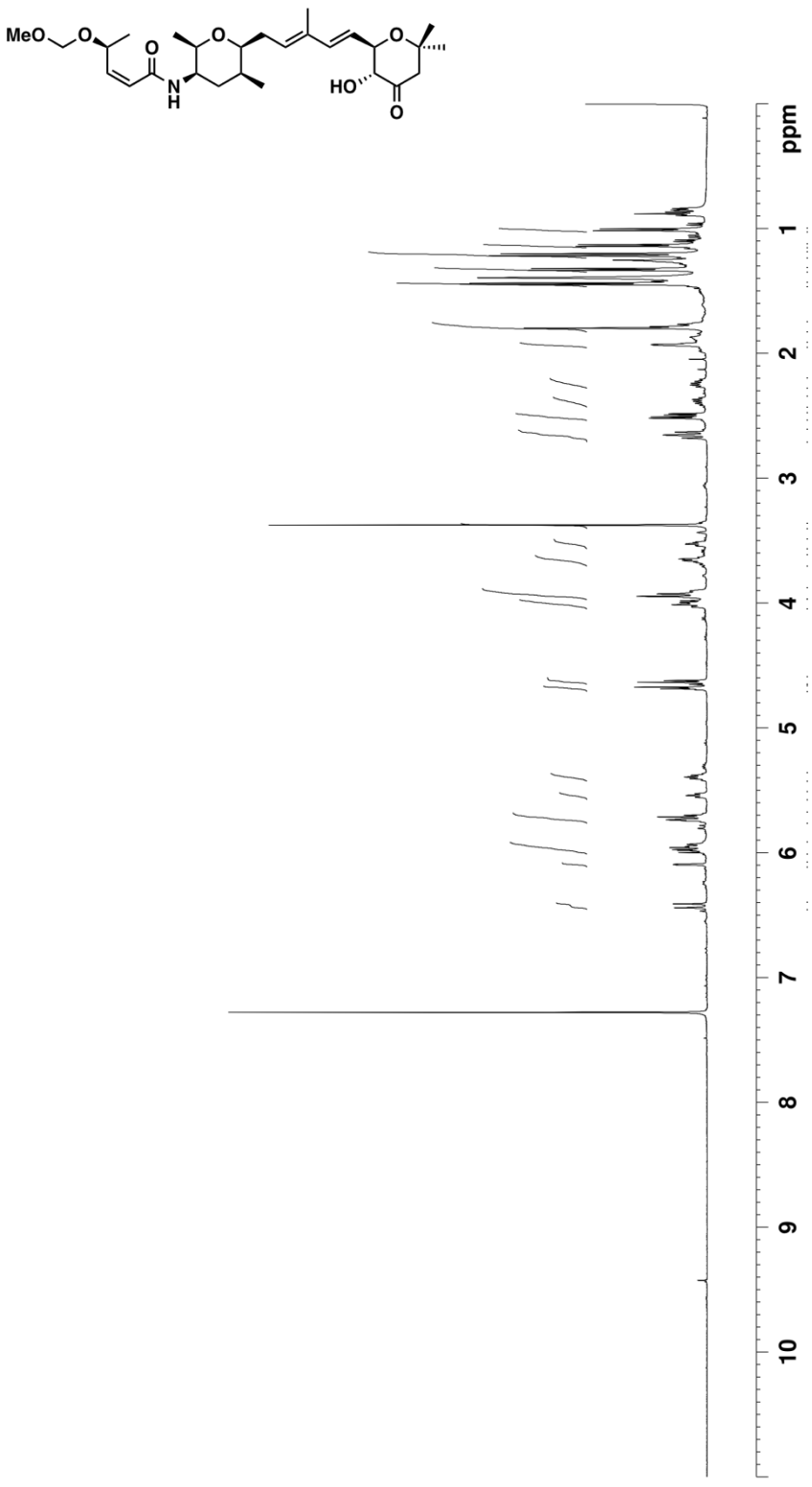

Spectrum 27. ^{1}H NMR spectrum of **1.83** (500 MHz, 293K)

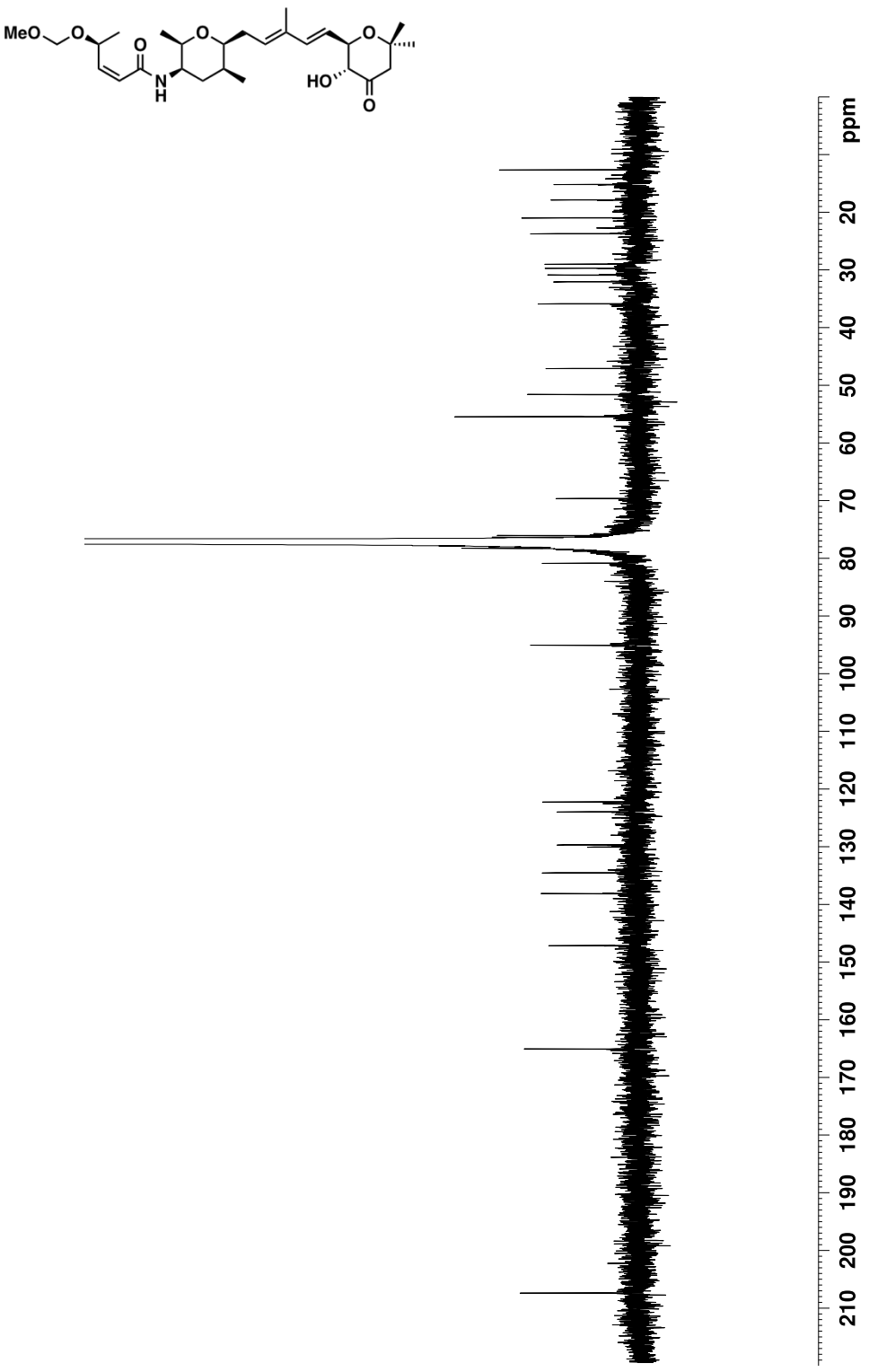

Spectrum 28. ^{13}C NMR spectrum of **1.83** (125 MHz, 293K)

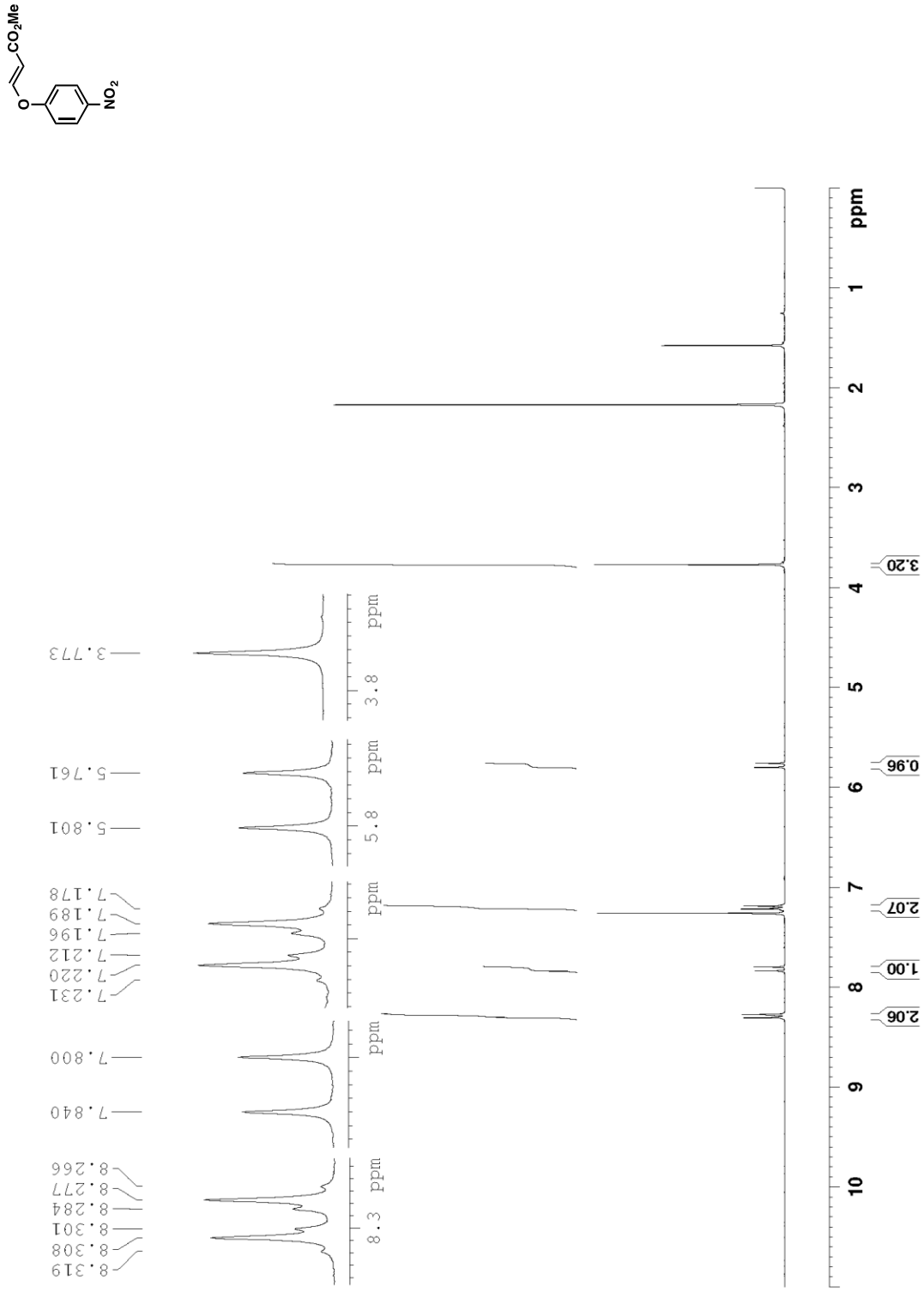

Spectrum 29. ^{1}H NMR spectrum of **2.25** (400 MHz, 293K)

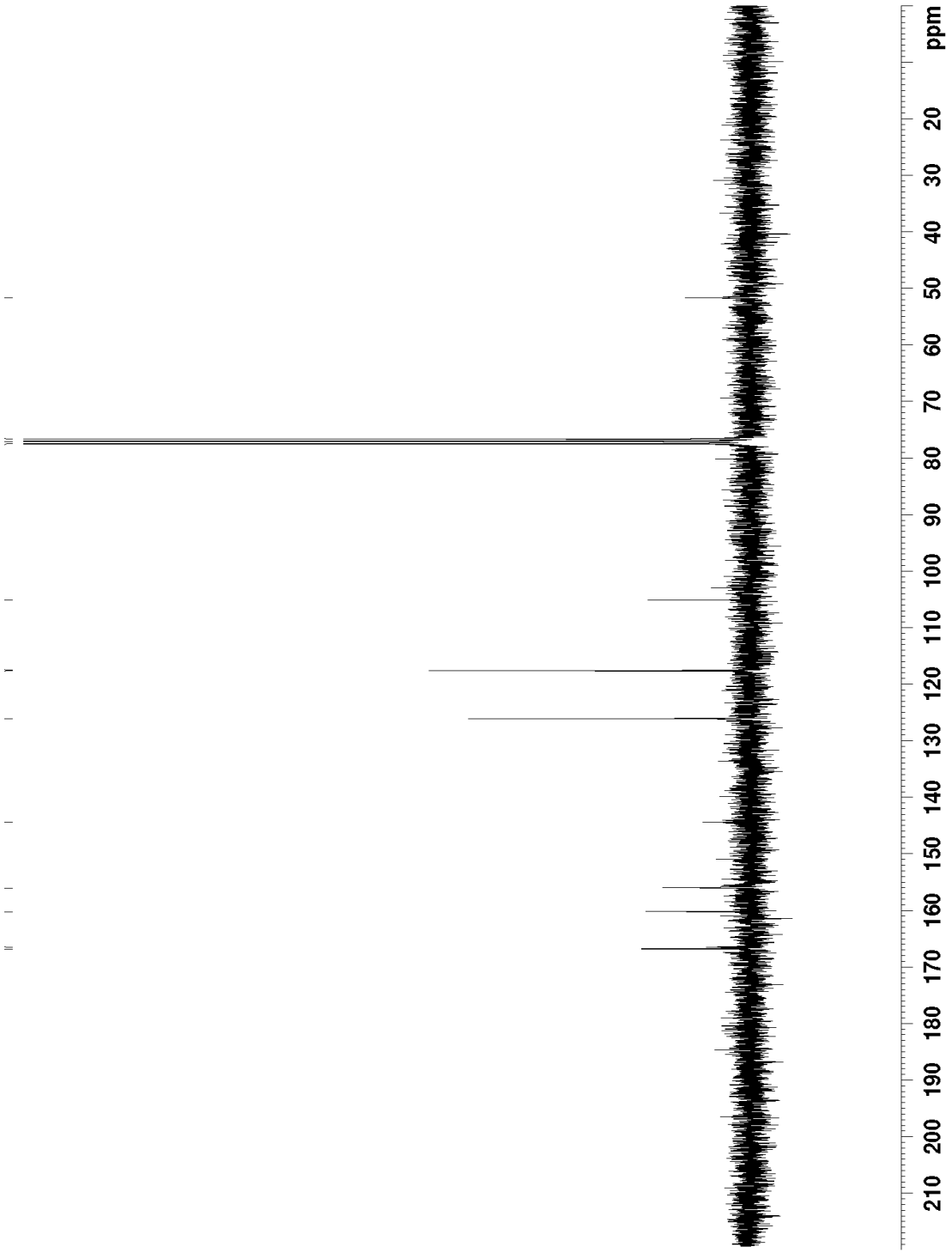

Spectrum 30. ^{13}C NMR spectrum of **2.25** (100 MHz, 293K)

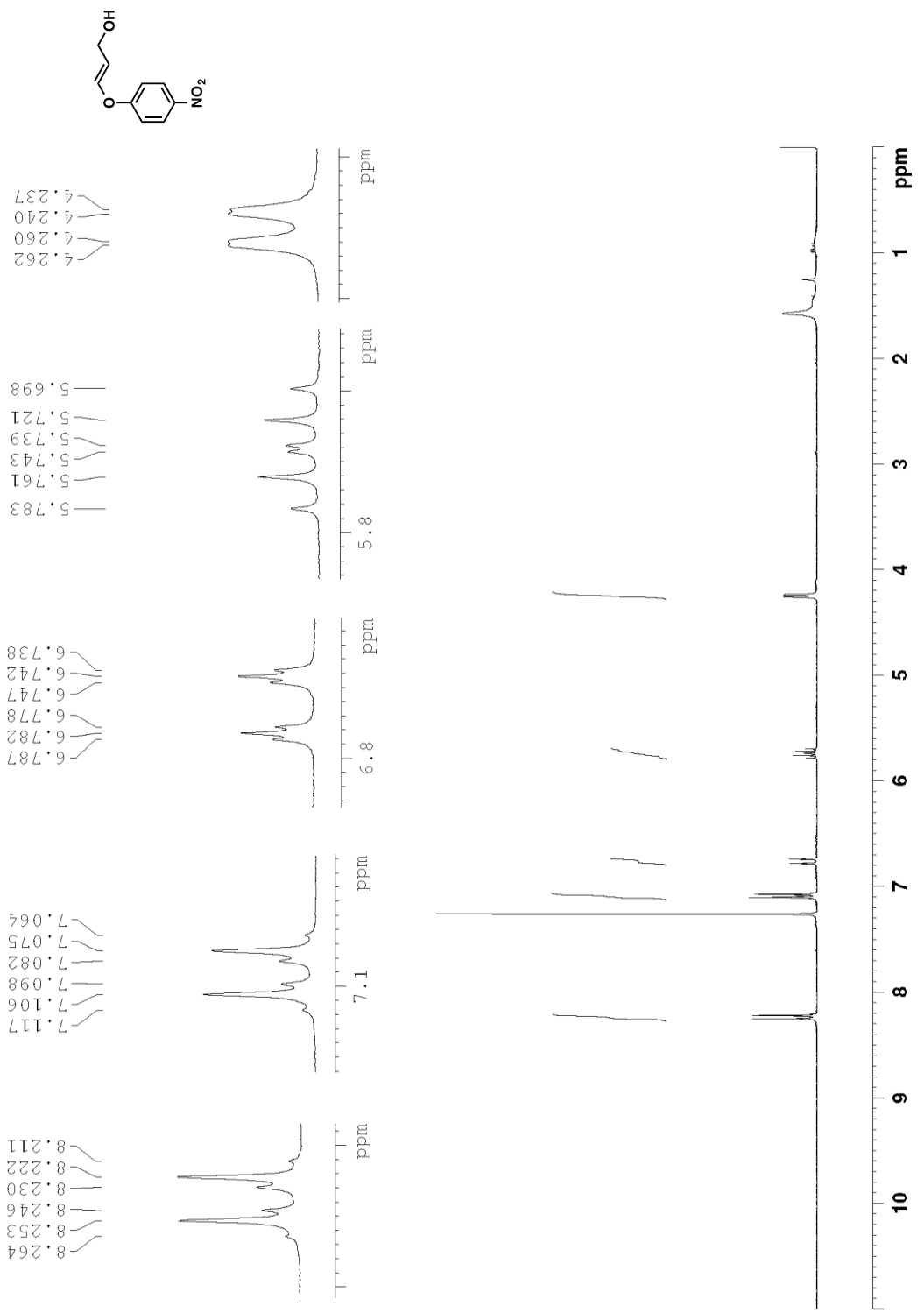

Spectrum 31. [1]H NMR spectrum of **2.26** (400 MHz, 293K)

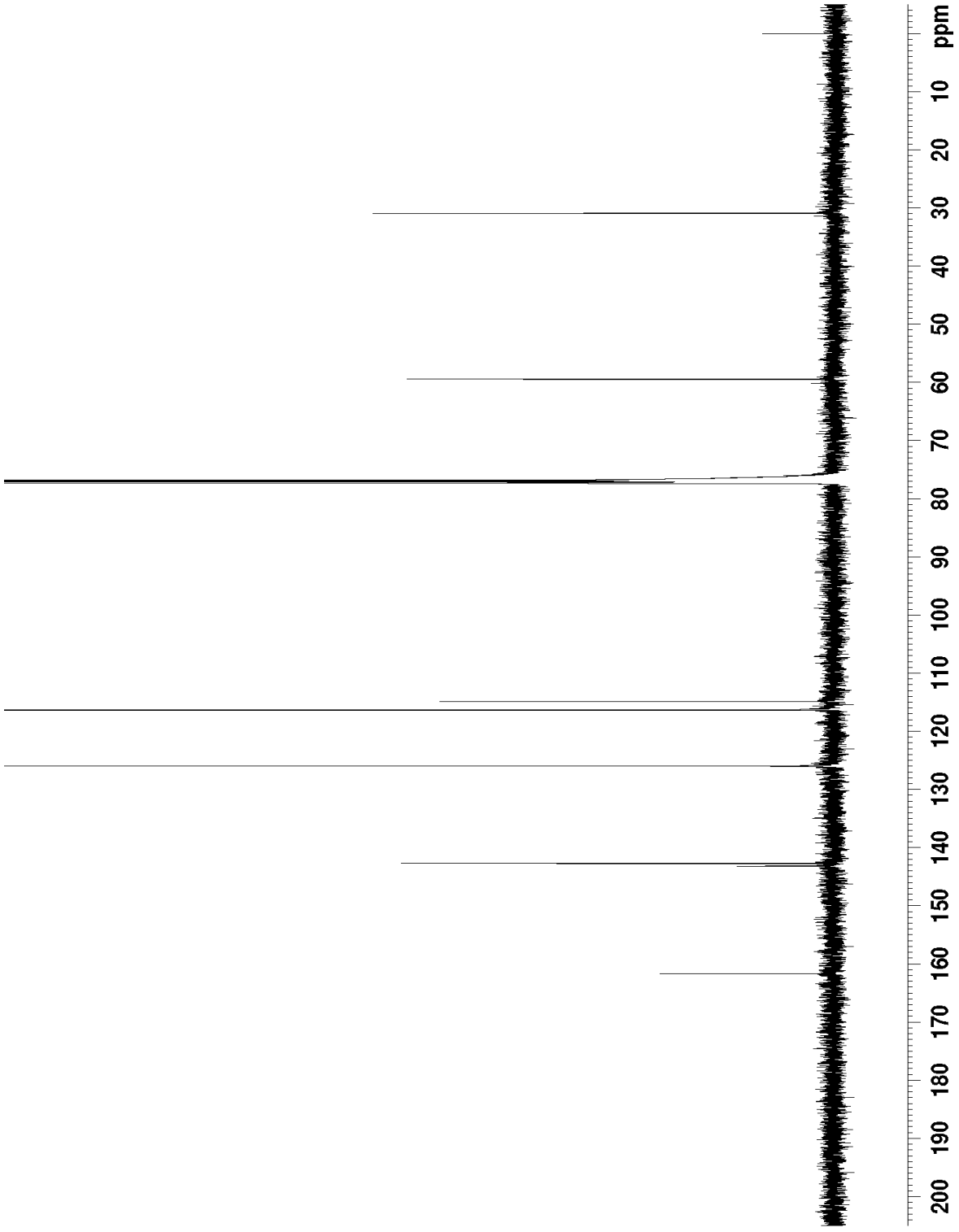

Spectrum 32. ^{13}C NMR spectrum of **2.26** ($CDCl_3$, 75MHz, 293K).

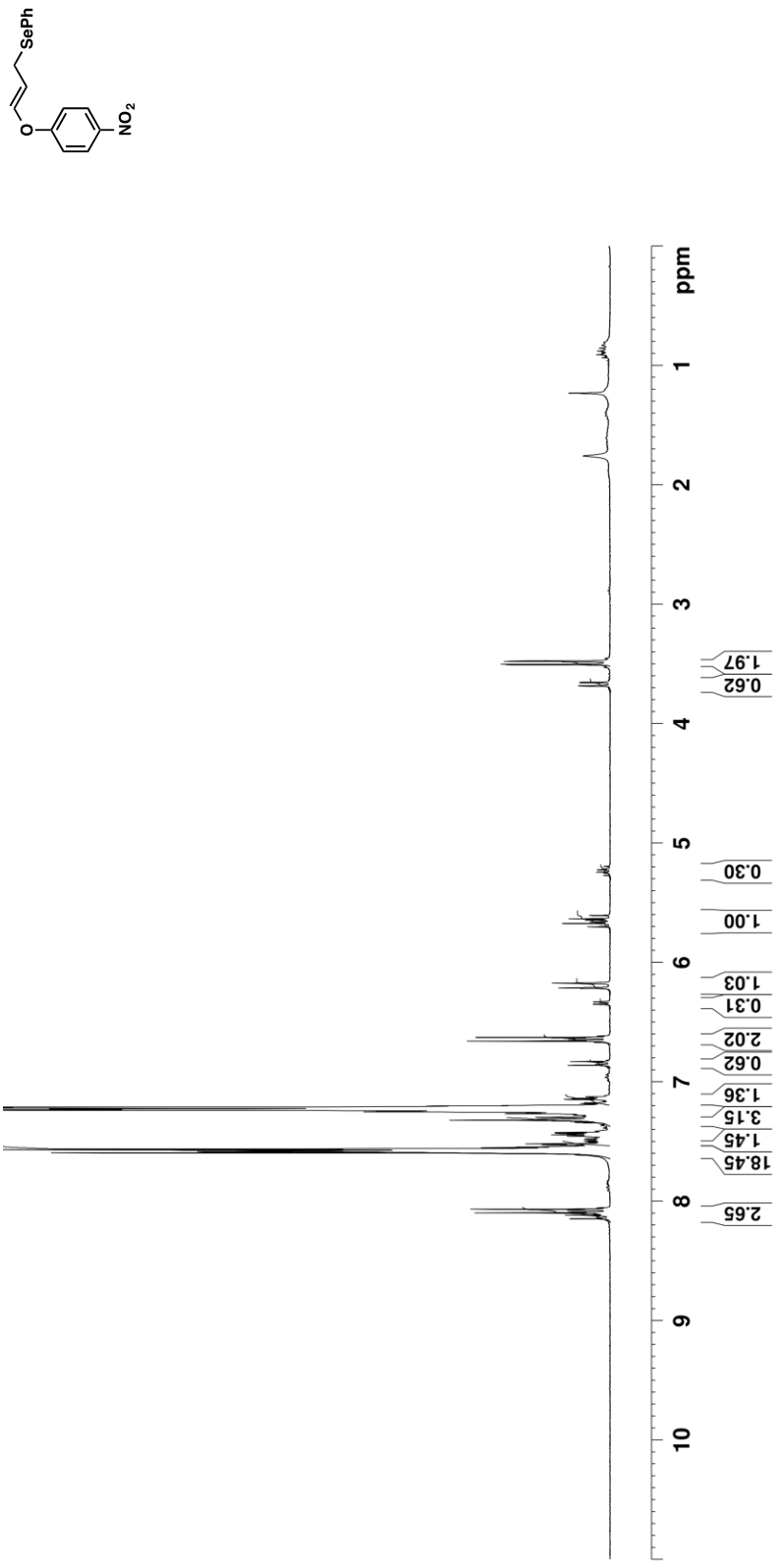

Spectrum 33. ^{1}H NMR spectrum of **2.27** ($CDCl_3$, 300 MHz, 293K).

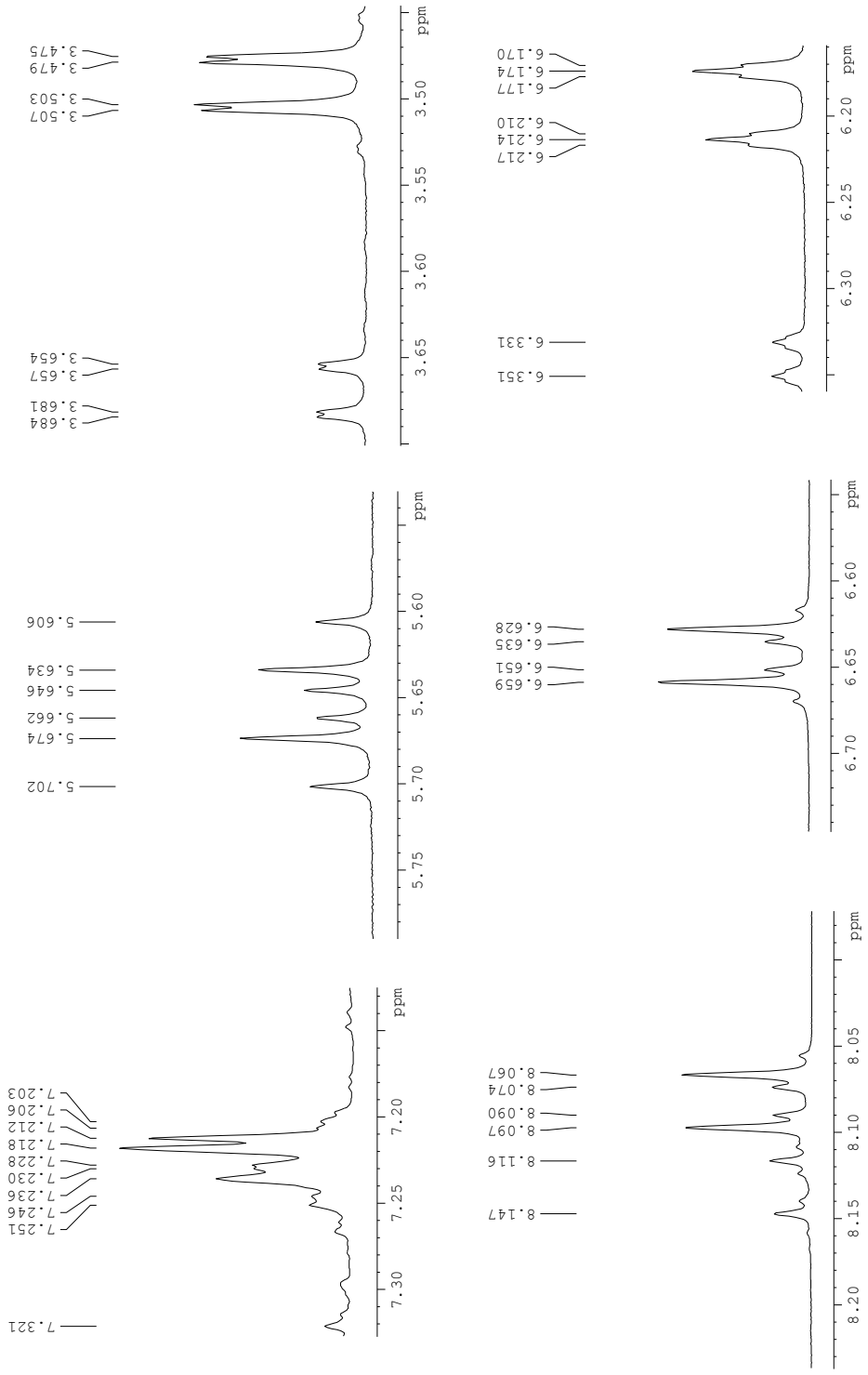

Spectrum 34. ^{1}H NMR spectrum of **2.27** ($CDCl_3$, 300 MHz, 293K).

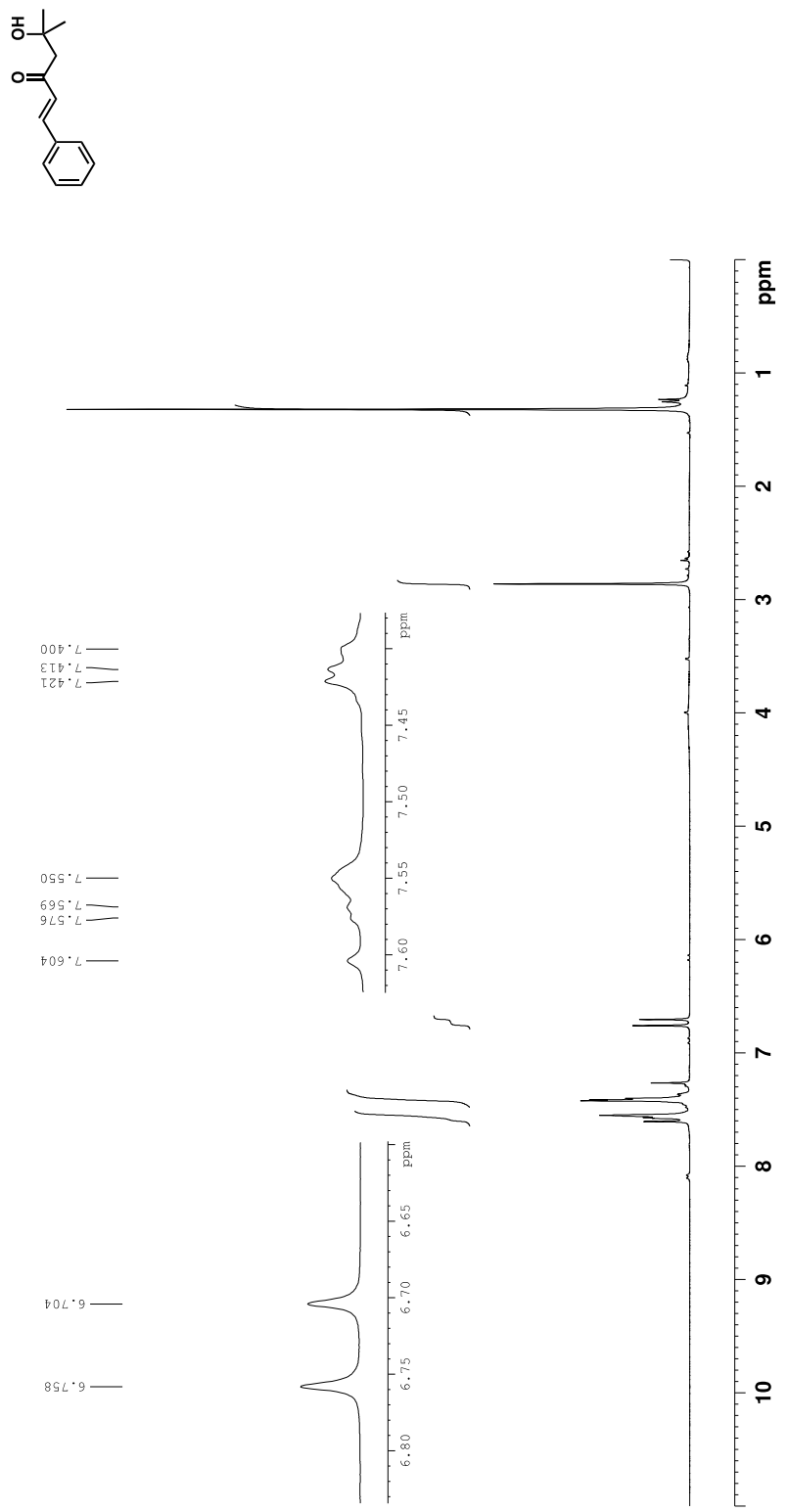

Spectrum 35. ^{1}H NMR spectrum of **1.71** ($CDCl_3$, 300 MHz, 293K)

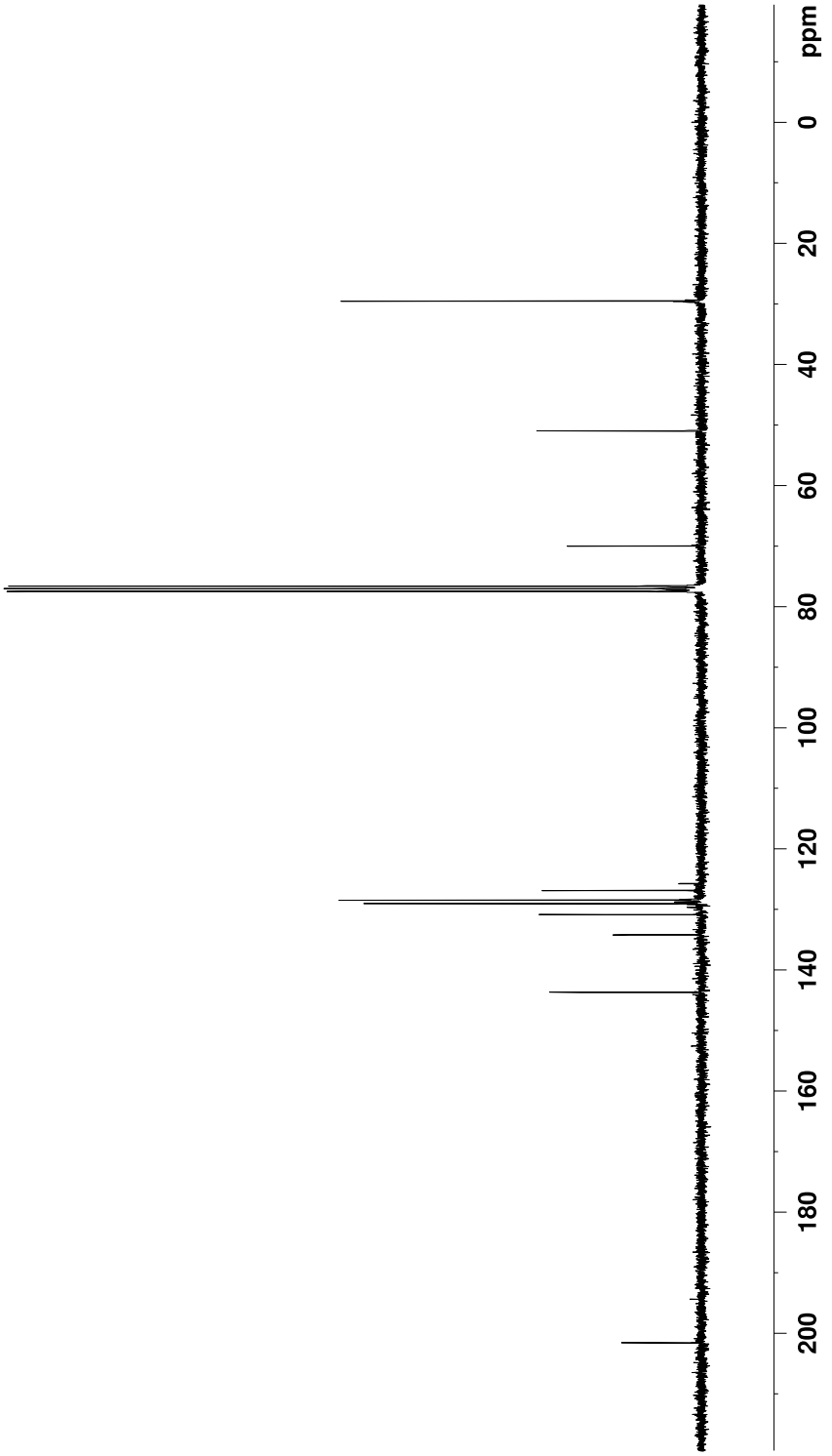

Spectrum 36. ^{13}C NMR spectrum of **1.71** ($CDCl_3$, 75 MHz, 293K)

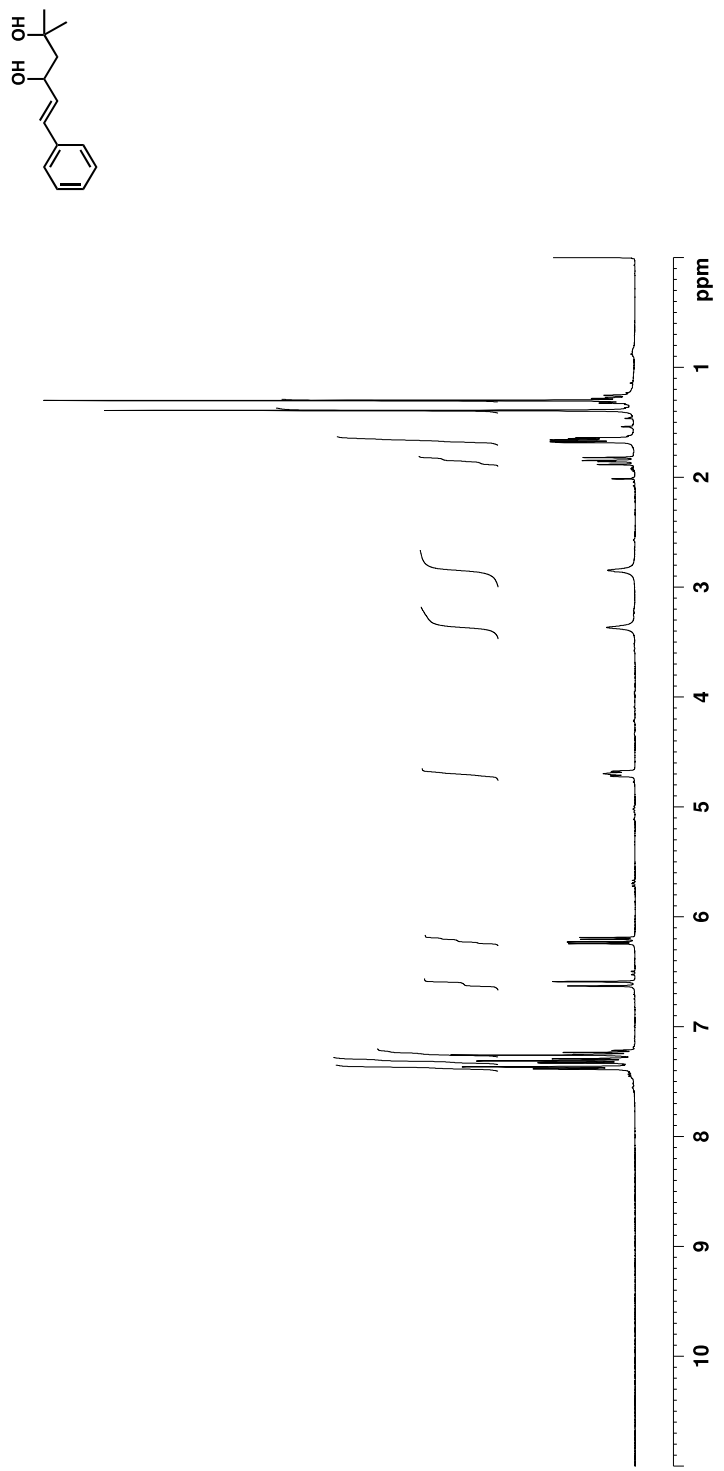

Spectrum 37. ^{1}H NMR spectrum of **1.72** ($CDCl_3$, 300 MHz, 293K)

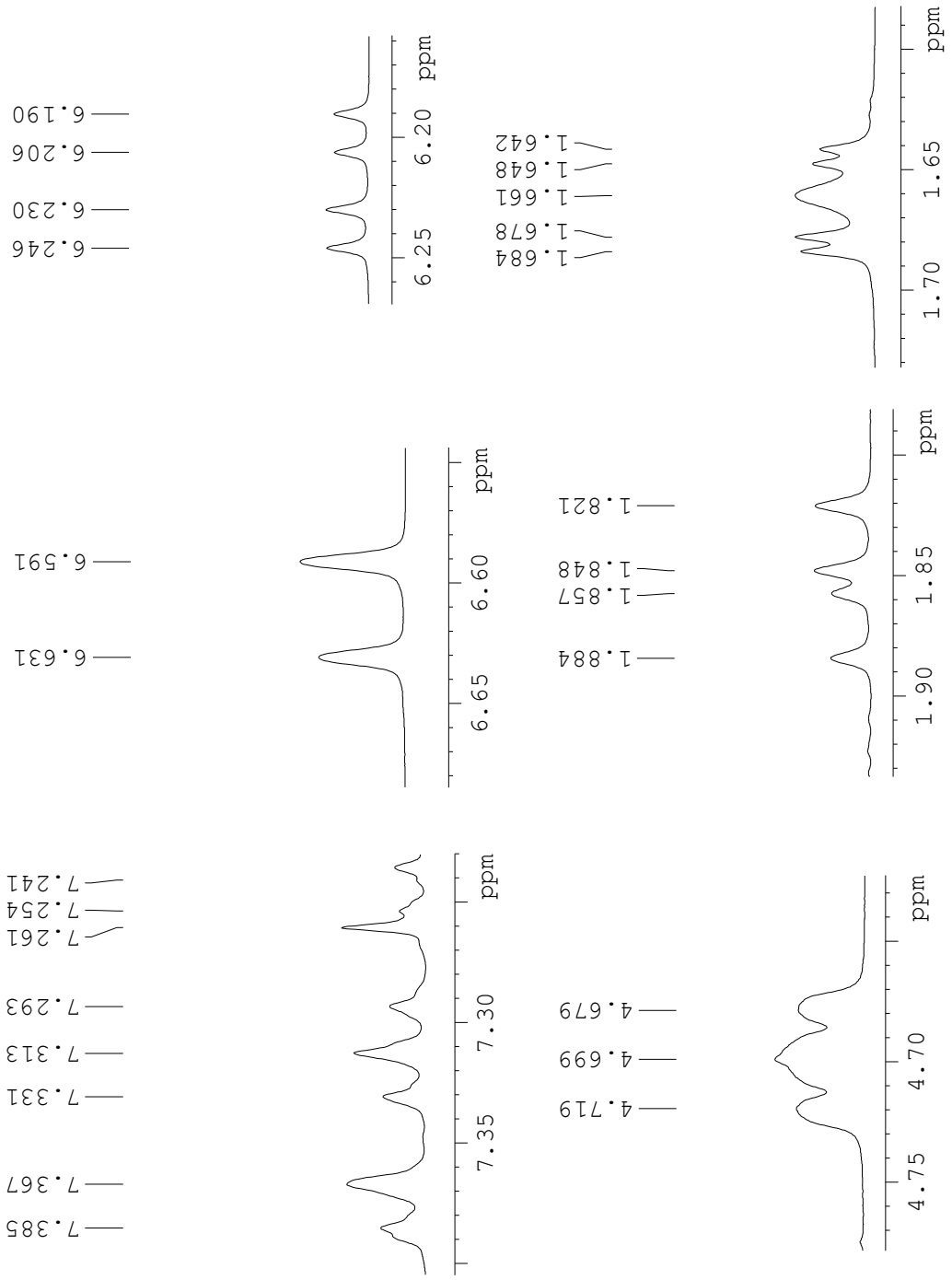

Spectrum 38. ^{1}H NMR spectrum of **1.72** ($CDCl_3$, 300 MHz, 293K)

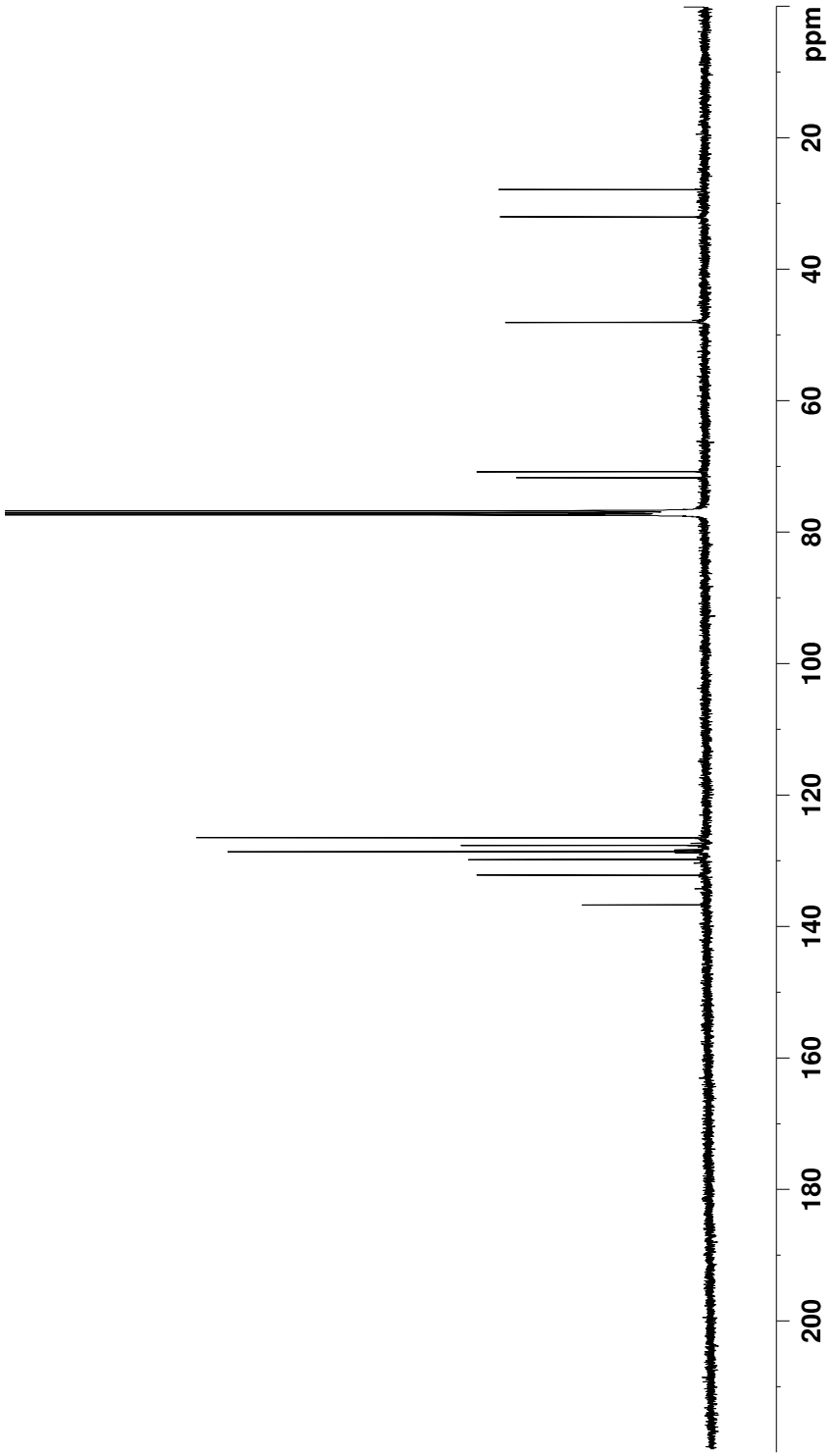

Spectrum 39. ^{13}C NMR spectrum of **1.72** ($CDCl_3$, 75 MHz, 293K)

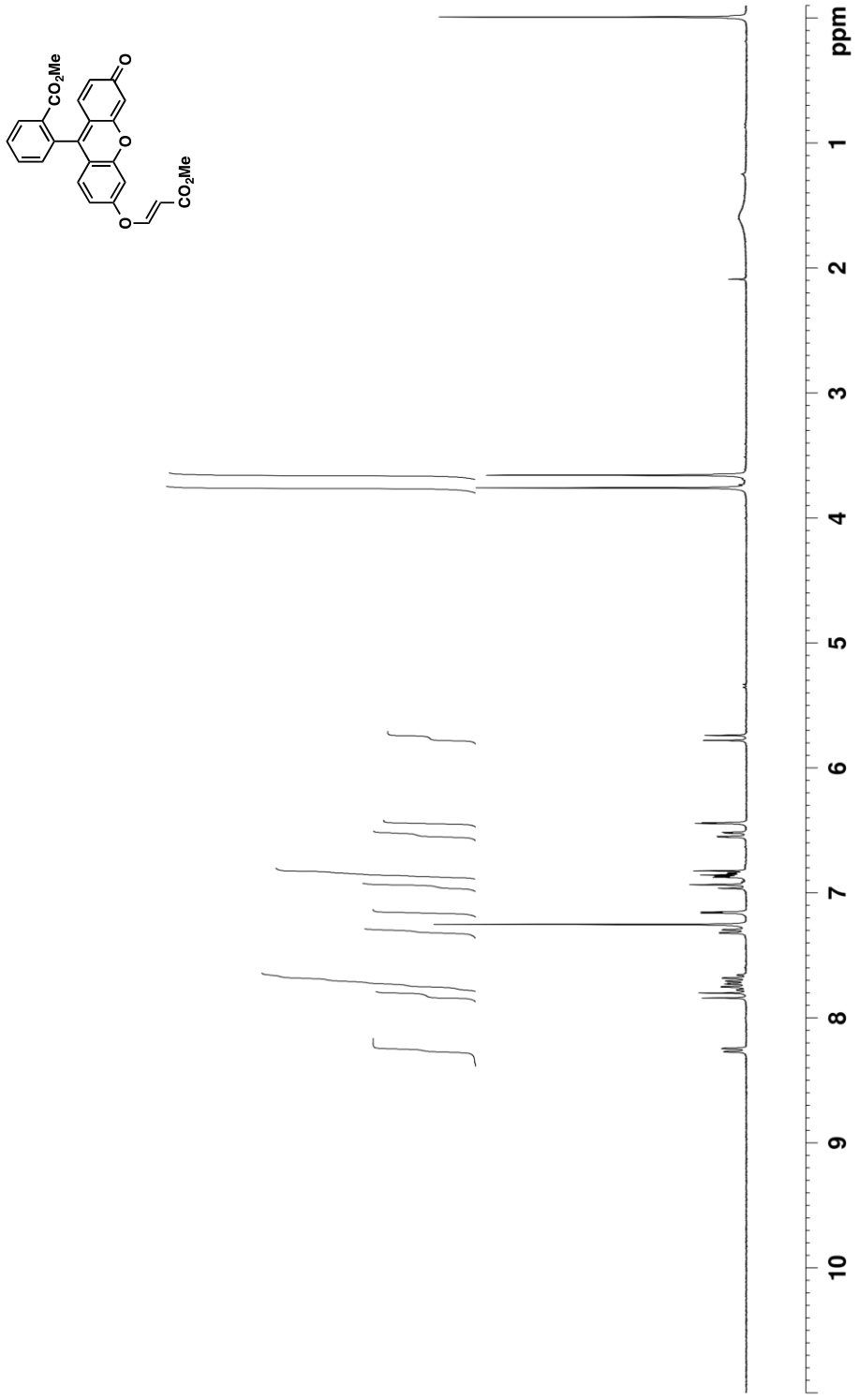

Spectrum 40. ^{1}H NMR spectrum of **2.35** (300 MHz, $CDCl_3$, 293K)

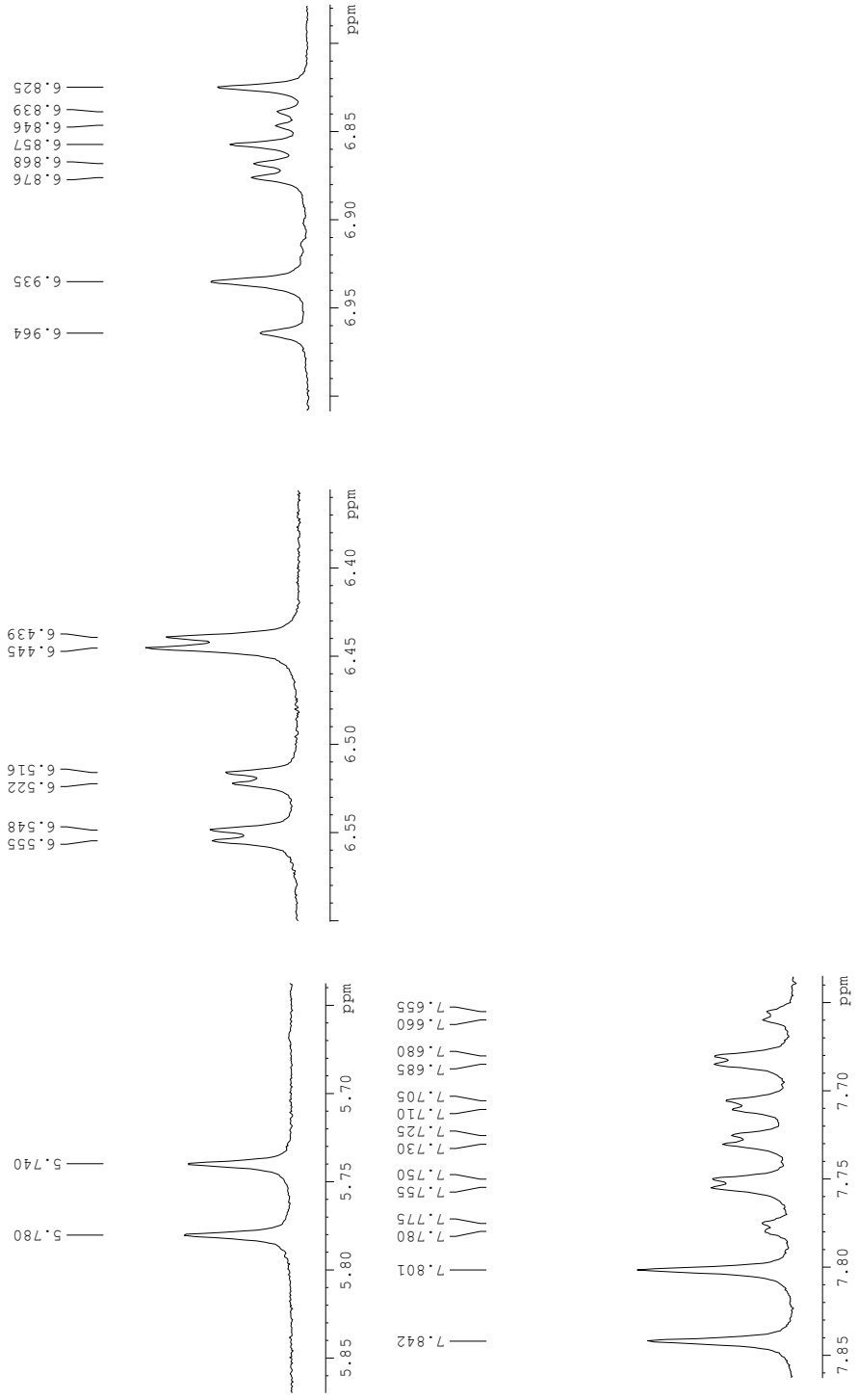

Spectrum 41. ^{1}H NMR spectrum of **2.35** continued

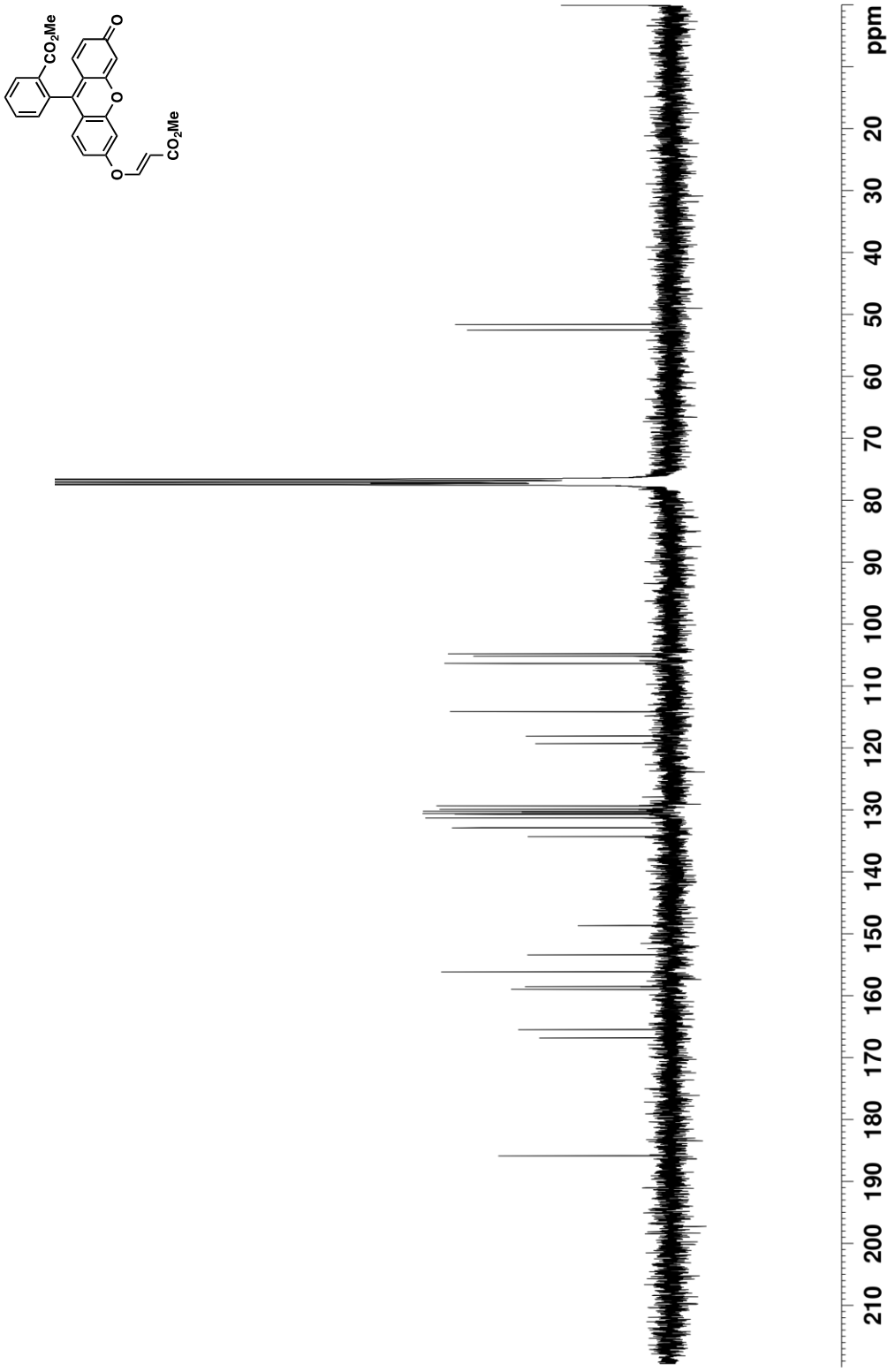

Spectrum 42. ^{13}C NMR spectrum of **2.35** (75 MHz, $CDCl_3$, 293K)

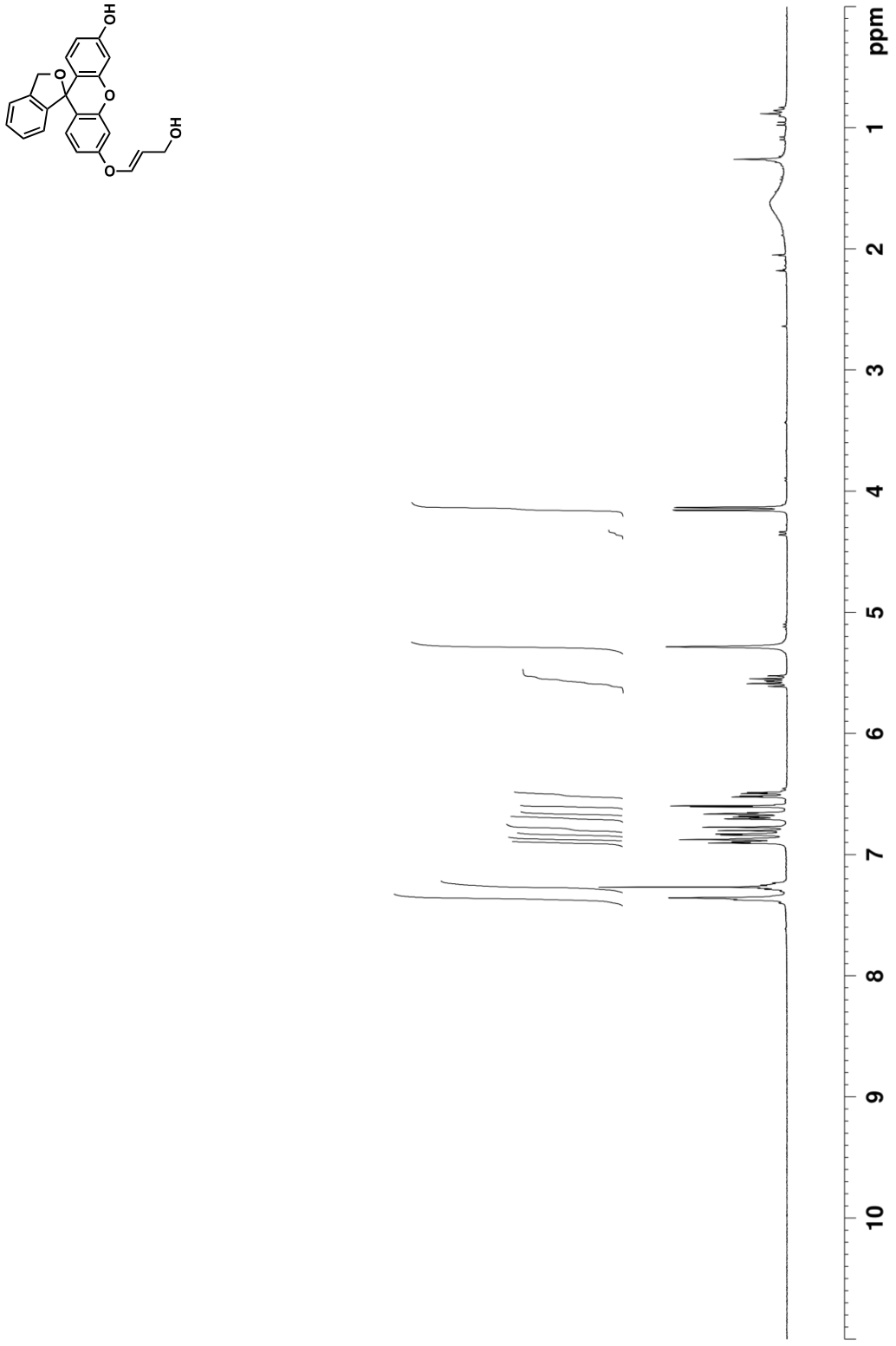

Spectrum 43. ^{1}H NMR spectrum of **2.37** (300 MHz, $CDCl_3$, 293K)

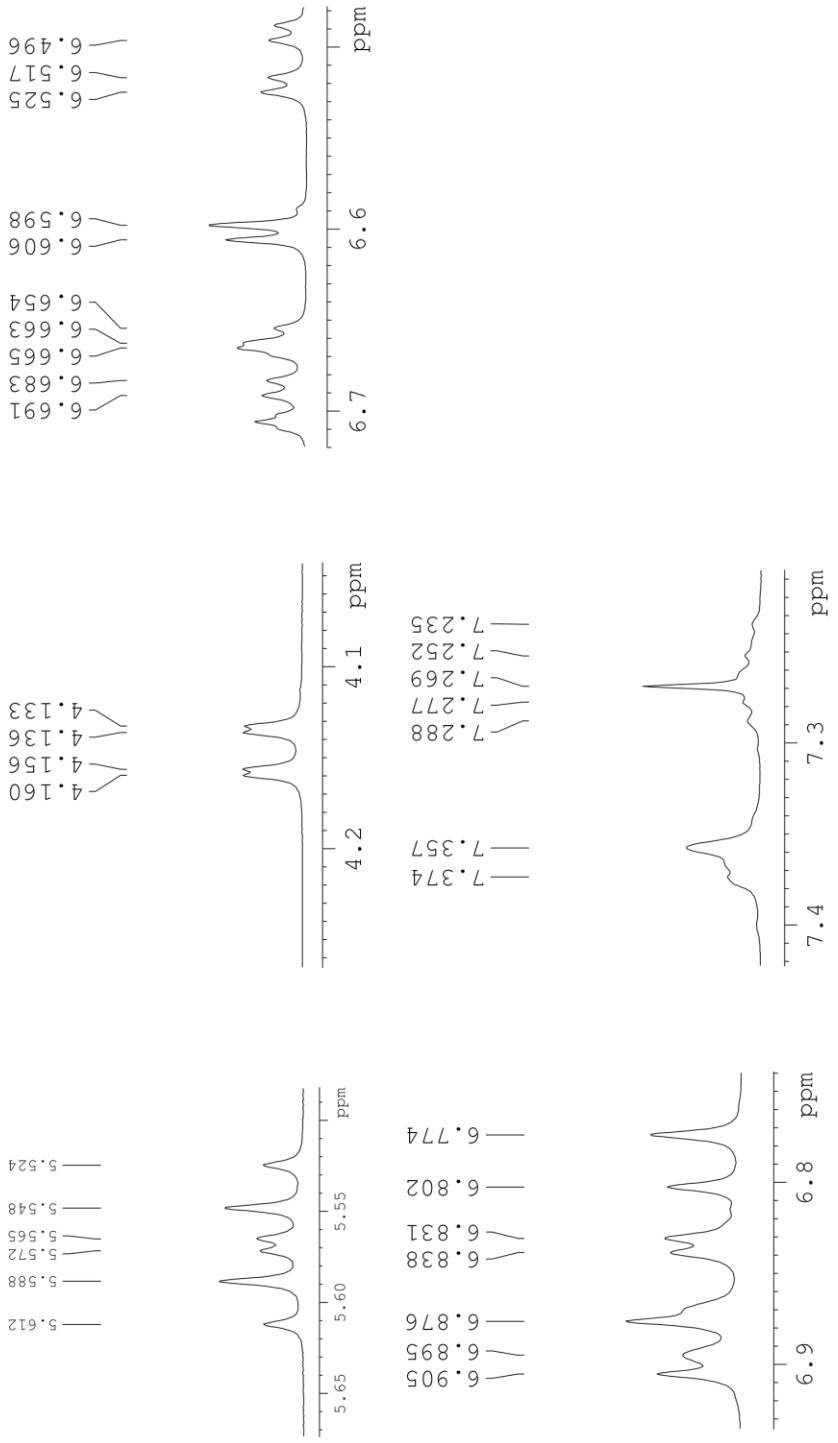

Spectrum 44. ^{1}H NMR spectrum of **2.37** continued

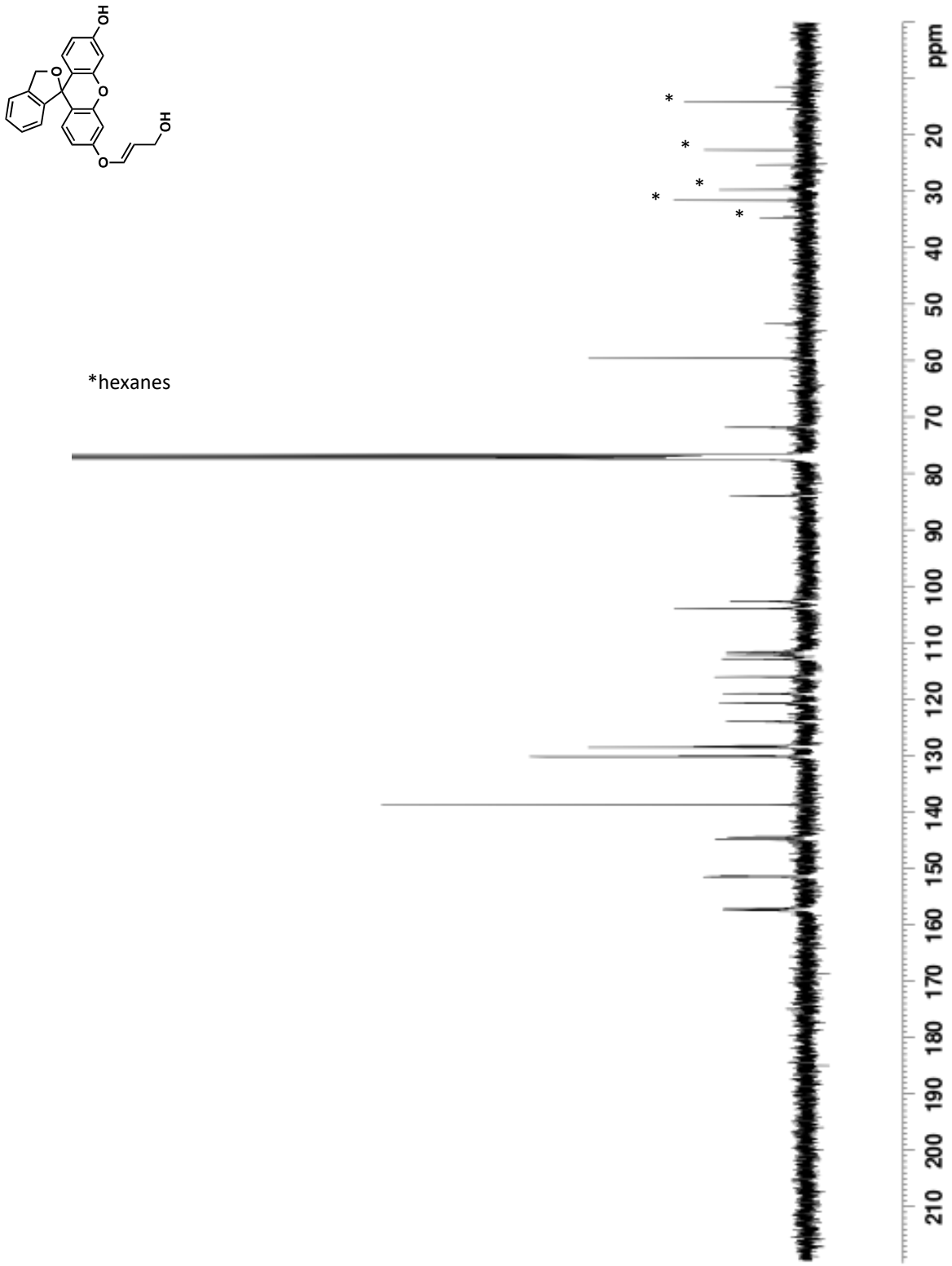

Spectrum 45. ^{13}C NMR spectrum of **2.37** (100 MHz, $CDCl_3$, 293K)

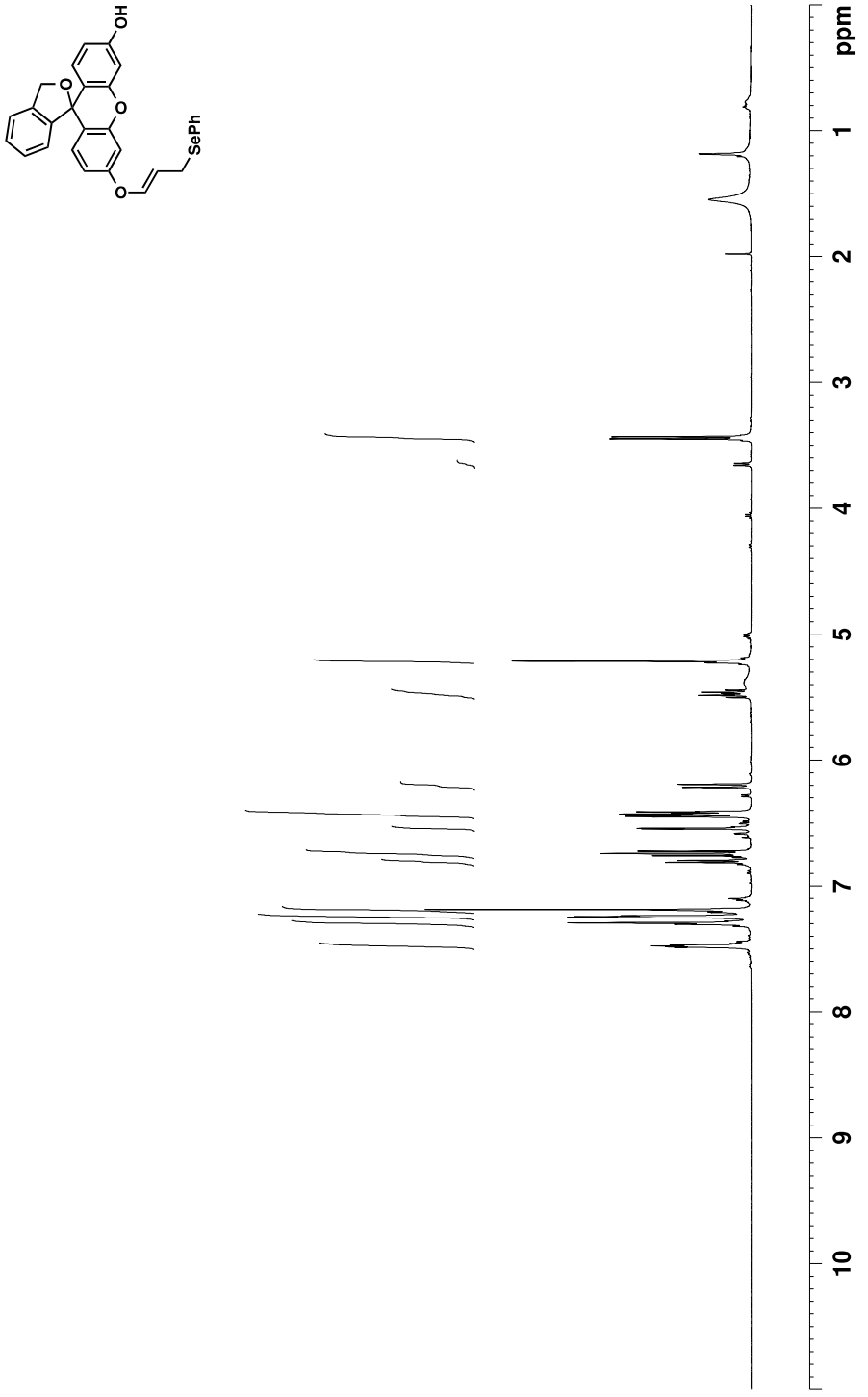

Spectrum 46. ^{1}H NMR spectrum of **2.17** (300 MHz, $CDCl_3$, 293K)

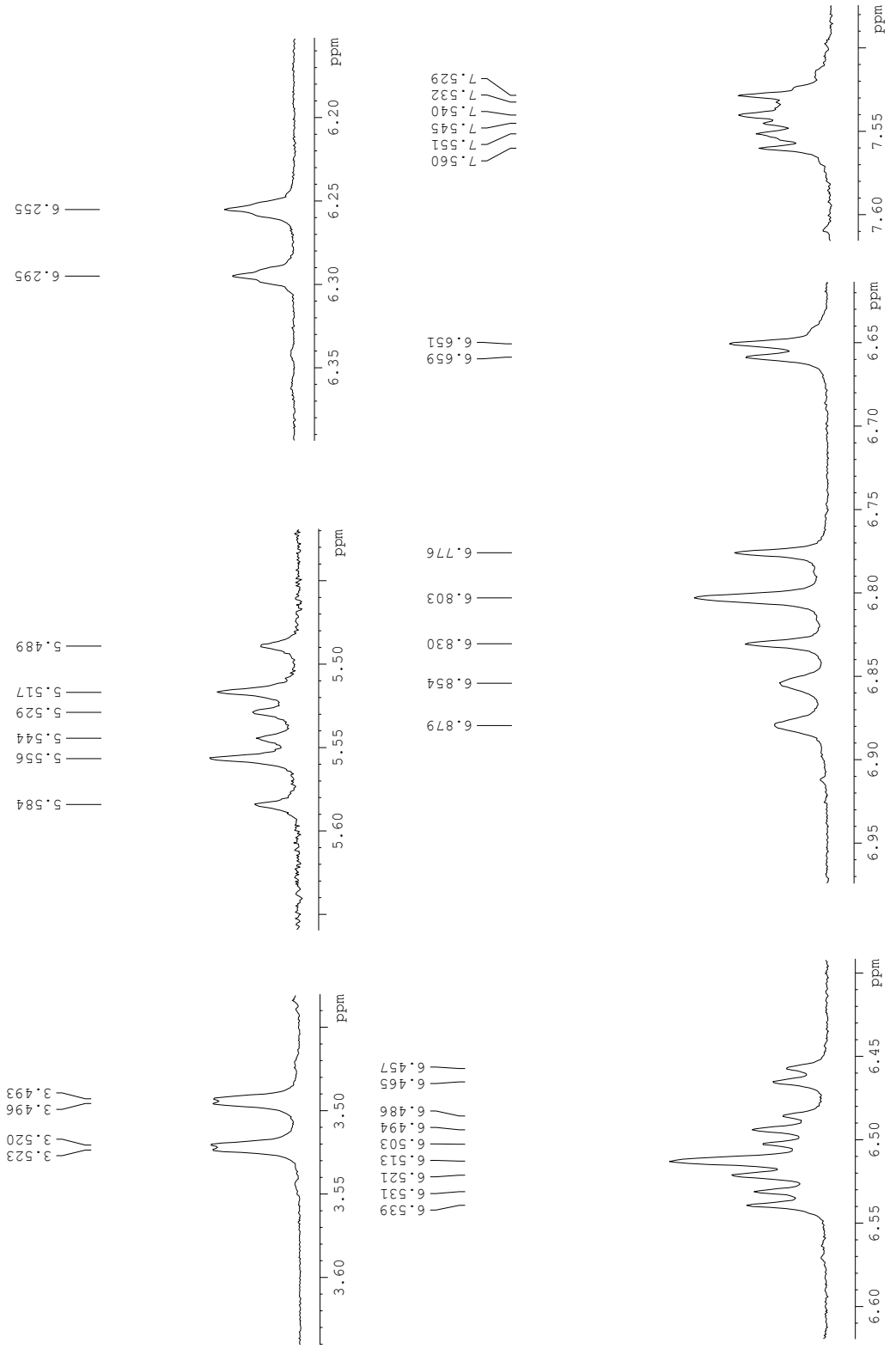

Spectrum 47. ^{1}H NMR spectrum of **2.17** continued

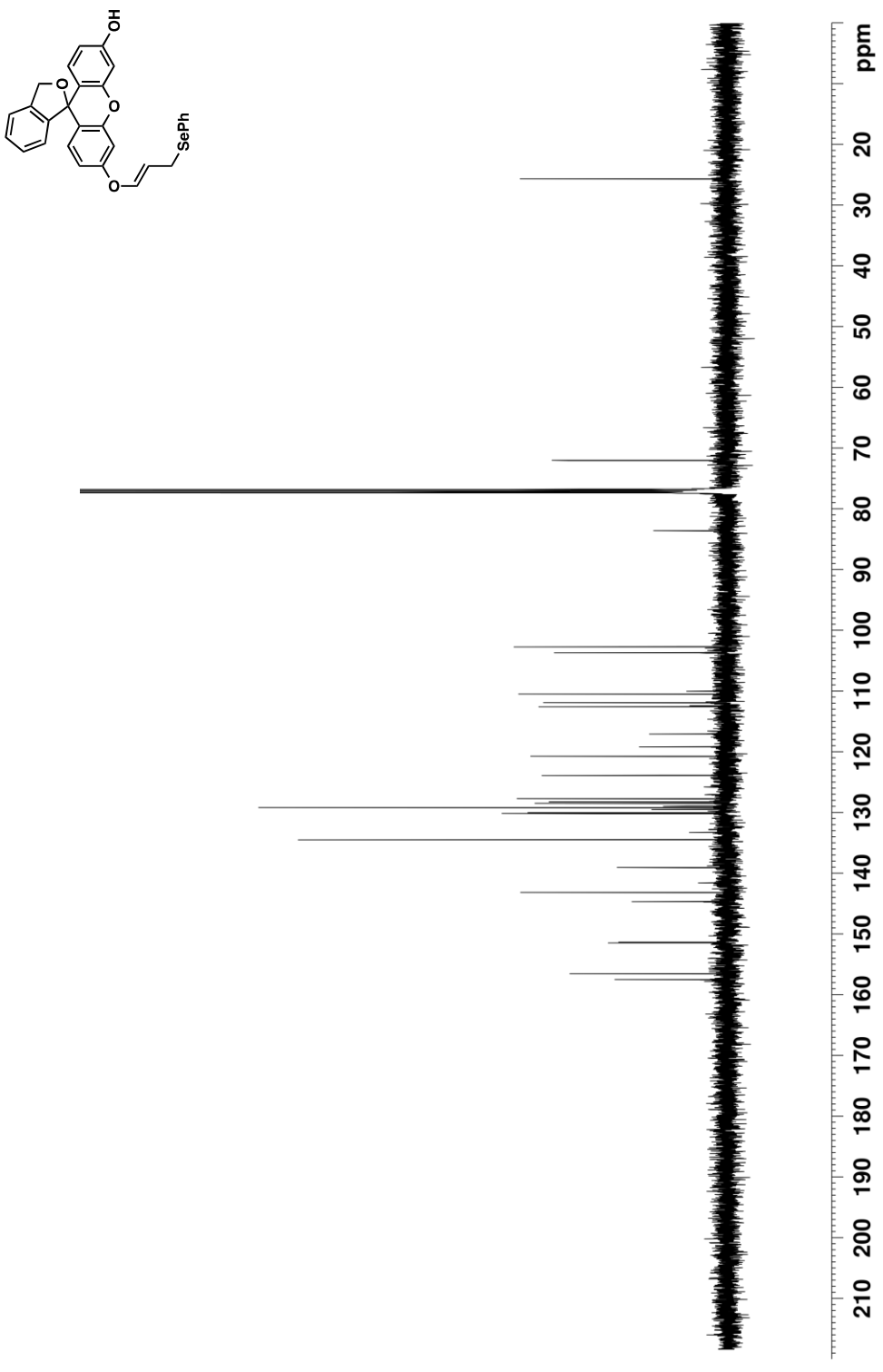

Spectrum 48. ^{13}C NMR spectrum of **2.17** (125 MHz, $CDCl_3$, 293K)

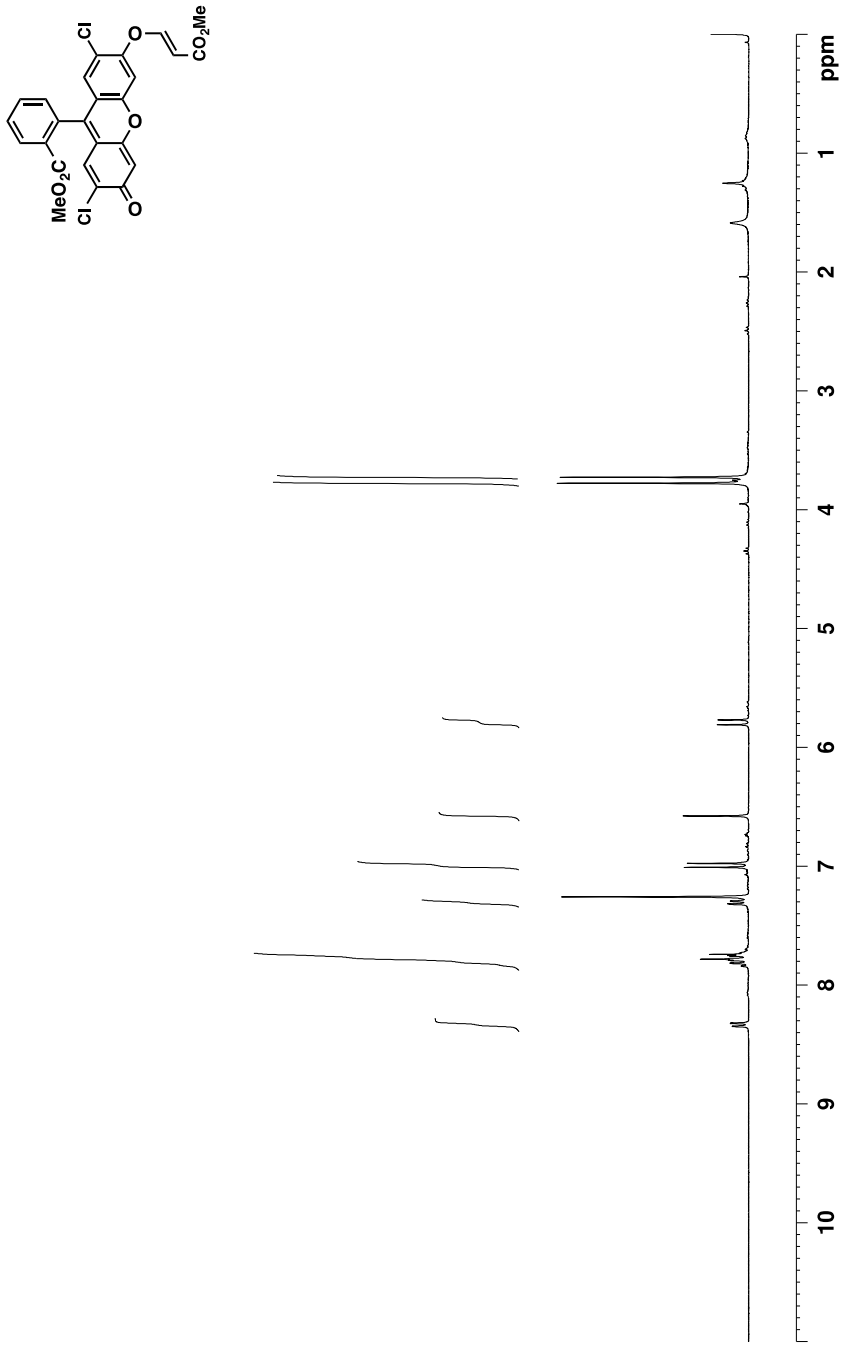

Spectrum 49. ^{1}H NMR spectrum of **2.38** (300 MHz, $CDCl_3$, 293K)

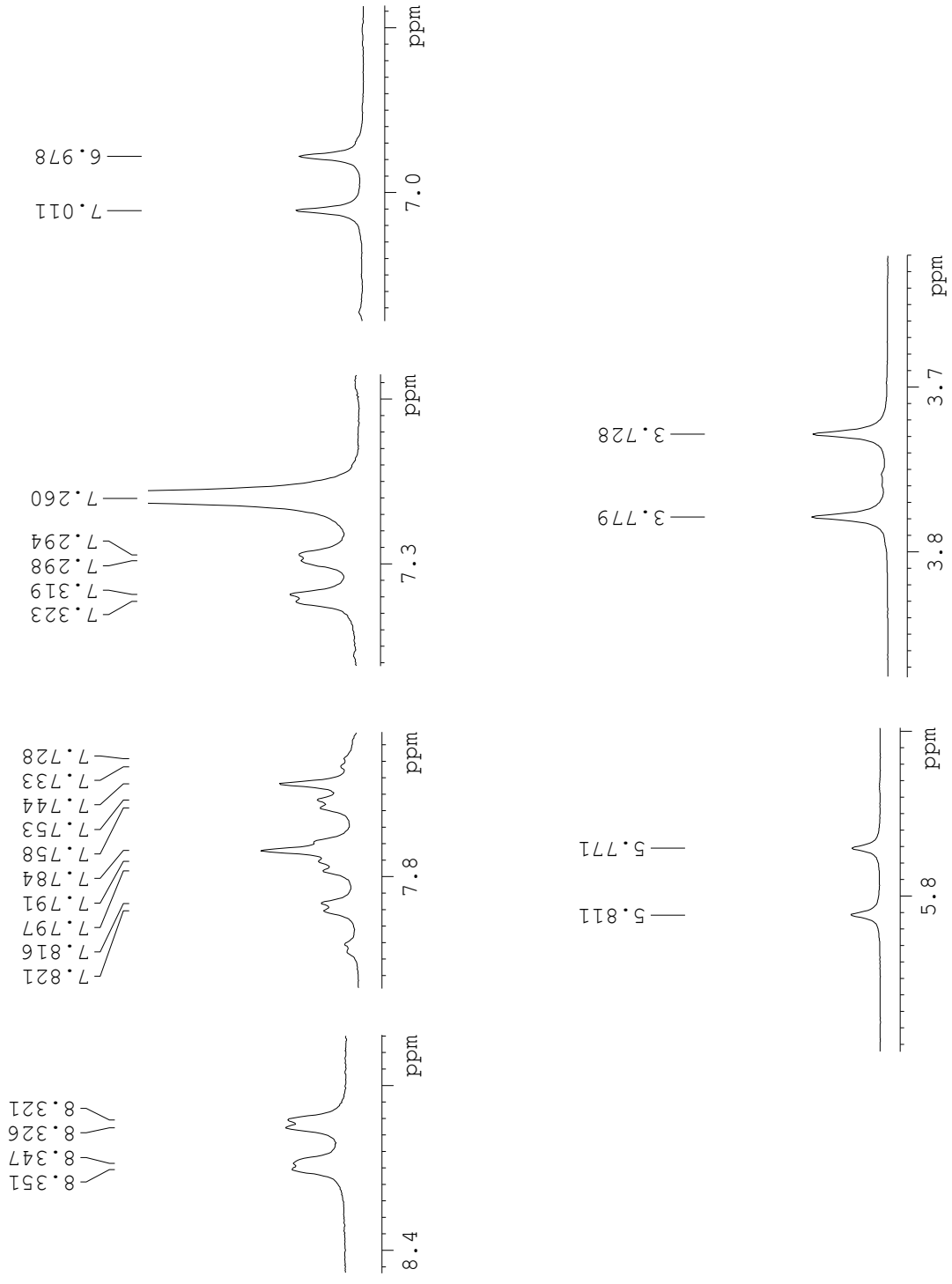

Spectrum 50. ^{1}H NMR spectrum of **2.38** (300 MHz, $CDCl_3$, 293K)

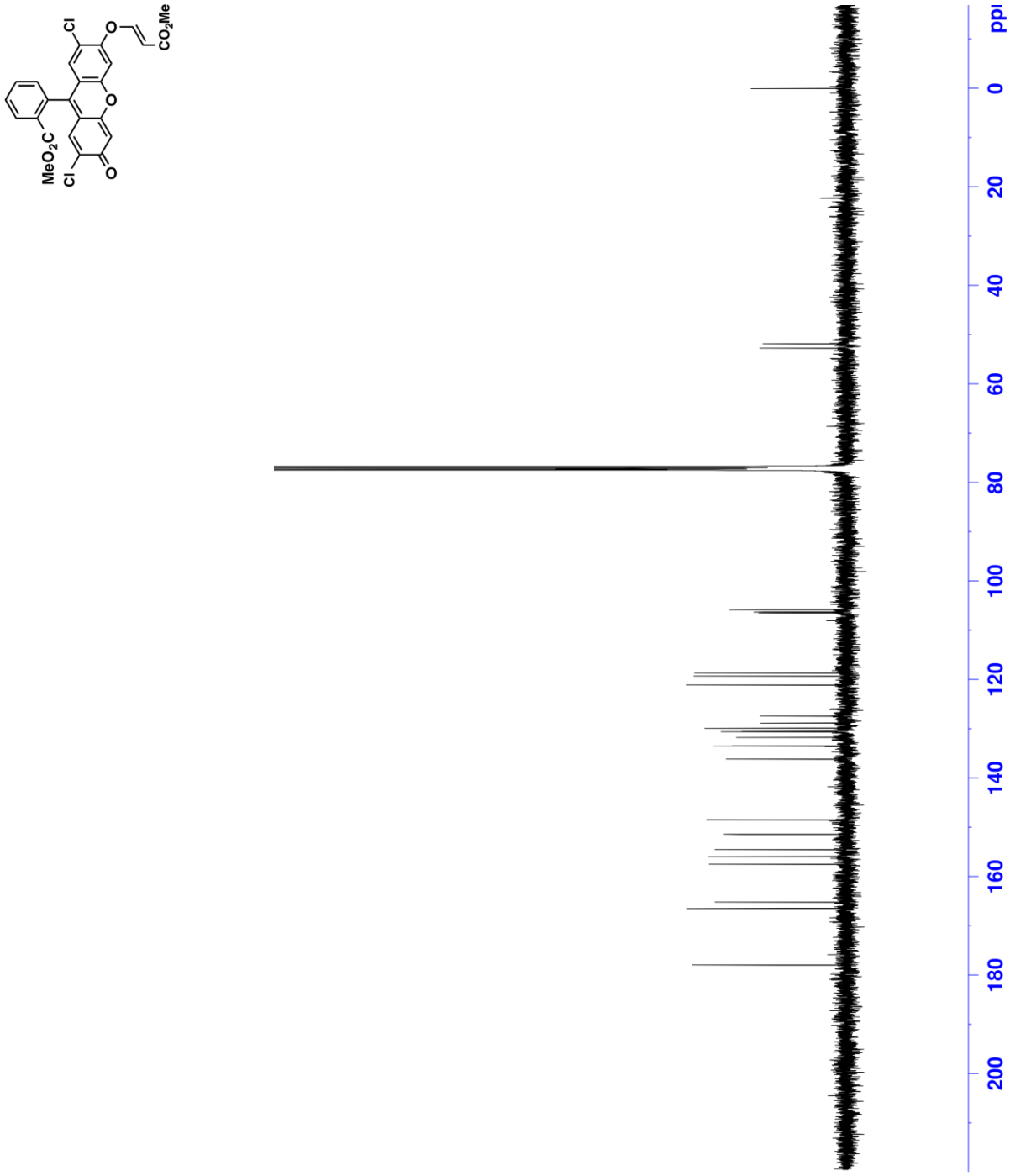

Spectrum 51. ^{13}C NMR spectrum of **2.38** (100 MHz, $CDCl_3$, 293K)

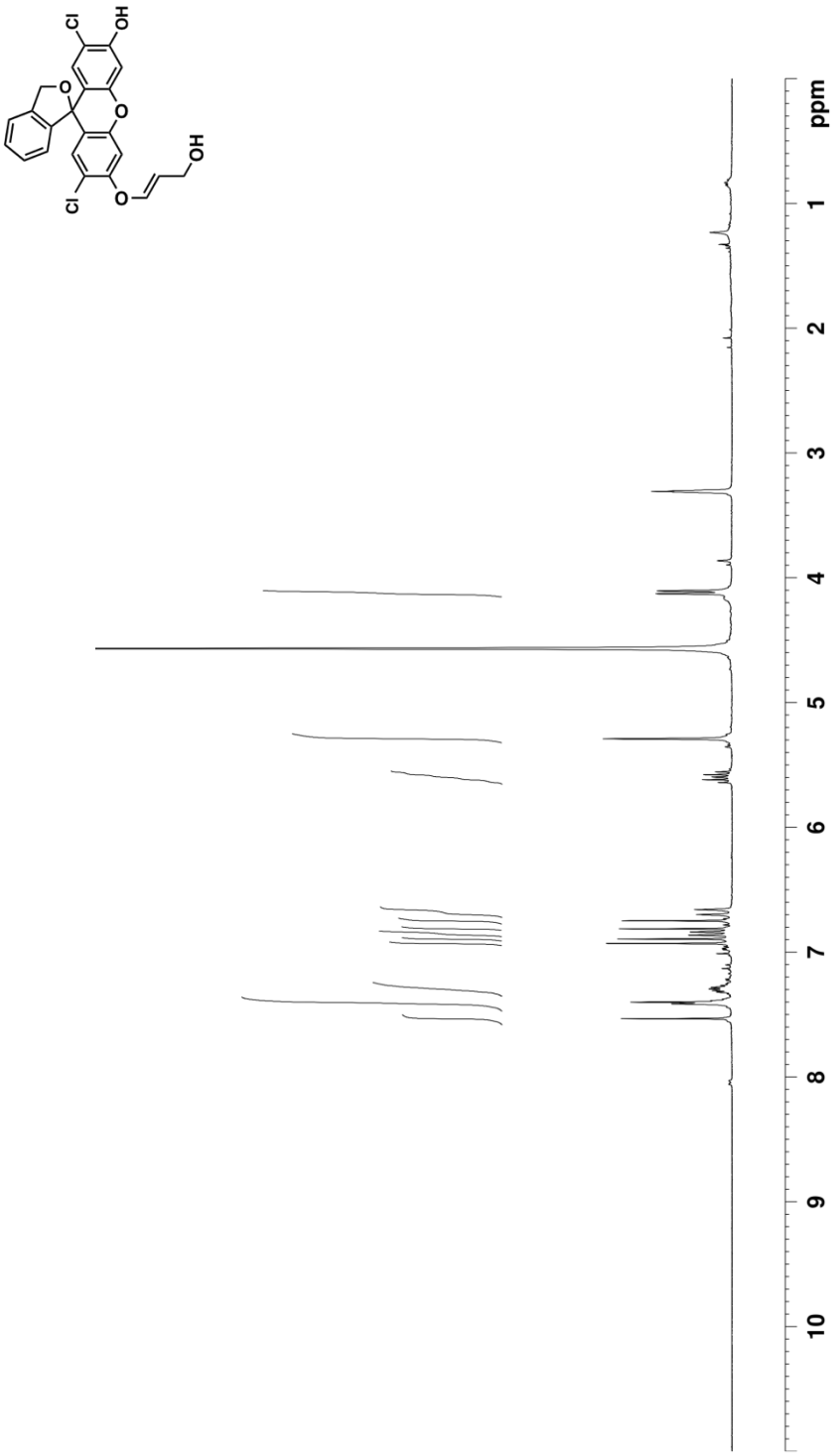

Spectrum 52. ^{1}H NMR spectrum of **2.40** (300 MHz, CD_3OD, 293K)

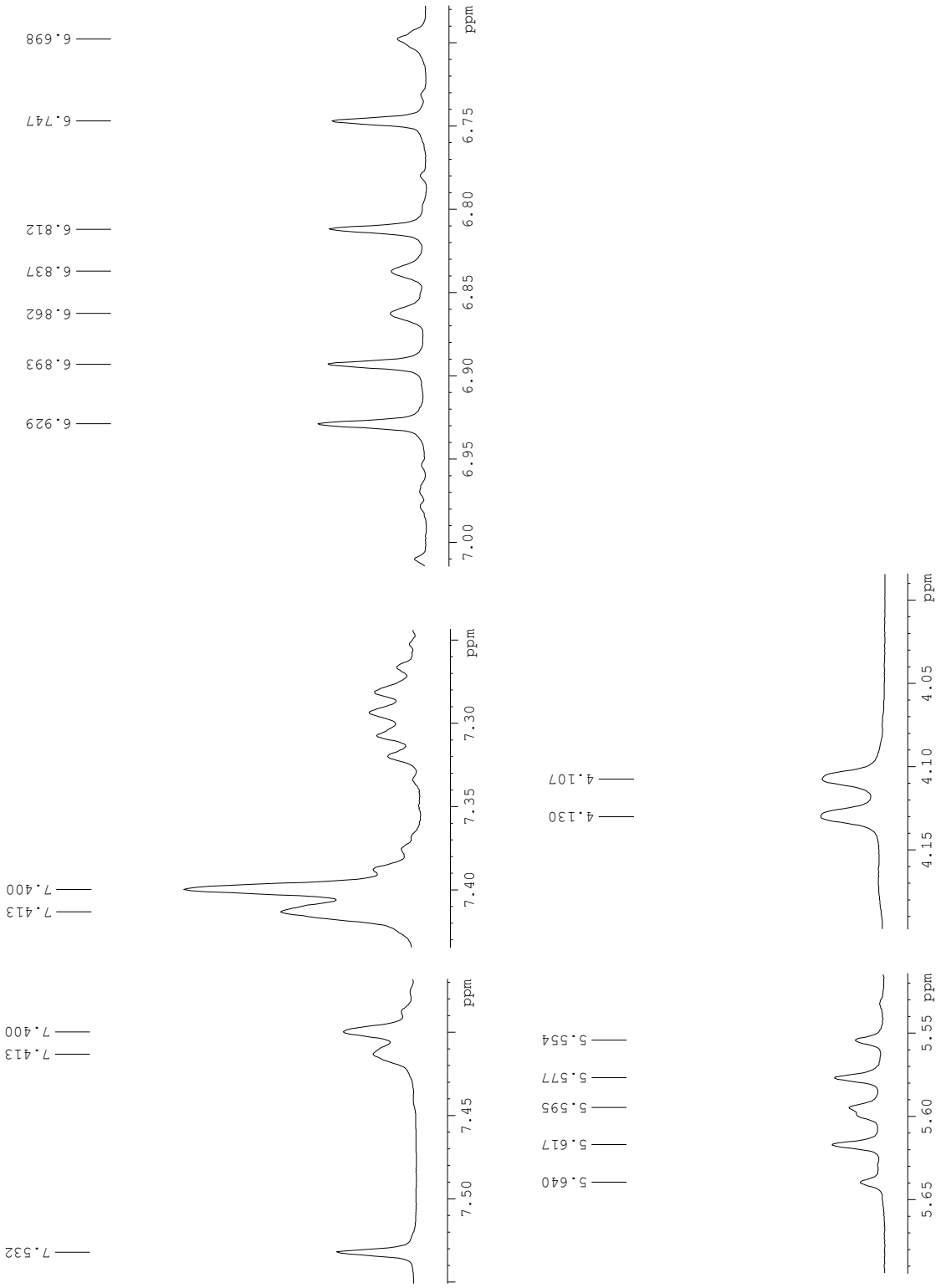

Spectrum 53. ^{1}H NMR spectrum of **2.40** (300 MHz, CD_3OD, 293K)

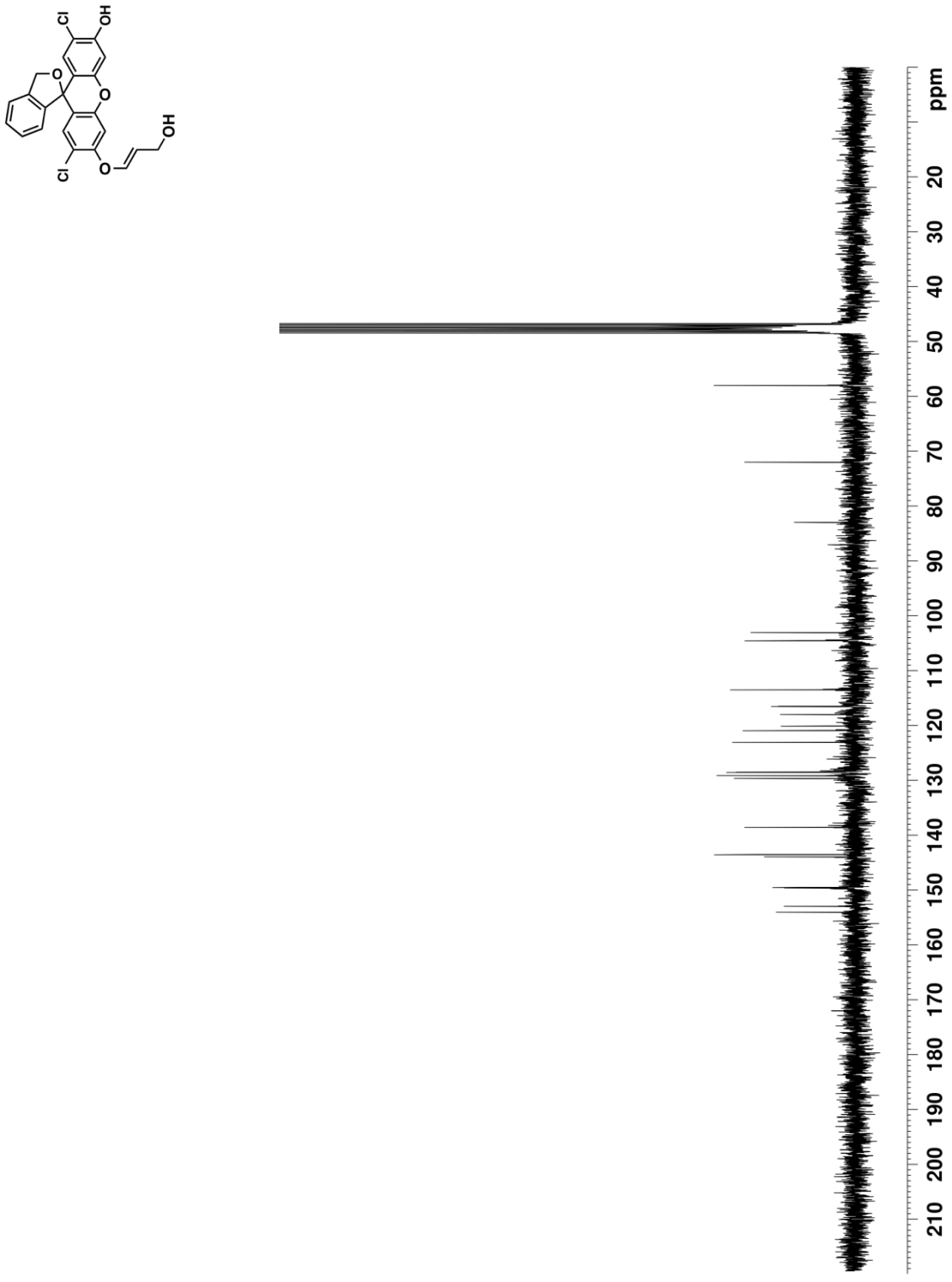

Spectrum 54. ^{13}C NMR spectrum of **2.40** (75 MHz, CD_3OD, 293K)

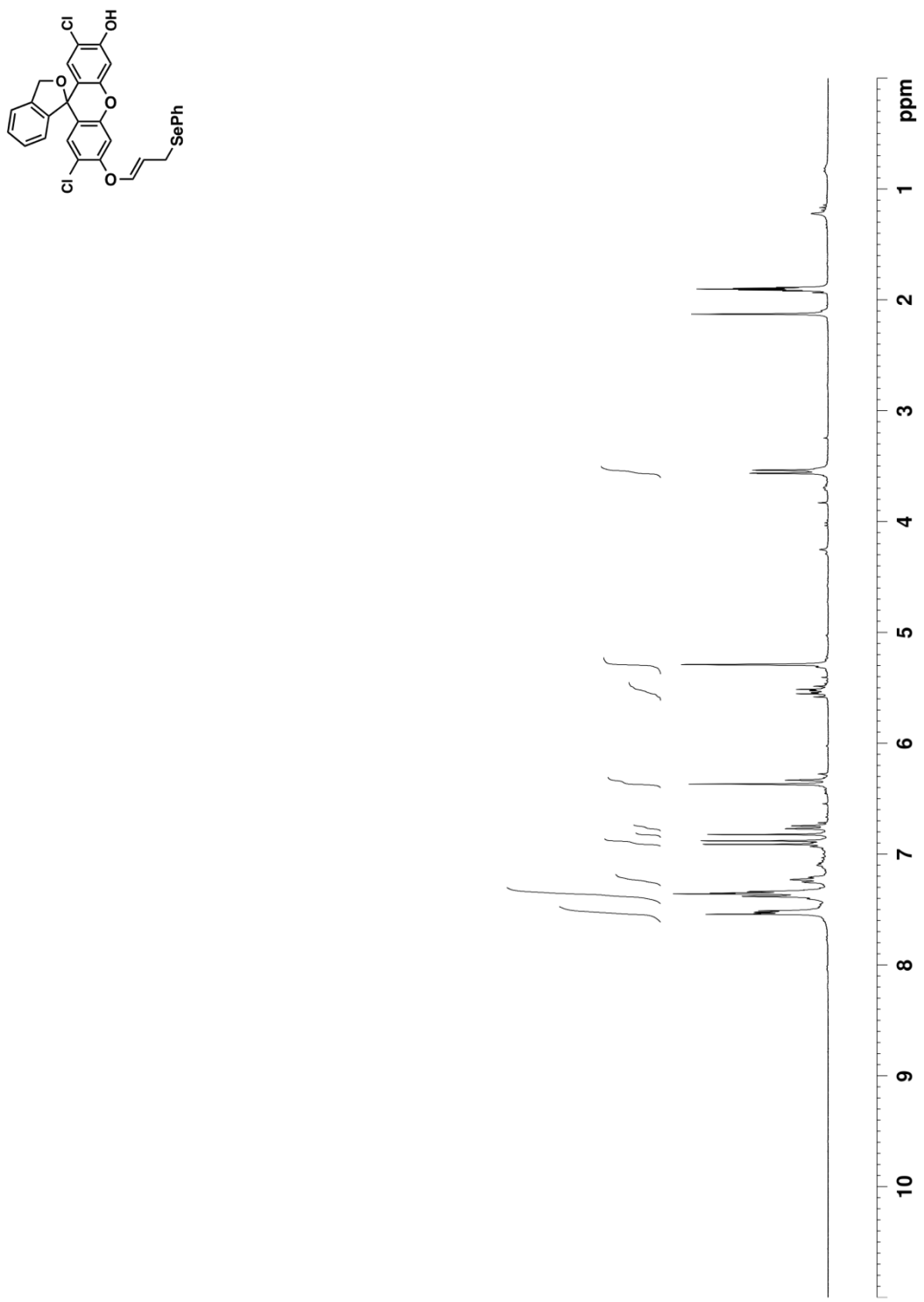

Spectrum 55. ^{1}H NMR spectrum of **2.41** (300 MHz, CD_3CN, 293K)

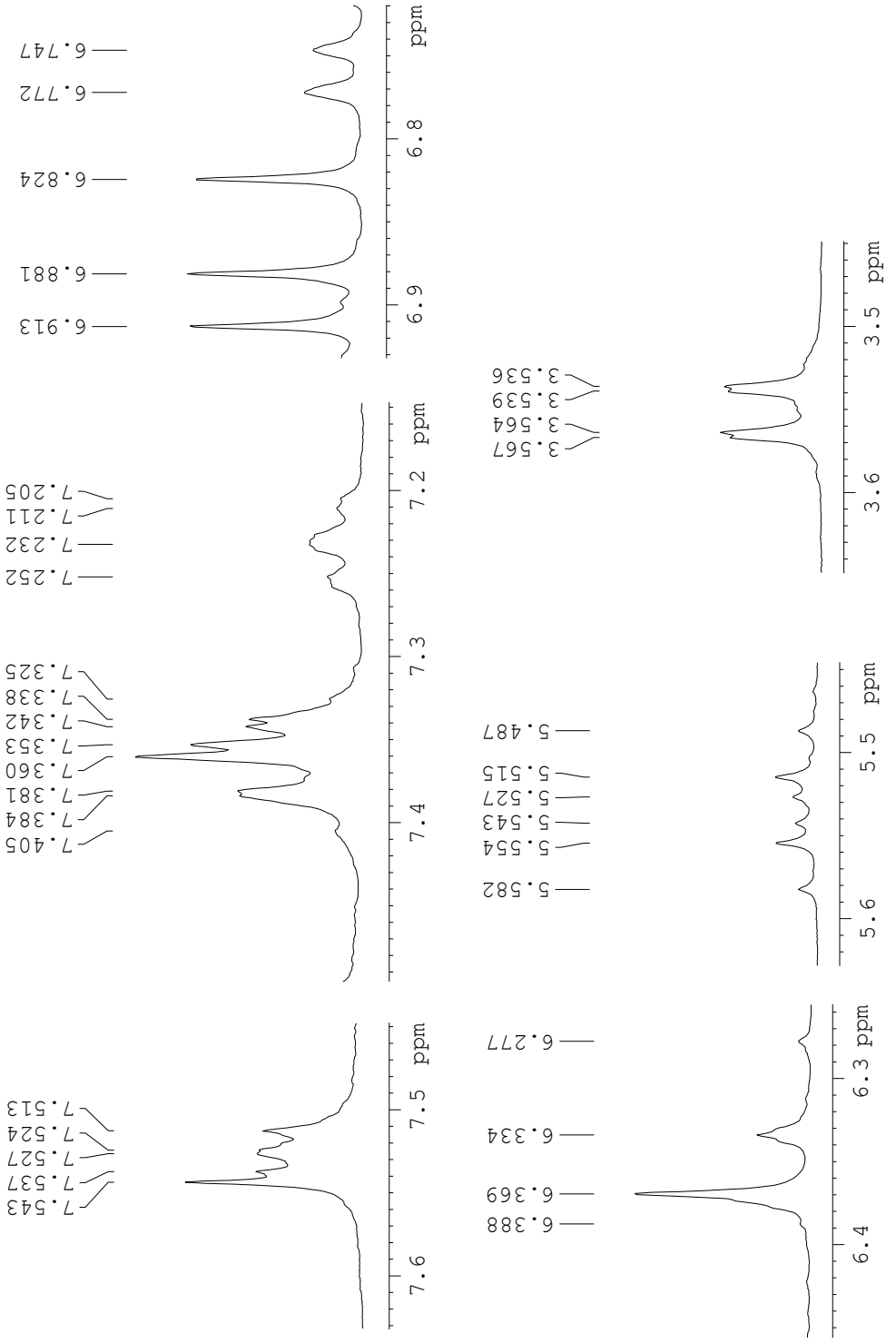

Spectrum 56. ^{1}H NMR spectrum of **2.41** (300 MHz, CD_3CN, 293K)

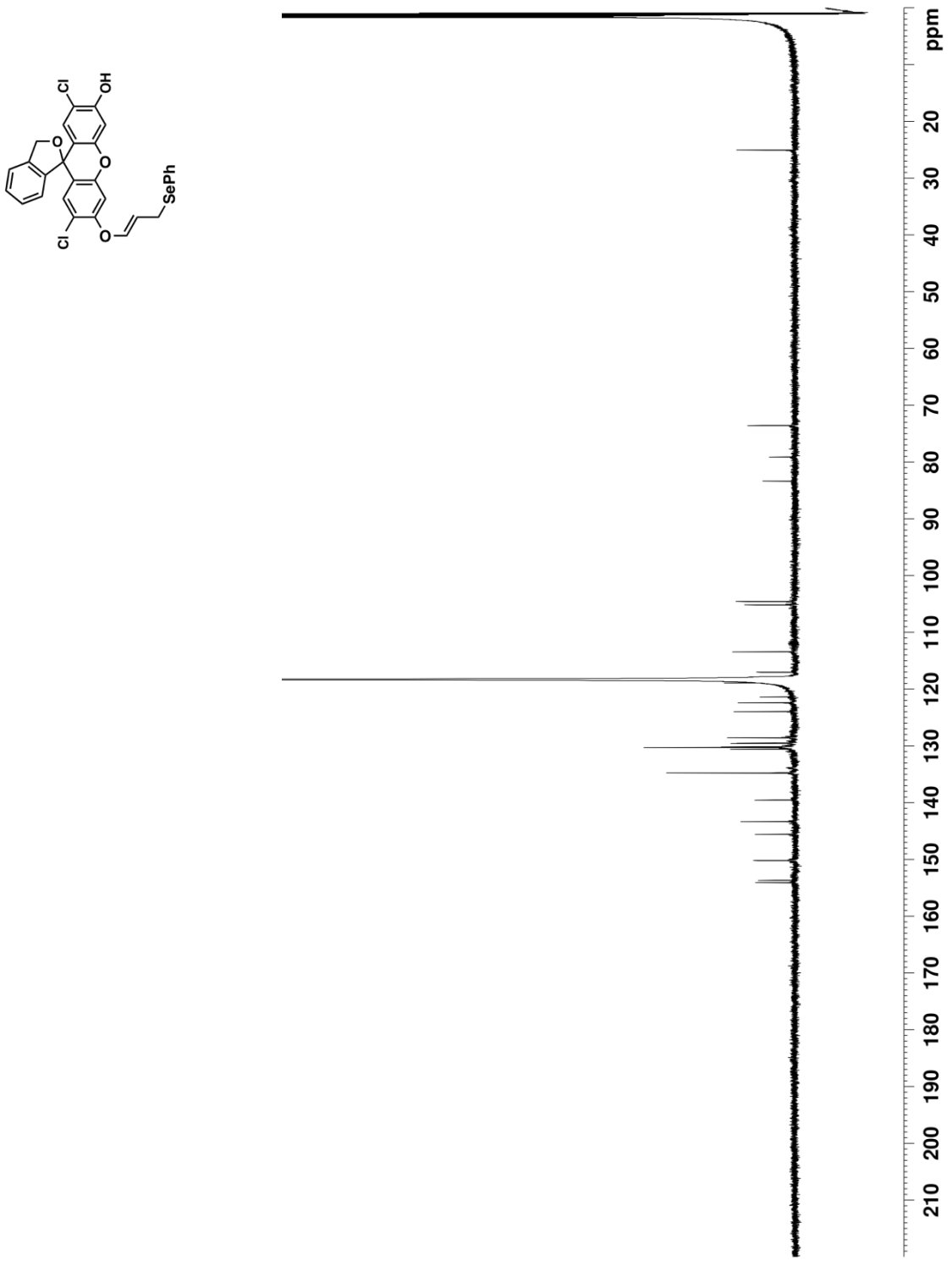

Spectrum 57. ^{13}C NMR spectrum of **2.41** (150 MHz, CD_3CN, 293K)

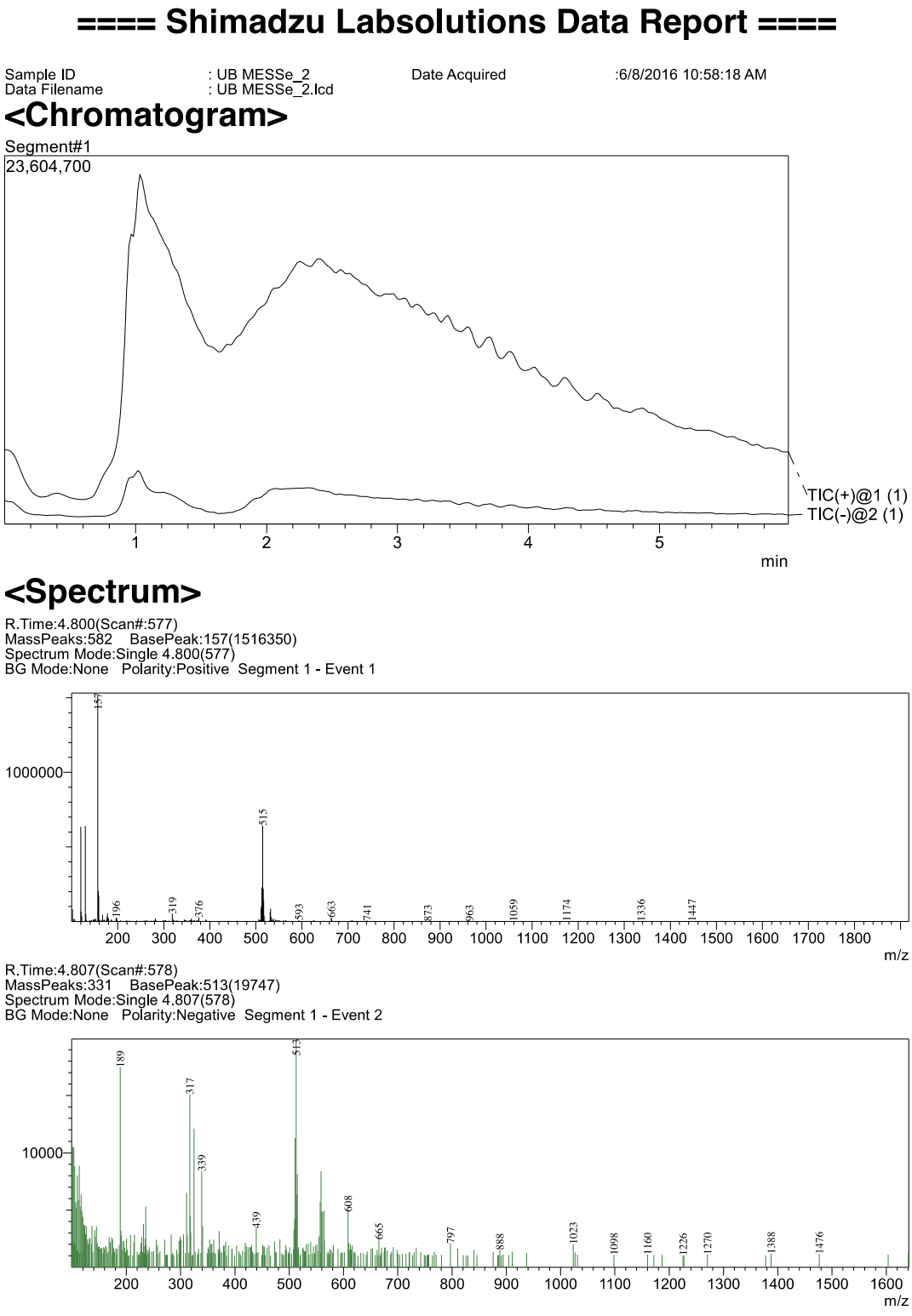

Spectrum 58. LCMS studies confirm formation of **2.17** by cross-metathesis approach

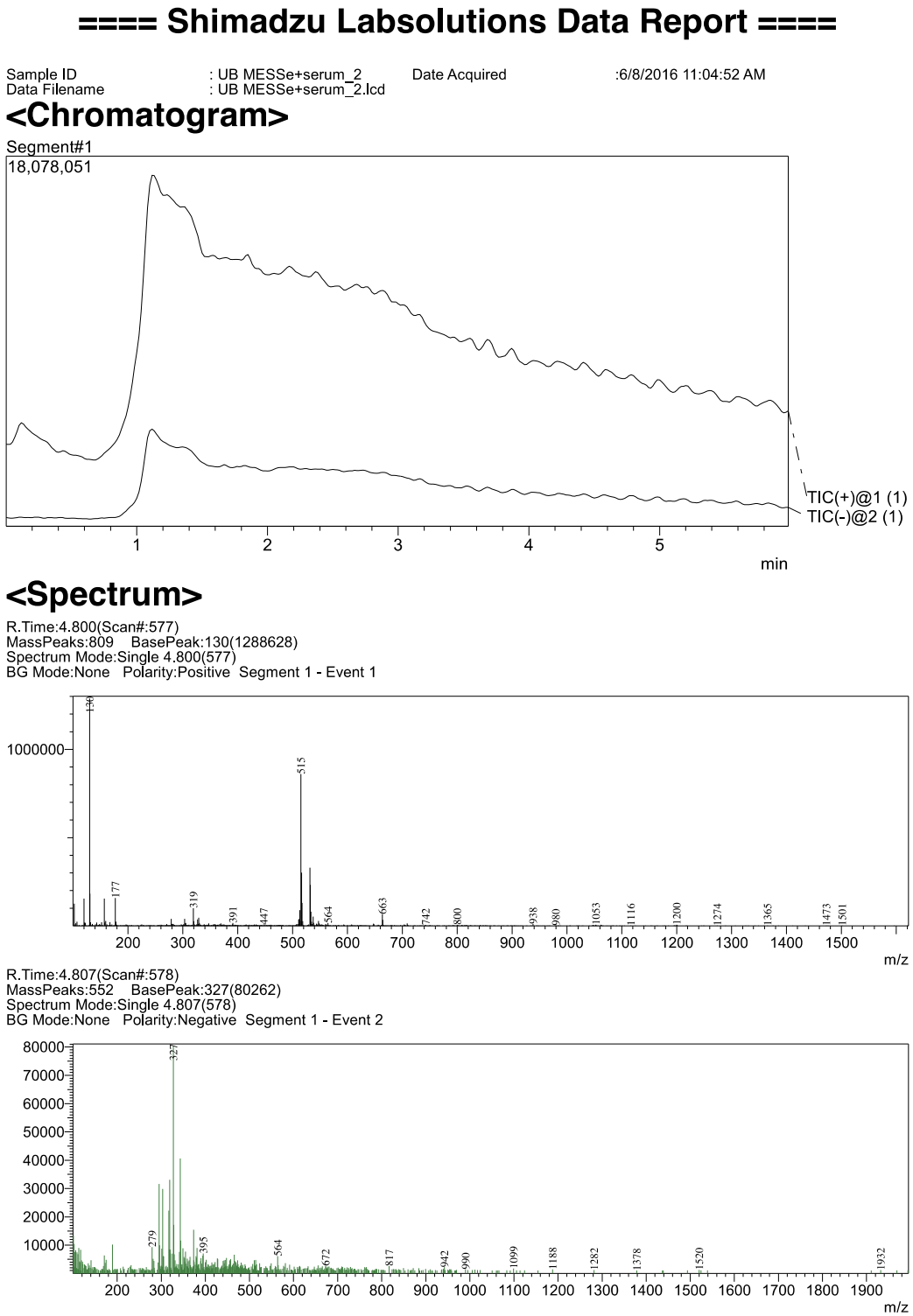

Spectrum 59. LCMS studies confirm **2.17** is stable in bovine serum

BIBLIOGRAPHY

1. Nakajima, H.; Sato, B.; Fujita, T.; Takase, S.; Terano, H.; Okuhara, M. *J Antibiot (Tokyo)* **1996**, *49*, 1196.

2. Nakajima, H.; Takase, S.; Terano, H.; Tanaka, H. *J Antibiot (Tokyo)* **1997**, *50*, 96.

3. Nakajima, H.; Hori, Y.; Terano, H.; Okuhara, M.; Manda, T.; Matsumoto, S.; Shimomura, K. *J Antibiot (Tokyo)* **1996**, *49*, 1204.

4. Eustáquio1, A. S.; Janso, J. E.; Ratnayake, A. S.; O'Donnell, C. J.; Koehn, F. E.; *Proc Natl Acad Sci U S A* **2014**, *111*, 3376–3385.

5. Thompson, C. F.; Jamison, T. F.; Jacobsen, E. N. *J Am Chem Soc* **2001**, *123*, 9974.

6. Horigome, M. M., H.; Watanabe, H.; Kitahara, T. *Tetrahedron Lett* **2001**, *42*, 8207.

7. Albert, B. J.; Sivaramakrishnan, A.; Naka, T.; Koide, K. *J Am Chem Soc* **2006**, *128*, 2792.

8. Ghosh, A. K.; Chen, Z; *Org. Lett.* **2013**, *15*, 5088.

9. Osman, S.; Albert, B. J.; Wang, Y.; Li, M.; Czaicki, N. L.; Koide, K. *Chemistry* **2011**, *17*, 895.

10. Motoyoshi, H.; Horigome, M.; Ishigami, K.; Yoshida, T.; Horinouchi, S.; Yoshida, M.; Watanabe, H.; Kitahara, T. *Biosci Biotechnol Biochem* **2004**, *68*, 2178.

11. Albert, B. J.; Sivaramakrishnan, A.; Naka, T.; Czaicki, N. L.; Koide, K. *J Am Chem Soc* **2007**, *129*, 2648.

12. Osman, S.; Waud, W. R.; Gorman, G. S.; Day, B. W.; Koide, K. *Med. Chem. Commun.* **2011**, *2*, 38-43

13. Kobayashi, S.; Hachiya, I.; Yamanoi, Y. *Bulletin of the Chemical Society of Japan* **1994**, *67*, 2342.

14. Nemoto, T.; Ohshima, T.; Yamaguchi, K.; Shibasaki, M. *J. Am. Chem. Soc.* **2001**, *123*, 2725.

15. Liu, Y.; Provencher, B. A.; Bartelson, K. J.; Deng, L. *Chem. Sci.* **2011**, *2*, 1301.

16. Wu, M. H.; Hansen, K. B.; Jacobsen, E. N. *Angewandte Chemie International Edition* **1999**, *38*, 2012.

17. Lebel, H.; Jacobsen, E. N. *Tetrahedron Lett.* **1999**, *40*, 7303.

18. Gao, Y.; Klunder, J. M.; Hanson, R. M.; Masamune, H.; Ko, S. Y.; Sharpless, K. B. *J. Am. Chem. Soc.* **1987**, *109*, 5765.

19. Ley, S. V.; Norman, J.; Griffith, W. P.; Marsden, S. P. *Synthesis* **1994**, *1994*, 639.

20. Nicolaou, K. C.; Prasad, C. V. C.; Somers, P. K.; Hwang, C. K. *J. Am. Chem. Soc.* **1989**, *111*, 5330.

21. Corey, E. J.; Bakshi, R. K.; Shibata, S. *J. Am. Chem. Soc.* **1987**, *109*, 5551.

22. Corey, E. J.; Bakshi, R. K.; Shibata, S.;Chen, C.-P.; Singh, V. K. *J. Am. Chem. Soc.* **1987**, *109*, 7925.

23. Corey, E. J.; Shibata, S.; Bakshi, R. K. *J. Org. Chem.* **1988**, *53*, 2861.

24. Corey, E. J.; Chen, C.-P.; Reichard, G. A. *Tetrahedron Lett.* **1989**, *30*, 5547.

25. Corey, E. J.; Link, J. O. *Tetrahedron Lett.* **1989**, *30*, 6275.

26. Corey, E. J.; Bakshi, R. K. *Tetrahedron Lett.* **1990**, *31*, 611.

27. Corey, E. J.; Reichard, G. A. *Tetrahedron Lett.* **1989**, *30*, 5207.

28. Waldrop, M. M. *Science* **1989**, *245*, 354.

29. Corey, E. J.; Gavai, A. V. *Tetrahedron Lett.* **1988**, *29*, 3201.

30. Corey, E. J.; Jardine, P. D. S.; Mohri, T. *Tetrahedron Lett.* **1988**, *29*, 6409.

31. Brown, H. C. *Organic Synthesis via Boranes*; Wiley-Interscience: NY, 1975.

32. Midland, M. M.; McDowell, D. C.; Hatch, R. L.; Tramontano, A. *J. Am Chem. Soc.* **1980**, *102*, 867.

33. Midland, M. M.; Tramontano, A.; Kazubski, A.; Graham, R. S.; Tsai, D. J. S.; Cardin, D. B. *Tetrahedron* **1984**, *40*, 1371.

34. Brown, H. C.; Chandrasekharan, J.; Ramachandran, P. V. *J. Am. Chem. Soc.* **1988**, *110*, 1539.

35. Brown, H. C.; Chandrasekharan, J.; Ramachandran, P. V. *J. Org. Chem.* **1986**, *51*, 3394.

36. Midland, M. M.; Zderic, S. A. *J. Am. Chem. Soc.* **1982**, *104*, 525.

37. Noyori, R.; Tomino, I.; Tanimoto, Y.; Nishizawa, M. *J. Am. Chem. Soc.* **1984**, *106*, 6709.

38. Noyori, R.; Tomino, I.; Yamada, M.; Nishizawa, M. *J. Am. Chem. Soc.* **1984**, *106*, 6717.

39. Chan, P. C.-M.; Chong, J. M. *J. Org. Chem.* **1988**, *53*, 5584.

40. Marshal, J.; Gung, W. Y. *Tetrahedron Lett*. **1990**, *31*, 1981.

41. Chong, J. M.; Mar, E. K. *Tetrahedron Lett.* **1990**, *31*, 1981.

42. Takaya, H.; Akutagawa, A.; Noyori, R. *Org. Synth.* **1989**, *67*, 20.

43. Kitamura, M.; Ohkuma, T.; Takaya, H.; Noyori, R. *Tetrahedron Lett.* **1988**, *29*, 1555.

44. Nishi, T.; Kitamura, M.; Ohkuma, T.; Noyori, R. *Tetrahedron Lett.* **1988**, *29*, 6327.

45. Nakatsuka, M.; Ragan, J. A.; Sammakia, T.; Smith, D. B.; Uehling, D. E.; Schreiber, S. L. *J. Am. Chem. Soc.* **1990**, *112*, 5583.

46. Noyori, R. *Science* **1990**, *248*, 1194.

47. Noyori, R. *Chem. Soc. Rev.* **1989**, *18*, 187.

48. Le Roux, J.; Le Corre, M. *Journal of the Chemical Society, Chemical Communications* **1989**, 1464.

49. Lifchits, O.; Mahlau, M.; Reisinger, C. M.; Lee, A.; Farès, C.; Polyak, I.; Gopakumar, G.; Thiel, W.; List, B. *J. Am. Chem. Soc.* **2013**, *135*, 6677−6693.

50. Chen, K.-M.; Hardtmann, G. E.; Prasad, K.; Repič, O.; Shapiro, M. J. *Tetrahedron Lett.* **1987**, *28*, 155.

51. Evans, D. A.; Chapman, K. T.; Carreira, E. M. *J. Am. Chem. Soc.* **1988**, *110*, 3560.

52. Carr, J. M.; Duggan, P. J.; Humphrey, D. G.; Platts, J. A.; Tyndall, E. M. *Aust. J. Chem.* **2011**, *64*, 495.

53. Noyori, R.; Tomino, I.; Tanimoto, Y. *J. Am. Chem. Soc.* **1979**, *101*, 3129.

54. Rossiter, B. E.; Verhoeven, T. R.; Sharpless, K. B. *Tetrahedron Lett.* **1979**, *49*, 4733.

55. Chatterjee, A. K.; Choi, T.-L.; Sanders, D. P.; Grubbs, R. H. *J. Am. Chem. Soc.* **2003**, **125**, 11360.

56. Nicolaou, K. C.; Rhoades, D.; Lamani, M.; Pattanayak, M. R.; Kumar, S. M. *J. Am. Chem. Soc.* **2016**, *138*, 7532–7535.

57. Blackmond, D. G. *Acc. Chem. Res.*, **2000**, *33*, 402–411.

58. Frisard, M.; Ravussin, E. Endocrine. **2006**, *1*, 27-32.

59. Harman, D. *Ann. N Y Acad. Sci.* **1998**, *854*, 1-7.

60. Balaban, R. S.; Nemoto, S.; Finkel, T. *Cell* **2005**, *120*, 483–495.

61. Chance, B; Sies, H.; Boveris, A. *Physiol Rev*. **1979**, *59*, 527–605.

62. Mueller, S. *Free Radic. Biol. Med.* **2000,** *29*, 410–415.

63. Giorgio, M.; Trinei, M.; Migliaccio, E.; Pelicci, P. G. *Nat. Rev. Mol. Cell Biol.* **2007**, *8*, 722-8.

64. Myhre, O.; Andersen, J. M.; Aarnes, H.; Fonnum, F. *Biochem Pharmacol* **2003**, *65*, 1575.

65. Riehl, T. E.; Malehorn, C. L.; Hinze, W. L. *Analyst* **1986**, *111*, 931.

66. Malehorn, C. L.; Riehl, T. E.; Hinze, W. L. *Analyst* **1986**, *111*, 941.

67. Arnold, R. S.; Shi, J.; Murad, E.; Whalen, A. M.; Sun, C. Q.; Polavarapu, R.; Parthasarathy, S.; Petros, J. A.; Lambeth, J. D. *Proc. Natl. Acad. Sci. U.S.A.* **2001**, *98*, 5550.

68. Pignatelli, P.; Pulcinelli, F. M.; Lenti, L.; Gazzaniga, P. P.; Violi, F. *Blood* **1998**, *91*, 484.

69. Dahlgren, C.; Aniansson, H.; Magnusson, K. E. *Infect. Immun.* **1985**, *47*, 326.

70. Faulkner, K.; Fridovich, I. *Free Radical Bio. Med.* **1993**, *15*, 447.

71. Gyllenhammar, H. *J Immunol Methods* **1987**, *97*, 209.

72. Warm, E.; Laties, G. G. *Phytochemistry* **1982**, *21*, 827.

73. Freeman, T. M.; Seitz, W. R. *Anal. Chem.* **1978**, *50*, 1242.

74. Thorpe, G. H. G.; Kricka, L. J.; Moseley, S. B.; Whitehead, T. P. *Clin. Chem.* **1985**, *31*, 1335.

75. Tarpey, M. M.; Fridovich, I. *Circ Res* **2001**, *89*, 224.

76. Kikuchi, K.; Nagano, T.; Hayakawa, H.; Hirata, Y.; Hirobe, M. *Anal. Chem.* **1993**, *65*, 1794.

77. Zielonka, J.; Lambeth, J. D.; Kalyanaraman, B. *Free Radic Biol Med* **2013**, *65*, 1310.

78. Boveris, A.; Martino, E.; Stoppani, A. O. M. *Anal. Biochem.* **1977**, *80*, 145.

79. Cohen, G.; Kim, M.; Ogwu, V. *J Neurosci Meth* **1996**, *67*, 53.

80. Tarpey, M. M.; Fridovich, I. *Circ Res* **2001**, *89*, 224.

81. Stone, J. R.; Yang, S. *Antioxidants & redox signaling* **2006**, *8*, 243.

82. Belousov, V. V.; Fradkov, A. F.; Lukyanov, K. A.; Staroverov, D. B.; Shakhbazov, K. S.; Terskikh, A. V.; Lukyanov, S. *Nat Methods* **2006**, *3*, 281.

83. Abo, M.; Terai, T.; Komatsu, T.; Nagano, T. *J. Am. Chem. Soc.* **2011**, *133*, 10629-10637.

84. Chang, M. C.; Pralle, A.; Isacoff, E. Y.; Chang, C. J. *J. Am. Chem. Soc.* **2004**, *126*, 15392–15393.

85. Weinstain, R.; Savariar, E. N.; Felsen, C. N.; Tsien, R. Y. *J. Am. Chem. Soc.* **2014**, *136*, 874.

86. Reich, H. J. *J. Org. Chem.* 1975, 40, 2570–2572.

87. Evans, D. A.; Andrews, G. C. *Acc. Chem. Res.* **1974**, *7*, 147–155.

88. Albert, B. J.; Sivaramakrishnan, A.; Naka, T.; Czaicki, N. L.; K. *J. Am. Chem. Soc.*, **2007**, *129*, 2648–2659.

89. Grieco, P. A.; Gilman, S.; Nishizawa, M. *J. Org. Chem.* **1976**, *41*, 1485-1486.

90. Ando, S.; Koide, K. *J Am Chem Soc*. **2011**,*133*, 2556-66.

91. Grela, K.; Harutyunyan, S.; Michrowska, A. *Angew. Chem. Int. Ed.* **2002**, *41*, 4038.

92. Rainier, J. D.; Cox, J. M.; Allwein, S. P. *Tetrahedron Letters* **2001**, *42*, 179–181;

93. Meek, S.J.; O'Brien, R. V.; Llaveria, J.; Schrock, R. R.; Hoveyda, A. H *Nature* **2011**, *471*, 461–466.

94. L. Ying; B. P. Bruce; *Bioconjugate Chemistry*, **2011**, *22*, 987–992.

95. Krief, A.; Lonez, F. *Tetrahedron Lett.* **2002**, *35*, 6255–6257.

96. Bickan, P.; Carson, F. W.; Jacobus, J.; Miller, E. G.; Mislow, K. *J. Am. Chem. Soc.* **1968**, *90*, 4869-4876.

97. Evans, D. A.; Andrews, G. C. *Accounts Chem. Res.* **1974**, *7*, 147.

98. Evans, D. A.; Andrews, G. C. *J Am Chem Soc* **1972**, *94*, 3672.

99. Advanced Organic Chemistry: Reaction Mechanisms By Reinhard Bruckner, 1st edition, Page 573, Chapter 14.

.